

Thesis submitted in partial fulfilment of the requirements  
for the degree of

***Master of Science***

Offshore and Dredging Engineering at  
Delft University of Technology

***Sand-Filled Monopiles: Strengthened Support Structures for  
Offshore Wind Turbines***

Panteleimon Rapis

16/10/2017

Graduation Committee:	Prof. Dr. A.V. Metrikine	TU Delft
	Ir. P. van der Male	TU Delft
	Ir. F. Renting	TU Delft
	Dr. D. Schraven	TU Delft
	Ir. J. van der Meer	Witteveen+Bos

An electronic version of this thesis is available at <http://repository.tudelft.nl>

*Page intentionally left blank*

# Abstract

In the early 1990's, the 1<sup>st</sup> wind turbine was installed offshore in Denmark. This 1<sup>st</sup> experimental application has nowadays turned to a constantly growing business sector, with an increasing number of offshore wind farms being developed in marine environment. The developments in Europe are mainly located at the North Sea, where the relatively shallow water ensures the technical and financial feasibility of this type of investment. The monopile is the prevailing foundation concept applied in those wind farms, mainly due to its' ability to support a wind generator ensuring at the same time the maximum production for the wind generator, since it can provide a foundation concept which does not exceed the displacement and rotation thresholds set by the wind turbine manufacturers. However, the trend nowadays is to develop wind farms in deeper water and to use wind turbines of higher capacity in order to increase the electricity production. This can be translated to an increased diameter and thickness demand for the monopile, leading to complications in the transportation and installation procedures. Therefore, the monopile concept is considered feasible only to water depths of approximately 30-35 m.

This thesis project focuses on the possibility to enhance the structural and dynamic behavior of the monopile by filling it with sand. The monopile design presented in Upwind report is being taken into consideration, since this design has been created specifically for reference purposes and comparison of the results of the researchers. The effect of the sand-fill on the following parameters has been investigated:

- Local Buckling
- Static Displacement
- Natural Frequency
- Damping Ratio

For the effect of sand-fill on local buckling, the effect of sand-fill on the ovalization of the monopile's cross-section was estimated using the relevant European and Dutch standards. The analysis has shown that for an increasing Youngs Modulus (E) of the sand-fill, the ovalization of the monopile at the critical cross-section decreases significantly, which in turn increases the bending resistance of the filled monopile in comparison with an empty monopile. The effect of the sand-fill on the static displacement has been done by modeling the monopile in Plaxis 3D, a finite element software specializing in the modeling of the soil. The effect of sand-fill appears to be more significant for lower static loads. As the static loads increase, the sand-fill reaches its' plastic region and its effect on the bending stiffness on the composite section is limited. The effect of sand-fill on the fundamental natural frequency of the structure was estimated analytically by using the approximate normal modes obtained by the Euler Bernoulli beam equations and numerically, using the finite difference method to model the structure. The results of the analysis have shown that the total effect of the sand-fill on the natural frequency of the structure is negative, and sand-fill should be applied only in cases when a decrease of the natural frequency of an existing structure is required. The effect of sand-fill on the damping ratio of the structure has been performed through Free Vibration Tests which have been simulated in Plaxis 3D. The hysteretic behavior of the sand-fill leads to an increase of the damping ratio of the structure. The beneficial effect of the sand-fill on the damping ratio increases as the initial displacement applied at the top of the structure increases.

Finally, a financial analysis was performed in order to identify the influence of sand-fill on the foundation cost. This additional cost sets the minimum threshold to be exceeded by the benefits to be obtained by the higher damping ratio, in order that the sand-fill can be applied as a financially feasible solution.

# Preface

This report is part of my Masters studies in Offshore & Dredging Engineering. The research which is presented has been performed under the support of a Witteveen+Bos, which was the sponsor company.

First of all, I would like to deeply thank Mr. Pim van der Male and Mr. Joost van der Meer, who trusted me and assigned to me this project and for their constant willingness to support me. Moreover, I would like to thank also my university supervisors, Mr. Frank Renting and Dr. Daan Schraven, who assisted me and shared their expertise on various aspects related to this topic. My supervisors' knowledge and their ability to guide me was vital in order to successfully complete this research project.

This thesis project was performed at Witteveen+Bos' offices in Rotterdam. At this point I would like express my gratitude to Mr. van der Meer, for providing to me a very pleasant working environment, and for ensuring that I will feel comfortable at the new working environment from the beginning. Along with Mr. van der Meer, I would also like to thank all my colleagues at the geotechnical department of Witteveen+Bos, who made me feel as part of their team, and for their willingness to share their knowledge with me. I would also like to thank Prof. A. Metrikine, for his guidance on my project, but also for being the academic who instilled to me significant knowledge in structural dynamics.

Finally, I would like to thank my family for their constant support and encouragement. I also want to thank Cristina, who is by my side and she has always patiently supported me to help me fulfill my goals.

Panteleimon Rapis

Delft, October 2017

*Page intentionally left blank*

# Contents

<b>1. Introduction</b> .....	1
1.1 Foundation Options .....	2
1.2 Monopile Concept.....	3
1.3 Problem Statement .....	3
1.4 Loading Conditions for an Offshore WTG .....	3
1.5 Laterally Loaded Piles Behavior - Requirement of Vertical Stability.....	4
1.6 Natural Frequency of a Monopile .....	5
1.7 Maximum Amplitude of Response - Damping Ratio.....	6
1.8 Research Objectives .....	7
1.9 Methodology and Outline .....	8
<b>2. Site Description – Load Calculations</b> .....	9
2.1 Location.....	9
2.2 Turbine Characteristics .....	9
2.3 Environmental Conditions.....	10
2.3.1 Water Depth .....	10
2.3.2 Water levels .....	10
2.3.3 Currents .....	11
2.4 Extreme Value Analysis – Ultimate Limit State (ULS) .....	11
2.4.1 Extreme Water Depth.....	11
2.4.2 Extreme Wave Heights .....	11
2.4.3 Extreme Wind Speed .....	11
2.5 Significant Elevations .....	12
2.6 Further meteorological - Oceanographical parameters .....	15
2.6.1 Ice.....	15
2.6.2 Marine growth .....	15
2.6.3 Soil conditions.....	15
2.6.4 Scour .....	16
2.7 Natural Frequencies.....	16
2.8 Dimensions of Structural Parts of a Wind Turbine Foundation .....	16
2.9 Loads Acting on the Monopile .....	17
2.9.1 Hydrodynamic Loading .....	17
2.9.2 Total Loads Acting at Seabed Level.....	20

<b>3.</b>	<b>Section Classification – Local Buckling Check/Stress Check.....</b>	<b>21</b>
3.1	Section Classification.....	21
3.2	Composite Section Design Against Local Buckling .....	22
3.3	Design Loads at Pile Toe & Yield Stress Check .....	22
	3.3.1 Design Loads .....	22
	3.3.2 Yield Stress Check .....	23
3.4	Local Buckling Check – Combined Axial and Moment Check.....	23
3.5	Bending Moment Resistance & Ovalization for Empty Tubes .....	24
	3.5.1 Bending Moment Resistance.....	24
	3.5.2 Ovalization .....	25
3.6	Bending Moment Resistance & Ovalization for Sand-Filled Tubes.....	28
<b>4.</b>	<b>Effect of Sand-Fill on the Response of the Monopile to a Static Loading .....</b>	<b>31</b>
4.1	Validation of the Model .....	31
4.2	Model for the p-y curves – Upwind report .....	35
4.3	Effect of the Sand-fill on the Displacement of the Pile.....	36
<b>5.</b>	<b>Effect of Sand-Fill on the Natural Frequency of the Structure .....</b>	<b>43</b>
5.1	Finite Difference Method – Model A .....	43
	5.1.1 Model Validation .....	43
	5.1.2 Sand-Fill Effect & Sensitivity Analysis .....	46
	5.1.3 Natural Frequency Variation with Sand-fill .....	47
	5.1.4 Natural Frequency Variation with the Contribution of Sand-fill in the Bending Stiffness .....	48
	5.1.5 Natural Frequency Variation with Monopile’s Bending Stiffness ( $EI_{mp}$ ) .	49
	5.1.6 Natural Frequency Variation with Tower’s Bending Stiffness ( $EI_{tower}$ )....	50
	5.1.7 Natural Frequency Variation with Monopile & Tower Mass.....	51
	5.1.8 Natural Frequency Variation with Unit Weight of filling .....	53
5.2	Finite Difference Method – Model B .....	56
	5.2.1 Natural Frequency Variation with Monopile’s Bending Stiffness ( $EI_{mp}$ ) and Mass .....	57
5.3	Normal Modes of a Clamped-Free Beam – Model A .....	58
	5.3.1 Sensitivity Analysis - Upwind Report Support Structure (varying cross-section along the length).....	64
	5.3.2 Required Minimum Stiffness and Maximum Added Mass to Increase the Natural Frequency by 1 – 10%.....	67
5.4	Normal Modes of a Free-Free Beam – Model B .....	72



5.4.1	Sensitivity Analysis - Upwind Report Support Structure (varying cross-section along the length) .....	77
5.4.2	Required Minimum Stiffness and Maximum Added Mass to Increase the Natural Frequency by 1 – 10%.....	80
<b>6.</b>	<b>Effect of the Sand-fill on the Damping Ratio.....</b>	<b>85</b>
6.1	Estimation of the Damping Ratio of a monopile.....	85
6.1.1	Logarithmic Decrement Method .....	85
6.2	Components of Damping for an Offshore Monopile .....	86
6.3	Soil Damping .....	87
6.4	Parameters Affecting Shear Strength-Strain Relation .....	88
6.4.1	Effect of Shear Strain Amplitude .....	89
6.4.2	Effect of Effective Confining Pressure .....	90
6.4.3	Effect of Soil Type & Plasticity Index .....	91
6.4.4	Effect of Number of Cycles .....	92
6.4.5	Effect of the Frequency of Excitation .....	94
6.5	Model in Plaxis 3D for Free Vibration Analysis .....	94
6.5.1	Modelling the Structural Elements.....	94
6.5.2	Modelling the Soil.....	96
6.5.3	Model Size .....	100
6.5.4	Optimization of the Model in Plaxis 3D.....	101
6.6	Methodology.....	105
6.7	Sensitivity Analysis .....	108
6.7.1	Effect of the Density of the Surrounding Soil & the Sand-Fill.....	108
6.7.2	Effect of the Level of Filling .....	113
6.7.3	Effect of the Magnitude of the Initial Displacement Imposed to the Structure .....	114
6.8	Modal Analysis of Forced Vibrations [30] .....	117
6.8.1	Theoretical Part .....	117
6.8.2	Analysis .....	119
6.9	Identification of Damping Coefficient Corresponding to the Sand-Fill (c)....	123
<b>7.</b>	<b>Opportunity Window for the application of Sand-Fill Technology in the North Sea &amp; Financial Analysis.....</b>	<b>125</b>
7.1	Introduction .....	125
7.2	Opportunity Window for the Application of the “Sand-Fill” Technique on Monopiles .....	125

7.2.1	WindEurope Report.....	126
7.2.2	EWEA Report .....	126
7.2.3	GWEC Report.....	127
7.2.4	IRENA Report.....	128
7.3	Exclusive Economic Zones.....	129
7.4	Data Collection & Methodology to Process the Data .....	130
7.4.1	Current Situation North Sea .....	130
7.4.2	Variation of Parameters for the Planned Projects.....	134
7.4.3	Comparison between Constructed and Planned Projects.....	137
7.5	Financial Analysis for the Sand-Filled Monopiles Technique – Case Study ..	142
7.5.1	Material Unit Costs related to the Support Structure (Monopile) .....	142
7.5.2	Transportation and Installation Costs .....	145
7.5.3	Installation Time Estimation for a Single Monopile .....	148
7.5.4	Sand-Fill Transportation and Installation Cost Case Study - “Icarus” Offshore Wind Farm .....	149
7.6	Conclusion.....	150
<b>8. Conclusions &amp; Recommendations for Future Work.....</b>		<b>153</b>
8.1	Research Objective 1: Effect of Sand-Fill on the Local Buckling Resistance .	153
8.2	Research Objective 2: Effect of Sand-Fill on the Response of the Monopile to a Static Loading .....	153
8.3	Research Objective 3: Effect of Sand-Fill on the Natural Frequency of the Structure .....	154
8.4	Research Objective 4: Effect of the Sand-fill on the Damping Ratio.....	156
8.5	Financial Analysis of the “Sand-Filled Monopiles” Technique .....	157
8.6	Recommendations for Future Research .....	158
<b>References .....</b>		<b>159</b>
<b>APPENDIX A: Vertical &amp; Horizontal Effective Stresses of the Sand-Fill.....</b>		<b>163</b>
<b>APPENDIX B: Natural Frequency Estimation (Analytical Solution) .....</b>		<b>164</b>
<b>APPENDIX C: Finite Difference Method .....</b>		<b>168</b>
<b>APPENDIX D: Approximate Modes – Sensitivity Analysis (Clamped-Free Beam) .....</b>		<b>176</b>
Sensitivity Analysis .....		182
<b>APPENDIX E: Approximate Modes – Sensitivity Analysis (Free-Free Beam with Soil Springs) ...</b>		<b>185</b>
Sensitivity Analysis .....		192
<b>APPENDIX F: Effect of the Density of the Surrounding Soil &amp; the Sand-Fill.....</b>		<b>195</b>
<b>APPENDIX G: Modal Analysis – Frequency Response Functions .....</b>		<b>200</b>

## List of Figures

Figure 1.1: Cost Breakdown of an Offshore Wind Farm [1].....	2
Figure 1.2: Foundation Concepts for Various Water Depths [5] .....	2
Figure 1.3: Major Components of a Foundation on a Monopile .....	3
Figure 1.4: Kinematics of a Rigid (left) and a Flexible (right) Laterally Loaded Pile [7].....	4
Figure 1.5: Acceptable Aimed Frequencies for an Offshore Wind Turbine .....	5
Figure 1.6: Effect of Diameter, Thickness and Embedded Length Variation on the Natural Frequency of the Structure [10].....	6
Figure 1.7: DSDSS Device for Simple Shear Tests under Cyclic Loading [12] .....	7
Figure 2.1: Project Location [15].....	9
Figure 2.2: NREL 5 MW Turbine Side & Front View .....	10
Figure 2.3: 1P & 3P Frequencies Range .....	16
Figure 2.4: Formula to Calculate $C_{Ds}$ .....	17
Figure 2.5: Drag Force Representation .....	19
Figure 3.1: Loads Acting on Pile Toe .....	22
Figure 3.2: Change of Radius due to Ovalization [21].....	26
Figure 3.3: Bending Resistance Variation with Sand-Fill's Young Modulus .....	30
Figure 4.1: Soil Characteristics – Dense Sand .....	31
Figure 4.2: Soil Parameters – Hardening Soil Model .....	32
Figure 4.3: Monopile Material Parameters .....	32
Figure 4.4: Creation of Rahman & Achmus' Model in Plaxis .....	33
Figure 4.5: Displacement of Pile on the Seabed Level for Various Loadings [14].....	33
Figure 4.6: Correlation between Abaqus and Plaxis 3D Results .....	33
Figure 4.7: Model used in the Convergence Test to Allocate the Optimal Distance of the Boundaries .....	34
Figure 4.8: Convergence Test (Displacement vs. Boundaries Distance) .....	34
Figure 4.9: p-y Curve at Seabed Level (Rahman & Achmus).....	35
Figure 4.10: p-y Curves at Seabed Level – Upwind Report's Monopile.....	36
Figure 4.11: Empty Pile Model in Plaxis.....	36
Figure 4.12: Sand-Filled Pile Model in Plaxis .....	37
Figure 4.13: Parameters used to Model the Sand-Fill in Plaxis (1) .....	37
Figure 4.14: Parameters used to Model the Sand-Fill in Plaxis (26) .....	37
Figure 4.15: Phases to Calculate the Displacement of the Monopile for varying Lateral Loads .....	38

Figure 4.16: : P-Y curves at Seabed Level (Empty vs. Sand-Filled Monopile) .....	38
Figure 4.17: Percentage Decrease of Displacement .....	39
Figure 4.18: Points of Displacement A & B .....	40
Figure 4.19: Displacement at the Top of the Monopile – Empty Monopile .....	40
Figure 4.20: Displacement at the Top of the Monopile – Sand-Filled Monopile.....	40
Figure 5.1: Natural Frequency – Analytical Calculation vs. Matlab .....	44
Figure 5.2: Model Elevation for Dynamic Analysis .....	45
Figure 5.3: Graphic Representation of all the Parts of the Structure and their Elevations .....	46
Figure 5.4: Natural Frequency Variation with Sand-fill’s Young Modulus.....	48
Figure 5.5: Natural Frequency Variation with % Contribution of Sand in EI.....	49
Figure 5.6: Natural Frequency Variation with EI monopile .....	50
Figure 5.7: Natural Frequency Variation with EI Tower.....	50
Figure 5.8: Variation of Natural frequency with Upper Pile’s Mass .....	52
Figure 5.9: Variation of Natural frequency with Tower’s Mass.....	53
Figure 5.10: Variation of Natural Frequency with Filling’s Young Modulus .....	54
Figure 5.11: Variation of Natural Frequency with Filling’s Young Modulus .....	55
Figure 5.12: Variation of Natural Frequency with Filling’s Young Modulus .....	55
Figure 5.13: Variation of Natural Frequency with Filling’s Young Modulus .....	56
Figure 5.14: Normalized Natural Frequency variation with the Flexural Stiffness of the Upper Pile..	57
Figure 5.15: Normalized Natural Frequency variation with the Mass of the Upper Pile.....	58
Figure 5.16: Clamped-Free Beam .....	58
Figure 5.17: 1 <sup>st</sup> Normal Mode.....	60
Figure 5.18: 2 <sup>nd</sup> Normal Mode .....	60
Figure 5.19: 3 <sup>rd</sup> Normal Mode .....	60
Figure 5.20: Modal Stiffness Matrix.....	61
Figure 5.21: Modal Mass Matrix.....	62
Figure 5.22: Natural Frequencies (rad/sec) .....	62
Figure 5.23: Natural Frequencies Hz.....	62
Figure 5.24: Exact Natural Frequencies – Finite Difference Method.....	62
Figure 5.25: Modal Stiffness Matrix Figure.....	63
Figure 5.26: Modal Mass Matrix.....	63
Figure 5.27: Natural Frequencies (rad/sec) .....	63
Figure 5.28: Natural Frequencies (Hz) .....	64
Figure 5.29: Natural Frequencies (FDM –Hz).....	64
Figure 5.30: Support Structure with variable Mass & Stiffness of the Upper Monopile .....	65
Figure 5.31: Modal Mass Matrix Upwind .....	65
Figure 5.32: Modal Stiffness Matrix Upwind .....	65

Figure 5.33: Natural Frequencies (Normal Modes) .....	65
Figure 5.34: Exact Natural Frequencies (FDM) .....	66
Figure 5.35: Effect of added mass on the 1 <sup>st</sup> Natural Frequency .....	66
Figure 5.36: Effect of increased bending stiffness on the 1 <sup>st</sup> Natural Frequency .....	66
Figure 5.37: Increase of 1 <sup>st</sup> Natural Frequency for an increase of EI of the Upper Monopile by 1-100% .....	67
Figure 5.38: Interaction Diagram .....	68
Figure 5.39: Required Minimum Bending Stiffness and Maximum Mass for varying Increase of the Natural Frequency .....	68
Figure 5.40: Required Added Bending Stiffness and Maximum Added Mass for varying Increase of the Natural Frequency .....	69
Figure 5.41: Required Bending Stiffness Increase for $\rho = 500 \text{ kg/m}^3$ .....	69
Figure 5.42: Required Bending Stiffness Increase for $\rho = 1000 \text{ kg/m}^3$ .....	70
Figure 5.43: Required Bending Stiffness Increase for $\rho = 1500 \text{ kg/m}^3$ .....	70
Figure 5.44: Required Bending Stiffness Increase for $\rho = 2000 \text{ kg/m}^3$ .....	71
Figure 5.45: Required Bending Stiffness Increase for $\rho = 2500 \text{ kg/m}^3$ .....	71
Figure 5.46: Minimum Young Modulus required for the Filling Bending Modes of Free-Free Beam – Model A .....	72
Figure 5.47: Free-Free Beam with Soil Springs .....	72
Figure 5.48: 1 <sup>st</sup> Normal Mode .....	74
Figure 5.49: 2 <sup>nd</sup> Normal Mode .....	74
Figure 5.50: 3 <sup>rd</sup> Normal Mode .....	75
Figure 5.51: Natural Frequencies (rad/sec) .....	76
Figure 5.52: Natural Frequencies Hz .....	76
Figure 5.53: Natural Frequencies (rad/sec) .....	77
Figure 5.54: Natural Frequencies (Hz) .....	77
Figure 5.55: Natural Frequencies (FDM – Hz) .....	77
Figure 5.56: Modal Mass Matrix Upwind .....	78
Figure 5.57: Modal Stiffness Matrix Upwind .....	78
Figure 5.58: Natural Frequencies (Normal Modes) .....	78
Figure 5.59: Exact Natural Frequencies (FDM) .....	78
Figure 5.60: Effect of added mass on the 1 <sup>st</sup> Natural Frequency .....	79
Figure 5.61: Effect of increased bending stiffness on the 1 <sup>st</sup> Natural Frequency .....	79
Figure 5.62: Increase of 1 <sup>st</sup> Natural Frequency for an increase of EI of the Upper Monopile by 1-100% .....	80
Figure 5.63: Interaction Diagram .....	80
Figure 5.64: Required Added Bending Stiffness and Maximum Added Mass for varying Increase of the Natural Frequency .....	81
Figure 5.65: Required Added Bending Stiffness and Maximum Added Mass for varying Increase of the Natural Frequency .....	81

Figure 5.66: Required Bending Stiffness Increase for $\rho = 500 \text{ kg/m}^3$ .....	82
Figure 5.67: Required Bending Stiffness Increase for $\rho = 1000 \text{ kg/m}^3$ .....	82
Figure 6.1: Initial Displacement and Free Vibration Test [28] .....	85
Figure 6.2: Response of Damped Free Vibration .....	86
Figure 6.3: Potential Energy and Energy loss in a Hysteretic Loop.....	87
Figure 6.4: Potential Energy and Energy loss in a Hysteretic Loop.....	88
Figure 6.5: Typical Representation of Shear Strength and Damping Ratio Variation with Shear Strains [33] .....	88
Figure 6.6: Strain Dependent Behavior of Soil.....	89
Figure 6.7: Effect of Effective Confining Pressure for sands.....	90
Figure 6.8: Effective Confining Pressure Effect on Toyoura (silica) Sand (Oztoprak) .....	91
Figure 6.9: Effect of Confining Pressure on Sand.....	91
Figure 6.10: Effect of the Soil Type on the Normalized Shear Strength (Darendeli) .....	91
Figure 6.11: Effect Of Soil Plasticity on the Normalized Shear Modulus and Material Damping (Left-Vucetic, Right-Ishibashi) .....	92
Figure 6.12: Effect of Number of Cycles in Normalized Shear Strength and Damping (%).....	92
Figure 6.13: Effect of Cycles in Shear Strength and Material Damping of Toyoura Sand (Lanzo) [37] 93	
Figure 6.14: Effect of Number of Loading Cycles on Shear Stress [38].....	93
Figure 6.15: Effect of Loading Frequency on Shear Strength & Damping Ratio for Sand and Clay (32) .....	94
Figure 6.16: Effect of Frequency of Excitation on Shear Strength And Damping Ratio (Stokoe) .....	94
Figure 6.17: Model Created in Plaxis using Symmetry .....	95
Figure 6.18: Shear Strength/Strain Reduction Curve.....	97
Figure 6.19: Values of A, B and n for Empirical Formula .....	98
Figure 6.20: Normalized Shear Modulus variation with Strain (Toyourea Sand) .....	98
Figure 6.21: Normalized Shear Strength and Damping Curves Plaxis 3D .....	99
Figure 6.22: Various Mesh Settings Tested. From Top Left to Bottom Right: Very Coarse, Medium, Very Fine, Very Fine (Enhanced Element Size on Sand-Fill), Very Fine (Further Enhanced Element Size on Sand-Fill), Very Fine (Enhanced Element Size on Sand-Fill and around the Monopile).....	102
Figure 6.23: Variation of Natural Frequency & Damping Ratio with Mesh .....	103
Figure 6.24: Effect of Locally Enhanced Mesh on Natural Frequency & Damping Ratio .....	103
Figure 6.25: Very Fine Mesh – Enhanced Elements in Sand-Fill and Soil Surrounding the Monopile .....	104
Figure 6.26: Effect of Locally Enhanced Mesh (Sand-Fill & Monopile) on the Natural Frequency & Damping Ratio .....	104
Figure 6.27: Response of a Sand-Filled and an Empty Monopile .....	105
Figure 6.28: Example of Mismatch (Plaxis vs. Analytical Solution).....	107
Figure 6.29: Mismatch of an Exponent with Constant Value on Both Sides of the Peak Responses	108
Figure 6.30: Comparison of the Response of a Filled Monopile Embedded in Loose Soil (all Densities of Sand-Fill) with a Monopile Embedded in Dense Soil.....	109

Figure 6.31: Required Added Rayleigh Damping for Soil .....	110
Figure 6.32: Horizontal Displacement on Seabed Level – Empty (Left) & Filled (Right) .....	111
Figure 6.33: Horizontal Displacement Along the Monopile Sides (Dense Sand) .....	111
Figure 6.34: Horizontal Displacement Along the Monopile Sides (Medium Density Sand): .....	112
Figure 6.35: Horizontal Displacement Along the Monopile Sides (Loose Sand) .....	112
Figure 6.36: Variation of the Inclination of the Relative Displacement with the Density of the Surrounding Soil .....	113
Figure 6.37: Comparison of the Response of a Partially Filled with an Empty Monopile Embedded in Loose Soil .....	114
Figure 6.38: Comparison of the Response of a Fully Filled Monopile for Varying Amplitude of Initial Displacement .....	115
Figure 6.39: Variation of Natural Frequency with Initial Displacement .....	116
Figure 6.40: Variation of Damping Ratio with Initial Displacement .....	116
Figure 6.41: Point of Application of the Harmonic Load .....	120
Figure 6.42: Normal Modes calculated using Modal Displacement (Left) and with Modal FRF (Right) .....	120
Figure 6.43: FRF for varying Frequency of Excitation .....	121
Figure 6.44: Real Frequency Response Function in Relation with the Frequency of the Excitation ..	122
Figure 6.45: Displacement of each Part of the Structure for Varying Frequency of Excitation – (Left Empty – Right Filled).....	122
Figure 6.46: Maximum Displacement of each Element of the Structure –2 <sup>nt</sup> Mode.....	123
Figure 7.1: Current Situation of Offshore Installations in EU (2016) [48].....	126
Figure 7.2: Forecast Offshore Wind Energy Developments each Year between 2017 - 2020 [47] ..	126
Figure 7.3: Current Situation per Country (2015) [50] .....	126
Figure 7.4: Forecast Offshore/Onshore Wind Energy Developments on 2020 [51].....	127
Figure 7.5: Offshore Wind Energy Target per Country [51].....	127
Figure 7.6: Current Situation Offshore Wind Developments (2016) [52] .....	127
Figure 7.7: Forecasted Offshore/Onshore Wind Energy Developments on 2020 [52] .....	128
Figure 7.8: Forecast Offshore Wind Energy Developments on 2045 [53] .....	128
Figure 7.9: Forecasted Trend in the Offshore Wind Energy Market [53] .....	129
Figure 7.10: Borders of Area of Interest & EEZ ( <a href="https://upload.wikimedia.org">https://upload.wikimedia.org</a> ) .....	130
Figure 7.11: Current Installed Capacity (Offshore Wind) per Country.....	131
Figure 7.12: Average Turbine Capacity per Country.....	132
Figure 7.13: Mean Water Depth of Developed Fields per Country .....	132
Figure 7.14: Number of Monopiles Installed per Country.....	133
Figure 7.15: Average Total Length of Monopiles Installed in each Country.....	133
Figure 7.16: Planned to be in Installed Total Capacity per Country .....	134
Figure 7.17: Forecasted Installed Capacity per Country.....	135
Figure 7.18: Future Trend for Average Capacity per Wind Generator (Offshore) .....	136

Figure 7.19: Average Water Depth for Projects to be Developed per Country .....	136
Figure 7.20: Total Number of Monopiles to be Installed per Country .....	137
Figure 7.21: Total Length of Monopiles to be Installed per Country.....	137
Figure 7.22: Current vs. Planned Capacity Installed .....	138
Figure 7.23: Average Capacity per Turbine per Country .....	138
Figure 7.24: Average Water Depth of Current / Planned Projects per Country .....	139
Figure 7.25: Total Number of Monopiles Constructed and Forecasted per Country .....	139
Figure 7.26: : Total Length of Monopiles to be Installed per Country.....	140
Figure 7.27: Approximated Cost / MW for an Offshore Wind Turbine in the Netherlands (2014) [10] .....	142
Figure 7.28: Cost of Steel / Monopile / Country.....	144
Figure 7.29: Cost of Sand / Fully Filled Monopile / Country .....	144
Figure 7.30: Percentage Increase in the Material Cost due to Sand-Fill / Country .....	145
Figure 7.31: Flow Chart Describing the Transportation & Installation Process with a Jack-Up Vessel .....	145
Figure 7.32: Expected installation time for wind generators of 2.5 – 8 MW.....	146
Figure 7.33: Transportation from the port to the jack-up structure procedure.....	146
Figure 7.34: Conveyor Belt to Install Soil Offshore.....	147
Figure 7. 35: Indicative Mobilization Costs and Day Rates (Netherlands, 2002) .....	147
Figure 7.36: Average Load, Installation and Movement Time for Jack-Up Vessel.....	148
Figure 7.37: Percentage Increase of Cost / Monopile / Country due to Sand-Fill .....	150
Figure 8.1: Percentage Decrease of Displacement due to Sand-Fill for varying Lateral Loading .....	154



# List of Tables

Table 1. 1: Input Variables .....	5
Table 2.1: NREL Reference Wind Turbine Characteristics .....	9
Table 2.2: Measured Water Levels .....	10
Table 2.3: Measure Current Speed .....	11
Table 2.4: Extreme Wave Heights for Various Return Periods .....	11
Table 2.5: Conversion Factors for Averaging Values of Wind Speed .....	11
Table 2.6: Extreme Wind Speeds for Various Return Periods .....	12
Table 2.7: Input Parameters for Formula 2.6 .....	12
Table 2.8: Input Parametes for Formula 2.7 .....	13
Table 2.9: Load Combination for Extreme Value Analysis (DNV).....	13
Table 2.10: Updated Load Combination Table .....	13
Table 2.11: Input Parameters for Each Load Combination.....	13
Table 2.12: Thickness of Marine Growth.....	15
Table 2.13: Soil Profile .....	15
Table 2.14: Dimensions of Each Structural Part .....	16
Table 2.15: Modified Drag & Inertia Coefficients .....	17
Table 2.16: 5 & 50-Year Waves & Current .....	18
Table 2.17: Hydrodynamic Loads (Factored) .....	18
Table 2.18: Moments due to the Hydrodynamic Loading (Factored).....	18
Table 2.19: Distributed Load on the Tower due to the Drag Force (un-factored).....	19
Table 2.20: Loads at the Seabed Level to the Drag Force (factored).....	19
Table 2.21: Moments at the Seabed Level to the Drag Force (factored) .....	20
Table 2.22: Total Lateral Loading Acting on Seabed Level (factored).....	20
Table 2.23: Total Bending Moments on Seabed Level (factored) .....	20
Table 3.1: Steel Young Modulus variation with Thickness ( <a href="http://www.steelconstruction.info">www.steelconstruction.info</a> ) .....	21
Table 3.2: Classification of Circular Hollow Sections .....	21
Table 3.3: Input Parameters for Classification Check .....	22
Table 3.4: Axial Load due to Tower’s Self-Weight .....	23
Table 3.5: Axial Load due to Transition Piece’s Self-Weight.....	23
Table 3.6: Axial Load due to Monopile’s Self-Weight.....	23
Table 3.7: Maximum Allowable Diameter to Thickness Ratio to Avoid Local Buckling [3] .....	24
Table 3.8: Recommended values for Out-of-Roundness Tolerance .....	25
Table 3.9: Ovalization Formulas .....	25

Table 3.10: Inputs for Formulas.....	26
Table 3.11: Inputs for Formulas.....	27
Table 3.12: Plug Stiffness in Variation with Soil's Young Modulus .....	28
Table 3.13: Ovalization Variation for Filled Monopile .....	28
Table 3.14: Ovalized Section Radius Variation for Filled Monopile .....	29
Table 3.15: Deformation Variation with the Radius of the Ovalized Section for Filled Monopile.....	29
Table 3.16: Bending Moment Resistance Variation with Sand-Fill's Young Modulus .....	29
Table 5.1: Natural Frequency – Analytical Calculation vs. Matlab .....	44
Table 5.2: Mean Diameter & Thickness .....	45
Table 5.3: Natural Frequency Variation with Sand-fill's Young Modulus .....	47
Table 5.4: Natural Frequency Variation with % Contribution of Sand in EI.....	48
Table 5.5: Natural Frequency Variation with EI Upper Pile .....	49
Table 5.6: Natural Frequency Variation with EI Tower .....	50
Table 5.7: Inputs for Formula .....	52
Table 5.8: Variation of Natural frequency with Upper Pile's Mass.....	52
Table 5.9: Variation of Natural frequency with Tower's Mass .....	52
Table 5.10: Variation of Natural Frequency with Filling's Young Modulus.....	53
Table 5.11: Variation of Natural Frequency with Filling's Young Modulus.....	54
Table 5.12: Variation of Natural Frequency with Filling's Young Modulus.....	55
Table 5.13: Variation of Natural Frequency with Filling's Young Modulus.....	56
Table 5.14: Normalized Natural Frequency variation with the Flexural Stiffness of the Upper Pile ...	57
Table 5.15: Normalized Natural Frequency variation with the Mass of the Upper Pile .....	57
Table 6.1: Parameters which Affect Nonlinear Behavior of Soil and their Relative Importance.....	89
Table 6.2: Dimensions of Plate Elements .....	95
Table 6.3: Mean Effective Pressure [38].....	96
Table 6.4: Maximum Shear Modulus Toyoura Sand .....	98
Table 6.5: Input Parameters for Sand-Fill (Toyoura Sand) and Surrounding Soil (Typical Values: Very Dense Sand).....	99
Table 6.6: 1 <sup>st</sup> & 2 <sup>nd</sup> Fundamental Frequencies of Each Element .....	100
Table 6.7: Maximum Allowable Element Size for Each Layer .....	101
Table 6.8: Maximum Time Step & Minimum Number of Steps for Free Vibration Analysis .....	101
Table 6.9: Soil Properties for Sensitivity Analysis .....	106
Table 6.10: Effect of Sand-Fill on Natural Frequency and Damping Ratio.....	109
Table 6.11: Natural Frequency and Damping Ratio variation with Initial Displacement.....	116
Table 6.12: Natural Frequency & Damping variation with Initial Displacement (Filled & Empty Monopile) .....	117
Table 6.13: Natural Frequencies of the Structure (Hz) .....	120

Table 6.14: Equivalent Amplitude of the Harmonic Load .....	121
Table 6.15: Percentage Decrease of Top Mass Displacement for varying Loading .....	123
Table 7.1: Forecasts for the Developed Offshore Wind Capacity in the North Sea (2020) .....	134
Table 7.2: Wind Turbine and Minimum Tower Length Required .....	141
Table 7.3: Minimum Monopile Length and its Required Minimum Dimensions.....	141
Table 7.4: Area and Volume of the Upper Part of the Average Dimensions Monopile per Country.	141
Table 7.5: Cost / KW for the development of an offshore wind farm in the US [57] .....	142
Table 7.6: Mechanical Properties of S355 K2G3 Steel for Offshore Applications .....	143
Table 7.7: Expected Installation Time for Varying Wind Turbine Capacity [15] .....	146
Table 7.8: Present Value of the Cumulative Cost per Day for Transportation & Installation Vessels in the Netherlands.....	147
Table 7.9: Total Operational Time for a Jack-Up to Install a Monopile for each Country .....	148
Table 7.10: Total Transportation and Installation Cost per Monopile for each Country.....	149
Table 7.11: Total Cost of Sand Filling / Monopile for each country .....	149
Table 7.12: Percentage Increase of the Cost / Monopile for each Country due to the Sand-Fill .....	150
Table 8.1: Variation of Damping Ratio with the Presence of Sand-fill and the Density of Soil.....	156
Table 8.2: Natural Frequency and Damping Ratio variation with Initial Displacement.....	157

*Page intentionally left blank*

# 1. Introduction

During the last decades, the greenhouse effect with its subsequent impact on global warming has mobilized the citizens and the governments across the world to take actions to reduce CO<sub>2</sub> gas emissions. As a part of the aforementioned strategy, a goal has been set to reduce the usage of conventional energy sources, such as coal, for the energy production. In EU, a goal of generating 20% of the energy demands of the region by Renewable Energy Sources (RES) by the year 2020 has been established [1]. On the other hand, the growth on the human population and the constant economic development across the world, leads to an always increasing demand of energy. Therefore, the goal to reduce greenhouse gas emissions can only be achieved by introducing energy produced by renewable energy sources. One of the “most promising renewable energy sources” [2] is wind energy. Wind energy has many advantages, such as:

- It cannot be exhausted since the only required input for this type of energy is the wind
- Even though a wind turbine’s CO<sub>2</sub> footprint is not zero, wind energy’s effect on gas emissions is positive comparing to traditional sources of energy
- It can be generated locally, providing energy independency for the countries and supporting the local economy

Initially, wind energy generators were placed on the land. This decision led to a debate in the local societies. The main concerns of the societies with respect to wind energy are related to the noise disturbance and the landscape pollution, which subsequently has a negative effect on the value of the properties in the area. Offshore wind energy projects have been developed as an answer to these concerns, and also due to its advantages against the onshore option, which consist of [1]:

- The almost unlimited space available for the development of wind farms
- The higher wind speeds offshore, which leads to an increase in the energy production
- The lower wind turbulence and wind shear, as a result of the absence of obstacles

However, development of offshore wind farms has an increased cost comparing to developments onshore. Madabhushi et al [1] states, that the goal for the UK is to reduce the cost per unit of energy by 28.6% by the year 2020 in order to make the cost per MWh, comparable with the cost of other energy sources. The cost breakdown of an offshore wind farm is being shown in Figure 1.1.

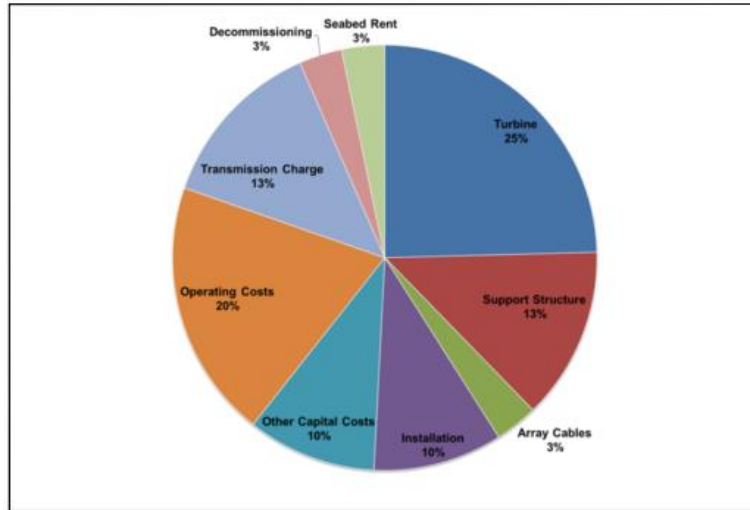


Figure 1.1: Cost Breakdown of an Offshore Wind Farm [1]

The foundation and installation cost combined is approximately equal to 27% of the total costs [3]. As shown in the figures above, reducing the foundation related costs can affect significantly the total cost.

## 1.1 Foundation Options

Foundation selection is primarily based on the water depth of the area under consideration. Foundation concepts and the corresponding depth limitations are being presented by Musial et al. [5] (Figure 1.2).

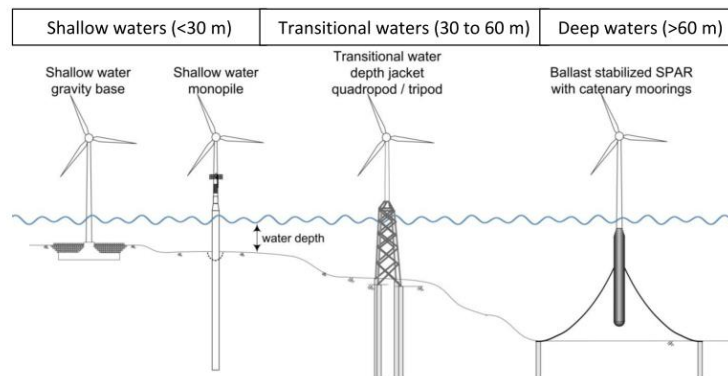


Figure 1.2: Foundation Concepts for Various Water Depths [5]

Despite the wide variety of foundation options, the most common foundation concept is the monopile. The monopile provides a technically and economically feasible solution for shallow water depths, like the average water depth near the coasts of the North Sea. This thesis project focuses entirely on the possibility to optimize the design of a monopile. The reference design of a monopile at shallow water (MSL=25m), as described in the Upwind report [6], will be used in this thesis project. The Upwind reference design is being widely used by researchers in order to calibrate the models and validate the results of their analyses.

## 1.2 Monopile Concept

Upwind's reference monopile has an average diameter of 6.1 m and thickness of 0.08 m [6]. Those dimensions are indicative for a monopile which can be used as a foundation for a medium/high capacity wind energy generator. The monopiles are usually applied on water depths of maximum 30 meters, therefore, their typical total length varies between 40 – 60 meters. On top of the monopile, the transition piece is being placed, using a grouted connection between the two parts. In Figure 1.3 more details of the major structural components and their relative position is being shown.

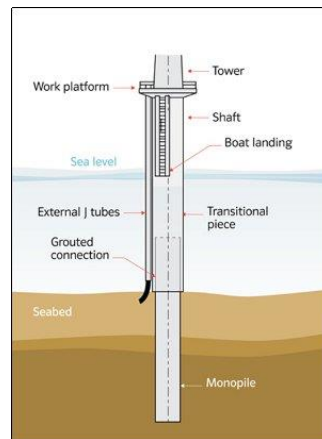


Figure 1.3: Major Components of a Foundation on a Monopile

The monopiles are usually driven into the soil (or drilled in very tough soils), having the embedded length required to provide the required stability to the structure.

## 1.3 Problem Statement

The need to significantly decrease the cost of the foundations, in order to reach the goal which is set for the overall cost reduction of the offshore wind farms, leads to the need to investigate alternative techniques in order to reduce the steel needed for the monopiles. Reducing the diameter/thickness of the monopile, can also positively affect the transportation and installation costs of the foundations. The main design requirements for the monopiles are being determined by the specific loading conditions applicable for a wind turbine generator at an offshore environment.

## 1.4 Loading Conditions for an Offshore WTG

There are significant differences between the offshore wind turbines and the oil & gas industry. The most important difference between those industries are:

- Ratio of horizontal to vertical loading is between 1.4 - 2.6 for the wind industry, whereas, in the oil and gas industry the vertical loading is approximately four times higher than the horizontal loading [2].
- Dynamic effects on the wind turbines are of high importance, because:
  - a) the dimensions of the structure are being mainly determined by the need to avoid resonance between the support structure's natural frequency and the rotor (1P), the blade (3P) the wind and wave loadings frequencies

- b) the fatigue damage to the structure determines its' design life. The fatigue damage depends on the number of cycles for various stress amplitudes which are being applied on the structure.

The differences of the monopile used in the wind energy and the piles used as foundations in the oil & gas industry, highlight also the main structural requirements for the monopiles, which are:

- The need to ensure the vertical stability of the laterally loaded pile, as well as, to reduce the maximum rotation of the monopile to ensure the optimal energy production
- The need to determine accurately the natural frequency of the structure, because a resonance would have a catastrophic effect on the structure
- The need to increase the period and/or reduce the amplitude of the response of the structure, by increasing the damping ratio of the structure

More details on each of the structural requirements for an offshore monopile are given in the following paragraphs.

## 1.5 Laterally Loaded Piles Behavior - Requirement of Vertical Stability

As explained above, monopiles function mainly as laterally loaded piles under cyclic loading. The magnitude of the shear force and the bending moment at the seabed level is high. For a typical wind turbine, the overturning moment in extreme conditions can reach up to 120 MNm [2]. Two failure mechanisms are common for laterally loaded piles, namely, the failure due to rigid or flexible pile behavior. The behavior of a pile as "rigid" or "flexible" is being determined by its' length to diameter ratio and by the relative stiffness between the monopile and the soil. The difference between the two failure mechanisms are shown schematically in Figure 1.4.

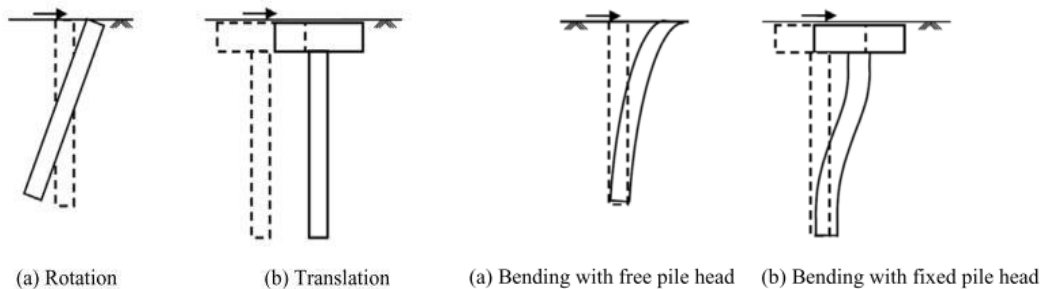


Figure 1.4: Kinematics of a Rigid (left) and a Flexible (right) Laterally Loaded Pile [7]

Tomlinson [8] suggests that a pile with length to diameter ratio of less than 10-12, behaves as a rigid pile. Poulos et al [9], suggests that the behavior of the monopile depends on its flexibility factor ( $k_R$ ). The flexibility factor is given by the formula 1.1:

$$k_R = \frac{E_p I_p}{E_s L^4} \quad (1.1)$$

The input variables are being presented in Table 1.1. The specific values used in this calculation are there calculation is being presented in Chapter 2.



$E_p$ : Young Modulus Pile (MPa)	$E_s$ : Young Modulus Dense Sand (MPa)	$I_p$ : 2 <sup>nd</sup> Moment of Area Pile (m <sup>4</sup> )	L: Embedded Length Pile (m)
210,000	65	6.855	24

Table 1. 1: Input Variables

Using these variables in Formula 1.1, it yields:

$$k_R \approx 0.067 > 0.01$$

which refers to a stiff pile, which is expected to behave similarly to a rigid pile. Poulos [9] has described the behavior of a pile according to Formula 1.1, using the following four categories:

- Very flexible piles ( $K_R < 10^{-5}$ )
- Flexible piles ( $K_R < 10^{-2}$ )
- Stiff piles ( $K_R > 10^{-2}$ )
- Perfectly stiff piles ( $K_R > 1$ )

According to Tomlinson [8], “at low loading the soil compresses elastically and the movement is sufficient to transfer some pressure from the pile to the soil at a greater depth”. Then, and as the magnitude of the loading increases, the soil yields plastically and again “transfer its’ load to greater depths”. A rigid pile rotates as the lateral load increases, mobilizing the passive stress of the soil at the head of the pile and at the toe of the pile (for the toe the plastic resistance of the soil is developed on the opposite side of the direction of loading). The stiff pile fails by rotation, which will take place “when the passive resistance of the head and toe are exceeded”. Since a “rigid pile” tends to rotate under the lateral load and the bending moment acting on it, reducing the angle of rotation could be beneficial for the stability of the structure, as well as, for the and the energy production of the system.

## 1.6 Natural Frequency of a Monopile

The initial dimensions of the monopile are being selected, such as to achieve a soft-stiff design for the structure.

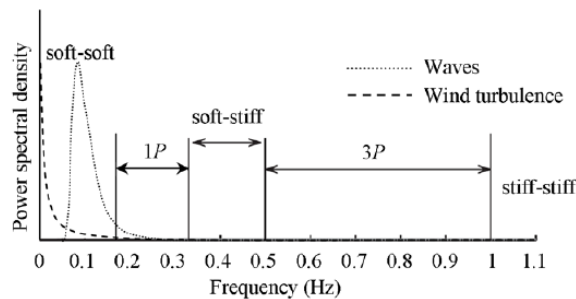


Figure 1.5: Acceptable Aimed Frequencies for an Offshore Wind Turbine

As shown in Figure 1.5, the soft-soft region needs to be avoided in the design, due to the high risk of resonance between the structure and the wind/wave loads. The stiff-stiff region could be chosen for a safe design, but it is usually avoided due to the high cost of the design. Therefore, the design usually aims for a structure with a natural frequency that falls in the soft-stiff region.

The effect of each of the main parameters which affect the natural frequency, namely the diameter, the thickness and the embedded length of the monopile on the natural frequency has been investigated by Arany et al. [10] (Figure 1.6).

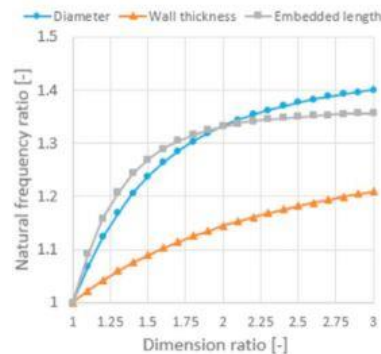


Figure 1.6: Effect of Diameter, Thickness and Embedded Length Variation on the Natural Frequency of the Structure [10]

In order to ensure the safety of the structure, usually the soft-stiff region is being reduced by increasing the upper rotor frequency limit (1P) and the minimum blade frequency limit (3P) by 10%. The fact that a resonance would lead to an almost certain collapse of the structure, signifies the importance of applying any techniques to achieve the minimum required natural frequency during the design phase and/or to adjust the natural frequency of an existing monopile.

## 1.7 Maximum Amplitude of Response - Damping Ratio

In the case than no damping effect was present in the system, any initial condition applied on the monopile (i.e. top mass displacement) would lead the monopile to vibrate infinitely at one of its' natural frequencies. However, in any system that exists in nature, some type of damping mechanism always acts and absorbs the energy of the system. More specifically, for offshore monopiles, the following damping mechanisms have been identified [11]:

1. Material Damping (Tower & Monopile)
2. Aerodynamic Damping
3. Hydrodynamic (viscous) Damping
4. Damping due to Wave Radiation
5. Soil Material Damping (hysteretic damping)
6. Soil Geometric Damping (radiation damping)

In the case of a stopped (parked) rotor, aerodynamic damping due to the rotor is not present in the system. In the case that no additional tuned mass damping system is installed on the tower, the most significant damping effect on the vibrations of the structure will be due to the soil related damping [11]. Lanzo et al. [12], has investigated the damping potential of the soil, after performing tests using a Double Specimen Direct Simple Shear (DSDSS) device (Figure 1.7) and analyzing the experimental results.

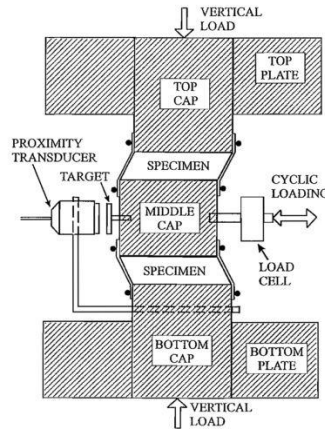


Figure 1.7: DSDSS Device for Simple Shear Tests under Cyclic Loading [12]

His research gave a better insight on the hysteretic damping mechanism of the soil. The increasing shear strains, lead to a significant reduction of the shear strength of the soil and the energy dissipation that is occurs in this mechanism adds damping (in hysteretic form) to the system as a whole. Introducing a new technique which could increase the damping ratio of the system could be highly beneficial for the monopile, since it would lead to a smaller amplitude and smaller number of loading cycles acting during the design on the monopile. This will lead to a smaller damage of the monopile due to fatigue and increase the lifetime of the structure.

## 1.8 Research Objectives

This thesis project investigates the possible positive effect of sand-fill on each of the structural requirements for the monopile, in order to reduce the foundation cost. The foundation cost could be affected positively directly or indirectly.

Directly, if the sand-fill:

- increases the resistance of the monopile against local buckling, reducing the steel demand for the monopile
- increases the stiffness of the structure, hence allows for the reduction of steel used for the monopile
- reduces the amplitude of the dynamic response or increases the damping ratio of the structure, which in turn could lead to lower maintenance costs and to an extension of the design life of the structure [1]

Indirectly, if the sand-fill has a positive effect on the static response of the monopile. This would lead to higher electricity production by reducing the maximum allowed displacement and rotation ( $<0.25^\circ$ ) at the mudline, as set by the operational requirements of the wind turbine manufacturers [13].

The possibility of improving each of the aforementioned attributes by adding sand in the monopile is the main research objective of this study. The effect of sand-fill on each of the four categories mentioned before, are the sub-objectives of the study.

## 1.9 Methodology and Outline

In order to investigate the effect of sand-fill each of the four categories mentioned in Paragraph 1.5, an equivalent number of chapters have been created.

Firstly, in chapter 2, the location and the environmental and site characteristics of the reference monopile (Upwind report) are being presented. The loads acting on the monopile are being calculated and a preliminary design is being performed.

In Chapter 3, a classification check along with the relevant yield stress and local buckling checks are being performed in order to ensure the static stability of the structure described in Upwind report.

In Chapter 4, the effect of the sand-fill on the horizontal displacement of the monopile is being calculated using Plaxis 3D. First, the model in Plaxis is getting validated using a reference model as described in the literature [14]. Also, a sensitivity analysis is being performed, in order to investigate the effect of sand-fill on the maximum displacement at the seabed level and at the top of the structure.

In Chapter 5, the natural frequency of the structure is being determined, using the Finite Difference Method to model all the parts of the structure along with the top mass, as described in the Upwind Report. Two models are being created using the fixity depth method and soil springs of constant stiffness. The cantilever beam model (fixity depth) is validated through simple hand calculations to calculate the natural frequency of a cantilever beam of a constant cross-section and through the analytical solution of the cantilever beam, using the approximate normal modes which are calculated for a beam with constant (average) area and stiffness. The model which includes the soil springs has been validated again through the approximate normal modes which are being calculated analytically, again for a beam with constant area and stiffness. After validating the models, a sensitivity analysis has been performed in order to identify the effect of sand-fill (or other materials) on the natural frequency of the structure. The sensitivity analysis has been performed using both the numerical and the analytical models.

In Chapter 6, the effect of the sand-fill on the damping ratio of the system has been examined using Plaxis 3D. A model which includes the hysteretic behavior of the sand-fill due to cyclic shear strains has been created and the damping ratio of the structure for an empty and filled monopile has been calculated using the exponential decrement method [11], after performing a free vibration test. The results have been compared and the difference in the damping is attributed to the sand-fill, since this is the presence of sand-fill is the only variable that changes between the empty and the filled-pile systems. Multiple sensitivity analyses have been performed, with parameters including the varying density of the surrounding soil, the varying density of the soil used a sand-fill and different magnitudes of initial displacement applied on the system.

In Chapter 7, the opportunity window for a new technology related to monopiles for the North Sea is being estimated. Then, the material, installation costs per monopile for the empty and the sand-filled monopile are being estimated. Finally, the added cost of placing sand-fill in the monopile is being estimated by performing a financial analysis of the costs related to the added sand.

In Chapter 8, the conclusions and recommendations for further research are being presented.

## 2. Site Description – Load Calculations

In this chapter, a brief description of the site conditions and the loads applied on the monopile under consideration is being presented. In the beginning, all the meteorological and site related parameters are being presented. In the last part of the chapter, the loads applied on the structure which correspond to the specific site conditions are being calculated.

### 2.1 Location

The design basis presented in [15] is based on a wind farm developed at a location in the Dutch North Sea. The climate information is obtained from the wave and wind data published by Rijkswaterstaat for the location “K13”. The coordinates of K13 are 53°13’04” north and 3°13’13” east, and the site has a water depth of 25 m.



Figure 2.1: Project Location [15]

### 2.2 Turbine Characteristics

The turbine that will be used for the design of the support structure will be UpWind report’s reference turbine [16], which is based on the NREL generic 5.0 MW turbine. The main characteristics of this wind turbine are shown in Table 2.1 and in Figure 2.2.

Rating	5 MW
Rotor Orientation, Configuration	Upwind, 3 Blades
Control	Variable Speed, Collective Pitch
Drivetrain	High Speed, Multiple-Stage Gearbox
Rotor, Hub Diameter	126 m, 3 m
Hub Height	90 m
Cut-In, Rated, Cut-Out Wind Speed	3 m/s, 11.4 m/s, 25 m/s
Cut-In, Rated Rotor Speed	6.9 rpm, 12.1 rpm
Rated Tip Speed	80 m/s
Overhang, Shaft Tilt, Precone	5 m, 5°, 2.5°
Rotor Mass	110,000 kg
Nacelle Mass	240,000 kg
Tower Mass	347,460 kg
Coordinate Location of Overall CM	(-0.2 m, 0.0 m, 64.0 m)

Table 2.1: NREL Reference Wind Turbine Characteristics

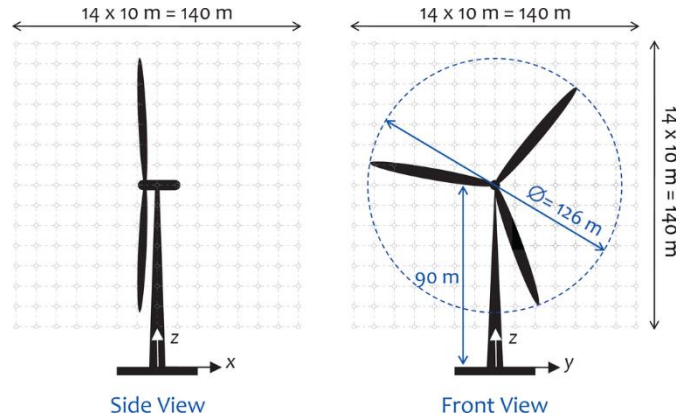


Figure 2.2: NREL 5 MW Turbine Side &amp; Front View

## 2.3 Environmental Conditions

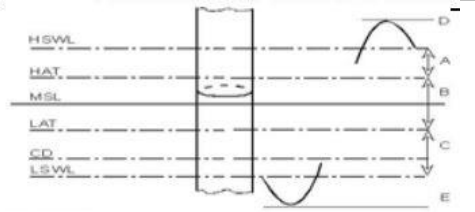
### 2.3.1 Water Depth

The water depth for the assumed wind park is 25 m. (Mean Sea Level (MSL)).

### 2.3.2 Water levels

Apart from the wind and wave measurements, there is also measured water level data and surge data available for the K13 site. The 50 year values for the minimum and maximum storm surge and for the tidal range have been calculated assuming that the extreme values of the aforementioned parameters follow the Gumbel distribution (Table 2.2).

<b>HSWL</b>	+ 3.29 m MSL
<b>HAT</b>	+ 1.16 m MSL
<b>MSL</b>	0 m
<b>LAT</b>	-1.06 m MSL
<b>LSWL</b>	-2.37 m MSL
<b>A</b>	+ 2.13 m MSL
<b>B</b>	2.22 m
<b>C</b>	-1.31 m MSL



HSWL highest still water level  
 HAT highest astronomical tide  
 MSL mean sea level  
 LAT lowest astronomical tide  
 CD chart datum (often equal to LAT)  
 LSWL lowest still water level  
 A positive storm surge  
 B tidal range  
 C negative storm surge  
 D maximum crest elevation  
 E minimum trough elevation

Table 2.2: Measured Water Levels

The splash zone has to be determined for later phase of the study. According to DNV the splash zone is determined as:

$$\text{Upper Limit: } SZ_U = HAT + 0.6 \cdot \left(\frac{1}{3}\right) \cdot H_{s,\max(100 \text{ years})} = 1.4 + 0.6 \cdot \left(\frac{1}{3}\right) \cdot 16.05 = +4.61 \text{ m MSL} \quad (2.1)$$

$$\text{Lower Limit: } SZ_L = LAT - 0.4 \cdot \left(\frac{1}{3}\right) \cdot H_{s,\max(100 \text{ years})} = -1.1 - 0.4 \cdot \left(\frac{1}{3}\right) \cdot 16.05 = -3.50 \text{ m MSL} \quad (2.2)$$

with,  $H_{s,max} = 16.05\text{m}$  [15]

### 2.3.3 Currents

Currents are considered to consist of sub surface currents, mainly driven by tide and wind generated near surface currents. The values for the currents are shown in Table 2.3.

Load situation	Current at MSL [m/s]
Normal current	0.6
Extreme current	1.2

Table 2.3: Measure Current Speed

## 2.4 Extreme Value Analysis – Ultimate Limit State (ULS)

For the extreme value analysis, the load combinations described in DNV [17] will be used. Based on the calculations in the previous paragraphs, and the given data for the return period of various wind speeds and wave heights, the following data will be used for the in order to calculate the load combinations which are needed.

### 2.4.1 Extreme Water Depth

The water depth with a return period of 50 years is required. The calculation is being done using Formula 2.3

$$Water\ depth_{50\ yrs} = LAT + \Delta z_{tide} + \Delta z_{surge} = 23.9 + 2.22 + 2.13 = 28.25 \quad (2.3)$$

### 2.4.2 Extreme Wave Heights

The extreme and significant wave heights for various return periods are shown in Table 2.4 [15]:

$T_{return}$ [yr]	$H_s$ [m]	$T_p$ [s]	$H_{max}$ [m]
1	6.05	10.12	11.25
5	6.95	10.54	12.93
10	7.34	10.69	13.65
50	8.24	10.97	15.33
100	8.63	11.05	16.05

Table 2.4: Extreme Wave Heights for Various Return Periods

### 2.4.3 Extreme Wind Speed

The wind speed distribution for the K13 site is given in [15]. The measured wind data first need to be translated from the reference height of 10 m to the hub height. A conversion factor of 0.9 [17] is used to obtain the 10-minute wind speed from the 1-hour average wind speed, as shown in Table 2.5.

Averaging Time	1 h	10 min	1 min	5 sec	3 sec
Factor	0.91	1.00	1.10	1.21	1.25

Table 2.5: Conversion Factors for Averaging Values of Wind Speed

The wind speed at the hub height will be calculated using the logarithmic law (for height up to 60m) and the power law for the wind speed at the height of the RNA. The formulas for both cases are:

$$U_{(60),50 \text{ yrs}} = U_{10} \cdot \frac{\ln\left(\frac{h}{z_0}\right)}{\ln\left(\frac{h_{ref}}{z_0}\right)} \quad (2.4)$$

And,

$$U_{(RNA),50 \text{ yrs}} = U_{60} \cdot \left(\frac{h}{h_{ref}}\right)^\alpha \quad (2.5)$$

where,  $\alpha = 0.11$  (offshore environment)

Table 2.6, shows the maximum wind speed at Upwind's Design Basis hub height (85.16m) as a function of the return period. The values averaged 10-min wind speeds, where the original 3-hrs stationary situations were converted with a factor 0.9 according to DNV [17].

$T_{return}$ [yr]	$V_w$ (10min) [m/s]
1	32.74
5	36.85
10	38.62
50	42.73
100	44.50

Table 2.6: Extreme Wind Speeds for Various Return Periods

## 2.5 Significant Elevations

The minimum required elevation for the transition piece and the hub height is being presented in this paragraph. These elevations are crucial in order to determine the hydrodynamic and aerodynamic loads on the structure.

$$Z_{interface} = LAT + Airgap + \Delta_{z,tide} + \Delta_{z,surge} + 1.86 \cdot H_{sig,50 \text{ yrs}} \cdot 0.65 \quad (2.6)$$

The input parameters for Formula 2.6 are being shown in Table 2.7.

LAT (m)	Airgap (m)	$\Delta_{z,tide}$ (m)	$\Delta_{z,surge}$ (m)	$H_{sig,50 \text{ yrs}}$ (m)
23.9	1.45	2.22	2.13	8.24

Table 2.7: Input Parameters for Formula 2.6

Also, a factor equal to 1.86 is being used to transform the significant wave height to the maximum wave height, and a factor equal to 0.65 is being used to calculate the wave elevation, assuming that the waves are not following completely the Airy Theory [17]. The elevation of the interface level is equal to:

$$Z_{interface} = 23.9 + 1.45 + 2.22 + 2.13 + 1.86 \cdot 8.24 \cdot 0.65 = 39.76 \text{ m}$$



The tower extends between the  $Z_{interface}$  and the hub Height. The interface is connected to the ground by the transition piece and the foundation pile. The hub height is being calculated as follows:

$$Z_{hub} = Z_{interface} + Safety\ Distance + \frac{D_{rotor}}{2} \quad (2.7)$$

The seabed is the reference point for the height calculated above. The input values for the Formula 2.7, are being shown in Table 2.8.

Safety Distance (m)	$D_{rotor}$ (m)
7.4	63

Table 2.8: Input Parametes for Formula 2.7

Therefore,

$$Z_{hub} = 39.76 + 7.4 + \frac{126}{2} = 110.2\ m$$

Having estimated the 5 and 50 -year values for the current, the waves and the wind speed and the water level which corresponds to a return period of 50 years, the load combination table has been created, as proposed by DNV [159].

		Environmental load type and return period to define characteristic value of corresponding load effect				
Limit state	Load combination	Wind	Waves	Current	Ice	Water level
ULS	1	50 years	5 years	5 years		50 years
	2	5 years	50 years	5 years		50 years
	3	5 years	5 years	50 years		50 years
	4	5 years		5 years	50 years	Mean water level
	5	50 years		5 years	50 years	Mean water level

Table 2.9: Load Combination for Extreme Value Analysis (DNV)

The maximum 5 and 50-year wind speed is higher than the cut-out speed of the NREL turbine, which is equal to 25m/sec. Therefore, a load combination including the cut-out speed of the turbine is included in this analysis, in order take into consideration also the thrust force on the rotor. Therefore, the load combination table will be adjusted to the following.

	Load Combination	Wind (m/sec)	Waves (m)	Current (m/sec)	Water Level (m)
ULS	I	50 years	5 years	5 years	50 years
	II	5 years	50 years	5 years	50 years
	III	Cut-Out	5 years	50 years	50 years

Table 2.10: Updated Load Combination Table

	Load Combination	Wind (m/sec)	Waves (m)	Current (m/sec)	Water Level (m)
ULS	I	42.73	12.93	0.6	33.29
	II	36.85	15.33	0.6	33.29
	III	25	12.93	1.2	33.29

Table 2.11: Input Parameters for Each Load Combination

*Page intentionally left blank*

## 2.6 Further meteorological - Oceanographical parameters

### 2.6.1 Ice

It is not likely that sea ice can occur in the specific site, therefore, ice-structure interaction is not considered in this analysis. However, an ice layer is expected to form around the part of the structure which is above the water level. The ice characteristic as described in [15] are:

- Atmospheric ice formation with a thickness of 30mm
- Ice formation due to sea water spray with a thickness of 100mm from MSL to HSWL
- Ice formation due to sea water spray from HSWL up to 60m above MSL with a thickness decreasing linearly to 30mm
- Density of ice of 900 kg/m<sup>3</sup>

### 2.6.2 Marine growth

For design purposes, a value for the marine growth around the monopile has to be estimated. 11 shows the thickness as determined according to DNV standard [17].

Level (m)]	Thickness (mm)
<b>MSL -2 to -40</b>	<b>100</b>

Table 2.12: Thickness of Marine Growth

### 2.6.3 Soil conditions

The hard soil profile as described in [15] is being assumed in this analysis. The profile characteristics are shown in Table 2.13.

Depths (m)	$\gamma'$ (N/m <sup>3</sup> )	$\Phi$ (°)
<b>0-3</b>	10000	38
<b>3-5</b>	10000	35
<b>5-7</b>	10000	38
<b>7-10</b>	10000	38
<b>10-15</b>	10000	42
<b>15-50</b>	10000	42.5

Table 2.13: Soil Profile

Where:

$\gamma'$ : effective soil unit weight

$\varphi$  : angle of internal friction

### 2.6.4 Scour

Scour protection is assumed in this report, therefore, the scouring effect is not included in the analysis.

## 2.7 Natural Frequencies

The fundamental natural frequency of the structure should be calibrated, in a way that it does not coincide with the main excitation frequencies of the structure. The main excitation frequencies during the rotor's operation are the 1P and the 3P frequencies. The 1P frequency is the range of frequencies of the rotor and the 3P frequency is the frequency of the blades and it is equal to the 1P frequency multiplied by three. The 1P and 3P frequencies refer to the excitation frequencies of the tower and the blades respectively. The values of the operating range of frequencies are being presented in [16]. The excitation frequencies of the wind and the waves are located below, or coincide, with the lower margin of the 1P frequency (Fig. 1.5). Taking into consideration that designing a structure with a natural frequency higher than the upper 3P frequency would lead to an expensive design, usually the target for the fundamental natural frequency is the soft-stiff region (Figure 2.3).

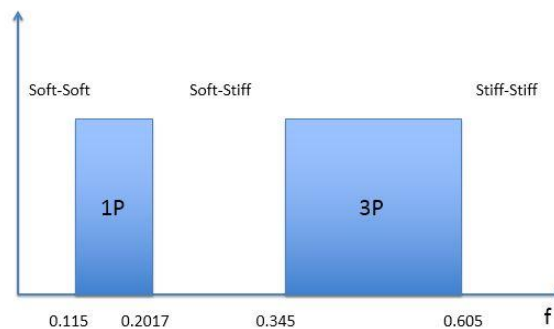


Figure 2.3: 1P & 3P Frequencies Range

## 2.8 Dimensions of Structural Parts of a Wind Turbine Foundation

In order to calculate the loads on the monopile, the dimensions given in the Upwind report's reference turbine will be used [15]. Since, in this report each structural member has a varying diameter, the average dimensions for each part will be evaluated. The average dimensions are shown in Table 2.14.

Part	Diameter (m)	Thickness (m)
Monopile	6.1	0.08
Transition Piece	5.65	0.06
Tower	4.85	0.03

Table 2.14: Dimensions of Each Structural Part

## 2.9 Loads Acting on the Monopile

### 2.9.1 Hydrodynamic Loading

For the calculation of the hydrodynamic loads, the Morrison equation was applied.

$$F = C_m \cdot \rho \cdot \frac{\pi}{4} \cdot D^2 \cdot \dot{u} + C_d \cdot \rho \cdot \frac{1}{2} \cdot D \cdot u \cdot |u| \quad (2.8)$$

To estimate if the Morrison load is drag or inertia dominated, the Keulegan-Carpenter number is being calculated. The KC formula is:

$$KC = \frac{2 \cdot \pi \cdot \zeta_\alpha}{D} \quad (2.9)$$

For the 5 and 50-year wave which are needed for the analysis, the formula yields:

- For the 5-year wave height = 12.93 m and D=6.1m,  $KC = 6.659 \Rightarrow 3 < KC < 15$ , which means that the force is neither Drag, nor inertia dominated.
- For the 50-year wave height = 15.33 m and D=6.1m,  $KC = 7.895 \Rightarrow 3 < KC < 15$ , which means that the force is neither Drag, nor inertia dominated.

Therefore, both the  $C_D$  and  $C_M$  coefficients are being calculated using the formula in Figure 2.4.

$$C_{Ds} = \begin{cases} 0.65 & \text{for } k/D < 10^{-4} \text{ (smooth)} \\ \frac{29 + 4 \log_{10}(k/D)}{20} & \text{for } 10^{-4} < k/D < 10^{-2} \\ 1.05 & \text{for } k/D > 10^{-2} \text{ (rough)} \end{cases}$$

Figure 2.4: Formula to Calculate  $C_{Ds}$

In order to include the diameter of the J-tubes ( $D_j$ ) and the boatlanding ( $D_{bl}$ ) in the total diameter which is affected by the hydrodynamic loading, the modified inertia ( $C_{M,mod}$ ) and drag ( $C_{D,mod}$ ) coefficients will be calculated according to the formulas.

$$C_{M,mod} = C_M \cdot \frac{D_{pile}^2 + D_j^2 + D_{bl}^2}{D_{pile}^2} \quad (2.10)$$

$$C_{D,mod} = C_D \cdot \frac{D_{pile} + D_j + D_{bl}}{D_{pile}} \quad (2.11)$$

The calculated coefficients are being shown in Table 2.15.

Wave Conditions	k	k/D	$C_{Ds}$	KC	$C_{M,mod}$	$C_{D,mod}$
5 - Year Wave (m)	0.02	0.00328	0.9307	6.659	1.855	0.791
50 - Year Wave (m)	0.02	0.00328	0.9307	7.895	1.80	0.778

Table 2.15: Modified Drag & Inertia Coefficients

The hydrodynamic loading will be calculated for all the 3 load combinations (Table 2.10) using the extreme values for the 5 and 50-year waves and current (Table 2.16).

<b>Hydrodynamic Loads</b>			
<b>5-Year Wave (m)</b>	<b>50-Year Wave (m)</b>	<b>5-Year Current (m/sec)</b>	<b>50-Year Current (m/sec)</b>
12.93	15.33	0.6	1.2

Table 2.16: 5 & 50-Year Waves & Current

The wave period according to DNV [17] is being calculated using the formula 2.11:

$$11.1 \cdot \sqrt{\frac{H_{S,NSS}(u_{10})}{g}} \leq T \leq 14.3 \cdot \sqrt{\frac{H_{S,NSS}(u_{10})}{g}} \quad (2.11)$$

Where,  $H_{S,NSS}(u_{10})$  is the significant wave height with a return period of 5 and 50 years, respectively.

- The 5-year significant wave height is equal to 6.95 m. Therefore:

$$9.3429 \leq T \leq 12.036$$

Since,  $T = 9.34$  is closer to the 1P natural frequency, this one will be chosen for the estimation of the hydrodynamic loads.

- The 50-year significant wave height is equal to 8.24 m. Therefore:

$$10.173 \leq T \leq 13.106$$

In order to calculate the extreme hydrodynamic loading, a specific value for the period needs to be chosen. For both the 5 and 50-year extreme wave conditions, the minimum frequency of the range corresponds to a frequency closer to the 1P frequency (Figure 2.3). Therefore, in both cases the smallest calculated frequency will be used in order to model the hydrodynamic loads of the waves. The hydrodynamic loads and moments calculated, multiplied with a safety factor equal to 1.35 [17], are being shown in Table 2.17 & Table 2.18.

<b>Hydrodynamic Loading</b>		<b>Force (kN)</b>
<b>5-Year Wave</b>	<b>5-Year Current</b>	5012
<b>5-Year Wave</b>	<b>50-Year Current</b>	5284
<b>50-Year Wave</b>	<b>5-Year Current</b>	6081

Table 2.17: Hydrodynamic Loads (Factored)

<b>Hydrodynamic Loading</b>		<b>Moments (kNm)</b>
<b>5-Year Wave</b>	<b>5-Year Current</b>	106770
<b>5-Year Wave</b>	<b>50-Year Current</b>	113766
<b>50-Year Wave</b>	<b>5-Year Current</b>	133889

Table 2.18: Moments due to the Hydrodynamic Loading (Factored)

### 2.9.1.1 Aerodynamic Loading

The aerodynamic loading consists of the thrust force acting on the rotor and the drag force which acts on the tower. The thrust force was calculated using a Matlab tool created in TUDelft and provided to the students attending the Wind Farm Design course (0E5662). The thrust force was calculated only for the cut-out wind speed (25 m/sec), since during the 5 and 50-year wind speed the rotor will be in idle mode. For a wind speed of 25 m/sec, the thrust force is equal to 845.82 kN. All the forces will be multiplied by 1.35 as DNV suggests in order to calculate the design loads [17]. The factored thrust force is equal to 1141.857 kN.

The Drag Force on the tower will be calculated using the following formula:

$$F_{Drag} = \frac{1}{2} \cdot C_D \cdot \rho_{air} \cdot D \cdot U^2 \quad (2.12)$$

In order to calculate the drag force, the distributed force of triangular shape was applied to the pile, as shown in Figure 2.5.

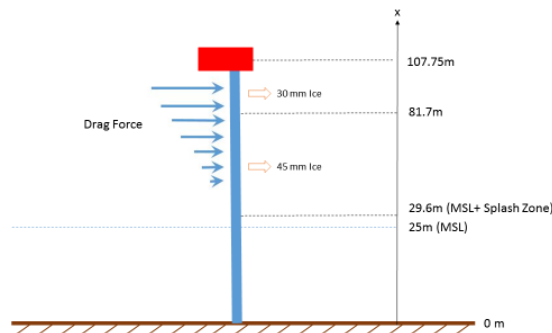


Figure 2.5: Drag Force Representation

The distributed load (non-factored) on the tower due to the drag force is shown in Table 2.19.

Wind Conditions	5-Year Wind Speed	50-Year Wind Speed	Cut-Out Wind Speed
Drag Load (kN/m)	4.83	6.49	2.22

Table 2.19: Distributed Load on the Tower due to the Drag Force (un-factored)

The resultant loads and moments on the seabed (factored), for each load case mentioned above, are being presented in the Table 2.20 and Table 2.21.

Load Case	Loads (kN)
5-year Wind Speed	254.781
50-year Wind Speed	342.577
Cut-out Wind Speed	1247.39

Table 2.20: Loads at the Seabed Level to the Drag Force (factored)

Load Case	Moments (kNm)
5-year Wind Speed	20818.16
50-year Wind Speed	27991.95
Cut-out Wind Speed	9581.81

Table 2.21: Moments at the Seabed Level to the Drag Force (factored)

## 2.9.2 Total Loads Acting at Seabed Level

The total loads and moments acting on the seabed level for each load case are being presented in Table 2.22 and Table 2.23.

FORCES	Load Combination	Forces due to Wind Loads (kN)	Forces due to Waves + Currents (kN)	Total Lateral Loads (kN)
ULS	I	342.6	5012.0	5354.6
	II	254.8	6081.0	6335.8
	III	1247.4	5284.0	6531.4

Table 2.22: Total Lateral Loading Acting on Seabed Level (factored)

Moments	Load Combination	Moment due to Wind Loads (kNm)	Moment due to Waves + Currents (kNm)	Total Moment (kNm)
ULS	I	27992.0	106770.0	134762.0
	II	20818.2	133889.0	154707.2
	III	106868.0	113766.0	220634.0

Table 2.23: Total Bending Moments on Seabed Level (factored)



### 3. Section Classification – Local Buckling Check/Stress Check

In this chapter a section classification check is being performed. Then a local buckling check is performed using CUE211 [21] guideline’s provisions. In this manner the effect of sand-fill on the ovalization and the local buckling of the section is being investigated, based on existing formulas in CUR211.

#### 3.1 Section Classification

The section classification is not expected to be influenced significantly by the presence of the sand-fill, due to the fact that the Young Modulus of the sand-fill is significantly lower than the steel’s Young’s Modulus. As Eurocode EN1993-1-1 [18] suggests, the yield stress of the cross-section is mainly affected by the thickness of the section, as shown in Table 3.1.

The variation of minimum yield strength (N/mm<sup>2</sup>) with thickness

Steel grade	Nominal thickness (mm)					
	≤ 16	> 16 ≤ 40	> 40 ≤ 63	> 63 ≤ 80	> 80 ≤ 100	> 100 ≤ 150
S275	275	265	255	245	235	225
S355	355	345	335	325	315	295
S420	420	400	390	370	360	340
S460	460	440	430	410	400	380

Table 3.1: Steel Young Modulus variation with Thickness ([www.steelconstruction.info](http://www.steelconstruction.info))

For a cross-section with a nominal thickness of 80 mm, the yield stress for S355 steel grade is equal to 315MPa. The section classification is being performed using the Table 3.2 of EN1993 [18]. A monopile for an offshore wind farm ideally should be designed using a cross-section which does not reach its’ plastic resistance. A Class 3 section can be chosen, which refers to cross-section which can develop their yield strength “but local buckling is liable to prevent development of the plastic moment resistance”. For a circular hollow section, the classification is being performed according to the table below.

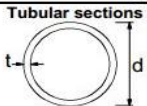
Tubular sections						
						
Class	Section in bending and/or compression					
1	$d/t \leq 50\epsilon^2$					
2	$d/t \leq 70\epsilon^2$					
3	$d/t \leq 90\epsilon^2$					
<b>NOTE</b> For $d/t > 90\epsilon^2$ see EN 1993-1-6.						
$\epsilon = \sqrt{235/f_y}$	$f_y$	235	275	355	420	460
	$\epsilon$	1,00	0,92	0,81	0,75	0,71
	$\epsilon^2$	1,00	0,85	0,66	0,56	0,51

Table 3.2: Classification of Circular Hollow Sections

The thickness of the monopile considered in Chapter 2 ( $t=0.08m$ ) was representing an average value. However, the monopile near the seabed level and until its’ toe has a constant thickness of 0.10m. The area near the seabed is more susceptible to local buckling [2], therefore the value of 0.10m. will be used for the thickness in the section classification and in the local buckling check. The values of the inputs needed to perform the cross-section classification are shown in Table 3.3.

D (m)	t (m)	f <sub>y</sub> (MPa)	ε	ε <sup>2</sup>	90ε <sup>2</sup>
6.1	0.1	315	0.850339	0.723077	65.07692

Table 3.3: Input Parameters for Classification Check

The cross-section is a Class 3 section, since  $\frac{d}{t} = 61 \leq 90 \cdot \epsilon^2 = 67.14$

### 3.2 Composite Section Design Against Local Buckling

Eurocode EN1994 [20] suggests two alternative methods in order to design composite steel and concrete structures. The simplified method can be used for columns of “doubly symmetric and uniform cross-section”, therefore this method could be followed for the design of the circular section of the monopile. As shown before, local buckling is not expected according to the local buckling check that EN1994 suggests. However, CUR211 [21], which in contrary with EN1994 provides specific guidelines for the design of empty and sand-filled piles against local buckling, suggests that the check presented in EN1994 is not valid. Since CUR211 provides specific formulas for sand-filled monopiles, the provisions of this guideline will be applied to check the combined effect of axial loads and moments, taking into consideration the local buckling effects. The biggest similarity between sand and concrete as structural materials, is their ability to withstand compressive loads. However, sand does not have the ability to develop any tensile stresses while concrete has a limited capacity against tensile loads. As far as the local buckling effects on the monopile are concerned, the sand is expected to support the section in order to prevent local buckling effects, and its influence will be investigated.

### 3.3 Design Loads at Pile Toe & Yield Stress Check

#### 3.3.1 Design Loads

The most critical section of the monopile is located just at the pile toe, because at this point the highest axial load and bending moments act. The levels of application for each type of application of environmental load is shown in the figure below.

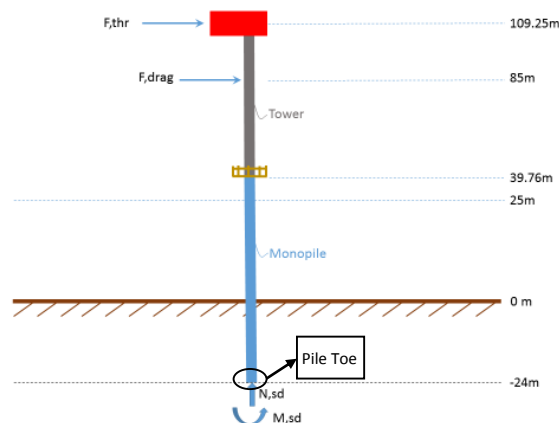


Figure 3.1: Loads Acting on Pile Toe

In order to calculate the axial loads acting at the pile toe of the monopile, the rotor/nacelle assembly mass and the geometrical characteristics of the tower and the monopile will be taken into consideration. The RNA has a total mass of 350 tonnes, which is equal to:

$$F_{RNA} = 350 \cdot 9.81 = 3433.5 \text{ kN} \quad (3.1)$$

In order to calculate the axial loads due to the self-weight of the tower, and taking into consideration the fact that all the structural elements have a variable cross-section along their length, the average value for the diameter and the thickness of each structural element will be used. Therefore, the cross-sections of the monopile, the transition piece and the tower are the same as presented in Table 3.4, Table 3.5, Table 3.6. The factored axial forces due to the tower and the monopile (as shown in Figure 3.1) are being shown in the tables below.

D (m)	t (m)	W <sub>el</sub> (m <sup>3</sup> )	W <sub>pl</sub> (m <sup>3</sup> )	A (m <sup>2</sup> )	E (MPa)	Length (m)	N <sub>sd</sub> (kN)
4.80	0.03	0.533	0.683	0.450	210000	69.250	2549.1

Table 3.4: Axial Load due to Tower's Self-Weight

D (m)	t (m)	W <sub>el</sub> (m <sup>3</sup> )	W <sub>pl</sub> (m <sup>3</sup> )	A (m <sup>2</sup> )	E (MPa)	Length (m)	N <sub>sd</sub> (kN)
5.65	0.06	1.457	1.875	1.054	210000	14.760	1269.8

Table 3.5: Axial Load due to Transition Piece's Self-Weight

D (m)	t (m)	W <sub>el</sub> (m <sup>3</sup> )	W <sub>pl</sub> (m <sup>3</sup> )	A (m <sup>2</sup> )	E (MPa)	Length (m)	N <sub>sd</sub> (kN)
6.10	0.10	2.782	3.600	1.885	210000	54.000	8487.6

Table 3.6: Axial Load due to Monopile's Self-Weight

Therefore, the total axial force at the fixity depth is equal to:

$$N_{sd} = F_{RNA} + F_{tower} + F_{TP} + F_{pile} = 15.77 \text{ MN} \quad (3.2)$$

The design moment at the pile toe is equal to:

$$M_{sd} = 6.53 \cdot 24 + 220.634 = 377.39 \text{ MNm} \quad (3.3)$$

### 3.3.2 Yield Stress Check

The yield stress check for a member under axial compression and bending moment is given in EN1993-1-3 [22]. The yield stress check for a section of Class 3 is being performed using the formula:

$$\frac{N}{A} + \frac{M}{W_{el}} \leq \frac{f_{yield}}{\gamma_{m0}} \quad (3.4)$$

$$\frac{15.77}{1.88} + \frac{377.39}{2.7819} \leq \frac{315}{1.1} \quad (3.5)$$

A safety factor ( $\gamma_{m0} = 1.1$ ) has been applied for a Class 3 steel section, as suggested by DNV [17].

### 3.4 Local Buckling Check – Combined Axial and Moment Check

Since the monopile has a “Class 3” cross-section, the possibility of failure due to local buckling is important to be investigated. EN1994 [20] suggests that the cross-section is not susceptible to

local buckling if the thickness of the section is bigger than 40 mm [23] and the limitations of the following table are being followed.

Table 6.3 : Maximum values  $(d/t)$ ,  $(h/t)$  and  $(b/t)$  with  $f_y$  in N/mm<sup>2</sup>

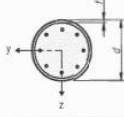
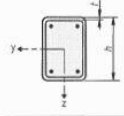
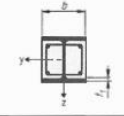
Cross-section	Max $(d/t)$ , max $(h/t)$ and max $(b/t)$
Circular hollow steel sections 	$\max (d/t) = 90 \sqrt{\frac{235}{f_y}}$
Rectangular hollow steel sections 	$\max (h/t) = 52 \sqrt{\frac{235}{f_y}}$
Partially encased I-sections 	$\max (b/t) = 44 \sqrt{\frac{235}{f_y}}$

Table 3 7: Maximum Allowable Diameter to Thickness Ratio to Avoid Local Buckling [3]

As shown before, the effects of local buckling can be neglected, since the section has a thickness equal to 0.10m and the ratio between the diameter and the thickness does not exceed the requirement for the circular section as shown in Table 3 7. As mentioned before, and to achieve a conservative design, the provisions of CUR211E will be applied in order to include the local buckling effect in the design of the section against combined axial loads and moments.

### 3.5 Bending Moment Resistance & Ovalization for Empty Tubes

In order to evaluate the effect of sand-fill on the ovalization of the monopile, which in turn affects its' bending moment resistance, the methodology described in CUR211E [21] and in EN1993-4-3 [24] is being followed. An empty monopile embedded in soil is filled with sand up to the sand plug level. The sand plugging occurs at a distance of about half pile diameter below the seabed, for a pile with a diameter bigger than 3m [19]. Therefore, the beneficial effect of sand fill on the reduction of the ovalization will be examined at this level, since at the distance between the plug level and the pile toe, the monopile is always filled with soil.

#### 3.5.1 Bending Moment Resistance

$$\text{For } \frac{D}{t} = \frac{6.1}{0.1} = 61 \leq 120 \Rightarrow$$

$$\varepsilon_{crit} = 0.25 \cdot \frac{t}{r} - 0.0025 = 0.005697 \quad (3.6)$$

$$\mu = \frac{\varepsilon_{crit}}{\varepsilon_{y,steel}} = \frac{0.005697}{0.002} = 2.848 > 1 \quad (3.7)$$

$$\sin(\theta) = \frac{1}{\mu}, \text{ for } \mu > 1 \quad (3.8)$$

$$\Rightarrow \theta = 0.3587 \text{ rad}$$

Bending moment as a function of plasticity (for  $\mu > 1$ ) is equal to:

$$M_R = \frac{1}{2} \cdot \left( \frac{\theta}{\sin(\theta)} + \cos(\theta) \right) \cdot M_{el,d} \quad (3.9)$$

The elastic resistance ( $M_{el,d}$ ) was chosen since the monopile has a Class 3 section.

where,

$$M_{el,d} = \frac{\pi \cdot D^2 \cdot t \cdot f_y}{4} = 836.89 \text{ MNm} \quad (3.10)$$

So,  $M_R = 819.36 \text{ MNm}$

### 3.5.2 Ovalization

The ovalization of the monopile will be due to the following reasons:

- Initial out-of-roundness which is permitted in the production process of the pile
- Ovalization due to direct and indirect soil pressure
- Ovalization as a 2<sup>nd</sup> order effect due to bending

The out-of-roundness tolerance during the production of the pile for a “Class B High” with a diameter of 6.1m can be calculated using Table 3.8 [21].

Recommended value of $U_{r,max}$	$D \leq 0.50 \text{ m}$	$0.50 \text{ m} < D < 1.25 \text{ m}$	$1.25 \text{ m} \leq D$
Class A Excellent	0.014	$0.007 + 0.0093 (1.25 - D)$	0.007
Class B High	0.020	$0.010 + 0.0133 (1.25 - D)$	0.010
Class C Normal	0.030	$0.015 + 0.0200 (1.25 - D)$	0.015

Table 3.8: Recommended values for Out-of-Roundness Tolerance

The ovalization due to the imperfections during the production phase is equal to:

$$\alpha = \frac{1}{4} \cdot U_r \cdot D = \frac{1}{4} \cdot 0.010 \cdot 6.1 = 0.01525 \text{ m} \quad (3.11)$$

The ovalization due to the surrounding soil pressure is being calculated using Table 3.9.

Case with soil pressure from two opposite sides		
	$M_A = -\frac{1}{4}qr^2$	-0.2500
	$M_B = \frac{1}{4}qr^2$	0.2500
	$M_C = \frac{1}{4}qr^2$	0.2500
	$\Delta D_y = \frac{1}{6} \frac{qr^4}{EI}$	0.1667
	$\Delta D_z = -\frac{1}{6} \frac{qr^4}{EI}$	-0.1667

Table 3.9: Ovalization Formulas

The ovalization due to direct soil pressure is calculated using the formula 3.12 [24]:

$$\alpha_{qd} = \frac{k_{yd} \cdot \sigma_{xx,eff}^2 \cdot r^4}{EI_w} \quad (3.12)$$

and

$$EI_w = \frac{E_{steel} \cdot t^3}{12 \cdot (1 - \nu^2)} \quad (3.13)$$

The ovalization due to the indirect soil pressure is calculated using the formula 3.14:

$$\alpha_{qi} = \frac{0.5 \cdot k_{yi} \cdot \sigma_{xx,eff}^2 \cdot r^4}{EI_w} \quad (3.14)$$

The ovalization due to curvature is calculated using the formula 3.15:

$$\alpha_C = \frac{C^2 \cdot r^5}{t^2} \quad (3.15)$$

and,

$$C = \frac{M_{plug\ level}}{\pi \cdot E_{steel} \cdot r^3 \cdot t} \quad (3.16)$$

The inputs for the formulas are being presented in Table 3.10.

<b>E<sub>steel</sub></b> <b>(GPa)</b>	<b>v</b>	<b>t</b> <b>(m)</b>	<b>k<sub>yd</sub></b>	<b>k<sub>yi</sub></b>	<b>q<sub>i</sub></b> <b>(kPa)</b>	<b>r</b> <b>(m)</b>	<b>C</b>	<b>M<sub>plug</sub></b> <b>(MNm)</b>
210	0.3	0.1	0.083	0.042	140.27	3.05	0.000129	240.55

Table 3.10: Inputs for Formulas

The calculation of the effective horizontal stress applied on the circumference on the pile ( $q_i$ ) is shown in Appendix A.

The ovalization due to the direct soil pressures (Eq 3.12) is equal to:

$$\alpha_{qd} = 0.05239 \text{ m}$$

The ovalization due to the indirect soil pressures (Eq. 3.14) is equal to:

$$\alpha_{qi} = 0.02651 \text{ m}$$

The ovalization due to the bending curvature (Eq. 3.15) is equal to:

$$\alpha_C = 0.00044 \text{ m}$$

The effect of the ovalization on the radius on both sides of the pile, is shown in Figure 3.2.

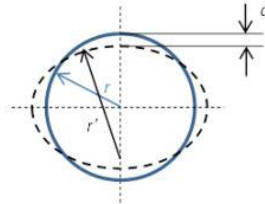


Figure 3.2: Change of Radius due to Ovalization [21]

In Figure 3.2, “ $r$ ” is the initial radius and “ $r'$ ” is the radius after the ovalization which can be determined by formula:

$$r' = \frac{r}{1 - \frac{3 \cdot \alpha}{r}} = \frac{3.05}{1 - \frac{3 \cdot 0.09458}{3.05}} = 3.368 \text{ m} \quad (3.17)$$

Since  $r' > r$ , the critical strain of the section will be equal to:

$$\varepsilon_{cr} = 0.25 \cdot \frac{r}{r'} - 0.0025 = 0.0057 \quad (3.18)$$

The resistant bending moment will be further reduced due to the ovalization, and will be calculated using the following formula.

$$M_{Rd} = g \cdot \beta_g \cdot \beta_s \cdot M_{R,oval} \quad (3.19)$$

where,

$$g = \frac{c_1}{6} + \frac{2}{3} \quad (3.20)$$

$$c_1 = \sqrt{4 - 2 \cdot \sqrt{3} \cdot \frac{m_{eff,sd}}{m_{el,Rd}}} \quad (3.21)$$

$$\beta_g = 1 - \frac{2 \cdot \alpha}{3 \cdot r} \quad (3.22)$$

$$\beta_s = 0.625 + 0.125 \cdot \mu \quad (3.23)$$

and

$$m_{eff,sd} = \frac{M_A + M_B}{2} \quad (3.24)$$

$M_A$  and  $M_B$  (Table 3.9) are related to the soil stress at the respective depth (Appendix A). The inputs for Eq. 3.19 are being presented in Table 3.11.

<b>g</b>	<b>c<sub>1</sub></b>	<b>m<sub>eff,sd</sub> (kNm)</b>	<b>β<sub>g</sub></b>	<b>β<sub>s</sub></b>
0.999	1.999	155.39	0.808	0.933

Table 3.11: Inputs for Formulas

For the determination of the strength of the monopile against local buckling, the quasi-static behavior of the monopile is taken into consideration, therefore the monopile is considered vertical and motionless and the relevant horizontal stress on it will be equal to the passive horizontal stress of the surrounding soil. The elastic bending resistance of the section has been calculated before and it is equal to  $m_{el,Rd} = 836.89 \text{ MNm}$ . Therefore,

$$M_{Rd} = g \cdot \beta_g \cdot \beta_s \cdot M_R = 0.99923 \cdot 0.9748 \cdot 0.9445 \cdot 658.54 = 609.46 \text{ MNm}$$

The resistant axial force will be due to the axial resistance of the composite section. This axial resistance for composite sections is given by the following formula (EN1994):

$$N_{pl,Rd} = A_{steel} \cdot f_{yd} \quad (3.25)$$

where,

$$A_{steel} = 2 \cdot \pi \cdot r \cdot t = 2 \cdot \pi \cdot 3.05 \cdot 0.1 = 1.916 \text{ m}^2 \quad (3.26)$$

with  $f_{yd} = 315 \text{ MPa}$

$$A_{sand} = \frac{\pi \cdot (D_{out} - 2 \cdot t)^2}{4} = \frac{\pi \cdot (6.1 - 2 \cdot 0.1)^2}{4} = 27.34 \text{ m}^2 \quad (3.27)$$

$$f_{sand} = \sigma_{zz} \text{ (at } -3.05\text{m below mudline)} = 0.140 \text{ MPa}$$

$$\text{So, } N_{pl,Rd} = \frac{1.916 \cdot 315}{1.1} = 548.67 \text{ MN}$$

and,

$$N_{Rd} = g \cdot N_{pl,Rd} = 0.999 \cdot 548.67 = 548.12 \text{ MN} \quad (3.28)$$

So, the combined bending and normal force check for the empty pile will be equal to:

$$\frac{M_{Sd}}{M_{Rd}} + \left(\frac{N_{Sd}}{N_{Rd}}\right)^{1.7} \leq 1 \Rightarrow \frac{473.098}{609.46} + \left(\frac{12.474}{548.12}\right)^{1.7} = 0.778 < 1 \quad (3.29)$$

The effect of the sand-fill to the ovalization of the section, and consequently, to the structural capacity of the cross section is being presented in the next paragraph.

### 3.6 Bending Moment Resistance & Ovalization for Sand-Filled Tubes

The bending stiffness of the steel section is equal to CUR211E [21]:

$$E \cdot I = \frac{1}{12} \cdot E_{steel} \cdot t^3 = \frac{1}{12} * 210000 \cdot 10^3 \cdot 0.1^3 = 175 \text{ MN} \cdot \text{m}^2 \quad (3.30)$$

also,

$$k_{steel} = \frac{12 \cdot E \cdot I}{r^4} = \frac{12 \cdot 175 \cdot 10^6}{3.05^4} = 2.427 \frac{\text{MN}}{\text{m}^3} \quad (3.31)$$

and,

$$k_{plug} = \frac{E_{plug}}{r} = \frac{E_{plug} \text{ (variable)}}{3.05} \quad (3.32)$$

The stiffness of the sand-fill is directly related to the material characteristics of the sand-fill. Literature suggests values of Young Modulus ranging from 10 – 80 MPa for dense sand and from 50 – 190 for sand and gravel mixture. However, at fixity depth, the material which will be present will have the characteristics of the surrounding soil. In this case, sand is considered to surround the monopile. For a varying stiffness for the sand, the  $k_{plug}$  will be equal to:

$E_{sand}$ (MPa)	10	20	30	40	50	60	70	80
$k_{sand}$ (kN/m)	3278.7	6557.4	9836.1	13114.8	16393.4	19672.1	22950.8	26229.5

Table 3.12: Plug Stiffness in Variation with Soil's Young Modulus

The ovalization of the cross-section at the plug level depth due to the presence of the sand-fill for various values of  $k_{sand}$  will be calculated using the formula below.

$$\alpha_{sand-fill} = \alpha_{empty} \cdot \frac{k_{steel}}{k_{steel} + k_{sand}} \quad (3.33)$$

$k_{sand}$ (kN/m)	3278.69	6557.38	9836.07	13114.75	16393.44	19672.1	22950.8	26229.5
$\alpha_{sand-fill}$ (m)	0.04023	0.025548	0.018718	0.014769	0.012196	0.010387	0.009045	0.00801

Table 3.13: Ovalization Variation for Filled Monopile

The monopile at the fixity depth is constantly plugged, therefore the factor  $c_1$ , which takes into consideration the ovalization due to soil pressure from the surrounding soil will be modified. As Winkel [19] suggest, the effect of the soil pressure on the circumferential stress is negligible, since



the soil plug is assumed to absorb the stresses and ensure the stability of the wall. ". Therefore, Equations 3.21, 3.20 and 3.17 yield:

$$c_1 = \sqrt{4 - 2 \cdot \sqrt{3} \cdot \frac{m_{eff;Sd}}{m_{el;Rd}}} = \sqrt{4} = 2$$

and,

$$g = \frac{c_1}{6} + \frac{2}{3} = 1$$

The new radius after ovalization, "r'", can be determined using the following formula:

$$r' = \frac{r}{1 - \frac{3 \cdot \alpha_{sand-fill}}{r}}$$

For various values of  $\alpha_{sand-fill}$  the values of the adjusted radius is being shown in Table 3.14.

$\alpha_{sand-fill}$ (m)	0.04023	0.02555	0.01872	0.01477	0.01220	0.01039	0.00904	0.00801
r' (m)	3.18	3.13	3.11	3.09	3.09	3.08	3.08	3.07

Table 3.14: Ovalized Section Radius Variation for Filled Monopile

The critical strains on the pile will be calculated using Eq. 3.18:

$$\varepsilon_{cr} = 7 \cdot \left(\frac{t}{r'}\right)^2 = 7 \cdot \left(\frac{0.085}{r'}\right)^2$$

For various values of  $r'$ ,  $\varepsilon_{crit}$  varies as shown in Table 3.15.

r' (m)	3.18	3.13	3.11	3.09	3.09	3.08	3.08	3.07
$\varepsilon_{crit}$	0.00694	0.00715	0.00725	0.00731	0.00735	0.00737	0.00739	0.00741

Table 3.15: Deformation Variation with the Radius of the Ovalized Section for Filled Monopile

All the coefficients, namely  $\beta_s$ ,  $\beta_g$ ,  $g$ ,  $c_1$ , which will be introduced in the formula, in order to calculate the effect of the ovalization on the bending resistance of the section, have been calculated for the varying parameters. The bending resistance variation for the varying Young's Modulus (E) of the plug is shown in Table 3.16 and in Figure 3.3.

$E_{sand}$ (Mpa)	10	20	30	40	50	60	70	80
$M_{Rd}$ (MNm)	736.70	772.13	788.92	798.72	805.13	809.66	813.03	815.64

Table 3.16: Bending Moment Resistance Variation with Sand-Fill's Young Modulus

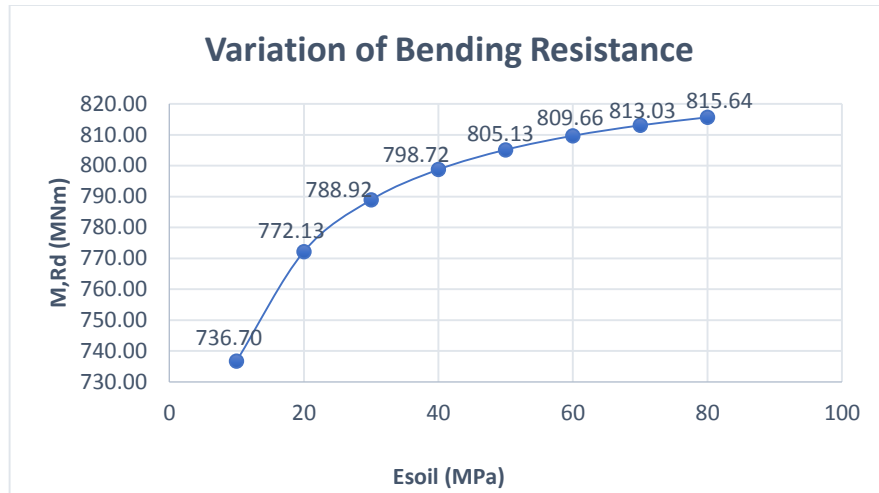


Figure 3.3: Bending Resistance Variation with Sand-Fill's Young Modulus

As it is shown in Figure 3.3 above, an increase of the sand-fill's Young's Modulus from 10 to 20 MPa has a higher effect on the bending resistance, and then for higher values increases but with smaller percentage. This is due to the fact, that the ovalization decreases non-linearly. Using for the sand-fill dense sand ( $E = 80$  MPa) instead of a loose sand ( $E = 10$  MPa), will increase the bending resistance of the monopile by:

$$\frac{815.64 - 736.70}{736.70} = 10.72 \%$$

The effect of sand-fill in the bending resistance, in comparison with the bending resistance of the empty pile is significant and is equal to (for an average value of  $E_{soil}=40$ MPa):

$$\frac{736.7 - 609.46}{609.46} = 20.09 \%$$

Therefore, it can be concluded that the presence of sand fill affects significantly the bending resistance of the section. However, the only effect of the sand-fill in the bending resistance is expected to happen only due to the fact that the sand-fill will restrict the ovalization of the cross-section. The sand-fill cannot be considered to be able to develop bending resistance itself, because its' contribution under repeated loading should be further investigated.

## 4. Effect of Sand-Fill on the Response of the Monopile to a Static Loading

In this paragraph, the effect of the sand-fill on the horizontal response of the monopile is being investigated. To perform this analysis, the Plaxis 3D software was used. Alternatively, the p-y curves which are being presented in the API and GL codes could be used. However, these curves are not suitable for the analysis of piles with large diameter [14, 27]. The formulas presented in the codes were derived using experimental data which were produced by measuring the response of piles with smaller diameter and have been validated for diameters up to 2m [14]. Therefore, a FEM approach was chosen to calculate the accurate response of the monopile under consideration.

### 4.1 Validation of the Model

In order to validate the model, the model which is being presented in a scientific publication [14], was first analyzed using Plaxis 3D. The model refers to a monopile with a diameter of 7.5 m and a thickness of 9 cm and in the paper it has been analyzed using the Abaqus software. The specific model was chosen also for the reason that it refers to the response of a monopile located in the North Sea, embedded in dense sand. The monopile under consideration (Upwind report) is also embedded in dense sand, therefore, this model could be used to validate the correct input of the dense sand characteristics in Plaxis 3D. The sand characteristics as presented in [14] are given in Figure 4.1.

Unit buoyant weight $\gamma'$	11.0 kN/m <sup>3</sup>
Oedometric stiffness parameter $\kappa$	600
Oedometric stiffness parameter $\lambda$	0.55
Poisson's ratio $\nu$	0.25
Internal friction angle $\varphi'$	35.0°
Dilation angle $\psi'$	5.0°
Cohesion $c'$	0.0 kN/m <sup>2</sup>

Figure 4.1: Soil Characteristics – Dense Sand

The authors apply a Hardening soil model to model the sand. In this model, the stress is dependent of the stiffness modulus,  $\kappa$ .

$$E_s = \kappa \cdot \sigma_{at} \cdot \left( \frac{\sigma}{\sigma_{at}} \right)^\lambda \quad (4.1)$$

$$\text{Where, } \sigma_{at} = 100 \frac{kN}{m^3}.$$

The model of Hardening soil in Plaxis requires the input of the following parameters:

$$E_{50}^{ref}, E_{oed}^{ref}, E_{ur}^{ref}$$

$$E_{oed}^{ref} = \sigma_{at} \cdot \kappa = 60000 \frac{kN}{m^2} \quad (4.2)$$

$$E_{50}^{ref} = E_{oed}^{ref} = 60000 \frac{kN}{m^2} \quad (4.3)$$

$$E_{ur}^{ref} = 3 \cdot E_{oed}^{ref} = 180000 \frac{\kappa N}{m^2} \quad (4.4)$$

according to [26].

Those parameters have been used in Plaxis 3D as shown in Figure 4.2

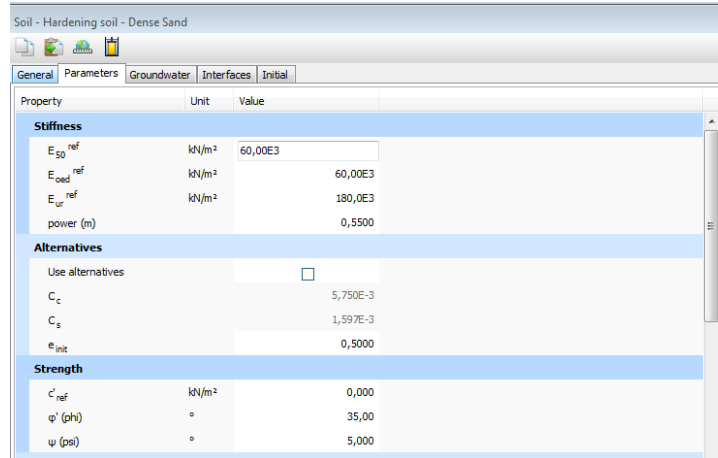


Figure 4.2: Soil Parameters – Hardening Soil Model

The monopile has been modelled using a Linear Elastic material, with the characteristics that the authors suggest. Symmetry has been used to model the pile in order to reduce the time of the analysis.

Properties		
d	m	0,09000
$\gamma$	kN/m <sup>3</sup>	77,08
Linear		<input checked="" type="checkbox"/>
Isotropic		<input checked="" type="checkbox"/>
End bearing		<input type="checkbox"/>
$E_1$	kN/m <sup>2</sup>	210,0E6
$E_2$	kN/m <sup>2</sup>	210,0E6
$\nu_{12}$		0,2000
$G_{12}$	kN/m <sup>2</sup>	87,50E6
$G_{13}$	kN/m <sup>2</sup>	87,50E6
$G_{23}$	kN/m <sup>2</sup>	87,50E6

Figure 4.3: Monopile Material Parameters

In this publication, only the part of the monopile which is embedded has been analyzed, by the means of applying the static equivalent lateral loading and moment on the monopile, just above the seabed. The lateral loading varies between 1 -18 MN, therefore, the equivalent moment for a pile with a typical length of 30m above the ground varies between 30 - 540 MNm. Since only half of the pile has been modelled, the applied lateral loading and moment is varying between 0.5 – 9 MN and the resultant moment between 15 -270 MNm. The side boundary conditions have been set using a diameter of 12D and the bottom boundary has been placed at a distance of 15m

beyond the pile tip. The embedded length is set to 30m. The model which was created in Plaxis 3D for the analysis is being shown in Figure 4.4.

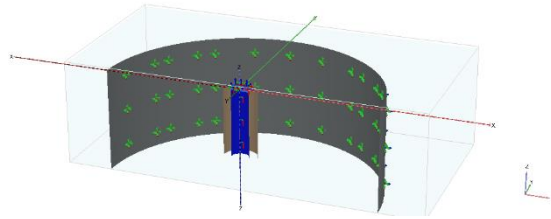


Figure 4.4: Creation of Rahman & Achmus' Model in Plaxis

Using the medium element distribution in the meshing options, and running the analysis for a number of lateral loadings, the displacements of the pile on the seabed calculated using Plaxis 3D, appear to correlate well with the results presented by Rahman and Achmus. The resultant displacements from the publication were estimated graphically using Figure 4.5.

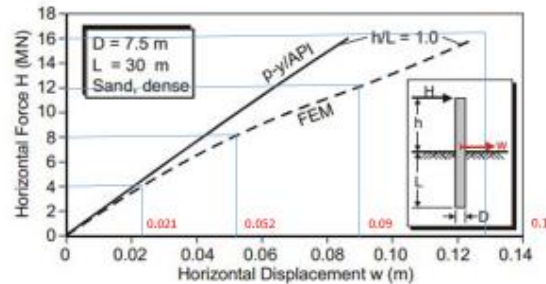


Figure 4.5: Displacement of Pile on the Seabed Level for Various Loadings [14]

The correlation between the results is shown in Figure 4.6.

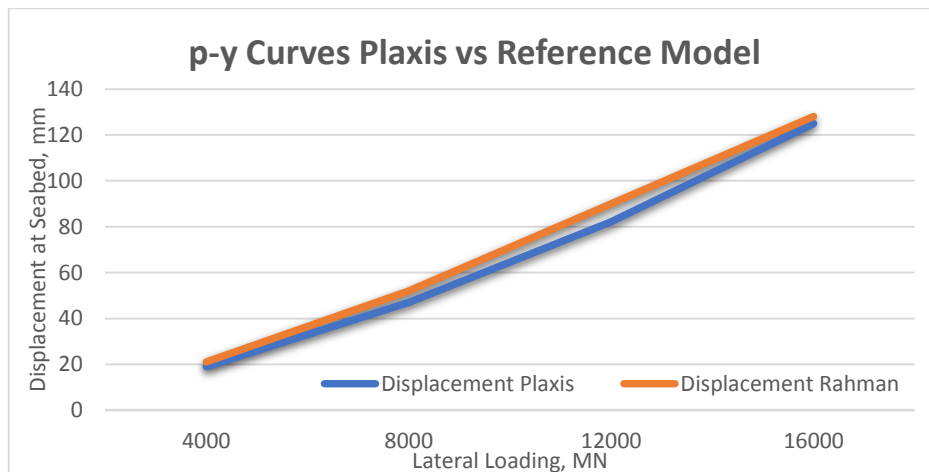


Figure 4.6: Correlation between Abaqus and Plaxis 3D Results

The average difference between Plaxis 3D and Abaqus results is about 6%, which can be considered reasonable taking into consideration the differences in the mesh and the constitutive models used in Plaxis 3D and Abaqus.

Having validated the soil model which was used in Plaxis in order to model the dense sand, a convergence test has been performed to identify the optimal distance for the boundary conditions. The boundary conditions have been placed at a distance which varies between 6D-16D as shown in Figure 4.7. The results of the analysis are being shown in Figure 4.8. In order that the results between the different cases are comparable, the different boundaries were set in the same model and the mesh was created only once. Therefore, in the resultant displacements between the cases are comparable.

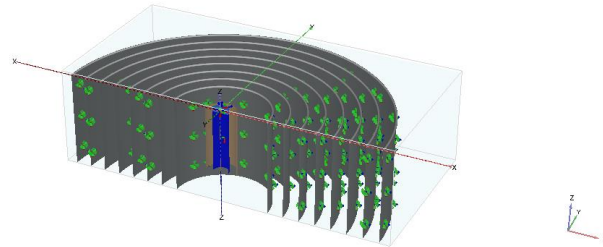


Figure 4.7: Model used in the Convergence Test to Allocate the Optimal Distance of the Boundaries

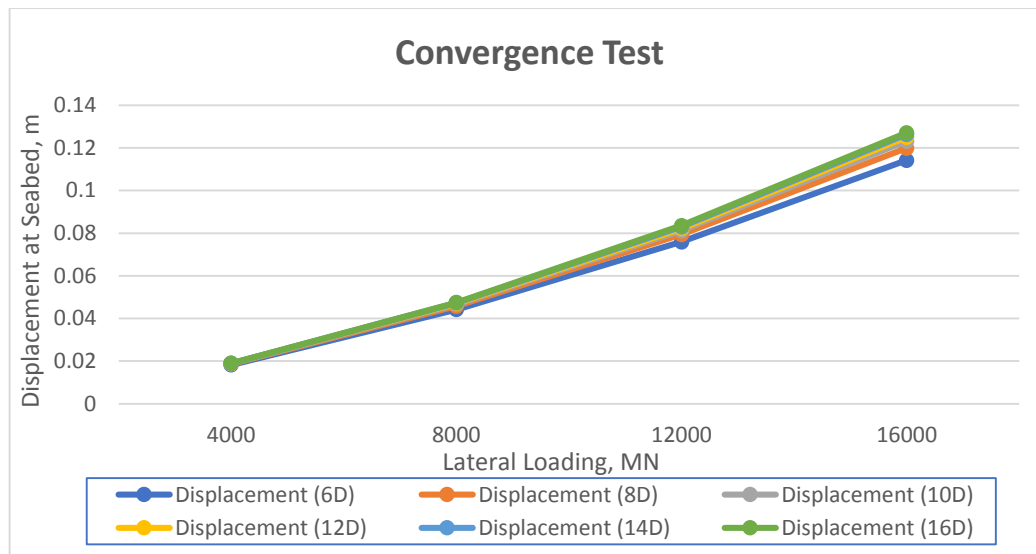


Figure 4.8: Convergence Test (Displacement vs. Boundaries Distance)

As shown in the figure above, the results converge sufficiently (0.46%) when the boundaries are being placed at a semi-circle with a diameter equal to 16 pile diameters. Therefore, in any further analysis which is presented in this paragraph, this distance has been implemented. The p-y curve for all the load cases, as presented in the paper, has been also created and is being shown in Figure 4.9.

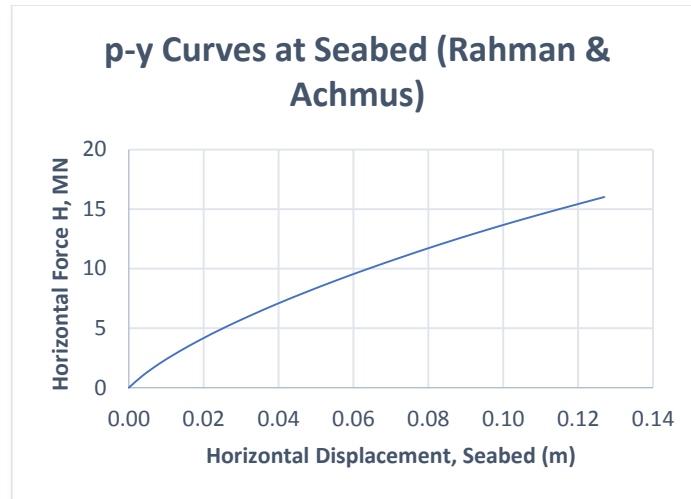


Figure 4.9: *p-y* Curve at Seabed Level (Rahman & Achmus)

## 4.2 Model for the *p-y* curves – Upwind report

Having validated the model in Plaxis 3D, the monopile presented in the Upwind report was modelled. The characteristics of the pile are:

$$D_{avg} = 6.1 \text{ m}$$

$$t_{avg} = 8 \text{ cm}$$

$$\text{Embedded Length} = 24 \text{ m}$$

and the loads applied on the half section of the pile on the seabed are:

$$\text{Lateral Load} = \frac{6531.39}{2} = 3265.7 \text{ kN}$$

$$\text{Axial Load} = \frac{11528}{2} = 5764 \text{ kN}$$

$$\text{Bending Moment} = \frac{220600}{2} = 110300 \text{ kNm}$$

The analysis has been done in phases. First, the initial stress state has been calculated using the K0 procedure as specified in Plaxis manual and then the monopile was generated replacing soil elements. Afterwards, the monopile was modelled in the soil, and a phase to apply the axial loading on the pile was created. Then, 10 phases were added in order to calculate the effect of varying lateral loads (and moments) on the displacement. The lateral loading and moment applied at the first phase was equal to 10% of the total loading and was increasing by 10% at each phase. The resultant *p-y* curve is being shown in Figure 4.10.

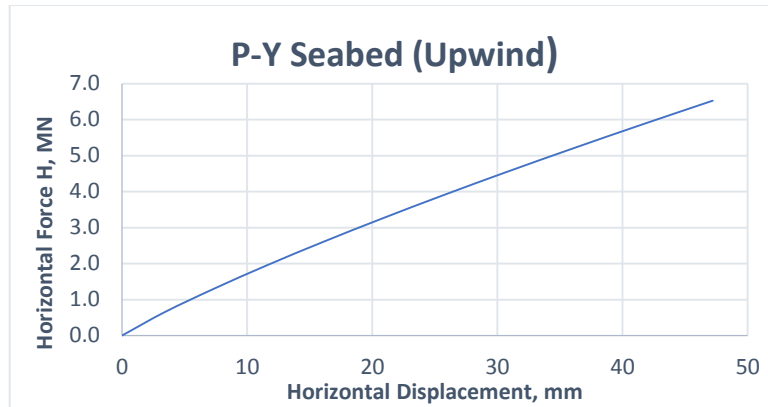


Figure 4.10: *p-y* Curves at Seabed Level – Upwind Report’s Monopile

As is being shown, calculating the displacement on the seabed, by applying the equivalent static loads and moments 1m above the seabed leads to a maximum displacement of about 47 mm for an applied load of 6.53 MN and a bending moment of 220.6 MNm.

### 4.3 Effect of the Sand-fill on the Displacement of the Pile

In this paragraph the effect of the sand-fill on the *p-y* curves of the monopile at the seabed level is being investigated. In order to include the added mass and stiffness of the sand-fill in the analysis, the pile was extended 33.78 m. above the seabed. This exact length was chosen in order to create a statically equivalent model with the one which was analyzed in the previous paragraph. Using a statically equivalent model should lead to the same *p-y* curves as before, and in that way the results of the new model can be validated. The applied load in the model with the pile ending 1 m above the seabed was 6.53 MN and the bending moment 220.6 MNm, therefore:

$$\text{Equivalent Pile Length} = \frac{220600}{6531.39} \approx 33.78 \text{ m} \quad (4.5)$$

Hence, an applied load with a magnitude of 6.531 MN at a height of 33.78m will lead to a statically equivalent model. The models which have been created in Plaxis 3D for the analysis of the empty and the sand-filled pile are being shown in Figure 4.11 & Figure 4.12.

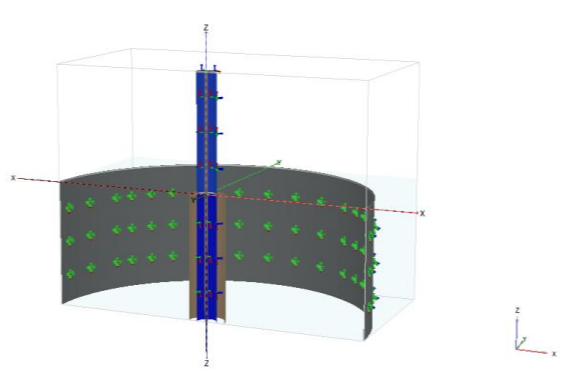


Figure 4.11: Empty Pile Model in Plaxis



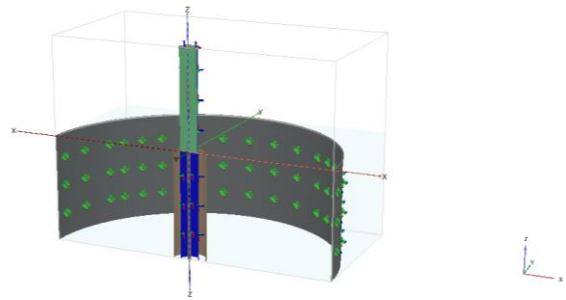


Figure 4.12: Sand-Filled Pile Model in Plaxis

In order to model the sand-fill in the monopile, a simpler model was chosen than the HS model which was used to model the surrounding soil. An elasto-plastic behavior of the sand in the monopile has been assumed, and a Mohr-Coulomb model was applied. The model parameters are being shown in Figure 4.13 & Figure 4.14.

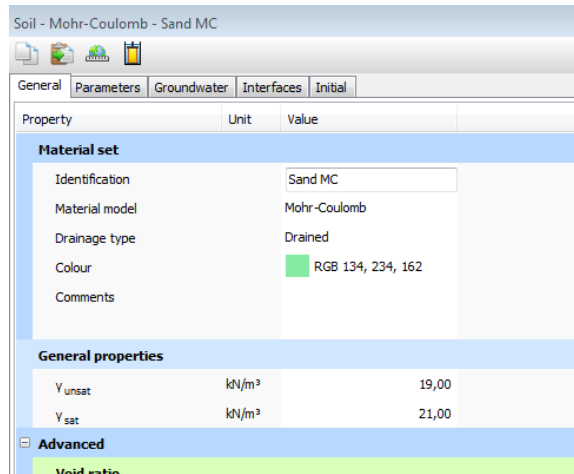


Figure 4.13: Parameters used to Model the Sand-Fill in Plaxis (1)

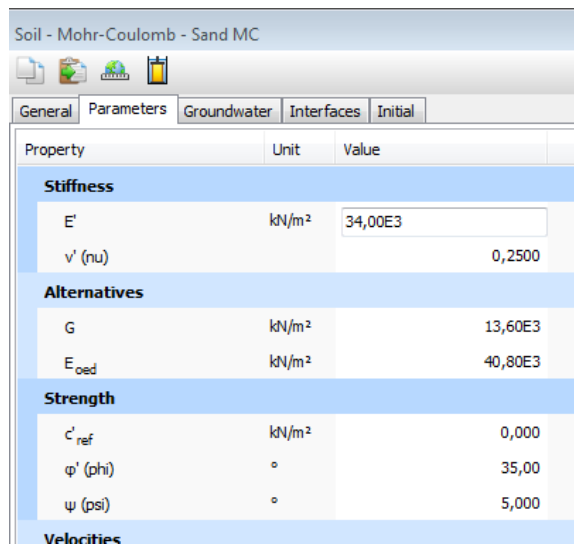


Figure 4.14: Parameters used to Model the Sand-Fill in Plaxis (26)

The analysis was performed again in various phases, and in each phase the lateral loading was increased by 10% comparing to the previous one.

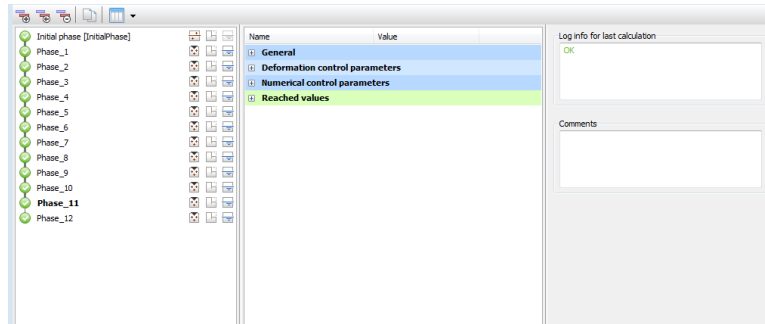


Figure 4.15: Phases to Calculate the Displacement of the Monopile for varying Lateral Loads

Figure 4.16 presents the p-y curves at the seabed level for the empty and the sand-filled pile.

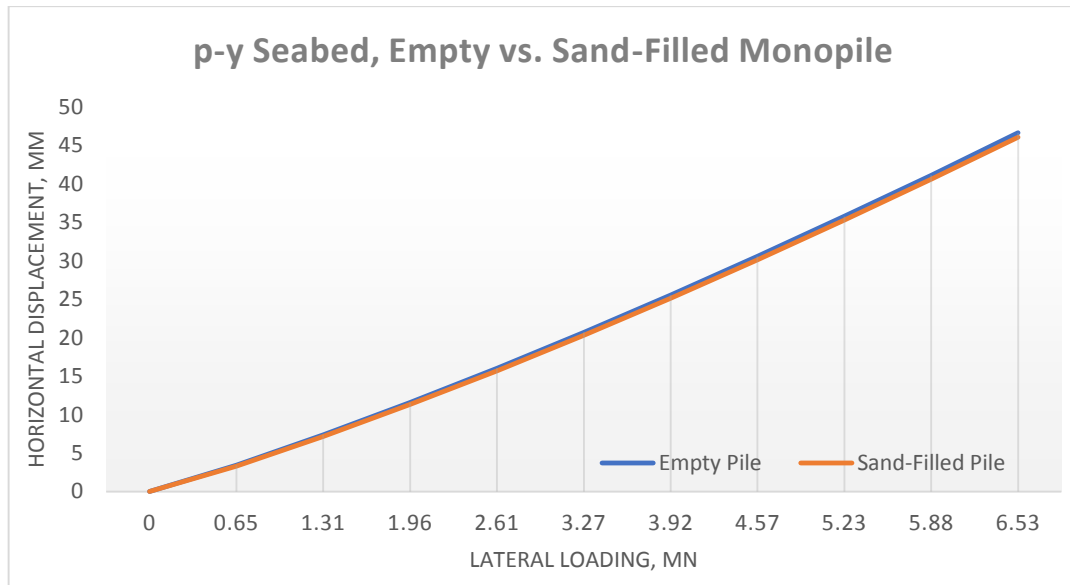


Figure 4.16: : P-Y curves at Seabed Level (Empty vs. Sand-Filled Monopile)

The decrease of the displacement due to the presence of sand-fill (%) for the varying values of lateral loading is also being presented in Figure 4.17.

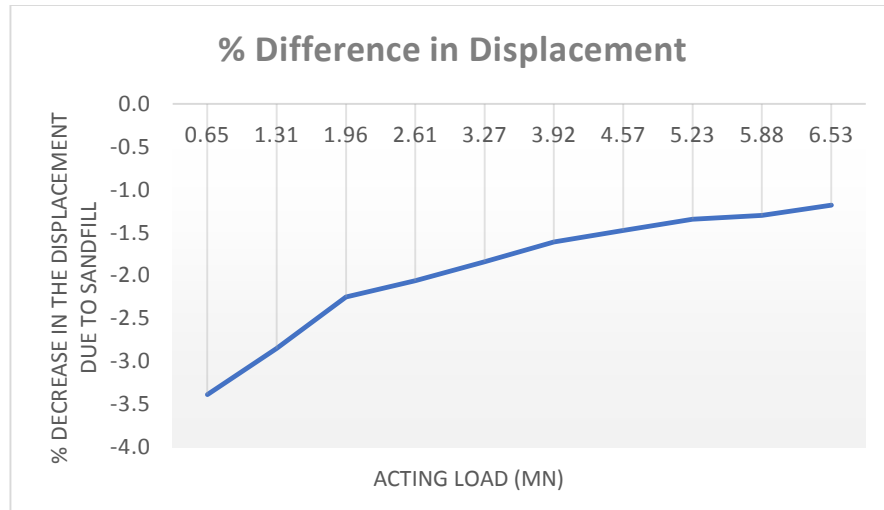


Figure 4.17: Percentage Decrease of Displacement

As shown in Figure 4.17, as the sand-fill increased the mass of the structure, the structure's displacements at the seabed were reduced. The decrease of the displacement for a given load is smaller for higher lateral loads. For a loading of 650 kN, the sand-fill reduces the displacement on the seabed by almost 3.5%, whereas, for a lateral load of 6.5 MN, the decrease is less ( $\approx 1\%$ ). This can be explained by the fact that increasing magnitude of the applied loading and using an elastoplastic (Mohr-Coulomb) model for the sand-fill will lead to plastification of the soil. This will reduce its' bending stiffness, therefore lower positive effect on the static displacement is expected for higher loads. In any case, the effect of the presence of sand-fill is always positive in contrast with the effect of sand-fill in the natural frequencies of the structure (will be presented in Chapter 5). The reason is, that the p-y curves are being created through a static analysis, therefore, the effect of the additional mass of the sand-fill also contributed positively to the displacement of the monopile. This effect is due to the fact that the added sand in the monopile increases the vertical stresses and, consequently, the horizontal stresses below the seabed and also, due to the fact that the mass of the structure when the monopile is filled with sand is increased and the same horizontal loading is expected to have a lower effect when applied to a bigger mass. In the following chapter the effect of the added mass due to the sand-fill in the dynamic analysis is presented. As it will be shown, the mass of the sand-fill is the key parameter which led to the reduction in the natural frequencies of the structure.

The effect of the additional stiffness due to the sand-fill will also affect the response at the top of the monopile. The displacement at the top of the pile is given by the following formula:

$$u_A = u_B + u'_B + \frac{F \cdot H^3}{3 \cdot E \cdot I} \quad (4.6)$$

Where,

$u_A$  = the displacement of point A

$u_B$  = the displacement of point B

$u'_B$  = the rotation of point B

and points A and B are as shown in Figure 4.18.

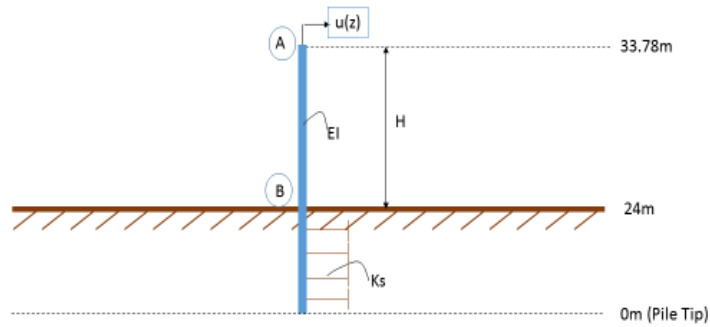


Figure 4.18: Points of Displacement A & B

As it shown in the formula above, the rotation of the point A, is related to the bending stiffness of the monopile. Therefore, a decrease in the displacement of point A is expected when the bending stiffness of the monopile increases due to the presence of sand-fill. However, and in accordance with the analysis of the effect of sand-fill in the natural frequency presented in the previous paragraphs, the increase of the stiffness of the structure due to the sand-fill is relatively low, therefore the expected difference is relatively small. This assumption is verified by Plaxis results as presented in Figure 4.19 & Figure 4.20.

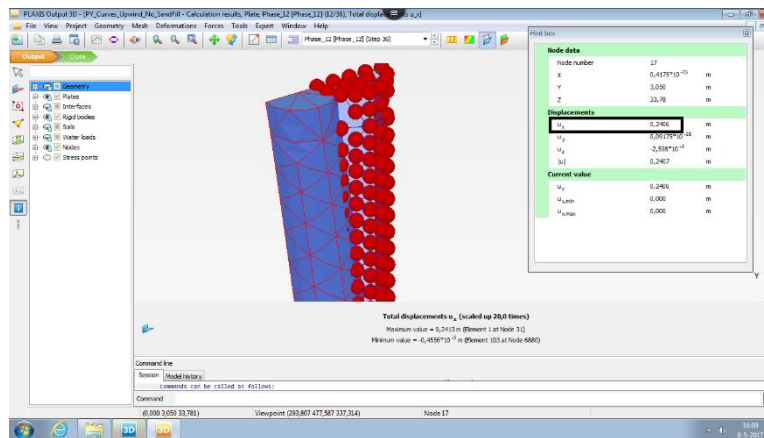


Figure 4.19: Displacement at the Top of the Monopile – Empty Monopile

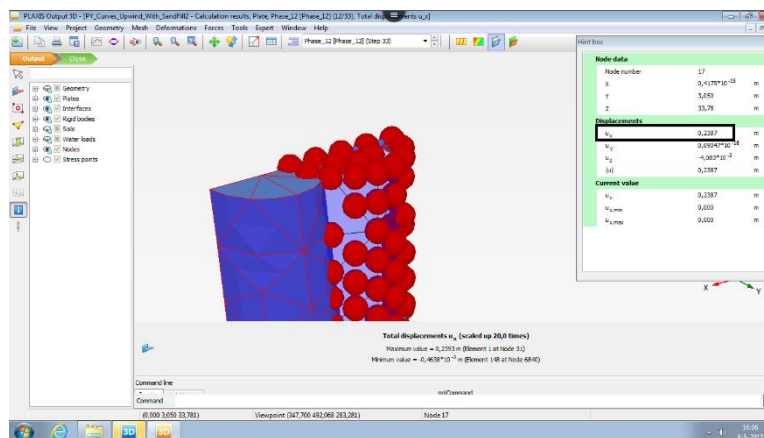


Figure 4.20: Displacement at the Top of the Monopile – Sand-Filled Monopile

The difference in the displacement at the top of the monopile is equal to:

$$\frac{0.2387 - 0.2406}{0.2406} = 0.8\%$$

This difference was calculated using a dense sand with Young's Modulus,  $E_s = 34$  MPa. The above analysis shows that the effect of the added mass on the displacement of the monopile at the seabed (point B) is much more significant than the effect of the added stiffness on the displacement at the top of the monopile (point A).

*Page intentionally left blank*

## 5. Effect of Sand-Fill on the Natural Frequency of the Structure

The aim of this chapter is to quantify the effect of sand-fill on the natural frequency of the structure. In order to perform this analysis, the natural frequencies of the structure will be determined:

- Numerically, using the Finite Difference Method (FDM) in MATLAB
- Analytically, using the normal modes of the structure

For both methods, the natural frequencies are being determined using two methods to model the support of the monopile, namely:

- Using the equivalent fixity length method (Model A)
- Using soil springs of constant stiffness per meter attached on the monopile (Model B)

First, the finite difference method is being applied on a structure with constant area, in order to create a model which can be easily validated using the analytical solution for a cantilever beam (APPENDIX B). After validating the FDM code, the dimensions for the monopile, transition piece and tower are being adjusted to the ones described in Upwind report [13]. For model corresponding to Upwind report, the required length for the fixity depth and the required stiffness for the soil springs ( $N/m^2/m$ ) is being determined by adjusting the aforementioned parameters in order that the 1<sup>st</sup> natural frequency of the structure is equal to the one provided in the Upwind report (0.277 Hz).

After the identification of all the parameters needed to model the dynamic behavior of the structure, a sensitivity analysis is being performed to identify the sensitivity of the natural frequency on various parameters. The tested parameters are:

- The effect of the stiffness of sand-fill on the 1<sup>st</sup> natural frequency
- The effect of the percentage contribution of sand-fill in the “composite” cross-section on the 1<sup>st</sup> natural frequency
- The effect of changing the mass and/or the stiffness of the monopile and the tower on the 1<sup>st</sup> natural frequency
- Assuming an “artificial material” with a varying density, it’s required stiffness in order to increase the fundamental natural frequency of the structure by 0.01 Hz

Then, the same analysis is being performed using the normal modes of the structure. Again, two models are being created in MAPLE, corresponding to a fixed beam (Model A) and beam embedded in soil (Model B).

Finally, the results of both models and of the analytical and the numerical method are being discussed.

### 5.1 Finite Difference Method – Model A

For both models created using the finite difference method, a model is created in Matlab. The description of the model is shown in Appendix C.

#### 5.1.1 Model Validation

The natural frequency of the system for various diameters has been calculated and compared with the results obtained by Matlab. Since the approach presented in the previous paragraph,

refers to a beam of a constant diameter, a constant thickness and diameter was used in the Matlab script for both the monopile and the tower in order to verify the results. In this analysis the diameter was a variable, ranging between 2m to 6m, while the thickness was calculated using a constant ratio:

$$t = \frac{D_{out}}{100} \tag{5.1}$$

As it is shown in Table 5.1 and Figure 5.1 below, the values of the natural frequency calculated analytically are almost identical with the Matlab results.

	Diameter	2	3	4	5	6
Natural Frequency (Hz)	Analytical Solution	0.0375	0.0804	0.1345	0.1964	0.2623
	Matlab	0.0373	0.0798	0.1345	0.1963	0.2627

Table 5.1: Natural Frequency – Analytical Calculation vs. Matlab

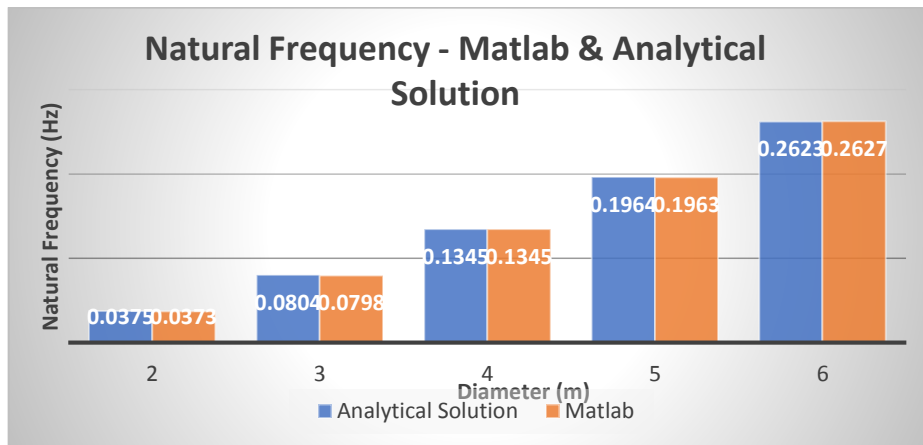


Figure 5.1: Natural Frequency – Analytical Calculation vs. Matlab

As shown in Figure 5.1, the results given by the analytical solution do almost perfectly match the results obtained using the Matlab script. After having validated the script, the structure presented in Upwind report was modeled using FDM. The structure presented in the Upwind report consists of a monopile, a transition piece and a tower all of them having varying diameter and thickness. In order to analyze the model in Matlab, each member had been assigned a constant diameter and thickness. In order to calculate the mean values for the diameter and thickness of each member, a weighted average was taken. The average values for each member are being presented in Table 5.2.



	Mean Value (m)
Thickness Tower	0.03
Diameter Tower	4.82
Thickness Transition	0.06
Diameter Transition	5.65
Thickness Pile	0.08
Diameter Pile	6.10

Table 5.2: Mean Diameter & Thickness

The length of the pile was taken equal to the total length of the support structure, which is equal to the combined length of the transition piece, the tower and the monopile length until the fixity depth. The fixity depth was taken equal to 14.4m. The fixed support was placed at a depth of 14.4m because that was the required length for the model in Matlab, in order to achieve the same natural frequency as the one presented in the Upwind report for the same structure. This natural frequency is equal to 0.277Hz. The difference between the model presented in Upwind report and the one modelled in the current project, is that in Upwind report the soil is being modelled using equivalent springs according to the p-y curves, when the model created in Matlab does not include any springs to model the soil, but instead a fixity depth which yields a dynamically equivalent system (i.e. same natural frequency) has been created. The total length of the structure is equal to:

$$L_{tower} + L_{trans.piece} + L_{monopile} = 68 + 14.76 + (25 + 14.4) = 122.16m.$$

A representation of the model of the structure along with all the relevant elevations is shown in Figure 5.2.

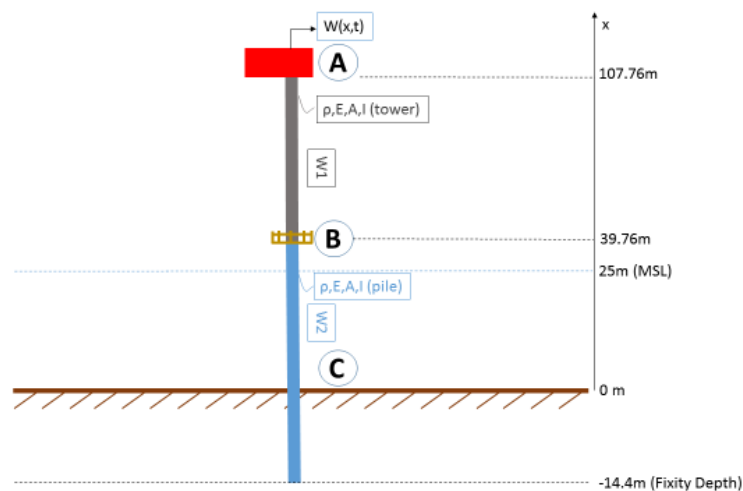


Figure 5.2: Model Elevation for Dynamic Analysis

### 5.1.2 Sand-Fill Effect & Sensitivity Analysis

In this paragraph, the effect of the presence of the sand-fill on the natural frequency of the structure will be investigated. The assumption made, is that sand will be added at the monopile, filling the part above the plug level and up until the upper tip of the monopile. Therefore, before calculating the effect of sand-fill on the 1<sup>st</sup> natural frequency due to the added sand, the natural frequency of the structure due to the presence of sand between the fixity depth and the plug level needs to be determined. Figure 5.3 shows the updated model of the structure, including the plug level.

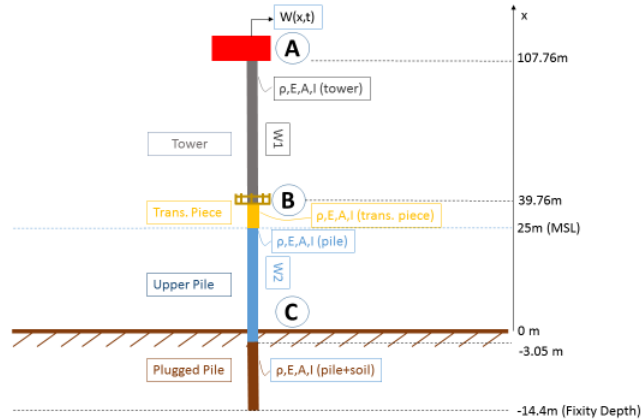


Figure 5.3: Graphic Representation of all the Parts of the Structure and their Elevations

In Figure 5.3, the monopile has been split in two parts. One part referring to the lower (plugged) part and one to the upper part, which initially is considered empty. The plug level for a pile with diameter bigger than 3m can be considered to be located at a distance of  $\frac{D_{pile,outer}}{2}$  below the seabed [19]. Therefore, the monopile has been split in two parts, one which spans between -14.4m (fixity depth) to  $-\frac{6.1}{2} = 3.05m$  (elevations are measured from seabed, with minus representing an elevation below the seabed) and an upper, empty part, which spans between -3.05m up to 30m above seabed.

At this point it is important to be mentioned that in order to allocate the fixity depth at the previous paragraph, the lower part of the monopile was also considered to be empty, due to the fact that the fixity depth method considers the soil to form a clamped connection at the tip of the pile. Therefore, the reference natural frequency which will be used to compare the results in this sensitivity analysis will be the one calculated taking into consideration the presence of sand in the plugged part of the monopile. The reference fundamental natural frequency in this analysis is equal to:

$$f_1 = 0.2762 \text{ Hz}$$

will be chosen.

Having estimated the reference value of the 1<sup>st</sup> natural frequency, a sensitivity analysis will be performed in order to investigate the influence of the variation of the physical characteristics of the tower/monopile to the natural frequency. To perform the sensitivity analysis, the model created in Matlab will be utilized. This model allows to input different diameter/thickness for the

monopile, the transition piece and the tower, and in that way can be used to simulate realistically the dynamic behaviour support structure. In order to model the changes in geometry using a finite difference model, three interfaces have been applied at the connection points between:

- 1) the plugged and the upper part of the monopile
- 2) the upper part of the monopile and the transition piece
- 3) the transition piece and the tower.

### 5.1.3 Natural Frequency Variation with Sand-fill

In this part of the analysis, the Upper Pile is considered to be fully filled with sand. Also, the sand is considered to contribute in the bending stiffness of the Upper Pile, in a similar manner as concrete contributes to the bending stiffness of composite, concrete-filled, steel columns. No friction effects between the sand and the pile have been taken into consideration at this stage. Eurocode 4 suggests that the effective flexural stiffness of a composite section can be calculated using the following formula [20]:

$$(E \cdot I)_{eff} = 0.9 \cdot (E_{steel} \cdot I_{steel} + K_{conc} \cdot E_{sand-fill} \cdot I_{sand-fill}) \quad (5.2)$$

The  $K_{conc}$  coefficient appearing in the formula, is a coefficient applied in concrete-filled sections in order to take into consideration the cracking of concrete under tensile stresses, and EN1994-1-1 suggests that  $K_{conc} = 0.5$ . Since the relevant Eurocode does not include steel-sand composite sections, the coefficients of “0.9” and  $K_{conc}$  will be omitted. For various values of the modulus of elasticity of sand, the natural frequency of the support structure has been calculated. The mass density of the sand was taken equal to:

$$\rho = 1900 \text{ kg/m}^3$$

which can be considered as a realistic value for saturated sand. The dimensions for all the members as presented in the previous paragraph have been used for the tower, the transition piece and the monopile. Assuming different compaction levels for the sand-fill of the upper part of the monopile (part above plugged level, shown in blue in the figure above) the modulus of elasticity is considered to vary between 20 to 80 MPa. The compaction level of the plug is considered as a constant, having a Young Modulus equal to  $E_{plug} = 80\text{MPa}$ . The higher Young Modulus of the sand in the Plugged pile in comparison with the Upper Pile is based on the assumption that the sand-fill which is located lower in the monopile will be compacted more than the sand-fill on the Upper Pile. The natural frequency variation with sand-fill’s modulus of elasticity is being presented in Table 5.3 and in Figure 5.4.

#### Sand Plug=80MPa

Sand-Fill Young Modulus ( $E_s$ ), MPa	20	40	60	80
$f_{n, \text{filled}}$ (Hz)	0.2745	0.2746	0.2746	0.2747
$f_{n, \text{filled}} / f_{n, \text{empty}}$	0.9938	0.9942	0.9942	0.9946

Table 5.3: Natural Frequency Variation with Sand-fill’s Young Modulus

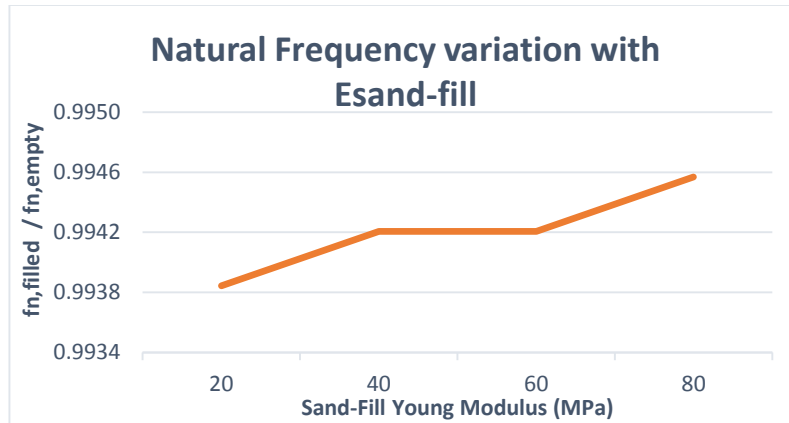


Figure 5.4: Natural Frequency Variation with Sand-fill's Young Modulus

As shown in Figure 5.4, the presence of sand-fill is estimated to reduce the natural frequency of the structure by approximately 0.6%. At this point it should be noted that filling the upper part of the monopile with a stronger material, such as, concrete which has the following physical properties:

$$\rho_{concr} = 2400 \text{ kg/m}^3$$

$$E_{concr} = 20000 \text{ MPa}$$

will increase the 1<sup>st</sup> natural frequency of the structure to:

$$f_1 = 0.2948 \text{ Hz}$$

which means that comparing to the hollow pile the natural frequency will increase by 6.7%.

#### 5.1.4 Natural Frequency Variation with the Contribution of Sand-fill in the Bending Stiffness

In the previous paragraph, the sand-fill was considered to contribute by 100% of its' bending stiffness to the total bending stiffness of the section. A sensitivity analysis has been performed to investigate the effect of sand-fill in the natural frequency using the percentage of contribution as a variable. The sensitivity analysis was performed taking into consideration a value of 80MPa for both the plug's and the sand-fill's Young Modulus. The dimensions of the monopile and the tower are the same as in the previous paragraph. The results of this analysis are being presented in Table 5.4 and in Figure 5.4.

##### Sand Plug=80MPa

Soil Contribution in Comp. Section's EI, %	20	40	60	80	100
$f_{n, \text{filled}}(\text{Hz})$	0.2745	0.2746	0.2746	0.2746	0.2747
$f_{n, \text{filled}} / f_{n, \text{empty}}$	0.9938	0.9942	0.9942	0.9942	0.9946

Table 5.4: Natural Frequency Variation with % Contribution of Sand in EI

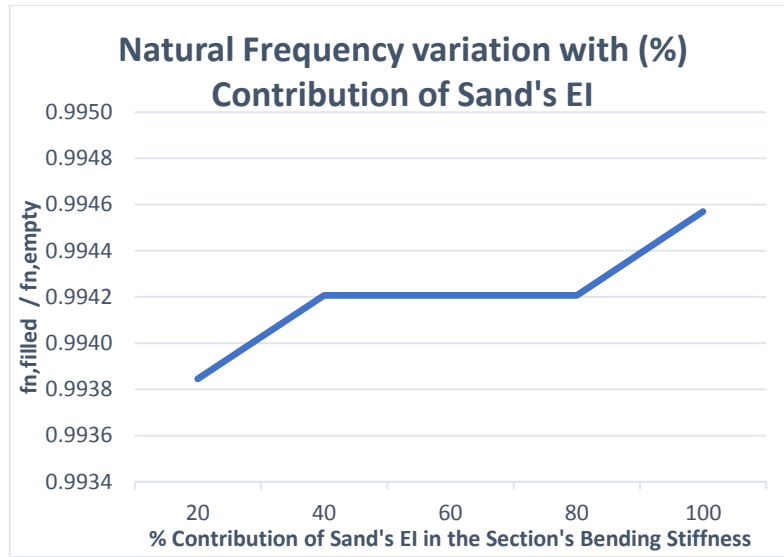


Figure 5.5: Natural Frequency Variation with % Contribution of Sand in EI

As it is shown in Figure 5.5, when the sand-plug/fill with  $E=80\text{MPa}$  contributes by 60% of its' bending stiffness in the composite section's stiffness, the natural frequency is equal to 0.2746 Hz. Figure 5.5 shows that even increasing sand's contribution to 100% will lead to an insignificant increase in the natural frequency, since sand's contribution to the section's bending stiffness is relatively small (comparing to steel's bending stiffness).

### 5.1.5 Natural Frequency Variation with Monopile's Bending Stiffness ( $EI_{mp}$ )

A sensitivity analysis was also performed to identify the effect of increasing the bending stiffness of the Upper Pile. Since the diameter and the thickness of the Upper Pile are constant, the second moment of area of the Upper Pile is also known. Therefore, in the sensitivity analysis the Young Modulus of the material of the pile is assumed to be variable. Hence, the effect of the bending stiffness of the Upper Pile on the natural frequency has been investigated, for various values of percentage increase in the section's bending stiffness. The results of this analysis are being presented in Table 5.5 and in Figure 5.6.

Increase in Flexural Stiffness (Upper Pile), %	5%	10%	15%	20%	25%	30%
Natural Frequency, Hz	0.2782	0.28	0.2817	0.2832	0.2847	0.2861
$f_{n, \text{incr stiffness.}} / f_{n, \text{empty}}$	1.007	1.014	1.020	1.025	1.031	1.036

Table 5.5: Natural Frequency Variation with EI Upper Pile

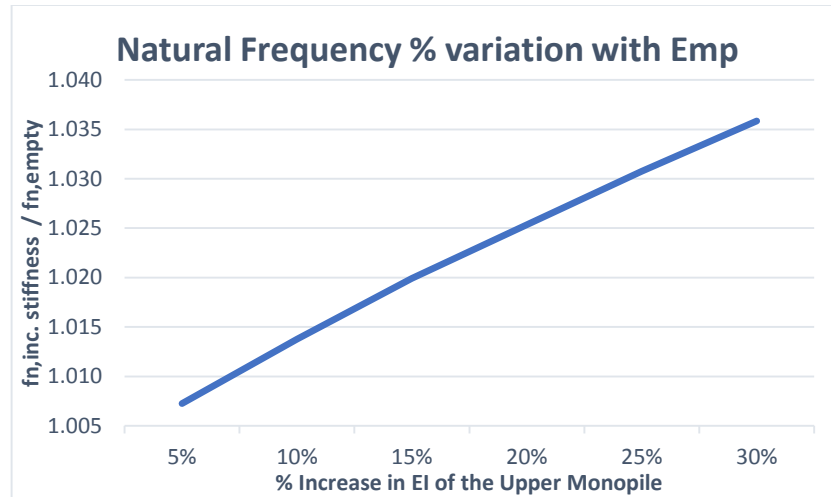


Figure 5.6: Natural Frequency Variation with EI monopile

As it is shown, an increase of the flexural stiffness of the monopile between 5 – 30%, will increase the natural frequency of the structure by 0.7 – 3.6%.

### 5.1.6 Natural Frequency Variation with Tower’s Bending Stiffness ( $EI_{tower}$ )

Increasing the tower’s bending stiffness again by 5 – 30% leads to an increase in the natural frequency, as shown in Table 5.6 and in Figure 5.7. In the figure, the results of this analysis are being presented together with the results obtained when the bending stiffness of the monopile was increased.

Increase of Flexural Stiffness (Tower), %	5%	10%	15%	20%	25%	30%
Natural Frequency, Hz	0.2794	0.2823	0.2851	0.2877	0.2902	0.2925
$f_{n, inc. stiffness} / f_{n, empty}$	1.012	1.022	1.032	1.042	1.051	1.059

Table 5.6: Natural Frequency Variation with EI Tower

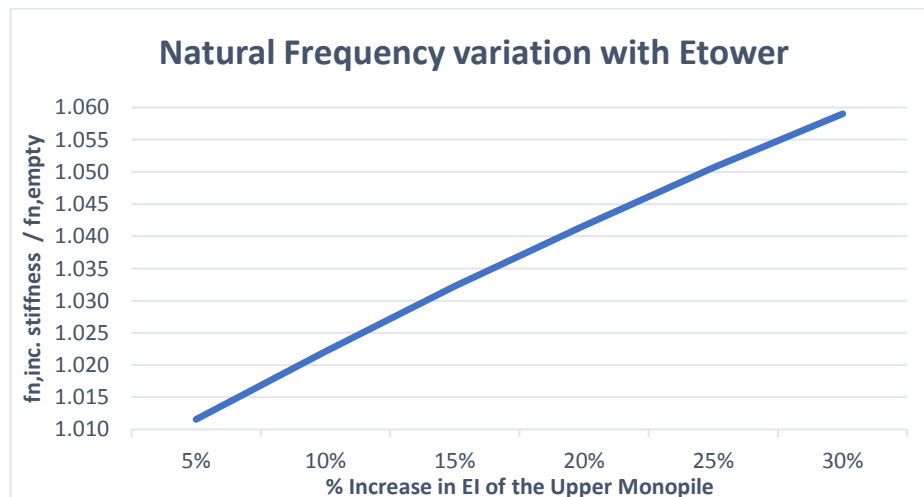


Figure 5.7: Natural Frequency Variation with EI Tower

It is shown, that increasing the bending stiffness of the monopile/tower will lead to a linear increase in the natural frequency of the structure for both cases. The only difference is related to the magnitude of the increase of the natural frequency. Increasing the bending stiffness of the tower by 20% will lead to an increase of approximately 4%, whereas, increasing the bending stiffness of the upper part of the monopile by 20% will cause an increase in the natural frequency by 2.5%. In order to increase the natural frequency by 0.01 Hz (i.e. from 0.2762 Hz to 0.2862 Hz) an increase of the bending stiffness of the Upper Pile by 30% is required (yielding a natural frequency of 0.2861Hz). A similar result could be achieved by increasing the tower's bending stiffness by about 18%. The bending stiffness can be increased either by increasing the moment of inertia of the Upper Pile itself, or by filling the hollow section with a material which will have the required physical characteristics (i.e. Young Modulus) to increase the bending stiffness accordingly. The moment of inertia of the filling will be considered to be constant, since in this analysis the model of the structure is specific, following the one suggested in the Upwind report. In order to calculate the required value for the Young Modulus of the filling, the following formula will be applied:

$$1.3 \cdot E_{steel} \cdot I_{up-pile} = E_{steel} \cdot I_{up-pile} + E_{fill} \cdot I_{fill} \quad (5.3)$$

$$\Rightarrow 1.3 \cdot 210000 \cdot 6.8551 = 210000 \cdot 6.8551 + E_{fill} \cdot 61.1105$$

$$\Rightarrow E_{fill} = 7067 \text{ MPa}$$

Alternatively, the same effect could be achieved by keeping the pile empty, but adjusting the cross-section of the upper part of the pile itself, so that the moment of inertia of the section should be equal to:

$$1.3 \cdot 6.8551 = 8.9163 \text{ m}^4$$

A similar percentage increase in the natural frequency of the structure can be also achieved by increasing the bending stiffness of the tower by 18%. The required Young Modulus of the material which will be used to fill the pile is:

$$1.18 \cdot E_{steel} \cdot I_{tower} = E_{steel} \cdot I_{tower} + E_{fill} \cdot I_{fill}$$

$$\Rightarrow 1.18 \cdot 210000 \cdot 1.2948 = 210000 \cdot 1.2948 + E_{fill} \cdot 25.1998$$

$$\Rightarrow E_{fill} = 1942 \text{ MPa}$$

Due to the longer length of the tower (in comparison with the pile) and due to its position (near the free end), the same increase of the natural frequency of the structure can be achieved in the following two ways:

- Filling fully the upper part of the monopile with a material with a Young Modulus of 7067 MPa
- Filling fully the tower by a material with a Young Modulus of 1942 MPa

### 5.1.7 Natural Frequency Variation with Monopile & Tower Mass

A sensitivity analysis in order to investigate the impact of the increase in the mass of the Upper Pile and the Tower on the natural frequency of the structure has been performed. This is of high importance, because due to the large diameter of the monopile/tower, the mass which it will be added on the structure after filling the Upper Pile/Tower is significant and it will affect the

dynamic behavior of the structure. For instance, in this example, filling the 33.05 m. Upper Pile (distance between the plug level and the interface level), leads to an additional mass of:

$$m_{filling} = \rho \cdot A \cdot L \tag{5.4}$$

where,

$\rho$ , filling (kg/m <sup>3</sup> )	A, upper pile (m <sup>2</sup> )	L (m)
<b>1900</b>	27.7117	33.05

Table 5.7: Inputs for Formula

$$\Rightarrow m_{filling} = \rho \cdot A \cdot L = 1740.16 \text{ tonnes}$$

Increasing the mass of the Upper Pile by 20 – 100% will lead to the following values for the natural frequency.

Mass Increase - Upper Pile, %	100%	200%	300%	400%	500%
Natural Frequency, Hz	0.2759	0.2758	0.2748	0.2745	0.2742
$f_{n, \text{incr mass.}} / f_{n, \text{empty}}$	0.9989	0.9986	0.9949	0.9938	0.9928

Table 5.8: Variation of Natural frequency with Upper Pile’s Mass

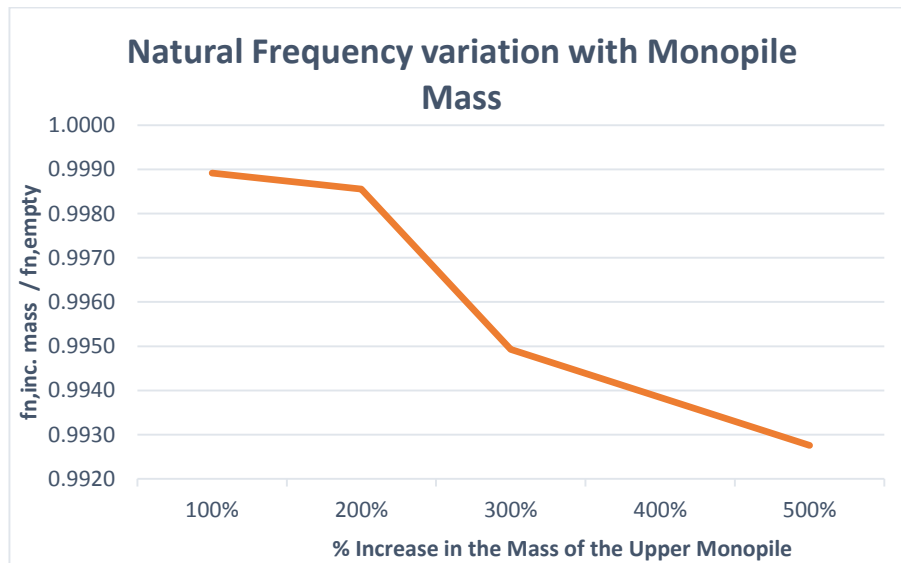


Figure 5.8: Variation of Natural frequency with Upper Pile’s Mass

Increasing the mass of the Tower by 20 – 100% will lead to the following values for the natural frequency.

Mass Increase - Tower, %	100%	200%	300%	400%	500%
Natural Frequency, Hz	0.2525	0.2339	0.2188	0.2062	0.1956
$f_{n, \text{incr mass.}} / f_{n, \text{empty}}$	<b>0.9142</b>	<b>0.8469</b>	<b>0.7922</b>	<b>0.7466</b>	<b>0.7082</b>

Table 5.9: Variation of Natural frequency with Tower’s Mass



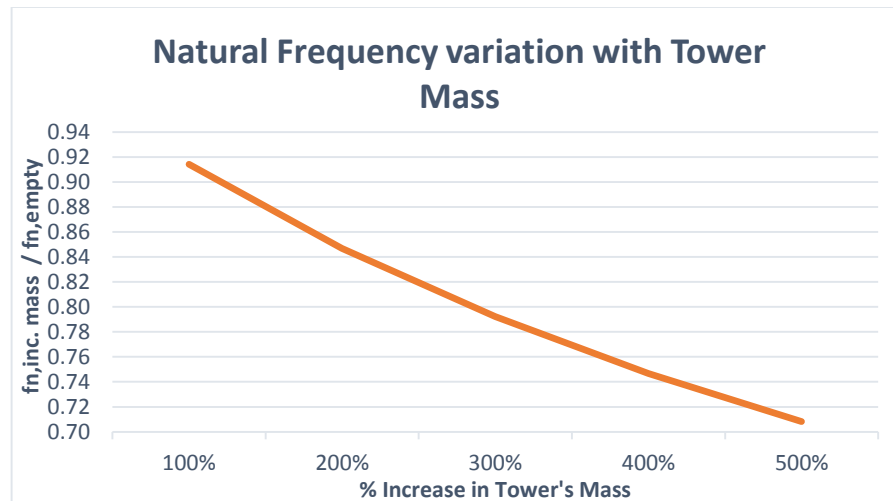


Figure 5.9: Variation of Natural frequency with Tower's Mass

As it is shown Figure 5.8 and Figure 5.9, an increase of the monopile's mass by 100% will lead to a decrease of the natural frequency by only 0.11% when an increase of the tower's mass by 100%, will lead to a decrease by 8.58%. This result is reasonable, since the tower refers to the biggest part of the support structure in this design (86m vs. 33.05m length of the Upper Pile) and since the mass of the tower is being located further than the support and closer to the mass at the free end, comparing to the mass of the monopile. Another model was tested, assuming that the monopile is half-filled with sand. In this case, the effect of the sand-fill on the natural frequency is neutral. This result is reasonable, because, as shown before, the increase of the bending stiffness of the composite section due to the sand-fill is small, and at the same time, placing the CoG of the added mass near the support, reduces the negative effect of the added mass in the natural frequency.

### 5.1.8 Natural Frequency Variation with Unit Weight of filling

In the previous paragraph, the effect on the natural frequency due to the filling added in the upper part of the monopile has been examined. At this point the combined effect of increased stiffness and mass will be examined, using varying values for the mass density of the material which will be used as filling.

- For  $\rho = 1000 \frac{kg}{m^3}$

$$\rho = 1000 \text{ kg/m}^3$$

Filling Young Modulus, MPa	100	1000	5000	10000
Natural Frequency, Hz	0.2760	0.2774	0.2831	0.2886
$f_n, \text{incr mass \& stiffness.} / f_{n, \text{empty}}$	0.9993	1.0043	1.025	1.0449

Table 5.10: Variation of Natural Frequency with Filling's Young Modulus

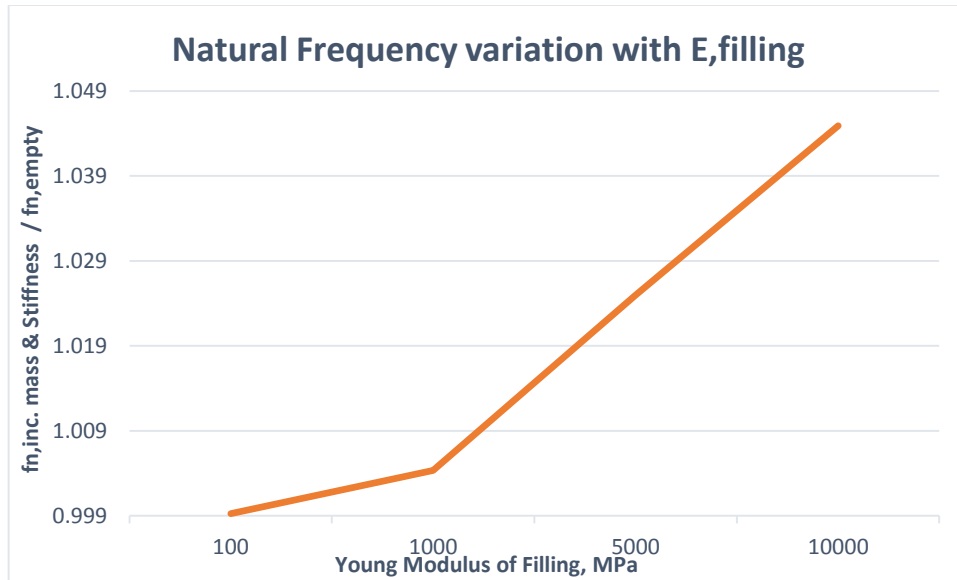


Figure 5.10: Variation of Natural Frequency with Filling's Young Modulus

As it is shown in Table 5.10 and Figure 5.10, the increase of 3.5% in the natural frequency for a density of the filling equal to:

$$\rho_{filling} = 1000 \frac{kg}{m^3}$$

can be achieved by filling the hollow pile with a material having a Young Modulus of:

$$E_{filling} \approx 7500 MPa$$

- For  $\rho = 1500 \frac{kg}{m^3}$

$\rho=1500 \text{ kg/m}^3$				
Filling Young Modulus, MPa	100	1000	5000	10000
Natural Frequency, Hz	0.2749	0.2764	0.2821	0.2875
$f_{n, \text{incr mass \& stiffness}} / f_{n, \text{empty}}$	<b>0.9953</b>	<b>1.0007</b>	<b>1.0214</b>	<b>1.0409</b>

Table 5.11: Variation of Natural Frequency with Filling's Young Modulus

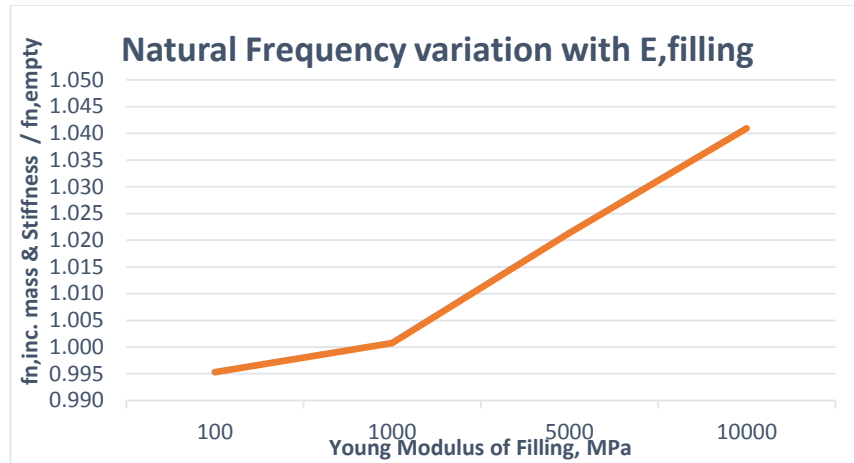


Figure 5.11: Variation of Natural Frequency with Filling's Young Modulus

As it is shown in Table 5.11 and Figure 5.11, the increase of 3.5% in the natural frequency for a density of the filling equal to:

$$\rho_{filling} = 1500 \frac{kg}{m^3}$$

can be achieved by filling the hollow pile with a material having a Young Modulus of:

$$E_{filling} \approx 8500 \text{ MPa}$$

- For  $\rho = 2000 \frac{kg}{m^3}$

**$\rho=2000 \text{ kg/m}^3$**

Filling Young Modulus, MPa	100	1000	5000	10000
Natural Frequency, Hz	0.2746	0.2761	0.2818	0.2874
$f_n, \text{incr mass \& stiffness.} / f_{n, \text{empty}}$	0.9942	0.9996	1.0203	1.0406

Table 5.12: Variation of Natural Frequency with Filling's Young Modulus

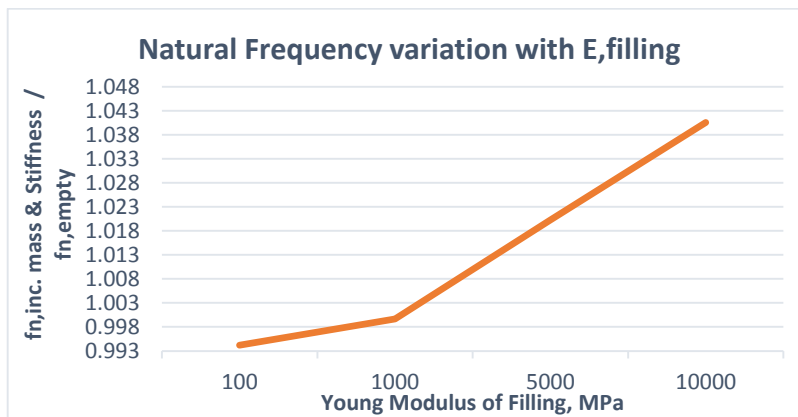


Figure 5.12: Variation of Natural Frequency with Filling's Young Modulus

As it is shown, the increase of 3.5% in the natural frequency for a density of the filling equal to:

$$\rho_{filling} = 2000 \frac{kg}{m^3}$$

can be achieved by filling the hollow pile with a material having a Young Modulus of:

$$E_{filling} \approx 9000 \text{ MPa}$$

- For  $\rho = 2500 \frac{kg}{m^3}$

**$\rho=2500 \text{ kg/m}^3$**

Filling Young Modulus, MPa	100	1000	5000	10000
Natural Frequency, Hz	0.2742	0.2757	0.2814	0.2870
$f_{n, \text{incr mass \& stiffness.}} / f_{n, \text{empty}}$	0.9928	0.9982	1.0188	1.0391

Table 5.13: Variation of Natural Frequency with Filling's Young Modulus

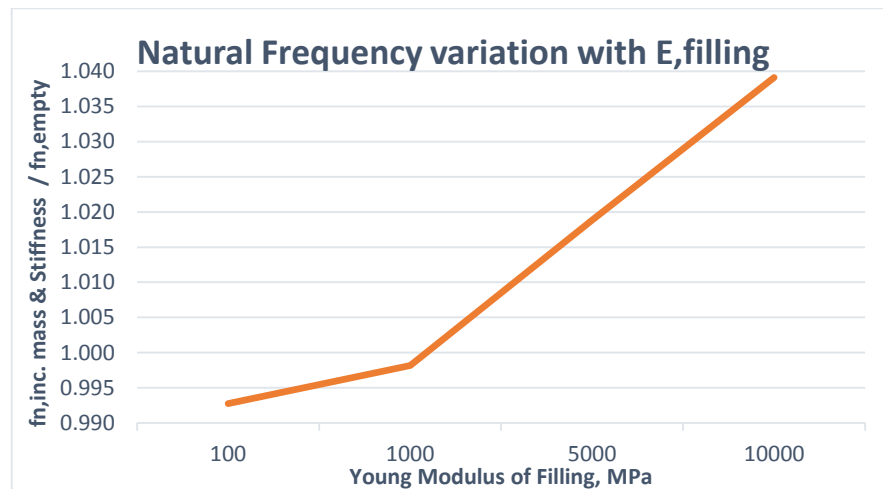


Figure 5.13: Variation of Natural Frequency with Filling's Young Modulus

As it is shown in Figure 5.13, the increase of 3.5% in the natural frequency for a density of the filling equal to:

$$\rho_{filling} = 2500 \frac{kg}{m^3}$$

can be achieved by filling the hollow pile with a material having a Young Modulus of:

$$E_{filling} \approx 9500 \text{ MPa}$$

## 5.2 Finite Difference Method – Model B

Having identified the insignificant contribution of the Young's Modulus of sand and of the contribution of the bending stiffness of sand in the composite section, the analysis will be limited to identify:

- the effect on the natural frequency of the varying mass and stiffness of the monopile and the tower
- the required Youngs Modulus in order to increase the fundamental natural frequency by 0.01 Hz

using the FDM model with the soil springs. The simulations ran, yielded almost identical results for the effect of added mass and/or stiffness on the natural frequency of the structure. For brevity, only the effect of added stiffness and mass on the monopile is being presented.

### 5.2.1 Natural Frequency Variation with Monopile’s Bending Stiffness ( $EI_{mp}$ ) and Mass

The effect on the fundamental natural frequency of a percentage increase in the bending stiffness of the monopile is shown in Table 5.14 & Figure 5.14.

Increase in Flexural Stiffness (Upper Pile), %	5%	10%	15%	20%	25%	30%
Natural Frequency, Hz	0.2782	0.28	0.2817	0.2832	0.2847	0.2861
$f_{n, \text{incr stiffness.}} / f_{n, \text{empty}}$	1.007	1.014	1.020	1.025	1.031	1.036

Table 5.14: Normalized Natural Frequency variation with the Flexural Stiffness of the Upper Pile

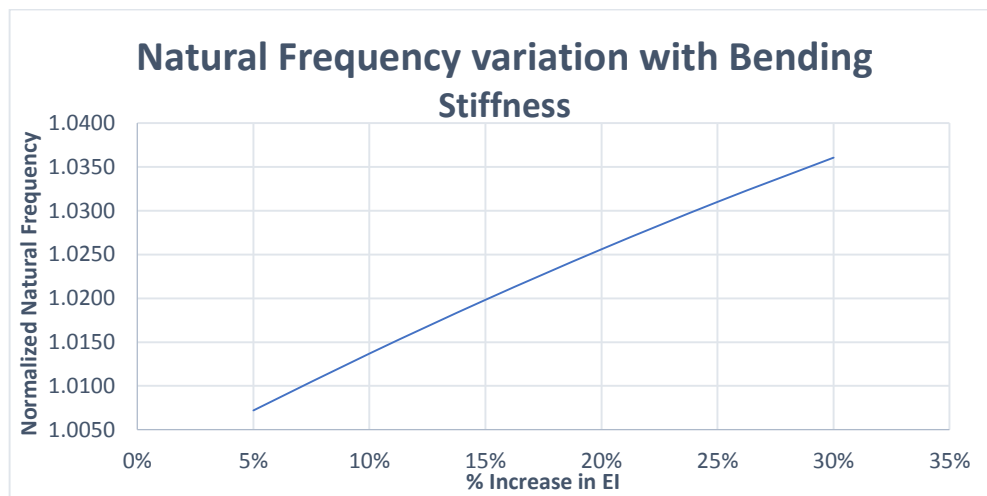


Figure 5.14: Normalized Natural Frequency variation with the Flexural Stiffness of the Upper Pile

The effect on the fundamental natural frequency of a percentage increase in the bending stiffness of the tower is shown in Table 5.15 & Figure 5.15.

Mass Increase - Upper part Monopile, %	100%	200%	300%	400%	500%
Natural Frequency, Hz	0.2771	0.2768	0.2763	0.2759	0.2755
Ratio (%)	<b>0.9989</b>	<b>0.9978</b>	<b>0.9960</b>	<b>0.9946</b>	<b>0.9932</b>

Table 5.15: Normalized Natural Frequency variation with the Mass of the Upper Pile

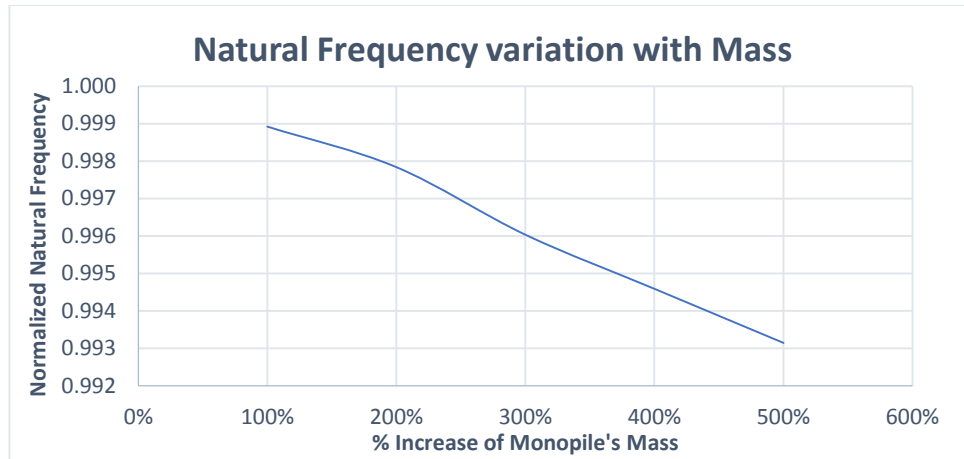


Figure 5.15: Normalized Natural Frequency variation with the Mass of the Upper Pile

It is shown, that when modelling the structure using the FDM method, using soil springs or an equivalent fixity depth does not significantly affect the estimation of the fundamental natural frequency.

### 5.3 Normal Modes of a Clamped-Free Beam – Model A

In this paragraph, the normal modes of a beam are being calculated, using the fixity depth method. In this method, the soil resistance on the embedded part of the monopile is being represented as a clamped connection at a specific depth under the seabed level. Therefore, this analysis refers to a beam with clamped-free boundary conditions. In the analysis of the structure modelled using fixity depth and soil springs, the normal modes will be used to create the modal mass and stiffness matrices which in turn will be utilized to calculate the natural frequencies of the beam.

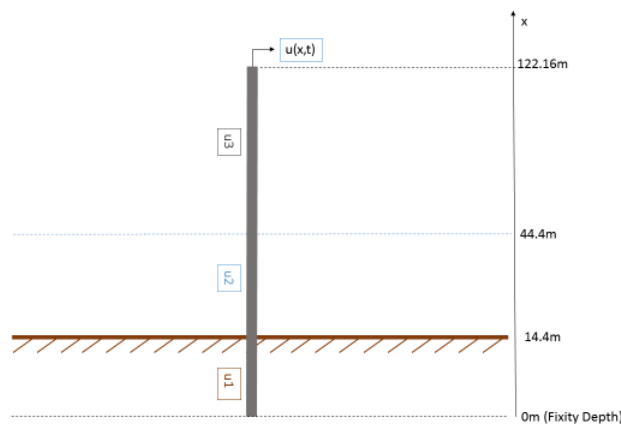


Figure 5.16: Clamped-Free Beam

First, the approximate modes will be calculated, for a structure of a constant cross-section as shown in Figure 5.16. The approximated modes refer to a structure with the same height as the one under consideration, but with the assumption that the cross-section is constant along the length and the top mass is not present. The column consists of 3 parts, each of them referring to a specific part of the structure, namely:

- Part 1: Embedded part of the monopile
- Part 2: Monopile above seabed
- Part 3: Tower

Therefore, 3 equations will be applied to determine the normal mode for each part. The three equations of motion are:

$$\rho \cdot A \cdot \ddot{u}_i + E \cdot I \cdot u_i'''' = 0 \quad (5.5)$$

For  $i = 1, 2, 3$

Where,

$\rho A$  = the mass per meter of the support structure

$EI$  = the bending stiffness per meter of the support structure

$u$  = the horizontal displacement

and,

$\ddot{u}$  = the horizontal acceleration ( $\frac{d^2u}{dt^2}$ ), as shown in the figure above

#### **Boundary Conditions**

$$u(0) = u'(0) = 0 \quad (5.6)$$

$$u''(122.16) = u'''(122.16) = 0 \quad (5.7)$$

#### **Interface Conditions**

$$u_1(14.4, t) = u_2(14.4, t) \quad (5.8)$$

$$\frac{du_1(14.4, t)}{dz} = \frac{du_2(14.4, t)}{dz} \quad (5.9)$$

$$\frac{d^2u_1(14.4, t)}{dz^2} = \frac{d^2u_2(14.4, t)}{dz^2} \quad (5.10)$$

$$\frac{d^3u_1(14.4, t)}{dz^3} = \frac{d^3u_2(14.4, t)}{dz^3} \quad (5.11)$$

and,

$$u_2(54.16, t) = u_3(54.16, t) \quad (5.12)$$

$$\frac{du_2(54.16, t)}{dz} = \frac{du_3(54.16, t)}{dz} \quad (5.13)$$

$$\frac{d^2u_2(54.16, t)}{dz^2} = \frac{d^2u_3(54.16, t)}{dz^2} \quad (5.14)$$

$$\frac{d^3u_2(54.16, t)}{dz^3} = \frac{d^3u_3(54.16, t)}{dz^3} \quad (5.15)$$

The detailed calculation of the normal modes is shown in Appendix D.

The first three normal modes have been calculated using the formulas above, and are being presented in the Figure 5.17, Figure 5.18 and Figure 5.19.

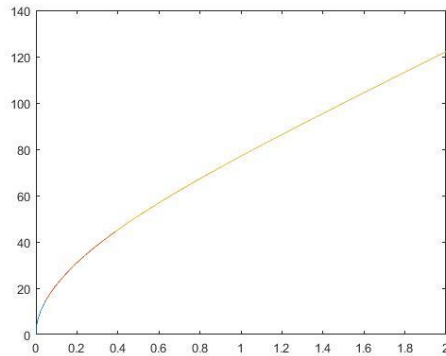


Figure 5.17: 1<sup>st</sup> Normal Mode

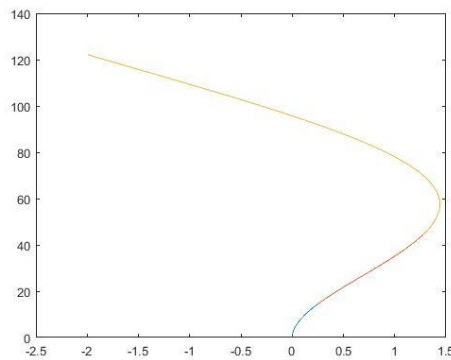


Figure 5.18: 2<sup>nd</sup> Normal Mode

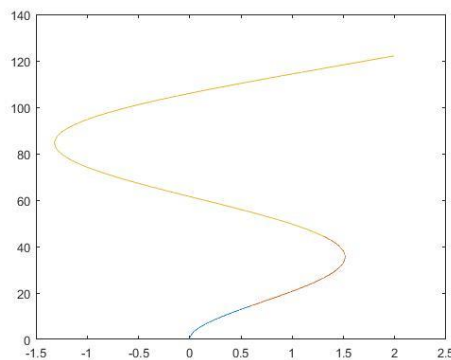


Figure 5.19: 3<sup>rd</sup> Normal Mode

Having calculated the first 3 normal modes for each part, the modal mass and stiffness matrix can be created using the integrals:

$$M_{i,j} = \int_0^{L=122.16} m(x) \cdot u_i \cdot u_j dx \quad (5.16)$$



$$K_{i,j} = \int_0^{L=122.16} E \cdot I(x) \cdot u_i'' \cdot u_j'' dx \quad (5.17)$$

Where, i,j are referring to number of modes (i,j=1,2,3).

In total 9 combinations of modes per part will be calculated. Also, the total mass and stiffness of the structure can be written as a summation of 3 integrals, each one referring to one of the three parts of the structure.

- For a structure without Top Mass

$$M_{i,j} = \int_0^{14.4} m(x) \cdot u_i \cdot u_j dx + \int_{14.4}^{44.4} m(x) \cdot u_i \cdot u_j dx + \int_{44.4}^{122.16} m(x) \cdot u_i \cdot u_j dx$$

and,

$$K_{i,j} = \int_0^{14.4} E \cdot I(x) \cdot u_i'' \cdot u_j'' dx + \int_{14.4}^{44.4} E \cdot I(x) \cdot u_i'' \cdot u_j'' dx + \int_{44.4}^{122.16} E \cdot I(x) \cdot u_i'' \cdot u_j'' dx$$

And since for the approximate modes, the mass and the stiffness is considered as a constant for the total length of the structure, the integrals can be re-written as:

$$M_{i,j} = \rho \cdot A \cdot \int_0^{14.4} u_i \cdot u_j dx + \rho \cdot A \cdot \int_{14.4}^{44.4} u_i \cdot u_j dx + \rho \cdot A \cdot \int_{44.4}^{122.16} u_i \cdot u_j dx$$

and,

$$K_{i,j} = E \cdot I \cdot \int_0^{14.4} u_i'' \cdot u_j'' dx + E \cdot I \cdot \int_{14.4}^{44.4} u_i'' \cdot u_j'' dx + E \cdot I \cdot \int_{44.4}^{122.16} u_i'' \cdot u_j'' dx$$

Calculating the stiffness and mass expressions for all the 9 possible combinations of normal modes per part, the following stiffness & mass matrices are being created.

where,

$$\rho \cdot A = 7140.85 \text{ kg (per meter length)}$$

$$E \cdot I = 5.6789 \cdot 10^{11} \text{ N} \cdot \text{m}^2 \text{ (per meter length)}$$

Calculating the stiffness and mass expressions for all the 9 possible combinations of normal modes per part, the following stiffness & mass matrices are being created (Figure 5.20 & Figure 5.21).

	1	2	3
1	3.8510e+06	-2.0348	-2.4721
2	-2.0348	1.5125e+08	-36.2391
3	-2.4721	-36.2391	1.1858e+09

Figure 5.20: Modal Stiffness Matrix

	1	2	3
1	8.7233e+05	-0.0136	-0.0429
2	-0.0136	8.7233e+05	0.0554
3	-0.0429	0.0554	8.7233e+05

Figure 5.21: Modal Mass Matrix

The three main natural frequencies have been calculated using the mass and stiffness matrices. The results, in rad/sec and Hz, are being presented in Figure 5.22 and Figure 5.23.

	1
1	2.1011
2	13.1675
3	36.8693

Figure 5.22: Natural Frequencies (rad/sec)

	1
1	0.3344
2	2.0957
3	5.8679

Figure 5.23: Natural Frequencies Hz

The natural frequencies which have been calculated using the modal mass and stiffness matrices are identical to the natural frequencies estimated graphically using Maple. Also, the exact solution for the natural frequencies, as being calculated for exactly the same structure and using the Finite Difference Method are being shown in Figure 5.24.

998	5.8189
999	2.0962
1000	0.3348

Figure 5.24: Exact Natural Frequencies – Finite Difference Method

As is being shown in the figure below, the approximated natural frequencies are almost equal to the exact ones. Therefore, the number of modes used is considered to be sufficient.

- For a structure with a Top Mass

The expressions to calculate the modal mass and stiffness matrices will be modified as follows:

$$M_{i,j} = \int_0^{14.4} m(x) \cdot u_i \cdot u_j dx + \int_{14.4}^{44.4} m(x) \cdot u_i \cdot u_j dx + \int_{44.4}^{122.16} m(x) \cdot u_i \cdot u_j dx + \int_{122.16}^{122.16} \delta(x - 131.76) \cdot M_{top} \cdot u_i \cdot u_j dx$$

and,

$$K_{i,j} = \int_0^{14.4} E \cdot I(x) \cdot u_i'' \cdot u_j'' dx + \int_{14.4}^{44.4} E \cdot I(x) \cdot u_i'' \cdot u_j'' dx + \int_{44.4}^{122.16} E \cdot I(x) \cdot u_i'' \cdot u_j'' dx$$

and for a constant cross-section along the structure's length, the expressions can be written as:

$$M_{i,j} = \rho \cdot A \cdot \int_0^{14.4} u_i \cdot u_j dx + \rho \cdot A \cdot \int_{14.4}^{44.4} u_i \cdot u_j dx + \rho \cdot A \cdot \int_{44.4}^{122.16} u_i \cdot u_j dx + M_{top} \cdot u_i(122.16) \cdot u_j(122.16)$$

$$K_{i,j} = E \cdot I \cdot \int_0^{14.4} u_i'' \cdot u_j'' dx + E \cdot I \cdot \int_{14.4}^{44.4} u_i'' \cdot u_j'' dx + E \cdot I \cdot \int_{44.4}^{122.16} u_i'' \cdot u_j'' dx$$

The stiffness and mass matrices in this case are:

	1	2	3
1	3.8510e+06	-2.0348	-2.4721
2	-2.0348	1.5125e+08	-36.2391
3	-2.4721	-36.2391	1.1858e+09

Figure 5.25: Modal Stiffness Matrix Figure

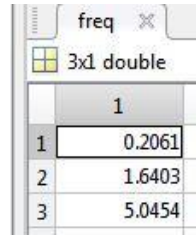
	1	2	3
1	2.2723e+06	-1.4000e+06	1.4000e+06
2	-1.4000e+06	2.2723e+06	-1.4000e+06
3	1.4000e+06	-1.4000e+06	2.2723e+06

Figure 5.26: Modal Mass Matrix

The three main natural frequencies have been calculated using the mass and stiffness matrices. The results, in rad/sec and Hz, are being presented in Figure 5.27 and Figure 5.28.

	1
1	1.2947
2	10.3065
3	31.7014

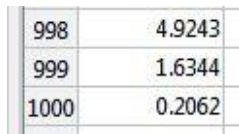
Figure 5.27: Natural Frequencies (rad/sec)



freq	
3x1 double	
1	
1	0.2061
2	1.6403
3	5.0454

Figure 5.28: Natural Frequencies (Hz)

Using the Finite Difference Method, the natural frequencies of the structure with the top mass would be:



998	4.9243
999	1.6344
1000	0.2062

Figure 5.29: Natural Frequencies (FDM –Hz)

As it is shown, the 1<sup>st</sup> natural frequency which has been calculated for the same structure using the finite difference method is almost equal to the one calculated using the eigenvalues of the modal mass & stiffness matrices. The exact values for 2<sup>nd</sup> and 3<sup>rd</sup> natural frequencies are marginally smaller. Also, using the equivalent cantilever beam method as presented in Appendix B, the resulting 1<sup>st</sup> natural frequency is equal to 0.2064 Hz. The perfect match of the results between the method which has been presented in this paragraph and the those of the equivalent cantilever beam and the finite difference method can be considered as a validation of the equations and formulas used to calculate the normal modes and the mass & stiffness matrices.

### 5.3.1 Sensitivity Analysis - Upwind Report Support Structure (varying cross-section along the length)

In this paragraph, a sensitivity analysis is being performed in order to identify the effect of the mass and the stiffness of the upper part of the monopile on the 1<sup>st</sup> natural frequency of the structure. The normal modes presented in the previous paragraph referred to a structure with constant stiffness and mass along its' length. In this analysis, the diameter of each part of the structure has been adjusted as it described in the Upwind report. The mass and stiffness of the upper part of the monopile is the variable under consideration. The equivalent model of the structure is being presented in Figure 5.30. Also the top mass of the RNA has been added to the model.

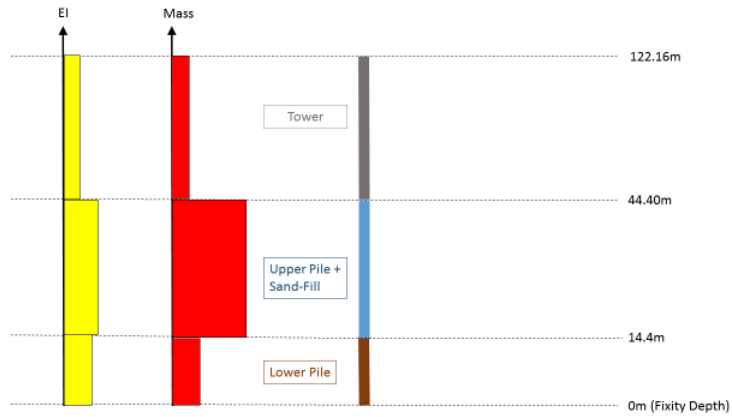


Figure 5.30: Support Structure with variable Mass & Stiffness of the Upper Monopile

Inputting the correct dimensions for each part of the support structure on the bending modes calculated using the approximate structure, the following modal mass and stiffness matrices are being created.

Mtot		Mtot{1, 1}	
Mtot{1, 1}			
	1	2	3
1	1.8816e+06	-1.3506e+06	1.4721e+06
2	-1.3506e+06	2.0616e+06	-1.1106e+06
3	1.4721e+06	-1.1106e+06	2.3252e+06

Figure 5.31: Modal Mass Matrix Upwind

Ktot		Ktot{1, 1}	
Ktot{1, 1}			
	1	2	3
1	8.6090e+06	1.4568e+07	-4.6289e+06
2	1.4568e+07	1.7806e+08	2.5889e+08
3	-4.6289e+06	2.5889e+08	1.5937e+09

Figure 5.32: Modal Stiffness Matrix Upwind

The above matrices have been used to calculate the natural frequency of the structure. The first three natural frequencies are being presented in Figure 5.33 and Figure 5.34.

freq		f
freq{1, 1}		
	1	
1	0.2712	
2	1.9417	
3	6.0218	

Figure 5.33: Natural Frequencies (Normal Modes)

98	5.0205
99	1.8308
000	0.2768

Figure 5.34: Exact Natural Frequencies (FDM)

The natural frequencies calculated by the approximated normal modes are having values of the same magnitude but are not exactly equal to the exact ones as expected.

The first analysis refers to the effect of increasing the upper pile’s mass and stiffness by 500% and 30%, respectively. This analysis has been performed also for the monopile using the FDM, so the results of both analyses will be compared. Increasing the mass of the Upper Monopile up to 500%, will lead to a decrease in the 1<sup>st</sup> natural frequency as shown in Figure 5.35.

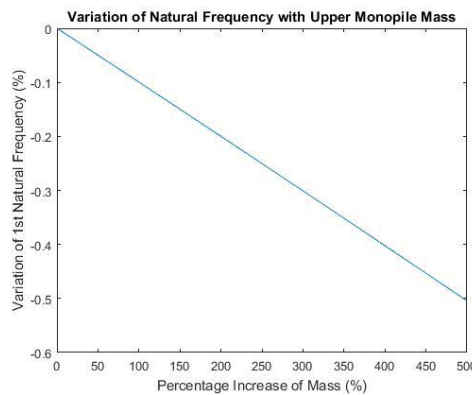


Figure 5.35: Effect of added mass on the 1<sup>st</sup> Natural Frequency

Figure 5.36, shows the effect of increasing the stiffness of the upper monopile by 1 – 30%.

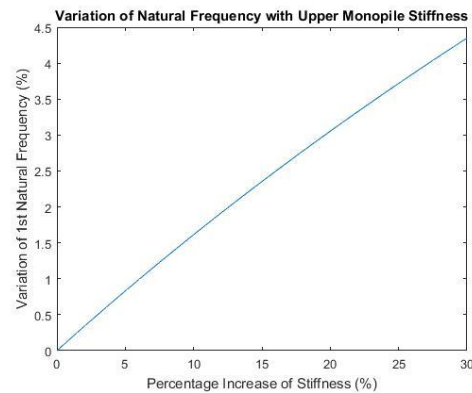


Figure 5.36: Effect of increased bending stiffness on the 1<sup>st</sup> Natural Frequency

It is shown, that increasing the bending stiffness by 30% will lead to an increase of about 4.25% in the 1<sup>st</sup> natural frequency. The analysis of the monopile presented in Upwind report has shown that for the same percentage increase, the 1<sup>st</sup> natural frequency was increased only by 3.5%. This difference can be explained because the normal modes are approximated and refer to a structure with constant diameter along its’ length. A sensitivity analysis will be performed to identify the maximum added mass along with the required additional bending stiffness in order to increase

the 1<sup>st</sup> natural frequency between 1 – 10%. Firstly, it was found that an increase of 100% in the bending stiffness would lead to an increase in the natural frequency by 10.8%.

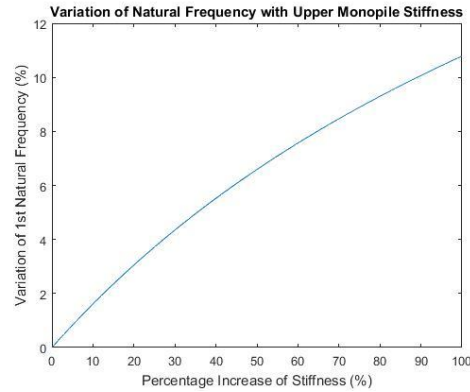


Figure 5.37: Increase of 1<sup>st</sup> Natural Frequency for an increase of  $EI$  of the Upper Monopile by 1-100%

A sensitivity analysis will be performed to identify the maximum added mass along with the required additional bending stiffness in order to increase the 1<sup>st</sup> natural frequency between 1 – 10%. In order to perform this analysis, the correlation between the added stiffness and the mass need to be specified. Assuming that the increase in the stiffness of the structure will occur by increasing the thickness of the steel pile the correlation is as follows:

In order to increase the bending stiffness by 1%, the second moment of area needs to be increased by:

$$\frac{\pi}{4} \cdot (3.05^4 - (3.05 - 0.08)^4) = 6.8551 \cdot 1.01 = 6.923651$$

Therefore, the thickness of the section should be increased to:  $t_{new} = 0.08083 \text{ m}$

This leads to a new section area of:  $A_{new} = \pi \cdot 3.05^2 - \pi \cdot (3.05 - 0.08083)^2 = 1.52848 \text{ m}^2$

Taking into consideration that the initial area of the section was equal to  $1.5130 \text{ m}^2$ , the percentage increase is equal to:  $\frac{1.52848}{1.5130} = 1.02\%$

With similar calculations, the added mass for a 1% increase in bending stiffness using concrete to fill the empty pile will be equal to 726%. For a dense sand with  $E = 50 \text{ MPa}$ , the increase 0.21% of the bending requires an increase of about 500% of the mass per meter length. In the following graphs, the bending stiffness and mass increased is assumed to be done by adding steel material and by filling the upper monopile with dense sand.

### 5.3.2 Required Minimum Stiffness and Maximum Added Mass to Increase the Natural Frequency by 1 – 10%

#### a) Increasing Stiffness with supplementary Steel

In Figure 5.38, the resultant 1<sup>st</sup> natural frequency for multiple combinations of increase in bending stiffness and mass is being presented, assuming steel as the supplementary material added to the section.

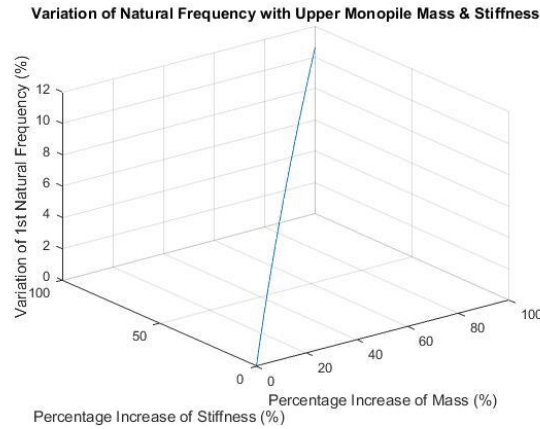


Figure 5.38: Interaction Diagram

The detailed results for the effect on the natural frequency of an increase of a bending stiffness by 1-10% are being shown in Appendix D.

In Figure 5.39, the minimum bending stiffness and the maximum added mass to achieve varying percentage increase in the natural frequency of the structure is being presented.

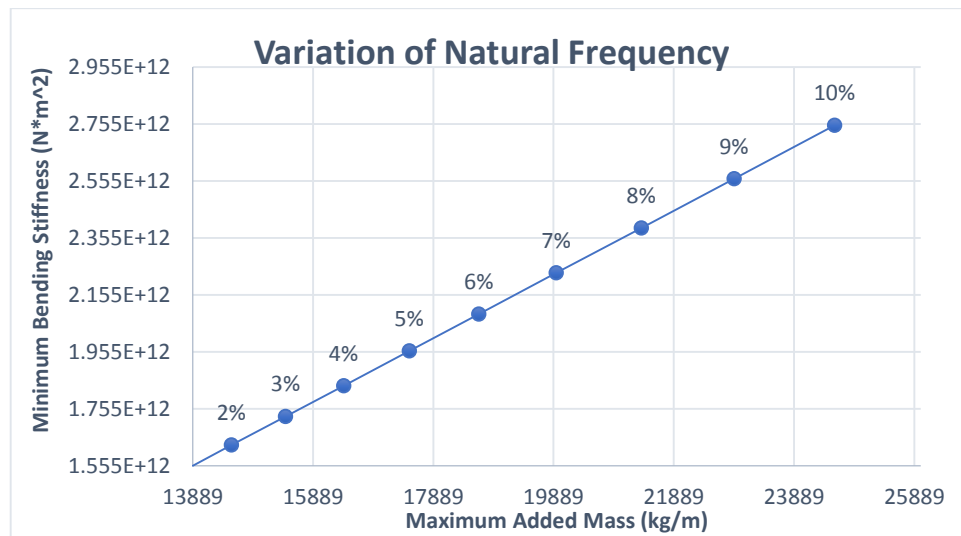


Figure 5.39: Required Minimum Bending Stiffness and Maximum Mass for varying Increase of the Natural Frequency

The variation of the natural frequency as a percentage increase of bending stiffness is being shown in Figure 5.40.



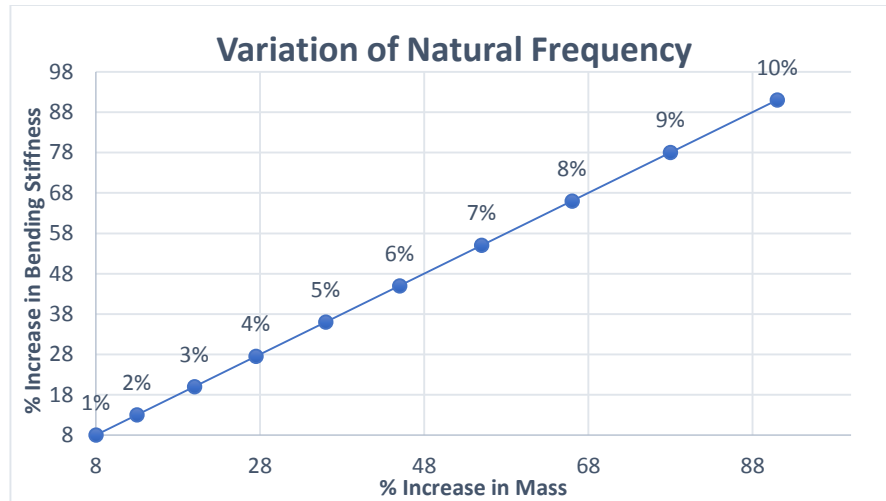


Figure 5.40: Required Added Bending Stiffness and Maximum Added Mass for varying Increase of the Natural Frequency

In order to perform this analysis a required percentage increase of the 1<sup>st</sup> natural frequency is being set. The goal it is to achieve an increase in the 1<sup>st</sup> natural frequency of the structure by 0.01 Hz (to 0.2812 Hz). This is equal to a percentage increase of 3.69%. The aim of this analysis is to determine for various mass densities the required Young modulus of the material which will be used to fill the monopile.

- Assuming a material with  $\rho = 500 \frac{kg}{m^3}$

The total mass per meter length of the upper monopile is equal to  $12860.5 + 500 \cdot 27.7117 = 26716.35 \text{ kg/m}$ . This means an increase of the mass per meter equal to 207.7%. For the given dimensions of the hollow section, an increase of 26.26% in the bending stiffness is required for an increase of 3.69% of the natural frequency as shown in Figure 5.41.

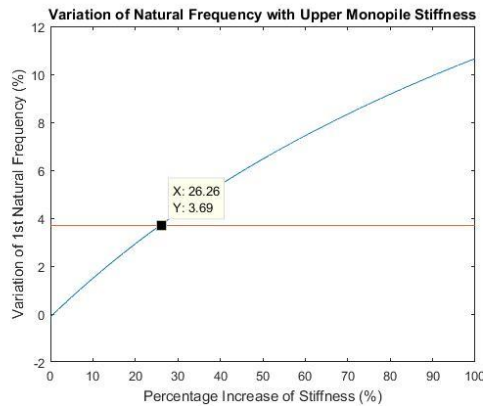


Figure 5.41: Required Bending Stiffness Increase for  $\rho = 500 \text{ kg/m}^3$

To achieve this increase in the bending stiffness, the Young Modulus of the material should be equal to:

$$1.2626 \cdot E \cdot I_{empty} = 1.8176 \cdot 10^{12} (N \cdot m^2) = 1.4396 \cdot 10^{12} + x \cdot 61.1105 \Rightarrow x \approx 6200 \text{ MPa}$$

- Assuming a material with  $\rho = 1000 \frac{kg}{m^3}$

The total mass per meter length of the upper monopile is equal to  $12860.5 + 1000 \cdot 27.7117 = 40572.2 \text{ kg/m}$ . This means an increase of the mass per meter equal to 315.5%. For the given dimensions of the hollow section, an increase of 27.27% in the bending stiffness is required for an increase of 3.69% of the natural frequency as shown in Figure 5.42.

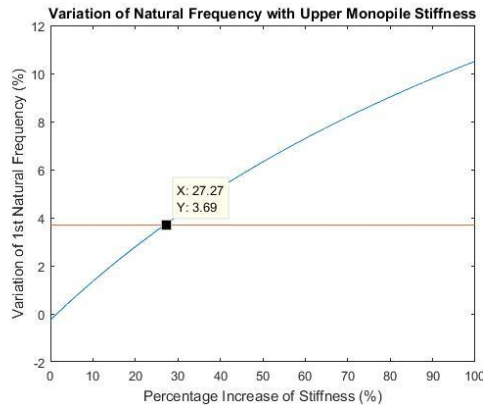


Figure 5.42: Required Bending Stiffness Increase for  $\rho = 1000 \text{ kg/m}^3$

To achieve this increase in the bending stiffness, the Young Modulus of the material should be equal to:

$$1.2727 \cdot E \cdot I_{empty} = 1.8322 \cdot 10^{12} (N \cdot m^2) = 1.4396 \cdot 10^{12} + x \cdot 61.1105 \Rightarrow x \approx 6425 \text{ MPa}$$

- Assuming a material with  $\rho = 1500 \frac{kg}{m^3}$

The total mass per meter length of the upper monopile is equal to  $12860.5 + 1500 \cdot 27.7117 = 54428.05 \text{ kg/m}$ . This means an increase of the mass per meter equal to 423.2%. For the given dimensions of the hollow section, an increase of 28.28% in the bending stiffness is required for an increase of 3.69% of the natural frequency as shown in Figure 5.43.

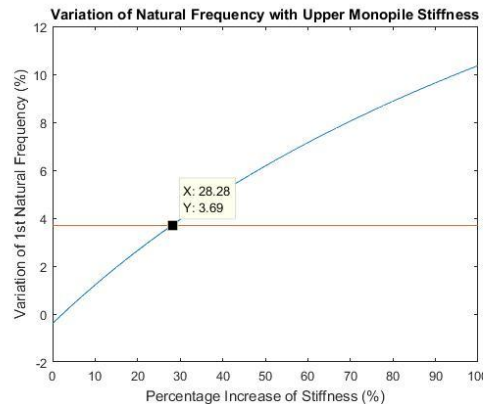


Figure 5.43: Required Bending Stiffness Increase for  $\rho = 1500 \text{ kg/m}^3$

To achieve this increase in the bending stiffness, the Young Modulus of the material should be equal to:

$$1.2828 \cdot E \cdot I_{empty} = 1.8467 \cdot 10^{12} (N \cdot m^2) = 1.4396 \cdot 10^{12} + x \cdot 61.1105 \Rightarrow x \approx 6660 \text{ MPa}$$

- Assuming a material with  $\rho = 2000 \frac{kg}{m^3}$

The total mass per meter length of the upper monopile is equal to  $12860.5 + 2000 \cdot 27.7117 = 68283.9 \text{ kg/m}$ . This means an increase of the mass per meter equal to 530.9%. For the given dimensions of the hollow section, an increase of 29.29% in the bending stiffness is required for an increase of 3.69% of the natural frequency as shown in Figure 5.44.

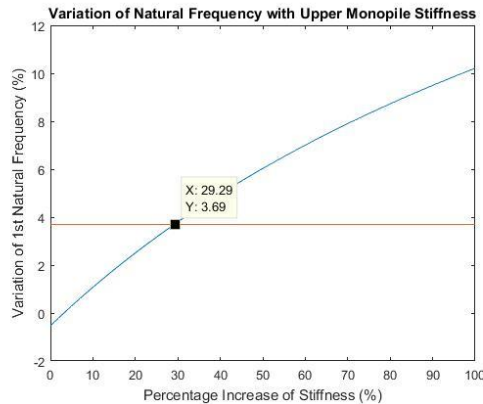


Figure 5.44: Required Bending Stiffness Increase for  $\rho = 2000 \text{ kg/m}^3$

To achieve this increase in the bending stiffness, the Young Modulus of the material should be equal to:

$$1.2929 \cdot E \cdot I_{empty} = 1.8467 \cdot 10^{12} (N \cdot m^2) = 1.4396 \cdot 10^{12} + x \cdot 61.1105 \Rightarrow x \approx 6900 \text{ MPa}$$

- Assuming a material with  $\rho = 2500 \frac{kg}{m^3}$

The total mass per meter length of the upper monopile is equal to  $12860.5 + 2500 \cdot 27.7117 = 82139.75 \text{ kg/m}$ . This means an increase of the mass per meter equal to 638.7%. For the given dimensions of the hollow section, an increase of 30.3% in the bending stiffness is required for an increase of 3.69% of the natural frequency as shown in Figure 5.45.

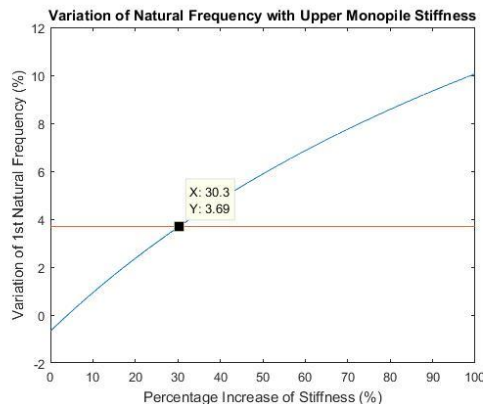


Figure 5.45: Required Bending Stiffness Increase for  $\rho = 2500 \text{ kg/m}^3$

To achieve this increase in the bending stiffness, the Young Modulus of the material should be equal to:

$$1.3003 \cdot E \cdot I_{empty} = 1.8719 \cdot 10^{12} (N \cdot m^2) = 1.4396 \cdot 10^{12} + x \cdot 61.1105 \Rightarrow x \approx 7075 \text{ MPa}$$

In Figure 5.46, the minimum value of Young Modulus required for each density of the material in order to achieve an increase of 3.69% in the natural frequency is being presented.

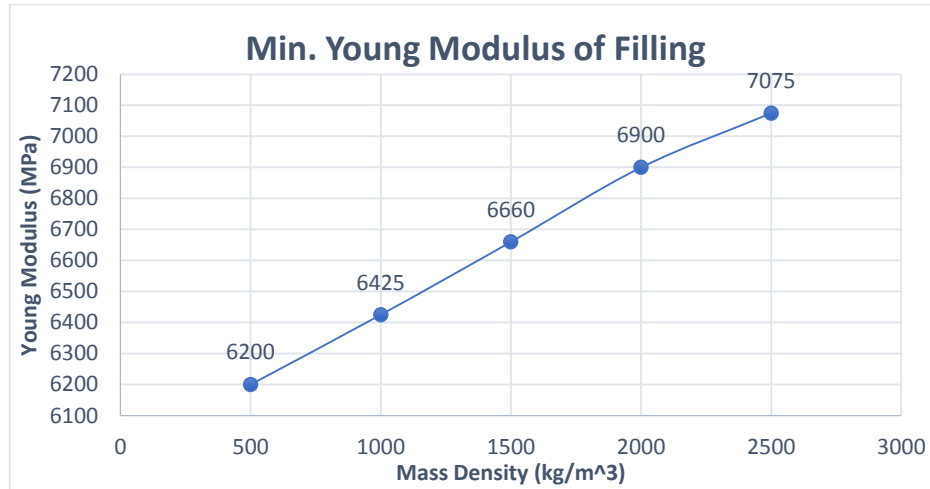


Figure 5.46: Minimum Young Modulus required for the Filling Bending Modes of Free-Free Beam – Model A

## 5.4 Normal Modes of a Free-Free Beam – Model B

In this paragraph, the normal modes of a beam, assuming free-free boundary conditions and soil springs attached to its lower part, are being calculated. The normal modes will be used to create the modal mass and stiffness matrices which in turn will be utilized to calculate the natural frequencies of the beam.

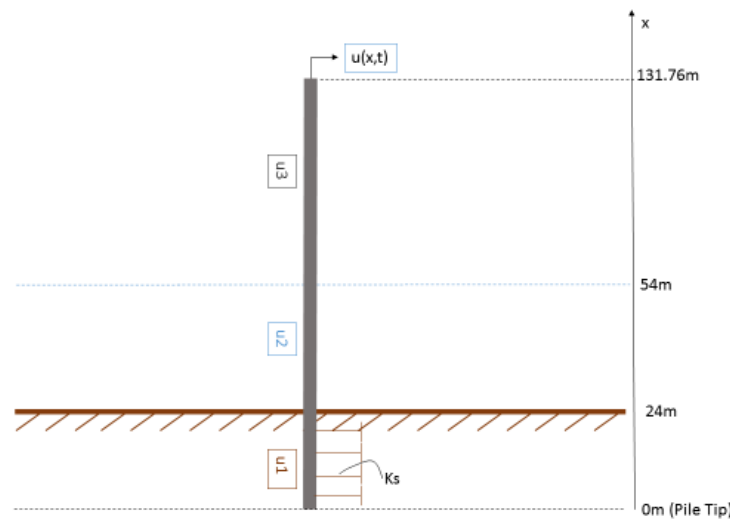


Figure 5.47: Free-Free Beam with Soil Springs

First, the approximate modes will be calculated. The approximated modes refer to a structure with the same height as the one under consideration, but with the assumption that the cross-section is constant along the length and the top mass is not present. In order to calculate the approximate modal mass & stiffness matrices, the normal modes of a column with constant cross-section/bending stiffness will be calculated (Figure 5.47). The column is considered to consist of 3 parts, each of them referring to a specific part of the structure, namely:

- Part 1: Embedded part of the monopile
- Part 2: Monopile above seabed
- Part 3: Tower

Therefore, 3 equations will be applied to determine the normal mode for each part. The three equations of motion are:

$$\rho \cdot A \cdot \ddot{u}_1 + E \cdot I \cdot u_1'''' + k_d \cdot u_1 = 0 \quad (5.18)$$

$$\rho \cdot A \cdot \ddot{u}_2 + E \cdot I \cdot u_2'''' = 0 \quad (5.19)$$

$$\rho \cdot A \cdot \ddot{u}_3 + E \cdot I \cdot u_3'''' = 0 \quad (5.20)$$

Where,

$\rho A$  = the mass per meter of the support structure

$EI$  = the bending stiffness per meter of the support structure

$u$  = the horizontal displacement

and,

$\ddot{u}$  = the horizontal acceleration ( $\frac{d^2u}{dt^2}$ ), as shown in the figure above

### **Boundary Conditions**

$$u''(0) = u'''(0) = 0 \quad (5.21)$$

$$u''(131.76) = u'''(131.76) = 0 \quad (5.22)$$

### **Interface Conditions**

$$u_1(24, t) = u_2(24, t) \quad (5.23)$$

$$\frac{du_1(24, t)}{dz} = \frac{du_2(24, t)}{dz} \quad (5.24)$$

$$\frac{d^2u_1(24, t)}{dz^2} = \frac{d^2u_2(24, t)}{dz^2} \quad (5.25)$$

$$\frac{d^3u_1(24, t)}{dz^3} = \frac{d^3u_2(24, t)}{dz^3} \quad (5.26)$$

and,

$$u_2(54, t) = u_3(54, t) \quad (5.27)$$

$$\frac{du_2(54, t)}{dz} = \frac{du_3(54, t)}{dz} \quad (5.28)$$

$$\frac{d^2 u_2(54, t)}{d_z^2} = \frac{d^2 u_3(54, t)}{d_z^2} \quad (5.29)$$

$$\frac{d^3 u_2(54, t)}{d_z^3} = \frac{d^3 u_3(54, t)}{d_z^3} \quad (5.30)$$

The detailed calculation performed to calculate the normal modes are being presented in Appendix E. The first three normal modes have been calculated using the formulas above, and are being presented in Figure 5.48, Figure 5.49 and Figure 5.50.

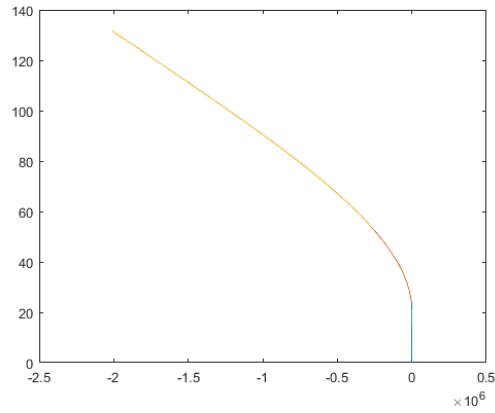


Figure 5.48: 1<sup>st</sup> Normal Mode

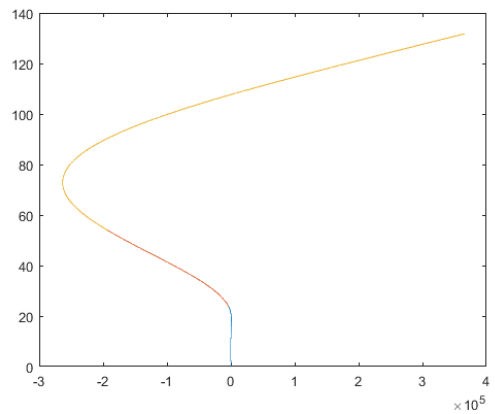
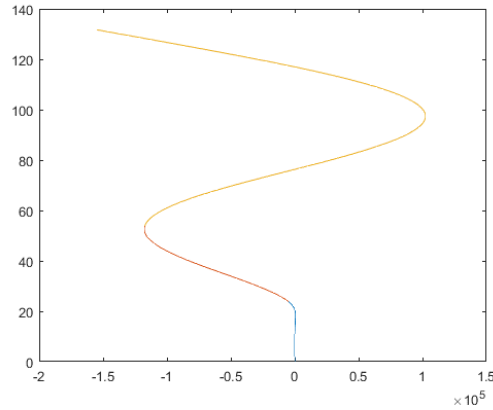


Figure 5.49: 2<sup>nd</sup> Normal Mode


 Figure 5.50: 3<sup>rd</sup> Normal Mode

Having calculated the first 6 normal modes for each part, the modal mass and stiffness matrix can be created using the integrals:

$$M_{i,j} = \int_0^{L=131.76} m(x) \cdot u_i \cdot u_j dx$$

$$K_{i,j} = \int_0^{L=131.76} E \cdot I(x) \cdot u_i'' \cdot u_j'' dx$$

where, i,j are referring to number of modes (i,j=1,2,3,4,5,6).

In total 9 combinations of modes per part will occur. Also, the total mass and stiffness of the structure can be written as a summation of 3 integrals, each one referring to one of the three parts of the structure.

- For a structure without Top Mass

$$M_{i,j} = \int_0^{24} m(x) \cdot u_i \cdot u_j dx + \int_{24}^{54} m(x) \cdot u_i \cdot u_j dx + \int_{54}^{131.76} m(x) \cdot u_i \cdot u_j dx$$

And,

$$K_{i,j} = \int_0^{24} E \cdot I(x) \cdot u_i'' \cdot u_j'' dx + \int_{24}^{54} E \cdot I(x) \cdot u_i'' \cdot u_j'' dx + \int_{54}^{131.76} E \cdot I(x) \cdot u_i'' \cdot u_j'' dx$$

And since for the approximate modes, the mass and the stiffness is considered as a constant for the total length of the structure, the integrals can be re-written as:

$$M_{i,j} = \rho \cdot A \cdot \int_0^{24} u_i \cdot u_j dx + \rho \cdot A \cdot \int_{24}^{54} u_i \cdot u_j dx + \rho \cdot A \cdot \int_{54}^{131.76} u_i \cdot u_j dx$$

and,

$$K_{i,j} = E \cdot I \cdot \int_0^{24} u_i'' \cdot u_j'' dx + E \cdot I \cdot \int_{24}^{54} u_i'' \cdot u_j'' dx + E \cdot I \cdot \int_{54}^{131.76} u_i'' \cdot u_j'' dx$$

Calculating the stiffness and mass expressions for all the 9 possible combinations of normal modes per part, the following stiffness & mass matrices are being created.

where,

$$\rho \cdot A = 7140.85 \text{ kg (per meter length)}$$

$$E \cdot I = 5.6789 \cdot 10^{11} \text{ N} \cdot \text{m}^2 \text{ (per meter length)}$$

The six main natural frequencies have been calculated using the mass and stiffness matrices. The results, in rad/sec and Hz, are being presented in Figure 5.51 and Figure 5.52.

	1
1	2.4923
2	15.3746
3	35.3296
4	80.9154
5	130.8352
6	195.0274

Figure 5.51: Natural Frequencies (rad/sec)

	1
1	0.3967
2	2.4469
3	5.6229
4	12.8781
5	20.8231
6	31.0396

Figure 5.52: Natural Frequencies Hz

The natural frequencies which have been calculated using the modal mass and stiffness matrices are almost equal to the natural frequencies estimated graphically using Maple.

- For a structure with Top Mass

The expressions to calculate the modal mass and stiffness matrices will be modified as follows:

$$M_{i,j} = \int_0^{24} m(x) \cdot u_i \cdot u_j dx + \int_{24}^{54} m(x) \cdot u_i \cdot u_j dx + \int_{54}^{131.76} m(x) \cdot u_i \cdot u_j dx + \int_{131.76}^{131.76} \delta(x - 131.76) \cdot M_{top} \cdot u_i \cdot u_j dx$$

and,

$$K_{i,j} = \int_0^{24} E \cdot I(x) \cdot u_i'' \cdot u_j'' dx + \int_{24}^{54} E \cdot I(x) \cdot u_i'' \cdot u_j'' dx + \int_{54}^{131.76} E \cdot I(x) \cdot u_i'' \cdot u_j'' dx$$

and for a constant cross-section along the structure's length, the expressions can be written as:



$$M_{i,j} = \rho \cdot A \cdot \int_0^{24} u_i \cdot u_j dx + \rho \cdot A \cdot \int_{24}^{54} u_i \cdot u_j dx + \rho \cdot A \cdot \int_{54}^{131.76} u_i \cdot u_j dx + M_{top} \cdot u_i(131.76) \cdot u_j(131.76)$$

$$K_{i,j} = E \cdot I \cdot \int_0^{24} u_i'' \cdot u_j'' dx + E \cdot I \cdot \int_{24}^{54} u_i'' \cdot u_j'' dx + E \cdot I \cdot \int_{54}^{131.76} u_i'' \cdot u_j'' dx$$

The three main natural frequencies have been calculated using the mass and stiffness matrices. The results, in rad/sec and Hz, are being presented in Figure 5.53 and Figure 5.54.

freq2	
3x1 double	
	1
1	1.5016
2	12.2015
3	37.2779

Figure 5.53: Natural Frequencies (rad/sec)

freq	
3x1 double	
	1
1	0.2390
2	1.9419
3	5.9330

Figure 5.54: Natural Frequencies (Hz)

Using the Finite Difference Method, the natural frequencies of the structure with the top mass would be:

998	5.2599
999	1.7366
1000	0.2176

Figure 5.55: Natural Frequencies (FDM – Hz)

As it is shown, the natural frequencies which have been calculated for the same structure using the finite difference method are smaller than the ones calculated using the eigenvalues of the modal mass & stiffness matrices. This difference is reasonable, since the FDM calculates the exact natural frequencies, whereas, the modal mass and stiffness matrices are approximating the real mass and stiffness of the structure, due to the fact, that the normal modes had been calculated without taking into account the presence of the top mass on the structure.

### 5.4.1 Sensitivity Analysis - Upwind Report Support Structure (varying cross-section along the length)

In this paragraph, a sensitivity analysis is being performed in order to identify the effect of the mass and the stiffness of the upper part of the monopile on the 1<sup>st</sup> natural frequency of the structure. The normal modes presented in the previous paragraph referred to a structure with

constant stiffness and mass along its' length. In this analysis, the diameter of each part the structure has been adjusted as it described in the Upwind report. The mass and stiffness of the upper part of the monopile is the variable under consideration. The equivalent model of the structure is being presented in the figure below. Also the top mass of the RNA has been added to the model.

Inputting the correct dimensions for each part of the support structure on the bending modes calculated using the approximate structure, the following modal mass and stiffness matrices are being created.

	1	2	3	4	5	6
1	1.8543e+18	-2.5378e+17	1.1240e+17	-7.3529e+16	9.8573e+16	9.0630e+16
2	-2.5378e+17	6.4094e+16	-1.7646e+16	1.5255e+16	-1.6741e+16	-1.6010e+16
3	1.1240e+17	-1.7646e+16	1.2812e+16	-4.5750e+15	8.4451e+15	7.0210e+15
4	-7.3529e+16	1.5255e+16	-4.5750e+15	6.2743e+15	-4.2548e+15	-4.9890e+15
5	9.8573e+16	-1.6741e+16	8.4451e+15	-4.2548e+15	1.0123e+16	5.3607e+15
6	9.0630e+16	-1.6010e+16	7.0210e+15	-4.9890e+15	5.3607e+15	8.0513e+15

Figure 5.56: Modal Mass Matrix Upwind

	1	2	3	4	5	6
1	1.0475e+19	3.7724e+18	1.1274e+16	-3.3258e+18	-7.3758e+18	4.4092e+18
2	3.7724e+18	6.7995e+18	3.1440e+18	2.1111e+18	-6.7477e+17	5.8040e+18
3	1.1274e+16	3.1440e+18	1.0138e+19	6.9428e+18	6.7405e+18	4.2784e+18
4	-3.3258e+18	2.1111e+18	6.9428e+18	1.9317e+19	1.6644e+19	-4.3977e+18
5	-7.3758e+18	-6.7477e+17	6.7405e+18	1.6644e+19	7.7402e+19	-3.7435e+19
6	4.4092e+18	5.8040e+18	4.2784e+18	-4.3977e+18	-3.7435e+19	1.2389e+20

Figure 5.57: Modal Stiffness Matrix Upwind

The above matrices have been used to calculate the natural frequency of the structure. The first three natural frequencies are being presented in Figure 5.58 and Figure 5.59.

	1
1	0.2822
2	2.3436
3	5.9468
4	12.3511
5	21.6135
6	34.7220

Figure 5.58: Natural Frequencies (Normal Modes)

1498	5.0000
1499	1.8442
1500	0.2775

Figure 5.59: Exact Natural Frequencies (FDM)

The natural frequencies calculated by the approximated normal modes are having values of the same magnitude but are not exactly equal to the exact ones as expected.

The first analysis refers to the effect of increasing the upper pile's mass and stiffness by 500% and 30%, respectively. This analysis has been performed also for the monopile using the FDM, so the results of both analyses will be compared. Increasing the mass of the Upper Monopile up to 500%, will lead to a decrease in the 1<sup>st</sup> natural frequency as shown in Figure 5.60.

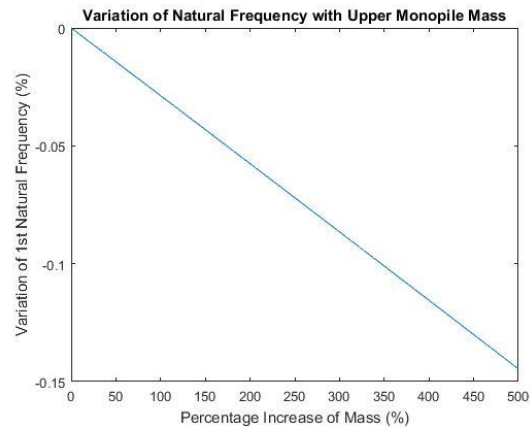


Figure 5.60: Effect of added mass on the 1<sup>st</sup> Natural Frequency

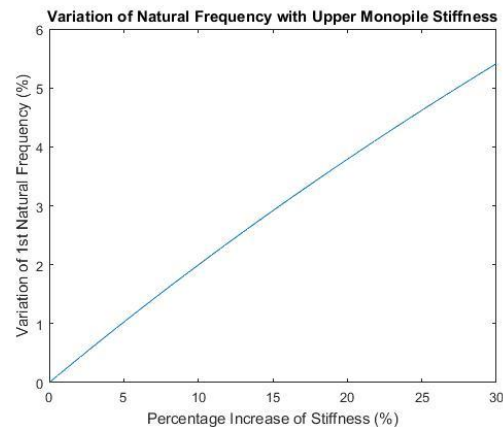


Figure 5.61: Effect of increased bending stiffness on the 1<sup>st</sup> Natural Frequency

As it is shown in Figure 5.61, increasing the bending stiffness by 30% will lead to an increase of about 5.5% in the 1<sup>st</sup> natural frequency, which is higher than the estimated increase predicted using the clamped-free model (4.25% increase). The analysis of the monopile presented in Upwind report has shown that for the same percentage increase, the 1<sup>st</sup> natural frequency was increased only by 3.5%. This difference can be explained because the normal modes are approximated and refer to a structure with constant diameter along its' length. A sensitivity analysis will be performed to identify the maximum added mass along with the required additional bending stiffness in order to increase the 1<sup>st</sup> natural frequency between 1 – 10%. Firstly, it was found that an increase of 100% in the bending stiffness would lead to an increase in the natural frequency by 13.6%.

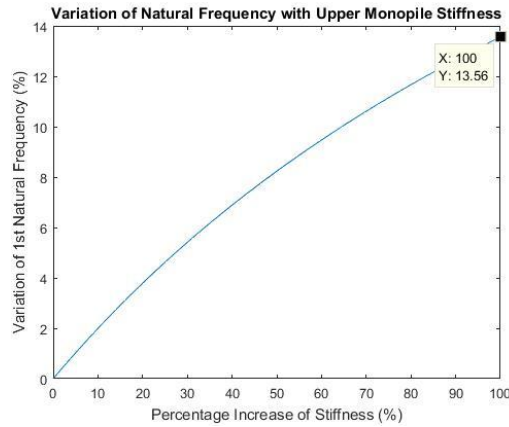


Figure 5.62: Increase of 1<sup>st</sup> Natural Frequency for an increase of EI of the Upper Monopile by 1-100%

A sensitivity analysis will be performed to identify the maximum added mass along with the required additional bending stiffness in order to increase the 1st natural frequency between 1 – 10%. In this analysis, again the additional stiffness is supposed to occur due to additional steel material on the monopile. As shown before, in order to increase the bending stiffness by 1% an increase of the mass of the pile by 1.02% is required.

#### 5.4.2 Required Minimum Stiffness and Maximum Added Mass to Increase the Natural Frequency by 1 – 10%

##### b) Increasing Stiffness with supplementary Steel

In Figure 5 63, the resultant 1<sup>st</sup> natural frequency for multiple combinations of increase in bending stiffness and mass is being presented, assuming steel as the supplementary material added to the section.

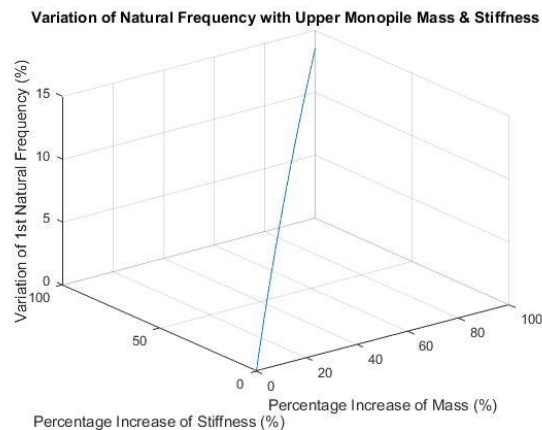


Figure 5 63: Interaction Diagram

In Figure 5.64, the minimum bending moment and the maximum added mass to achieve varying percentage increase in the natural frequency of the structure is being presented.

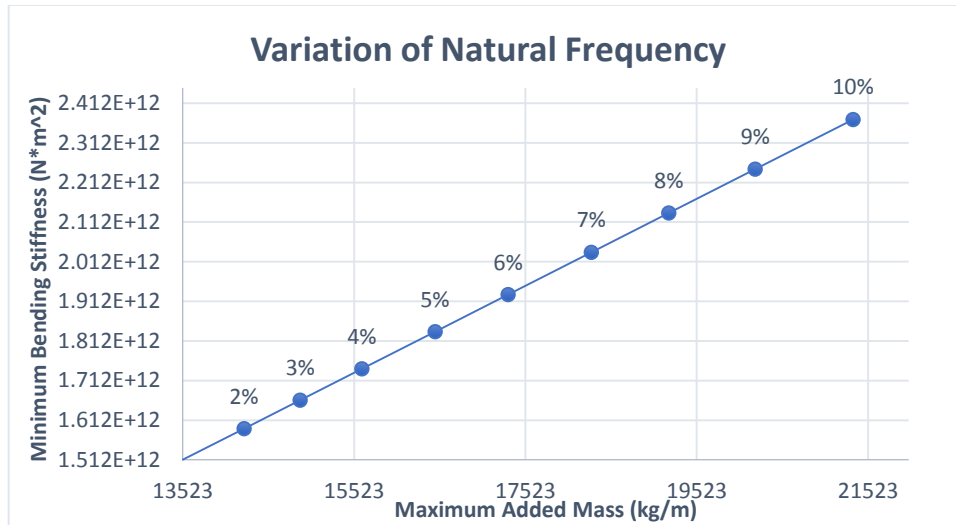


Figure 5.64: Required Added Bending Stiffness and Maximum Added Mass for varying Increase of the Natural Frequency

The variation of the natural frequency as a percentage increase of bending stiffness is being shown in Figure 5.65.

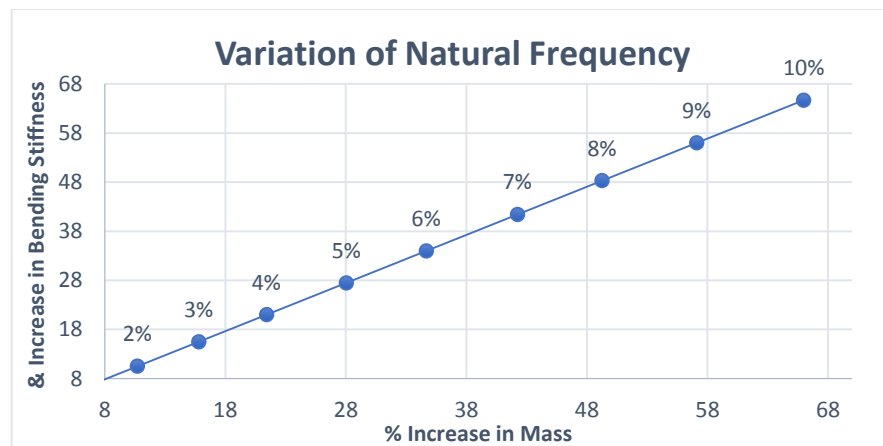


Figure 5.65: Required Added Bending Stiffness and Maximum Added Mass for varying Increase of the Natural Frequency

a) Increasing stiffness by filling the upper monopile with artificial material

In order to perform this analysis a required percentage increase of the 1<sup>st</sup> natural frequency is being set. The goal it is to achieve an increase in the 1<sup>st</sup> natural frequency of the structure by 0.01 Hz (to 0.3044 Hz). This is equal to a percentage increase of 3.40%. The aim of this analysis is to determine for various mass densities the required Young modulus of the material which will be used to fill the monopile.

- Assuming a material with  $\rho = 500 \frac{kg}{m^3}$

The total mass per meter length of the upper monopile is equal to  $12860.5 + 500 \cdot 27.7117 = 26716.35 \text{ kg/m}$ . This means an increase of the mass per meter equal to 207.7%. For the given

dimensions of the hollow section, an increase of 18% in the bending stiffness is required for an increase of 3.4% of the natural frequency as shown in Figure 5.66.

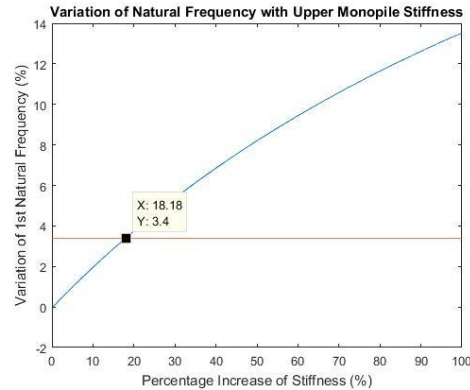


Figure 5.66: Required Bending Stiffness Increase for  $\rho = 500 \text{ kg/m}^3$

To achieve this increase in the bending stiffness, the Young Modulus of the material should be equal to:

$$1.1818 \cdot E \cdot I_{empty} = 1.8176 \cdot 10^{12} (\text{N} \cdot \text{m}^2) = 1.4396 \cdot 10^{12} + x \cdot 61.1105 \Rightarrow x \approx 4300 \text{ MPa}$$

- Assuming a material with  $\rho = 1000 \frac{\text{kg}}{\text{m}^3}$

The total mass per meter length of the upper monopile is equal to  $12860.5 + 1000 \cdot 27.7117 = 40572.2 \text{ kg/m}$ . This means an increase of the mass per meter equal to 315.5%. For the given dimensions of the hollow section, an increase of 18.18% in the bending stiffness is required for an increase of 3.4% of the natural frequency as shown in Figure 5.67.

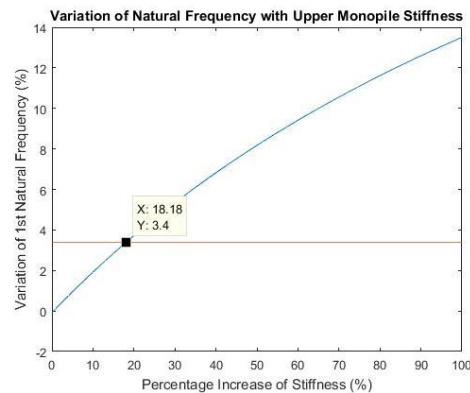


Figure 5.67: Required Bending Stiffness Increase for  $\rho = 1000 \text{ kg/m}^3$

Again, the required Young Modulus is approximately equal to 4300 MPa

- Assuming a material with  $\rho = 1500 - 2500 \frac{\text{kg}}{\text{m}^3}$

Again, an increase of 18.18% in the bending stiffness is required for an increase of 3.4% of the natural frequency as shown in the figure below. This result is reasonable since according to figure 2.20, a variation of the added mass from 1 – 500% affects the 1<sup>st</sup> natural frequency only by about

0.15%. Therefore, the required Young Modulus in any case is equal to 4300 MPa. It is shown that modelling the structure using soil springs, which at the same time, leads to placing the “support” closer to the upper part of the monopile, shows a higher effect of the added stiffness on the fundamental natural frequency. This result can be explained, by the fact that adding stiffness closer to the support of the structure, has a higher effect on the total stiffness of the structure.

*Page intentionally left blank*



## 6. Effect of the Sand-fill on the Damping Ratio

### 6.1 Estimation of the Damping Ratio of a monopile

This chapter focuses on the effect of the sand-fill on the rate at which the amplitude of a free damped vibration decreases. The method used to calculate the decay rate is called the logarithmic decrement method. The application of this method to calculate the damping ratio of a wind support structure application has been presented by Daamsgard et al. [11] and by Carswell et al. [28]. Carswell [28], performs a free vibration analysis in order to estimate the damping ratio of the structure. In this publication an initial displacement of 0.10m has been applied on the top of the monopile, and then the structure is let free to vibrate at each own natural frequency. The amplitude of the initial vibration applied is of high importance, since previous experiments [29] have revealed a dependency between the damping ratio and the amplitude of the dynamic excitation. More specifically, higher amplitudes can lead to bigger damping ratios, therefore, the initial displacement should be realistic for the given structure. Therefore, Carswell has chosen to impose an initial displacement of 0.1m, which “falls in the middle of the range of tower top displacements found during the stochastic time history analysis” [28]. Since the monopile presented in the given project has many similarities with the aforementioned one, the majority of the simulations have been performed assigning an initial displacement of 0.10 m at the top of the structure. Also, an initial displacement of 0.05m, 0.2m, 0.3m and 0.4m have been tested, in order to estimate the damping ratio in the case of the installation of a smaller or bigger wind turbines on the same structure (bigger rotor diameter leads to higher thrust force and thus to bigger displacements of the top of the monopile).

#### 6.1.1 Logarithmic Decrement Method

The initial displacement of 0.10m and the free vibration response is being shown in Figure 6.1 [28].

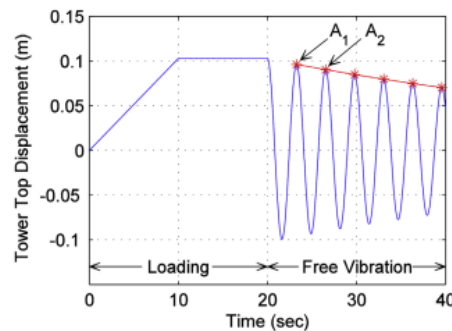


Figure 6.1: Initial Displacement and Free Vibration Test [28]

The logarithmic decrement ( $\delta$ ) of the response is being calculated by the following formula:

$$\delta = \frac{1}{n} \cdot \ln \left( \frac{A_1}{A_n} \right) \quad (6.1)$$

where,

$A_1$  and  $A_n$  = amplitude of two successive peaks

$n$  = number of cycles between the peaks

Having calculated  $\delta$ , the damping ratio ( $\xi$ ) can be evaluated by the formula:

$$\xi = \frac{1}{\sqrt{1 + \left(\frac{2 \cdot \pi}{\delta}\right)^2}} [2] \approx \frac{\delta}{2 \cdot \pi} \text{ for } \delta \ll 1 [11] \quad (6.2)$$

Alternatively, the value of  $\xi$ , can be determined by adjusting the exponential part of the general solution for the response of a damped system under free vibration:

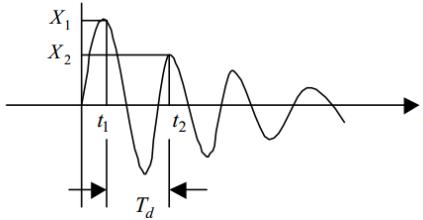


Figure 6.2: Response of Damped Free Vibration

$$X_1 = A \cdot e^{-\xi \cdot \omega_n \cdot t} \cdot \cos(\omega_d \cdot t - \varphi) \quad (6.3)$$

where,

$A$  = the Amplitude of the response along the longitudinal axis ( $x$ )

$\omega_n$  = the undamped natural frequency of the structure

$\phi$  = phase angle

$\omega_d$  = the damped natural frequency of the structure which is equal to [30]:

$$\omega_d = \omega_n \cdot \sqrt{1 - \xi^2} \quad (6.4)$$

$\omega_n$  = the undamped natural frequency of the structure

The latter approach was applied in order to estimate the damping ratio of the structure.

## 6.2 Components of Damping for an Offshore Monopile

Damgaard et al [11] suggest that the total energy dissipation for an offshore monopile is due to:

- Material damping of the monopile and the tower
- Aerodynamic damping (only when the rotor operates)
- Viscous hydrodynamic damping and damping created from wave radiation. The first one is considered to negligible due to the small relative velocities between the monopile and the and the waves [11]
- Soil induced damping

In this project, focus is given on the soil induced damping and on the damping due to the presence of sand-fill in the monopile. The rotor is considered to be parked, and the water damping which for a similar structure [11] is estimated about 0.12% is being neglected, since this damping depends on the radiation of the waves around the monopile, and the monopile's outer diameter does not vary with the presence of sand-fill. Therefore, is being omitted in the sensitivity analysis,

since it has a constant value in both cases. This assumption is valid, since the total damping of a structure is considered to be a “linear combination of independently modeled damping sources” [28]. The logarithmic decrement value for the material damping of both the monopile and the tower is equal to,  $\delta=0,012$  (in accordance with EN1991-1-4 [31]). This yields a material damping ratio of approximately 0.19%. This material damping has been added on the model developed in Plaxis 3D in the form of Rayleigh Damping. The soil damping is considered to have the maximum contribution on the total damping of the system, when the rotor is stopped [11]. Also, Damgaard et al. suggest, that the soil damping consists of material and geometric damping, but in the case of frequency below 1 HZ, the geometric damping can be neglected [11]. In this thesis project the focus is on the response of the structure mainly on its’ first two natural frequencies, which are smaller than the 1Hz threshold (1<sup>st</sup> natural frequency  $\approx 0.3$  Hz), therefore, this assumption is valid also for this project, since the free vibration test is performed by an excitation which enables the 1<sup>st</sup> normal mode of the structure.

### 6.3 Soil Damping

As mentioned in the previous paragraph, even though soil damping consists of material damping and geometric damping, only the material damping is of high importance for the case under consideration. Therefore, the analysis that follows focuses only on the hysteretic material damping from the soil and the sand-fill. The material damping of the soil is related to the energy dissipated during the loading and unloading of the soil. Hysteretic loops correspond to a cyclic application of a given load, which in turn corresponds to a specific level of shear strains in the soil. A simplistic representation of a hysteretic loop due to periodic loading applied on a single degree of freedom system is being shown in Figure 6.3 [28].

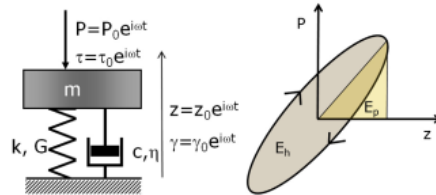


Figure 6.3: Potential Energy and Energy loss in a Hysteretic Loop

where,

$$E_h = 4 \cdot \pi \cdot E_p \cdot D \quad (6.5)$$

where,

$E_p$  = elastic strain energy (for all the elements of the soil)

$E_h$  = total hysteretic energy (for all the elements of the soil)

$D$  = Damping ratio

A most usual representation of hysteretic curves for soils is given by Darendeli [32] (Figure 6.4).

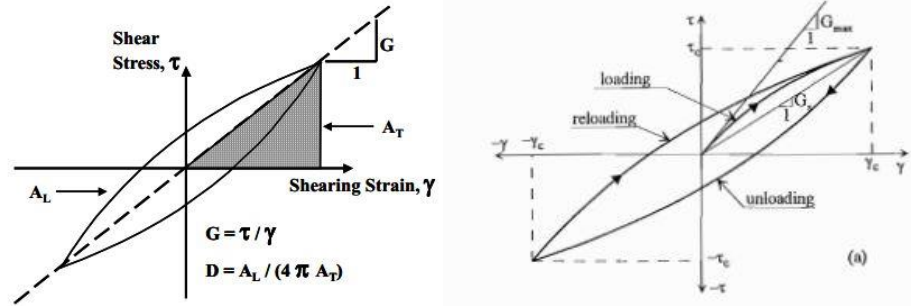


Figure 6.4: Potential Energy and Energy loss in a Hysteretic Loop

Obviously, as shown also in the p-y curves for soil, the strains vary along the length of the monopile, and consequently, the shear strength and the corresponding damping is also variable along the length. A graphic representation of the variation of the shear strength and the damping ratio with the shear strains is being shown in Figure 6.5.

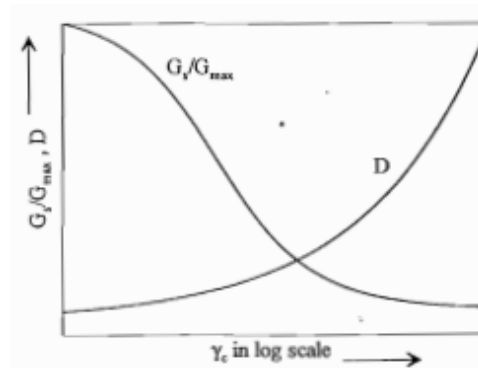


Figure 6.5: Typical Representation of Shear Strength and Damping Ratio Variation with Shear Strains [33]

## 6.4 Parameters Affecting Shear Strength-Strain Relation

In order to identify the damping effect due to the hysteretic behavior of the sand-fill, relevant shear strength-strain curves which have been created using experimental results are being used. Darendeli [32] executed a significant number of experiments on different type of soils and identified the effect of various parameters on the hysteretic behavior of them. For his experiments Combined Resonant Column and Torsional Shear (RCTS) equipment has been used. Firstly, he identified the main parameters which may affect the nonlinear behavior of soil. Then, he estimated each parameter's effect, depending on the type of soil. The results of his analysis are being summarized in Table 6.1.

Parameter	Impact on Normalized Modulus Reduction Curve	Impact on Material Damping Curve
Strain Amplitude	***	***
Mean Effective Confining Pressure	***	***
Soil Type and Plasticity	***	***
Number of Loading Cycles	* <sup>+</sup>	*** <sup>++</sup>
Frequency of Loading (above 1 Hz)	*	**
Overconsolidation Ratio	*	*
Void Ratio	*	*
Degree of Saturation	*	*
Grain Characteristics, Size, Shape, Gradation, Mineralogy	*	*

\*\*\* Very Important      <sup>+</sup> On competent soils included in this study  
 \*\* Important              <sup>++</sup> Soil Type Dependent  
 \* Less Important

Table 6.1: Parameters which Affect Nonlinear Behavior of Soil and their Relative Importance

As shown Table 6.1, the strain amplitude, mean effective confining pressure, the type of soil and its' plasticity are the parameters which mainly control the nonlinear behavior of any type of soil. The number of loading cycles' influence depends on the type of soil and the frequency of loading is of medium importance, and mainly relevant for frequencies of excitation above 1 Hz. These observations are being presented in detail in the following paragraphs and also compared with the results available by other researchers, when possible. This analysis is being presented in the following paragraphs.

### 6.4.1 Effect of Shear Strain Amplitude

The qualitative effect of shear strains on the decrease of the normalized shear strength and the consequent effect on the damping has been presented in Figure 6.6. The shear strain magnitude determines the behavior of soil, as linear elastic, nonlinear elastic and plastic material. A graphic representation is presented in Figure 2.6 [32].

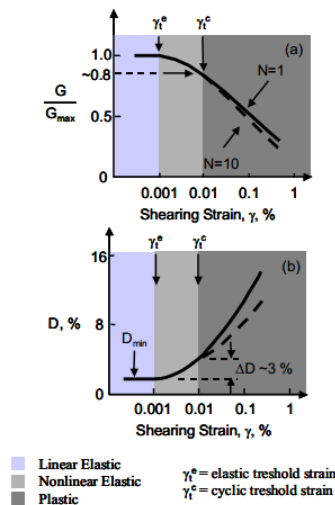


Figure 6.6: Strain Dependent Behavior of Soil

Where,

$G$  = Shear Strength of Soil

$G_{\max}$  = Maximum Shear Strength of Soil ( $G_{\max}$ )

$D$  = Damping Ratio

For very small strains ( $\leq 0.001\%$ ) the soil behaves linearly, therefore during a loading/unloading cycle no energy dissipation occurs, leading to a constant low value of damping. For strains between  $0.001$ - $0.01\%$ , the soil has a nonlinear elastic behavior, which enhances the damping effect (increase by approximately 3% comparing to the initial damping of the soil). For strains higher than  $0.01\%$ , the soil's normalized shear strength decreases drastically, and the rate of increase of the soil damping reaches its maximum value.

### 6.4.2 Effect of Effective Confining Pressure

The effect of the effective confining pressure on the shear strength/damping for a silty sand, as measured by Darendeli [32], is being shown in Figure 6.7.

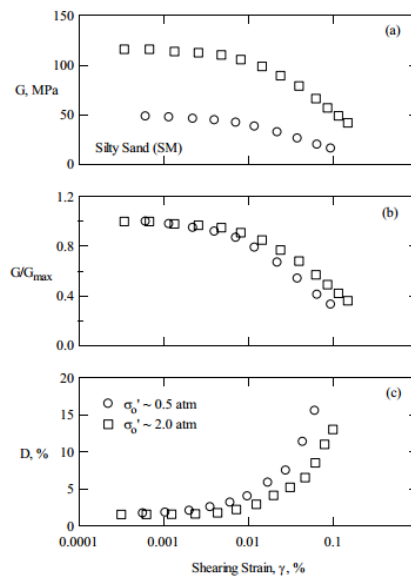


Figure 6.7: Effect of Effective Confining Pressure for sands

As shown in Figure 6.7, increasing the effective confining pressure has low effect on the normalized shear strength/damping curves at the linear and nonlinear elastic thresholds. For higher strains the normalized shear strength decreases drastically with a simultaneous increase on the damping. Similar effect on the normalized shear strength of a sand (Toyoura sand) has been identified by Oztoprak et al., through their analysis of a laboratory test database [33] (Figure 6.8). The behavior of sand in the latter report was identified through Cyclic Loading Triaxial Tests (CLTxT).

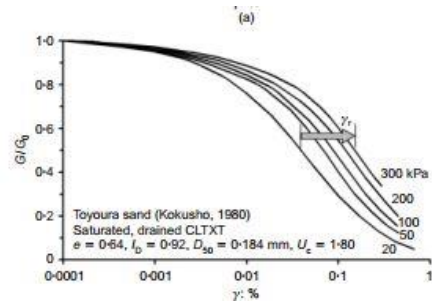


Figure 6.8: Effective Confining Pressure Effect on Toyoura (silica) Sand (Oztoprak)

The effect of confining pressure for Toyoura Sand was also investigated by Kokusho [34], showing again similar effect with Oztoprak’s and Darendeli’s result (Figure 6.9).

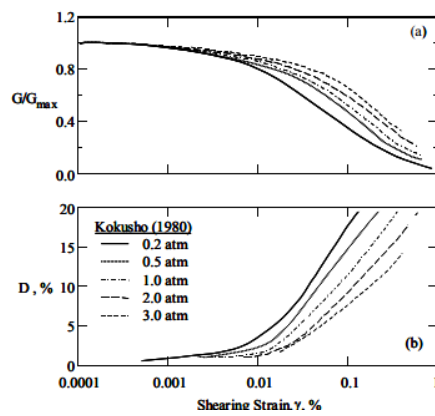


Figure 6.9: Effect of Confining Pressure on Sand

### 6.4.3 Effect of Soil Type & Plasticity Index

The effect of soil type is being shown in the normalized shear strength comparison between silty sand and sandy lean clay [32] (Figure 6.10)

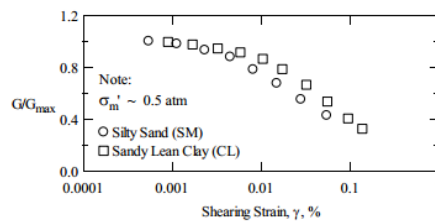


Figure 6.10: Effect of the Soil Type on the Normalized Shear Strength (Darendeli)

Curves which demonstrate a similar effect of the type of soil on the normalized shear strength and the material damping has been created by Vucetic & Dobry [35] and Ishibashi & Zhang [36].

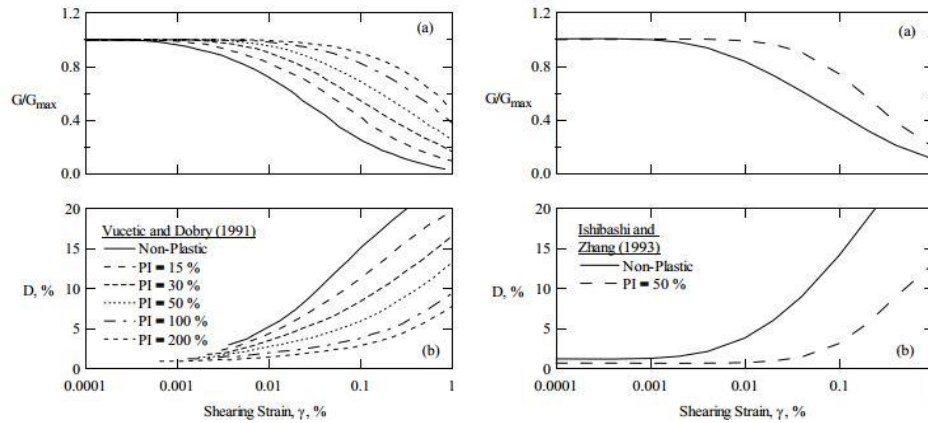


Figure 6.11: Effect Of Soil Plasticity on the Normalized Shear Modulus and Material Damping (Left-Vucetic, Right-Ishibashi)

Figure 6.11 clearly demonstrates the higher material damping of sands in comparison with soils with higher Plasticity Index (PI). Feyissa [37], also performed experiments to measure the effect of the Plasticity Index (PI), and his experimental data demonstrated damping ratio of soil with low PI is higher.

#### 6.4.4 Effect of Number of Cycles

Darendeli shown that for silty sands the effect of number of cycles on the shear strength of a silty sand is very low (Figure 6.12) [32].

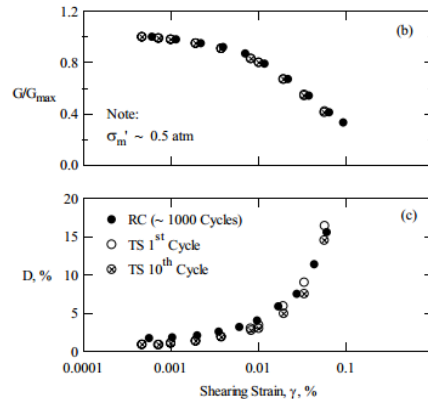


Figure 6.12: Effect of Number of Cycles in Normalized Shear Strength and Damping (%)

On Figure 6.12, the effect of the number of cycles on the nonlinear behavior is being shown for two different types of tests, namely, Resonant Column (RC) and Torsional Shear (TS) tests. It is shown that the highest impact of the number of cycles is during the first 10 cycles. Also it is shown that the effect on damping is higher than the effect on the shear strength, on which the effect is almost insignificant. The effect of number of cycles on Toyoura sand has been also investigated by Lanzo et al. [38]. In order to investigate the nonlinear behavior, Double Specimen Direct Shear tests (DSDSS) were performed on Toyoura sand. Their research shown that the number of cycles of loading has no impact on both the normalized shear strength and on the material damping for low strains. For medium strains, they identified an effect only on material damping, and the effect was significant only during the first 10 cycles. For high strains ( $\gamma \geq 0.027\%$ ), the shear strength



marginally decreases, while the material damping drops significantly between the 1<sup>st</sup> and the 10<sup>th</sup> cycle (Figure 6.13).

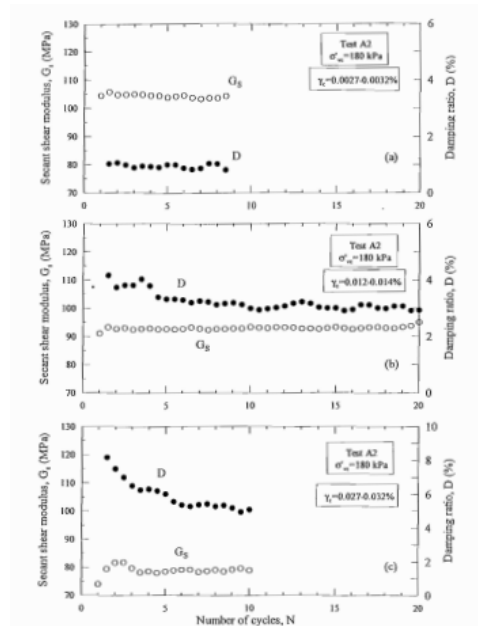


Figure 6.13: Effect of Cycles in Shear Strength and Material Damping of Toyoura Sand (Lanzo) [37]

Another publication by Jafarzadeh et al. [39] which is based on the results of experimental data acquired by Cyclic Simple Shear (CSS) tests on sand, have shown that the number of cycles for a Babolsar sand affect the shear stress during the first 80 circles, and then the shear stress is almost constant for the 20 more loading circles applied on the soil.

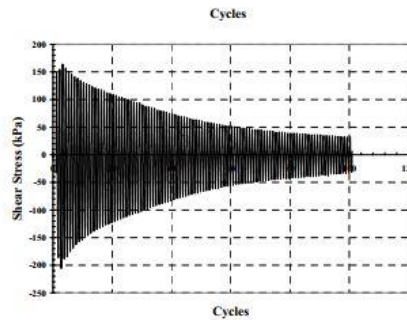


Figure 6.14: Effect of Number of Loading Cycles on Shear Stress [38]

Their test results diverge from the findings of [32] and [38], but their tests had been performed by the application of a load with a high frequency of excitation (1-15 Hz), whereas, Darendeli performed his tests using a frequency of 1 HZ, while Lanzo et al., tested the Toyoura sand on frequencies between 0.04 – 1 Hz. This variation in the results is in line with Darendeli’s [32] observation that the effect of the number of cycles on shear strength and damping ratio is overwhelmed by the frequency of excitation.

### 6.4.5 Effect of the Frequency of Excitation

The effect of the frequency of excitation on the shear strength & on the damping ratio for sand and clay is being shown in

Figure 6.15.

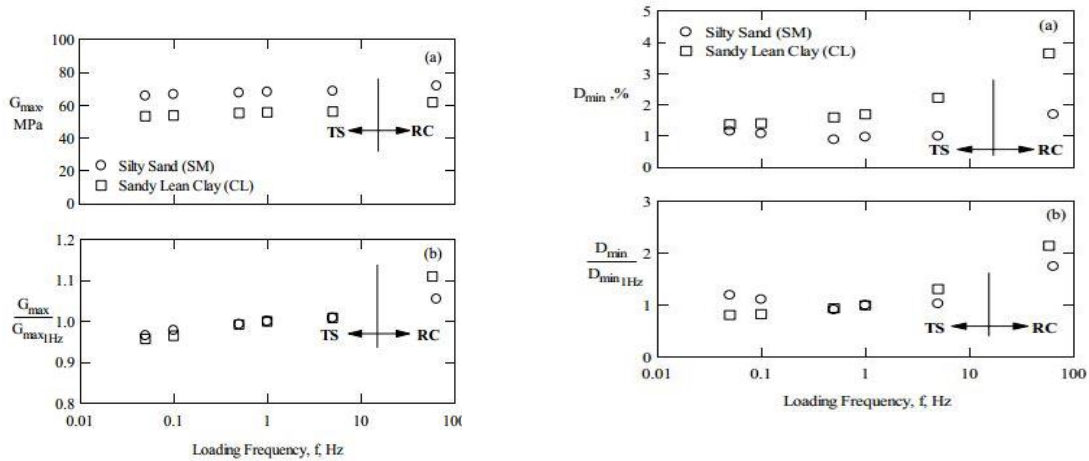


Figure 6.15: Effect of Loading Frequency on Shear Strength & Damping Ratio for Sand and Clay (32)

As shown in

Figure 6.15, the effect of the loading frequency of the damping ratio for a sand is minimal for low frequencies of excitation is insignificant. Similar trend was observed by Stokoe et al. [40] as shown in Figure 6.16.

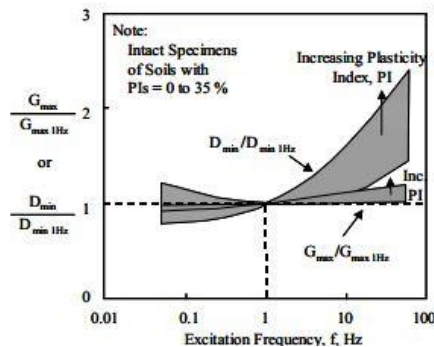


Figure 6.16: Effect of Frequency of Excitation on Shear Strength And Damping Ratio (Stokoe)

More specifically, for the frequency range of 0.02-1Hz (which corresponds to the 1<sup>st</sup> and 2<sup>nd</sup> natural frequency of the structure), [38] has shown that the stress strain loop is almost identical for a silica sand.

## 6.5 Model in Plaxis 3D for Free Vibration Analysis

### 6.5.1 Modelling the Structural Elements

For the creation of the model in Plaxis 3D, the rule of symmetry has been applied to model half of the structure and the soil and reduce the computational time (Figure 6.17).

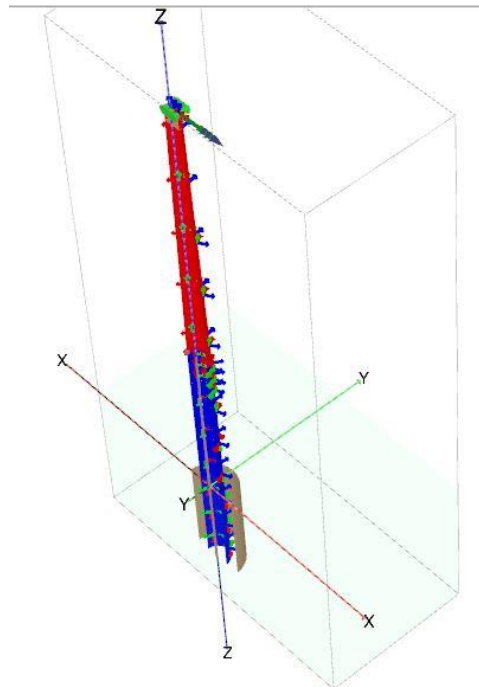


Figure 6.17: Model Created in Plaxis using Symmetry

The monopile and the tower parts were designed using plate elements, with the characteristics shown in Table 6.2.

	Length (m)	Diameter (m)	Thickness (m)	Self Weight (kN/m <sup>3</sup> )
<b>Monopile</b>	63.76	6.1	0.08	83.39
<b>Tower</b>	68	6.1 - 4.0 (Var.)	0.03	83.39
<b>RNA Mass (Dummy Plate)</b>	N/A	4	1	273.2

Table 6.2: Dimensions of Plate Elements

The tower has the exact dimensions described in Upwind [32]. The monopile described in Upwind report has a constant diameter until 11.4 m below MSL and then its' diameter and thickness varies to accommodate the assembly of the transition piece on top of it. Since the connection between the monopile and the transition piece is out of the scope of this project, the monopile (for simplicity in the geometry) was designed having a constant diameter and thickness along its' length, equal to the weighted average for each of the parameters. For both the monopile and the tower, a density of 8500 kg/m<sup>3</sup>w was used (83.39 kN/m<sup>3</sup>) as in all analyses in the previous chapters. Also, the transition piece was omitted in this analysis, therefore the monopile's length was extended up to the position where the top of the transition piece is located in the original report. In that way, the total length of the structure remained the same. The total length is a significant parameter when estimating the natural frequency and the free vibrations of the structure because it affects the total distance of the concentrated RNA mass from the support and also the exact location where the stiffness and mass per meter of the structure is located. The RNA mass was applied on a "dummy" plate with a radius of 2 m and a thickness of 1 m. On the

symmetrical model only half of the 350 tonnes mass is applied. This mass was distributed per  $m^2$  on the plate element, with a magnitude of:

$$Mass/m^2 = \frac{350 \cdot 9.81}{2 \cdot \left(\frac{\pi \cdot 2^2}{2}\right) \cdot 1} = 273.2 \frac{kN}{m^2}$$

## 6.5.2 Modelling the Soil

The soil was modelled in Plaxis using the HS Small model. The initial model for the surrounding soil corresponds to a dense sand, as used for the analysis presented in Chapter 4. The difference between the soil model used in the static analysis for the p-y curves and the dynamic analysis is the application of HS Small Model instead of the Hardening Soil Model. This model takes into account the higher stiffness for soils when deformed with small shear strains. In comparison with HS soil, it requires also the initial shear strength modulus ( $G_0$ ) and the shear strain which corresponds to a normalized reduction of the shear strength by 28.8% [43]. Comparing to the HS model the HS Small model also includes the following properties of soils under dynamic loading [41]:

- The very stiff behaviour at low strains
- The reduction of the stiffness on higher strains
- The energy dissipation due to the hysteretic behaviour of the soil

In order to evaluate the damping effect on the system, due to the presence of sand-fill, relevant shear strength/strain reduction curves should be used. The analysis presented in paragraphs 6.4.1 - 6.4.5 has shown that the curves used to model the hysteretic behaviour of the sand fill should have been produced by experimental data referring to similar effective confining pressure and soil type, whereas, the effect of the number of cycles and the effect of frequency of excitation (for the frequencies under consideration) are of low importance. Strength reduction curves for sand, which fulfil the aforementioned requirements have been created by Lanzo [38]. Considering the monopile fully filled with sand and with the dimensions shown in Table 6.2, the mean effective confining pressure at the seabed (using the soil properties presented by Lanzo [38]) is being shown in Table 6.3.

Toyoura Sand Properties / Mean Effective Stress		
Maximum Void Ratio ( $e_{max}$ )	97.5	%
Minimum Void Ratio ( $e_{min}$ )	56	%
Average Void Ratio ( $e_{avg}$ )	59	%
Relative Density (RD)	0.93	%
$\gamma$ (saturated sand)	20.5	kN/m <sup>3</sup>
$\phi$	40	degrees
K0	0.36	
$\sigma_{zz, effective}$ (mean)	314.64	kPa
$\sigma_{xx, effective}$ (mean)	112.4	kPa
$\sigma_m$ (mean effective pressure)	179.81	kPa

Table 6.3: Mean Effective Pressure [38]

Since the mean effective pressure is approximately 180 kPa, but this corresponds to the lowest level of the soil column in the monopile (seabed level), a mean effective confining pressure of 90-100 kPa can be supposed in order to estimate the maximum shear strength Figure 6.18.

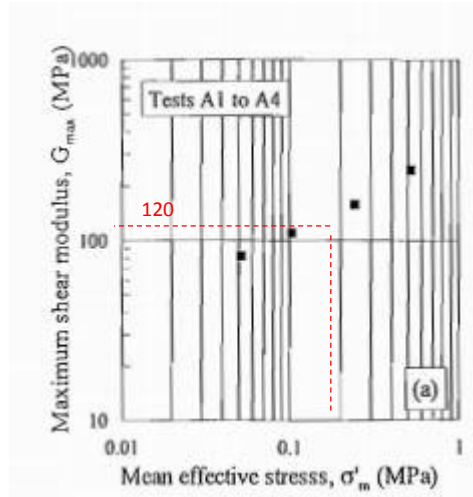


Figure 6.18: Shear Strength/Strain Reduction Curve

From Figure 6.18, the maximum shear modulus, for a mean shear strain of 100kPa, is approximately 120 MPa. From the same figure it can be shown that for a mean effective stress of 180 kPa, the shear strength is about 147 MPa. The validity of the results obtained graphically have been also verified by Giang et al [42]. Giang et al suggest an empirical equation for the estimation of the strain shear modulus as a function of the void ratio ( $e$ ) and the mean effective confining pressure ( $p'$ ). The formula which they suggest is:

$$G_{max} = A \cdot F_e \cdot \left( \frac{p^i}{p_a} \right)^n \quad (6.6)$$

where,

$$F_e = B \cdot \left( \frac{\alpha - e}{1 + e} \right)^2 \quad (6.7)$$

The values of A, B and n are found graphically as shown in Figure 2.18 [42] (for a Coefficient of Uniformity ( $C_u$ ) equal to 1.3 [38])

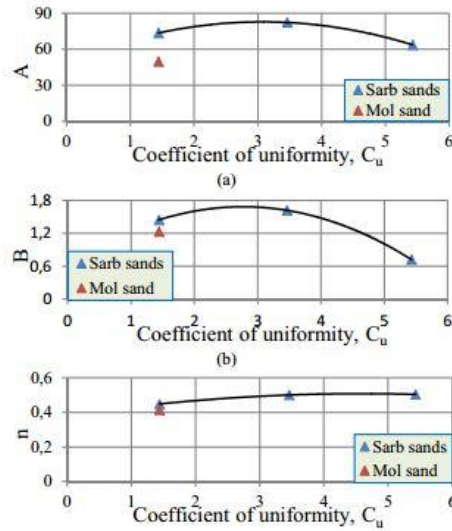


Figure 6.19: Values of A, B and n for Empirical Formula

The shear modulus for a fully filled monopile for a dense (Toyoura) sand is shown in Table 2.4.

Shear Modulus ( $G_{max}$ )		
<b>A</b>	50,00	
<b>B</b>	1,20	
<b>N</b>	0,41	
<b>Pa</b>	100,00	kPa
<b>E</b>	0,59	% [12]
<b>F(e)</b>	2,30	
<b>Gmax</b>	146,11	Mpa

Table 6.4: Maximum Shear Modulus Toyoura Sand

As shown in Table 6.4, the maximum shear strength obtained by the empirical solution are in agreement with the results obtained graphically. The shear strain which corresponds to a reduction of about 30% in shear strength is approximately equal to 0.021%, obtained graphically again by Figure 6.20.

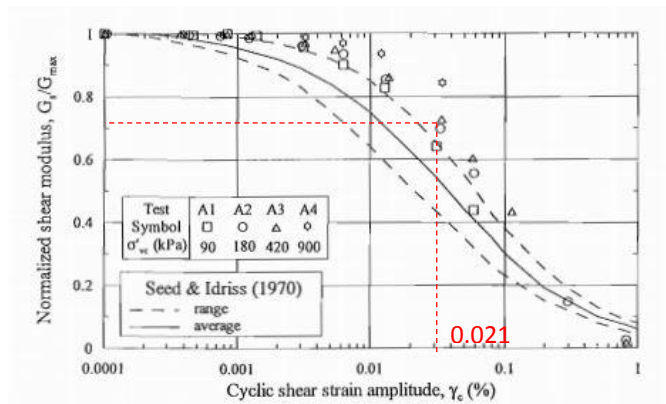


Figure 6.20: Normalized Shear Modulus variation with Strain (Toyoura Sand)

Graphically, the value obtained for  $\gamma_{0.7}$  is approximately 0.02%. The above values have been verified by the equations which correspond to the evaluation of the aforementioned parameters for sand by Brinkgreve et al. [43]. The proposed formulas are based on the relative density of sand and are the following:

$$G_0 = 60000 + 68000 \cdot \frac{RD}{100} \tag{6.8}$$

$$\gamma_{0.7} = \left(2 - \frac{RD}{100}\right) \cdot 10^{-4} \tag{6.9}$$

The formulas above are valid for a reference effective confining pressure of 100 kN/m<sup>2</sup> and a Poisson’s ratio of  $\nu=0.2$ , which are both valid for this analysis. Inputting the target initial shear strength in the first formula, the corresponding relative density is being determined. Then, the value of the reference shear strain is  $\gamma_{0.7} = 0.0207$ , and the corresponding curves created in Plaxis are shown in Figure 6.21.

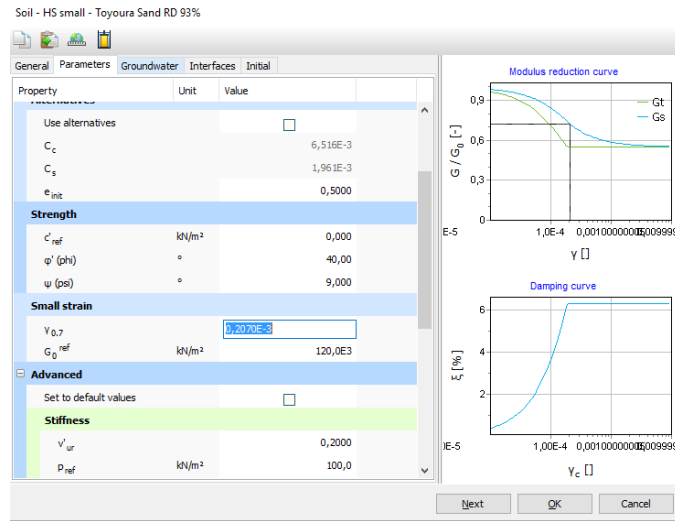


Figure 6.21: Normalized Shear Strength and Damping Curves Plaxis 3D

The values of all the necessary input parameters for the sand-fill, calculated using the formulas presented in [43], are being shown in Table 6.5. In the same table, the same parameters needed to model the surrounding soil (dense sand) are being presented.

Input Parameters for HSSmall Soil	$E_{50}$ (kN/m <sup>2</sup> )	$E_{oed}$ (kN/m <sup>2</sup> )	$E_{ur}$ (kN/m <sup>2</sup> )	$\phi$ (degrees)	$\psi$ (degrees)	Rf	$\gamma_{0.7}$ (%)	$G_0$ (kN/m <sup>2</sup> )
<b>Toyoura Sand (Sand Fill)</b>	52940	52940	158300	40	9	0.8897	0.0207	120000
<b>Dense Sand (Soil)</b>	60000	60000	180000	40.5	10.5	0.875	0.01	128000

Table 6.5: Input Parameters for Sand-Fill (Toyoura Sand) and Surrounding Soil (Typical Values: Very Dense Sand)

### 6.5.3 Model Size

In the horizontal direction the boundaries are located at a distance of 12D from the centerline of the monopile. The soil depth is equal to 36m, so that the bottom line of the model is located at a distance of 2D below the pile toe. The total model size was chosen, such as, it has a relatively small size, but at the same time it does not affect the deformation of the soil and the structure, as described by Fonseca A.C.V. [44].

#### 6.5.3.1 Maximum Element Size

For dynamic analysis the maximum element size and time step need to be determined. The maximum element size should be smaller than the length of the shear wave propagating for each soil layer and structural element [45].

$$Max\ Element\ Size_{layer} \leq \frac{V_{s,layer}}{5 \cdot f_{max}} \quad (6.10)$$

where,

$$V_{s,layer} = \sqrt{\frac{G}{\rho}} \quad (6.11)$$

and

G is the shear strength of the soil layer

$\rho$  is the density of the soil layer

and the maximum frequency  $f_{max}$  is the maximum of:

- The natural frequency of the soil deposit
- The natural frequency of the structural elements
- The frequency of the input signal

The two fundamental frequencies of the structure have been calculated using the relevant Matlab script. The two fundamental frequencies of the soil are being calculated using the formula:

$$f_n = \frac{V_s \cdot (2 \cdot n - 1)}{4 \cdot H} \quad (6.12)$$

where, “n” is the number of natural frequency under consideration.

The natural frequency of the structure and the soil layers are being shown in Table 6.6.

Element	1 <sup>st</sup> Natural Frequency	2 <sup>nd</sup> Natural Frequency
Structure	0.2775	1.844
Soil Deposit	1.715	5.144
Sand-Fill	2.213	6.638

Table 6.6: 1<sup>st</sup> & 2<sup>nd</sup> Fundamental Frequencies of Each Element

To determine the maximum allowable element size, the biggest natural frequency will be used. Therefore, the maximum element size for the soil deposit, the sand-fill and the structure are being shown in Table 6.7.



Element	G <sub>max</sub> (MPa)	γ (kN/m <sup>3</sup> )	Soil Depth (m)	Shear Wave Velocity (m/sec)	Max. Element Size (m)
Soil Deposit	128	20,6	36	247	28,8
Sand-Fill	120	20,4	30	266	24

Table 6.7: Maximum Allowable Element Size for Each Layer

Due to the high shear strength of the dense soil and sand-fill, the maximum allowable element size is large.

### 6.5.3.2 Maximum Time Step – Dynamic Analysis

In order to perform a dynamic analysis in Plaxis, the maximum time step needs to be estimated. Estimating the time step will be used to input the time of steps needed for any given duration used for the dynamic analysis. The maximum time step is given by the formula [45]:

$$\Delta_{t,max} \leq \frac{Element\ Size}{V_s \cdot \sqrt{\frac{2 \cdot (1 - \nu)}{1 - 2 \cdot \nu}}} \quad (6.13)$$

where, “ν” is the Poisson’s ratio

Since the element size calculated is larger than even the default element size for “Very Coarse” mesh option in Plaxis 3D, the default element size of Plaxis will be used in the sensitivity analysis which will be shown in the following paragraphs. The simulation time will be equal to 35 secs, in order that the simulation will run for approximately 10 circles, as suggested in the literature [32], [38]. The maximum time step allowed for each layer is shown in Table 6.8.

	Element Type	Max Element Size (Very Coarse Mesh) (m)	Max Element Size (Medium Mesh) (m)	Max Element Size (Very Fine Mesh) (m)
Max Element Size (m)	Soil Deposit	8.3	4.15	2.07
	Sand-Fill	8.3	4.15	2.07
Max Time Step (sec)	Soil Deposit	0.021	0.1	0.0051
	Sand-Fill	0.019	0.1	0.0048
Min Number of Steps	Soil Deposit & Sand-Fill	1830	3659	7318

Table 6.8: Maximum Time Step & Minimum Number of Steps for Free Vibration Analysis

### 6.5.4 Optimization of the Model in Plaxis 3D

In order to estimate the effect of the size of the mesh on the damped natural frequency and damping ratio of the structure, six mesh settings have been tested. These settings are being shown in Figure 6.22. The simulations were performed imposing a static displacement on the top of the tower and then measuring the varying displacement with time of a node at the top, as the structure vibrates freely.

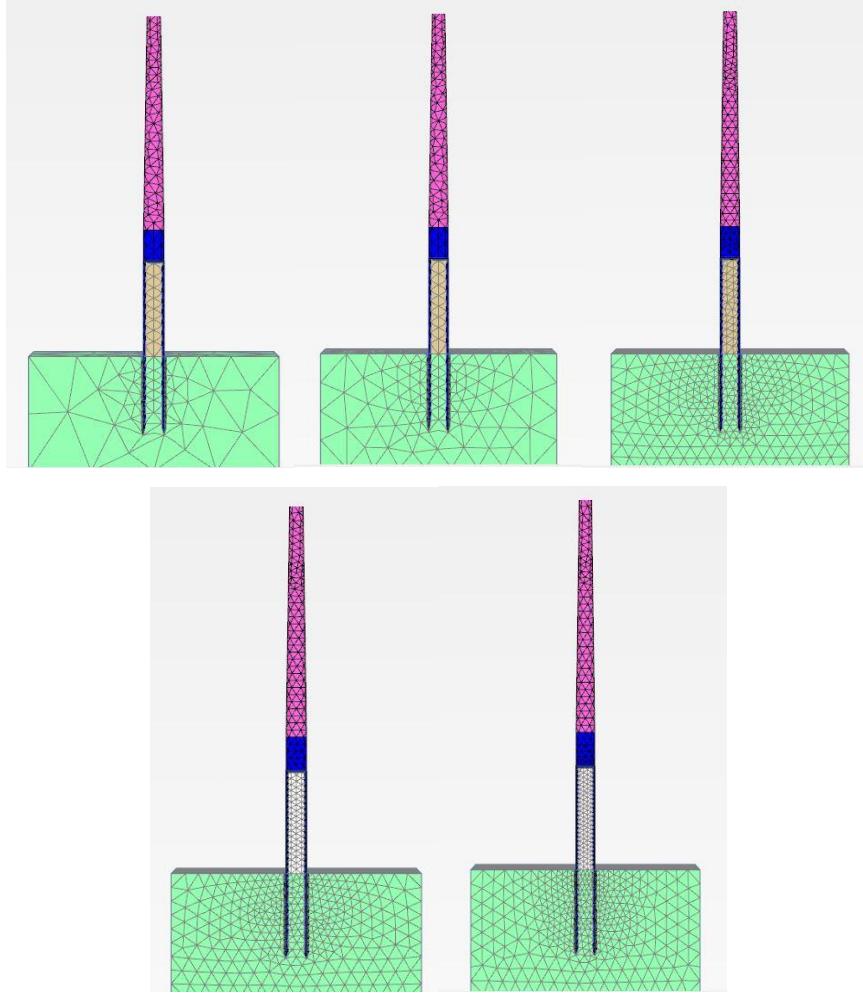


*Figure 6.22: Various Mesh Settings Tested. From Top Left to Bottom Right: Very Coarse, Medium, Very Fine, Very Fine (Enhanced Element Size on Sand-Fill), Very Fine (Further Enhanced Element Size on Sand-Fill), Very Fine (Enhanced Element Size on Sand-Fill and around the Monopile)*

The results of the sensitivity analysis performed are being shown in Figure 6.23.

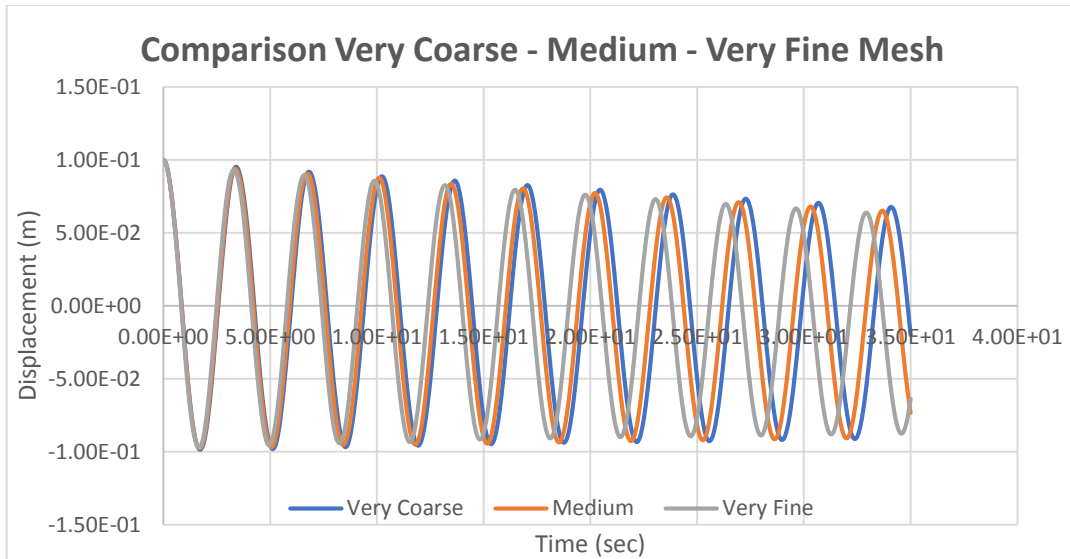


Figure 6.23: Variation of Natural Frequency & Damping Ratio with Mesh

As shown in Figure 6.23, during the first two cycles, there is almost no difference independently of the detail level of the mesh, and the effect becomes visible only after the 3<sup>rd</sup> circle of displacement. Moreover, it is shown that decreasing the element size, results to a higher zero-crossing period, thus to a lower fundamental natural frequency. Moreover, as the element size increases, the hysteretic damping of the sand fill is not fully captured, leading to a lower damping ratio for the structure. Further enhancing the mesh locally (more detailed mesh for the sand-fill) increased the simulation time significantly without any significant variation on the measured natural frequency and damping ratio (this simulation was performed for a loose soil deposit and loose sand-fill, as it will be presented in the following paragraphs).

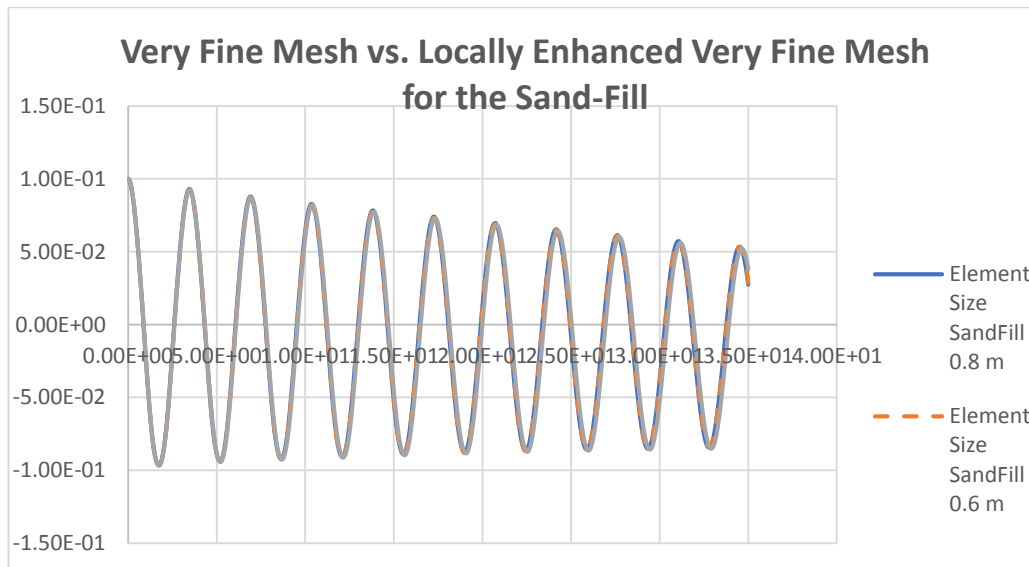


Figure 6.24: Effect of Locally Enhanced Mesh on Natural Frequency & Damping Ratio

Further enhancing the mesh for the sand-fill and for the soil around the monopile is shown in Figure 6.25.

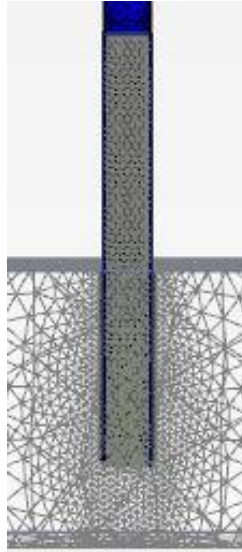


Figure 6.25: Very Fine Mesh – Enhanced Elements in Sand-Fill and Soil Surrounding the Monopile

The further enhancement of mesh led to the results presented in Figure 6.26.

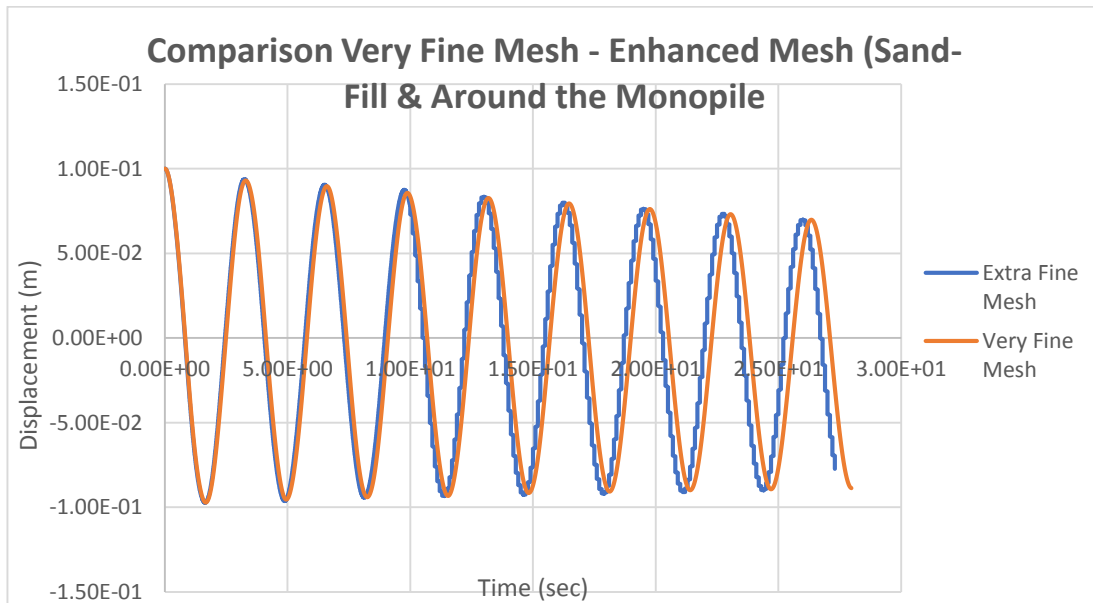


Figure 6.26: Effect of Locally Enhanced Mesh (Sand-Fill & Monopile) on the Natural Frequency & Damping Ratio

Creating a mesh with constant shape of the elements to model the sand-fill and the soil surrounding the monopile led to a small decrease in the natural frequency and an insignificant change on the damping ratio. The natural frequency calculated with the optimized mesh is the most accurate one, but the computational times increased by 10 times. Therefore, the very fine mesh option of Plaxis (Element Size of 2.07 m.) will be used further in the analysis.

### 6.5.4.1 Number of Cycles

In order to verify the variation of hysteretic damping of the sand-fill with increasing number of cycles a comparison between an empty and a sand-filled monopile's response will be compared (Figure 6.27).

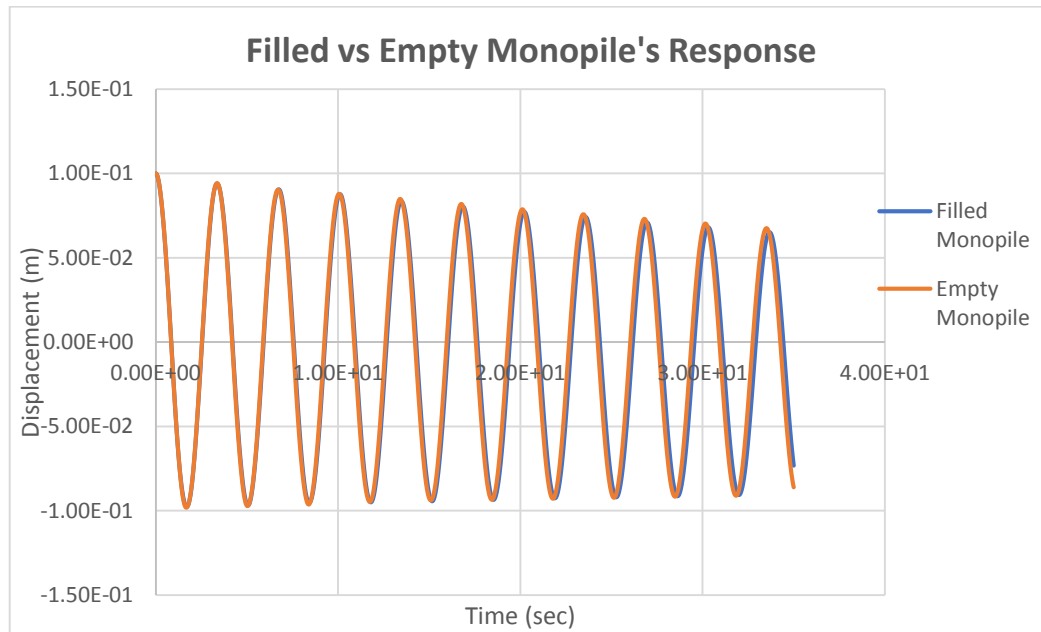


Figure 6.27: Response of a Sand-Filled and an Empty Monopile

As shown in Figure 6.27, for the initial 3 circles of displacement, there is almost no effect of the sand-fill's damping on the structure. After the 3<sup>rd</sup> circle the hysteretic damping of the sand-fill increases, leading to an increase of the total damping ratio and a decrease on the damped natural frequency of the structure.

### 6.5.4.2 Effect of Density of the Surrounding Soil and the Sand-Fill on the Structure's Response

In order to identify the effect of the density of soil to the structural response, free vibration tests have been simulated, using sand of varying density. Only sand was taken into consideration in the free vibration simulations. The damping induced in the system when adding clay in the monopile could be investigated and compared with sand in future research work. However, the total damping induced to the system when sand is used is higher comparing to clay, as shown in Figure 6.11.

## 6.6 Methodology

The methodology used in the sensitivity analysis is summarized in the following steps:

- The time history of the horizontal displacement of the structure for varying densities for the surrounding soil (loose, medium and dense sand) and for an empty monopile has been recorded. The properties of the loose and medium sand for the HSSmall soil are being taken by the literature [38, 43]. The properties of the dense (Toyoura) sand are as shown in Table 6.3. The collective table with all the sand properties used in the simulations are shown in Table 6.9.

<b>Input Parameters for HSSmall Soil</b>	<b>E50 (kN/m<sup>2</sup>)</b>	<b>Eoed (kN/m<sup>2</sup>)</b>	<b>Eur (kN/m<sup>2</sup>)</b>	<b>φ (degrees)</b>	<b>ψ (degrees)</b>	<b>Rf</b>	<b>γ 0.7 (%)</b>	<b>G0 (kN/m<sup>2</sup>)</b>
<b>Loose Sand</b>	15000	15000	45000	31.1	1.1	0.969	0.018	77000
<b>Medium Sand</b>	30000	30000	90000	34.3	4.3	0.938	0.015	94000
<b>Toyoura Sand (Sand-Fill)</b>	52940	52940	158300	40	9	0.8897	0.0207	120000
<b>Dense Sand (Surrounding Soil)</b>	60000	60000	180000	40.5	10.5	0.875	0.01	128000

Table 6.9: Soil Properties for Sensitivity Analysis

- For all the tested densities of the surrounding sand, the monopile was filled with sand of varying a density (Table 6.9). The same values for loose and medium sand have been used for both the sand-fill and the surrounding soil. The values of dense sand presented by [38] are used to simulate the dense sand-fill. Free vibration simulations were executed the displacement has been recorded
- The analytical solution has been used, in order to identify the fundamental natural undamped/damped frequency of the structure. However, if the analytical solution's curve is drawn on the same graph with the response curve calculated in Plaxis the curve cannot coincide (Figure 6.28). The reason is that all the curves produced in Plaxis are non-symmetrical (see Figure 6.24 – Figure 6.27). This is normal, since after applying the initial displacement of 0.10m, the properties of the soil on the two sides of the monopile are non-symmetrical. The initial strains taken at each step of the calculation on the soil located on the side of the displacement are higher, and the cumulative hysteretic damping which occurs on the side of the excitation refers to higher values of strains, thus the damping ratio is higher. The mismatch between the analytical solution for a damped system and the non-symmetrical curves in Plaxis is shown in Figure 6.27.

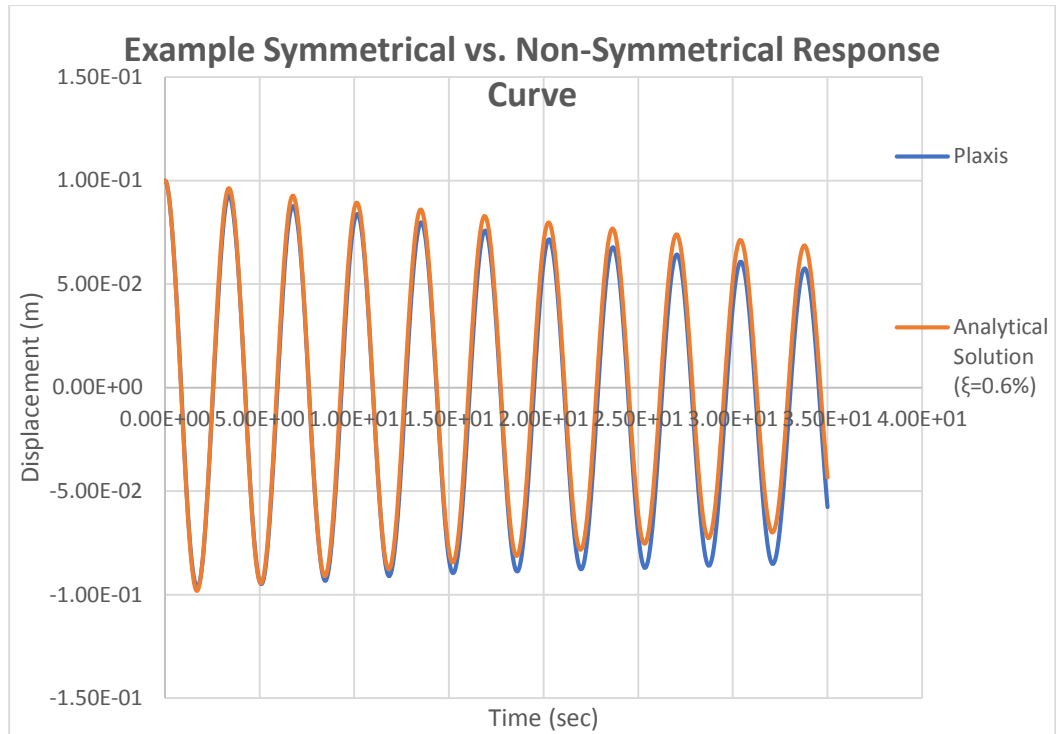


Figure 6.28: Example of Mismatch (Plaxis vs. Analytical Solution)

- In order to apply the logarithmic decrement method, a symmetrical time-response curve is required. If the graph is non-symmetrical two different exponential functions will be adjusted on the top and lowest peaks. An example of using the same power on the exponential function is shown in Figure 6.29.

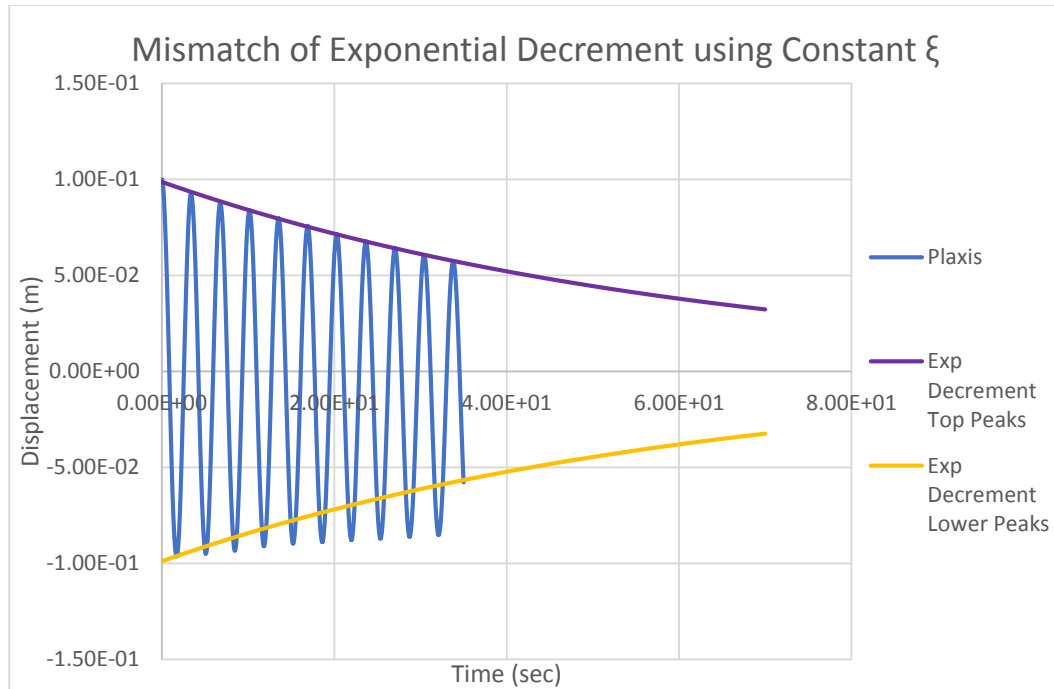


Figure 6.29: Mismatch of an Exponent with Constant Value on Both Sides of the Peak Responses

- Therefore, every graph presented in the following paragraphs has been created by the exact data obtained by Plaxis 3D, but by normalizing the data in order to fit with Eq. 2.3. The normalization is performed using the x-squared method.
- The x-squared method has been performed in order to identify all the parameters included in the Eq. 2.3 This method can be applied automatically in Microsoft Excel, by using the ability of its' Solver to adjust the unknown parameters in order to fit with the minimum error with the values obtained by Plaxis 3D. Using this error minimizing technique, the curve obtained by Plaxis is normalized in order to be symmetrical along the time axis.

## 6.7 Sensitivity Analysis

The results for the time history of the responses for every combination of soil types are being presented in this paragraph.

### 6.7.1 Effect of the Density of the Surrounding Soil & the Sand-Fill

The response time history for a fully filled monopile embedded on loose and dense sand is being shown in Figure 6.30. In this graph, the response for all the possible densities for the sand-fill are being presented and compared with the response of a fully filled monopile with dense sand, embedded in dense soil environment.



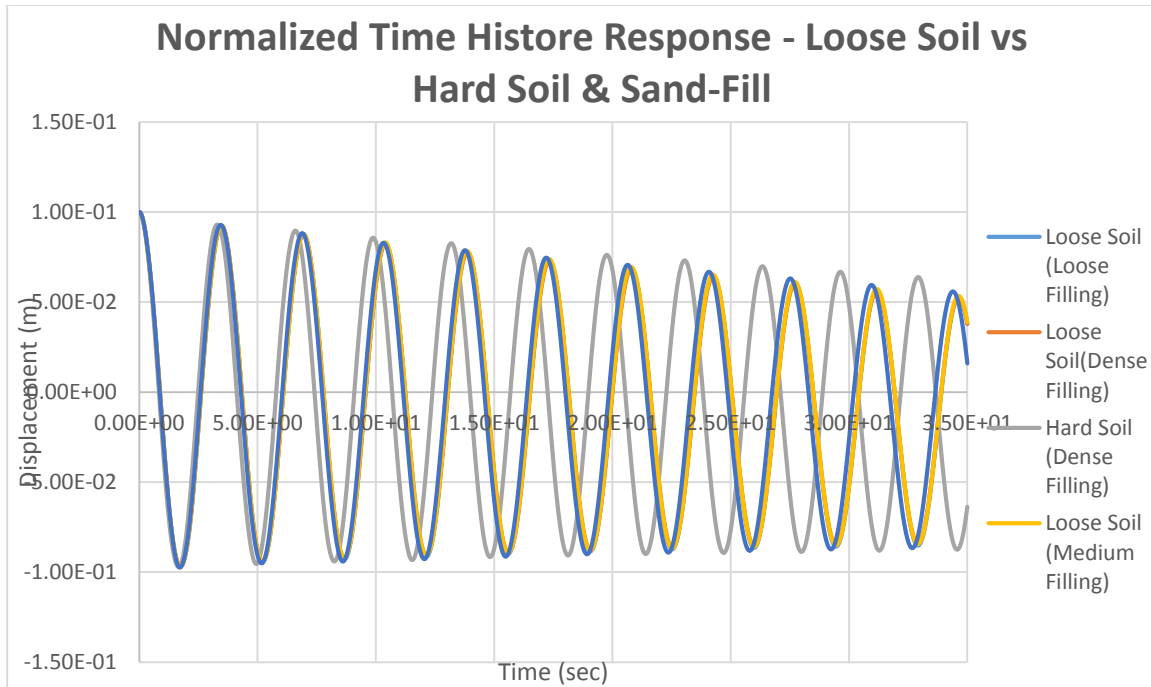


Figure 6.30: Comparison of the Response of a Filled Monopile Embedded in Loose Soil (all Densities of Sand-Fill) with a Monopile Embedded in Dense Soil

As shown in Figure 6.30, the embedded monopile in loose sand, demonstrates a higher level of damping ratio, and subsequently, a smaller damped natural frequency. This result is considered reasonable, due to the higher hysteretic damping of loose sands in comparison with dense sands. Again, the varying density of the sand-fill has an insignificant influence on the structure’s total response.

The natural frequencies and the corresponding damping ratios for all the densities of the surrounding soil and the sand-fill are being presented in Table 6.10.

Type of Surrounding Soil	Type of Filling	Natural Frequency (rad/sec)	Damping Ratio (%)	Increase on Damping Ratio due to Sand Fill (%)
Loose	Empty	1.825	0.58	N/A
	Loose	1.810	0.62	6.9
	Dense	1.810	0.62	6.9
Medium	Empty	1.870	0.5	N/A
	Loose	1.860	0.54	8
Dense	Empty	1.915	0.38	N/A
	Loose	1.910	0.42	10.5
	Dense	1.910	0.42	10.5

Table 6.10: Effect of Sand-Fill on Natural Frequency and Damping Ratio

As shown in Table 6.10, the added sand in the monopile reduces the natural frequency of the structure by a percentage of 0.3 – 0.8%. This result is in accordance with the results presented in Chapter 5. Using the analytical solution, the sand-fill reduces the natural frequency by approximately 0.6% (for a medium dense sand with  $E = 30$  (MPa) and  $\rho = 2$  kg/m<sup>3</sup>). The effect of sand-fill on the total damping ratio of the structure is positive, as calculated in Plaxis. The damping ratio in this analysis refers only to the Rayleigh (material) damping of the monopile and the tower and the damping due to the hysteretic behavior of the soil. This value of the damping ratio can be considered to be conservative and in reality a higher value of damping is being expected. Brinkgreve et al. [46] have shown that when simulating a dynamic analysis in Plaxis, additional Rayleigh damping should be added to the soil, to provide a realistic small amount of damping at small strains (Figure 6.31). The damping ratio suggested for sand [46] is approximately 3%. However, in the simulations performed in this chapter, no damping has been added manually, in order that any variation identified in the damping ratio to be only related to the hysteretic behavior of the soil.

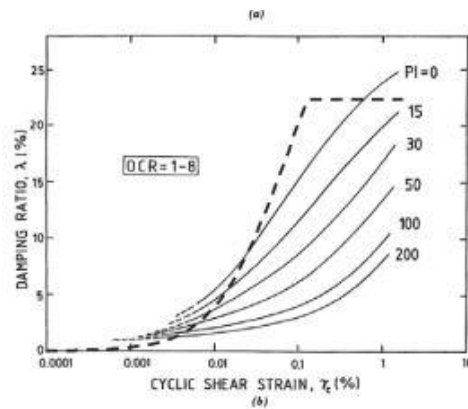


Figure 6.31: Required Added Rayleigh Damping for Soil

The damping ratio of an empty monopile embedded on dense sand is approximately 0.38%. If the monopile is located in sand with lower density, the damping ratio can be increased up to 0.58%. These results are giving slightly lower damping ratio in comparison with the damping ratio due to soil and material damping (steel) calculated by Damgaard et al. [11]. In their publication the combined damping is 0.77%. However, as it is explained before, Plaxis underestimates the value of soil damping at low strains, and in this analysis no Rayleigh damping has been added, in order to not affect the ending result by adding manually Rayleigh damping to the soil.

The density of the sand-fill is of bigger importance when the surrounding soil is dense sand or a sand with medium density. In these cases, the damping ratio increases by 10.5% and 8%, respectively. In the case that the surrounding sand is loose sand, the increase on the damping ratio due to the presence of sand-fill is about 6.9%. To conclude, the increase on the damping ratio of the structure when filling the monopile with sand is approximately 0.4%, independently of the surrounding soil environment. The density of the sand used is also of no importance. However, despite the fact that the total added damping to the structure is equal to 0.4% for all the cases, the source of this damping is not yet identified. The added damping in the presence of the sand-fill, could be either due to the hysteretic behavior of the sand-fill or due to the bigger strains developed on the ground. However, an empty monopile demonstrates bigger

displacements on the seabed level, therefore, adding sand-fill in the monopile is highly unlikely to lead to a development of higher shear strains on the soil located around it (Figure 6.32).

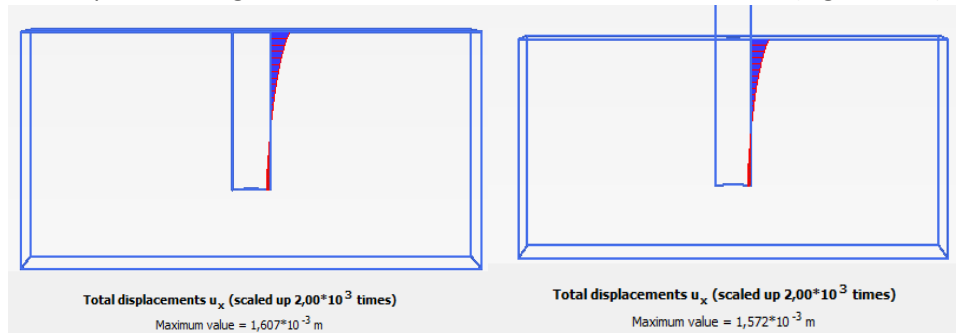


Figure 6.32: Horizontal Displacement on Seabed Level – Empty (Left) & Filled (Right)

Shear strains are being developed in the sand-fill due to the relative displacement along the height of the monopile. Embedding the monopile in a sand with higher density, reduces the relative displacement of the monopile on the seabed level without affecting significantly the relative displacement on the top of the monopile. The latter is normal, since the dense sand restricts the monopile on the ground, but the sand-fill does not affect significantly the stiffness of the monopile. The absolute displacement along both sides of the monopile embedded in dense, medium and loose sand is being shown in Figure 6.33, Figure 6.34 and Figure 6.35.



Figure 6.33: Horizontal Displacement Along the Monopile Sides (Dense Sand)

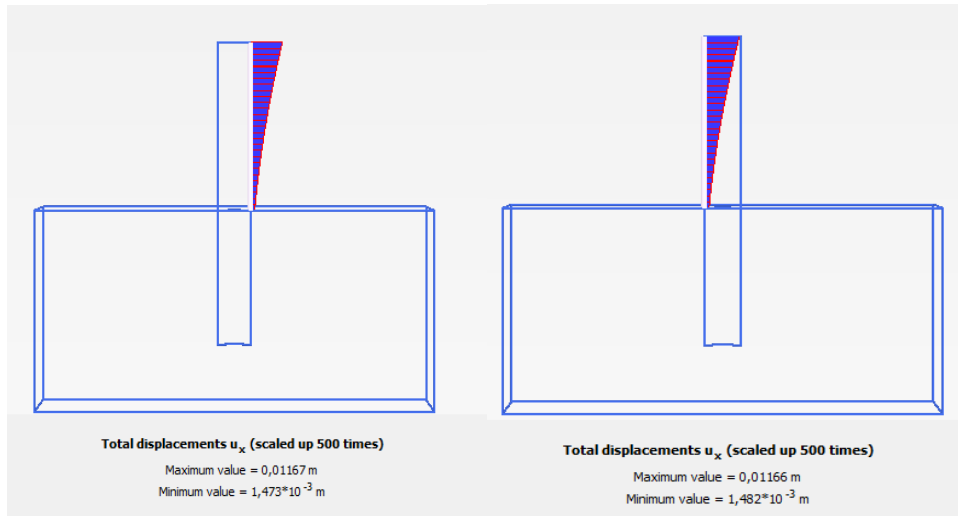


Figure 6.34: Horizontal Displacement Along the Monopile Sides (Medium Density Sand):

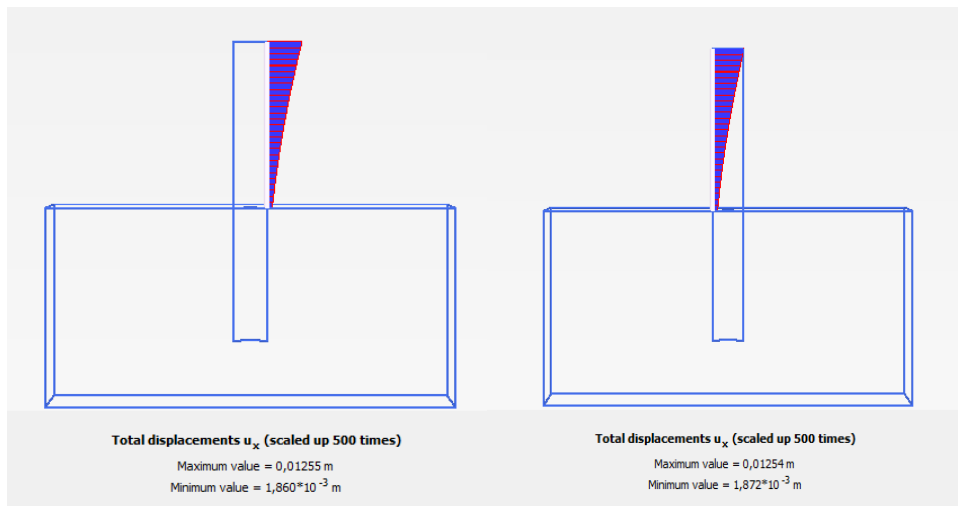


Figure 6.35: Horizontal Displacement Along the Monopile Sides (Loose Sand)

In Figure 6.36, a linear approximation of the horizontal relative displacement along the length of the monopile is being presented. The term “relative displacement” in this case refers to the difference on the horizontal displacement at each side of the monopile, at each point along its’ length.

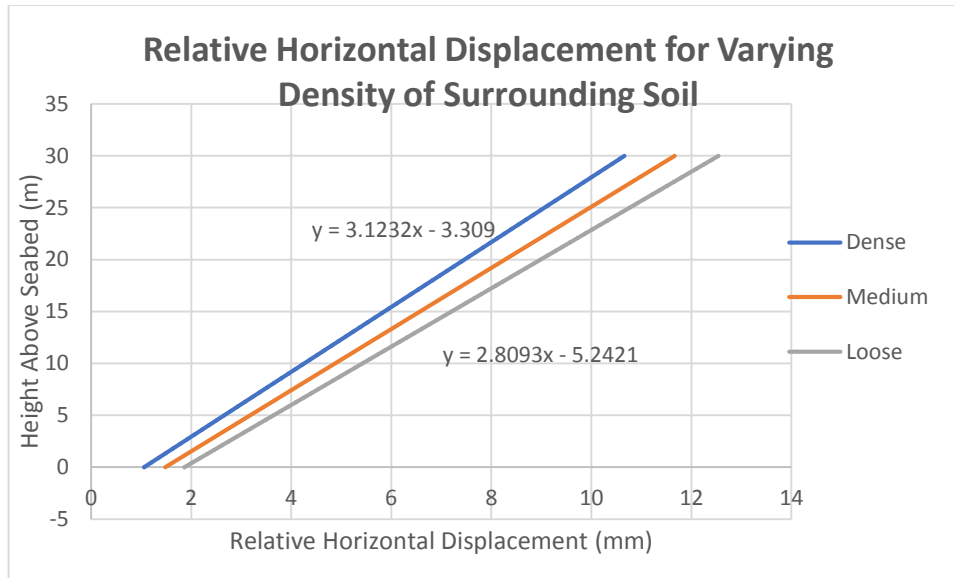


Figure 6.36: Variation of the Inclination of the Relative Displacement with the Density of the Surrounding Soil

As shown in Figure 6.36, the inclination of the relative horizontal displacement along the height of the monopile is the biggest for a monopile in a dense sand environment. This means that the shear deformation of the sand inside the monopile is bigger in the case of dense sand-fill. This leads to higher shear strains and, consequently, to higher damping due to the hysteretic behavior of the sand. This result is in accordance with Figure 6.30. This could lead to bigger shear strains in the sand-fill, but its' effect is negligible, since the difference between the slopes is very small.

### 6.7.2 Effect of the Level of Filling

In this paragraph, the effect of filling the monopile partially with sand is being investigated. Two models were used in this part. The percentage of filling for each model is 25% and 50%, respectively. The analysis has shown that the partially filled monopile has insignificant effect on the damping ratio of the total structure (Figure 6.37).

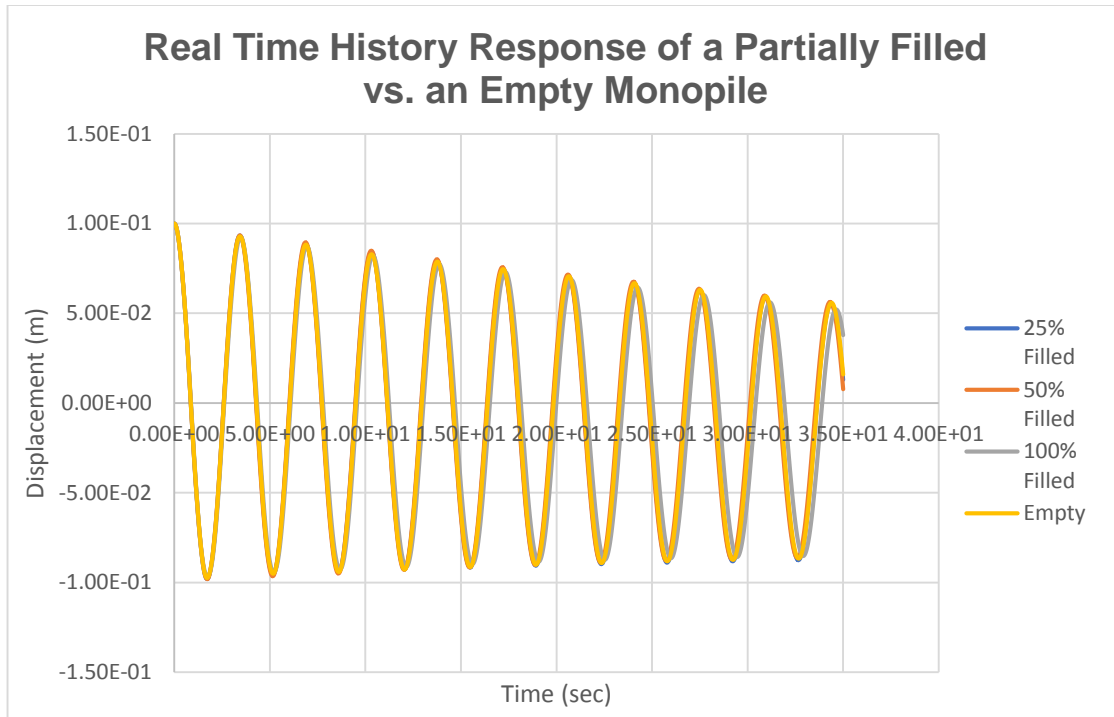


Figure 6.37: Comparison of the Response of a Partially Filled with an Empty Monopile Embedded in Loose Soil

To conclude, a bigger percentage of the volume inside the monopile should be filled with sand, in order to achieve the beneficial effect of the sand-fill on the total damping of the system.

### 6.7.3 Effect of the Magnitude of the Initial Displacement Imposed to the Structure

The effect of the initial displacement on the damping ratio and the natural frequency of the structure are being examined in this paragraph. In all the previous simulations, an initial displacement of 0.10 m was applied on the top of the structure. The effect on the total damping of the structure for an initial displacement of 0.05, 0.20, 0.30 and 0.40 m has been tested. The simulations have been performed on a monopile embedded in loose soil and filled with loose sand, since this combination was proven to have the higher effect on the damping ratio of the system. The results are being presented in Figure 6.38.

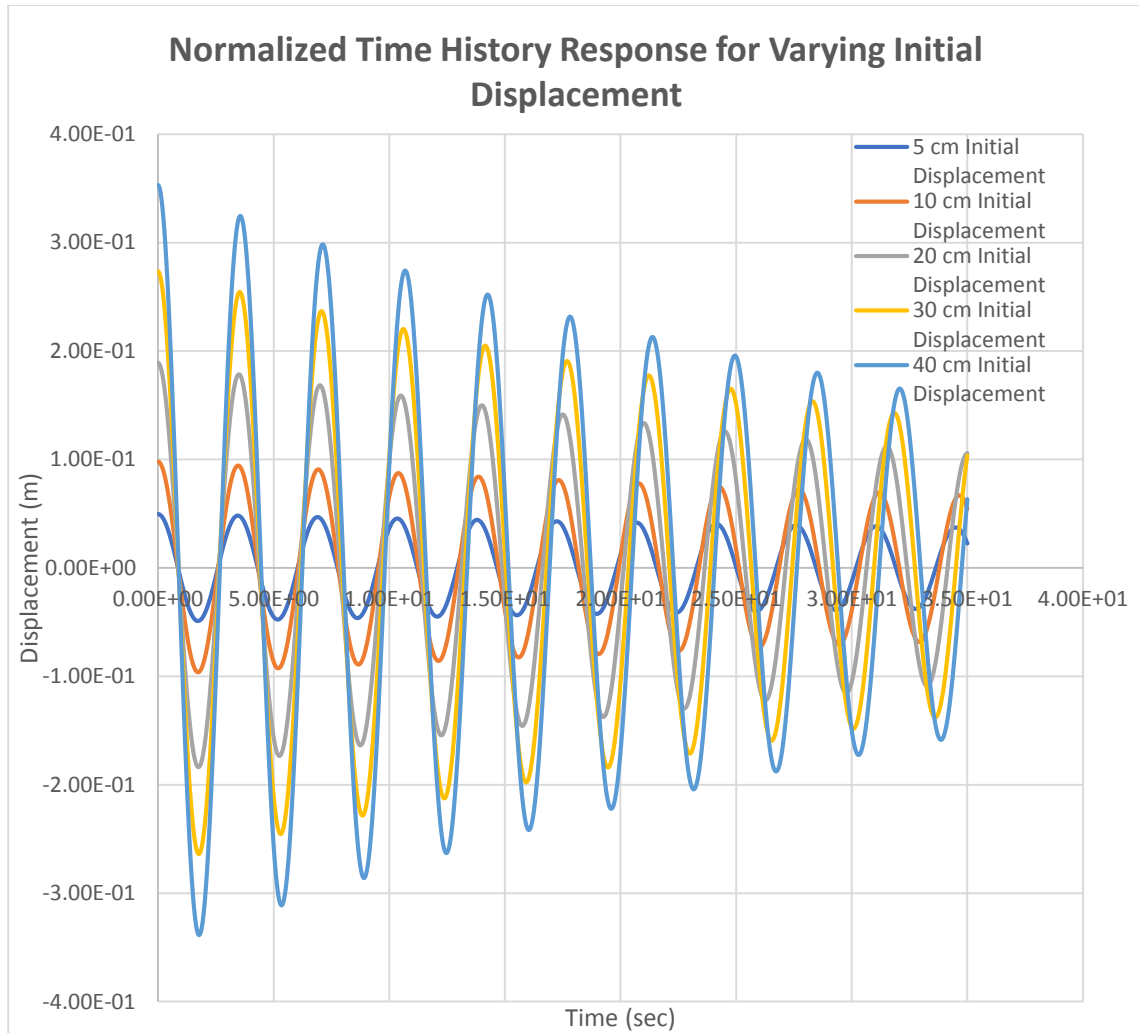


Figure 6.38: Comparison of the Response of a Fully Filled Monopile for Varying Amplitude of Initial Displacement

Imposing a higher initial displacement on the structure, leads to a bigger period of the vibration cycles, which leads to a lower damped natural frequency of the structure. This result is aligned with Chopra's [29] observation after the Lytle Creek and the San Fernando earthquakes in the US. Measurements on existing structures revealed a reduction of the stiffness of the structure during the earthquake. Also, during the dynamic loading, an increase in the damping ratio has been measured for an increasing amplitude of motion. The corresponding fundamental natural frequencies and damping ratios for each initial displacement amplitude are summarized in Table 6.11 and in Figure 6.39 & Figure 6.40.

<b>Initial Displacement (m)</b>	<b>Natural Frequency (rad/sec)</b>	<b>Damping Ratio (%)</b>
<b>0.05</b>	1.820	0.46
<b>0.10</b>	1.815	0.62
<b>0.20</b>	1.795	1.02
<b>0.30</b>	1.775	1.32
<b>0.40</b>	1.762	1.6

Table 6.11: Natural Frequency and Damping Ratio variation with Initial Displacement

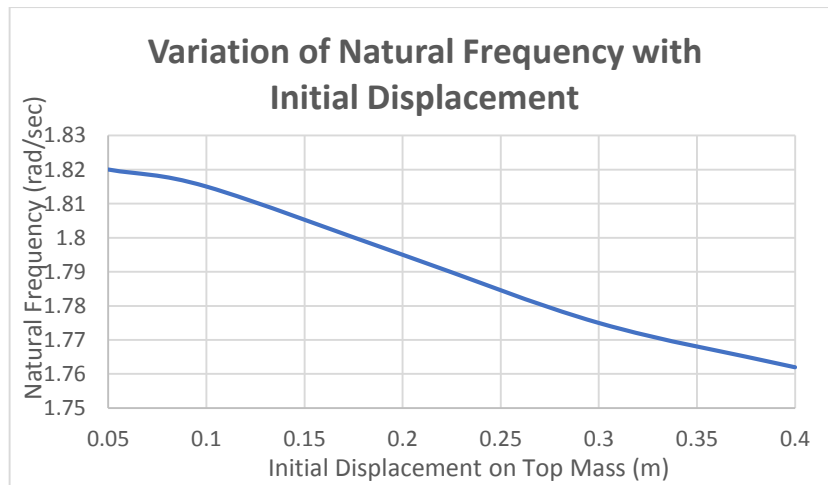


Figure 6.39: Variation of Natural Frequency with Initial Displacement

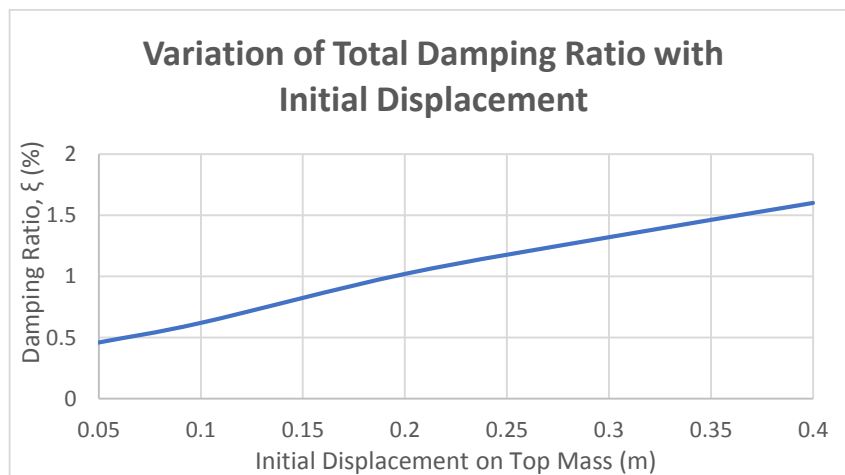


Figure 6.40: Variation of Damping Ratio with Initial Displacement

The collective table which includes the natural frequencies and the damping ratio of an empty monopile for various initial displacements is shown below.



Initial Displacement (m)	FILLED		EMPTY	
	Natural Frequency (rad/sec)	Damping Ratio (%)	Natural Frequency (rad/sec)	Damping Ratio (%)
0.05	1.820	0.46	1.835	0.42
0.10	1.815	0.62	1.825	0.58
0.20	1.795	1.02	1.810	0.92
0.30	1.775	1.32	1.795	1.20
0.40	1.762	1.60	1.785	1.40

Table 6.12: Natural Frequency & Damping variation with Initial Displacement (Filled & Empty Monopile)

## 6.8 Modal Analysis of Forced Vibrations [30]

In this paragraph, the Frequency Response Functions (FRF) and the corresponding displacements at the top of the wind turbine for varying frequencies of excitations are being presented. This analysis is restricted to a monopile embedded in loose sand, since it yields the optimal damping for the structure. The results for both empty and filled with loose sand monopiles are being presented. First, the theoretical part of the modal analysis is being presented and afterwards the technique is applied to an undamped system, as well as, to damped systems using the damping ratios identified in the previous paragraphs.

### 6.8.1 Theoretical Part

The equation of motion for the damped system (in matrix form) is:

$$M \cdot \ddot{x} + C \cdot \dot{x} + K \cdot x = f \quad (6.14)$$

The forced mode can be represented as the superposition of the normal modes of the free undamped vibrations multiplied by the modal displacement as a function of time.

$$x(t) = \sum_{i=1}^N \hat{x}_i \cdot u_i(t) = E \cdot u(t) \quad (6.15)$$

where, E is the eigenvector matrix of the undamped system. Substituting the expression above into the equation of motion it yields.

$$M \cdot E \cdot \ddot{u} + C \cdot E \cdot \dot{u} + K \cdot E \cdot u = f \quad (6.16)$$

Multiplying the expression above with the transpose of the Eigenmatrix, it yields:

$$E^T \cdot M \cdot E \cdot \ddot{u} + E^T \cdot C \cdot E \cdot \dot{u} + E^T \cdot K \cdot E \cdot u = E^T \cdot f \quad (6.17)$$

where,

$$E^T \cdot M \cdot E = M^* \rightarrow \text{Modal Mass Matrix} \quad (6.18)$$

$$E^T \cdot C \cdot E = C^* \rightarrow \text{Modal Damping Matrix} \quad (6.19)$$

$$E^T \cdot K \cdot E = K^* \rightarrow \text{Modal Stiffness Matrix} \quad (6.20)$$

Substituting the initial matrices with the modal ones, it allows to decouple the system. For the modal mass and stiffness matrices it can be proven (orthogonality property) that the matrices are diagonal, since the original mass and stiffness matrices are symmetric. The most important drawback of the analysis is that it assumes that the modal damping matrix is also diagonal, which usually is not the case. For the particular case that the modal damping matrix is diagonal, the equation above can be multiplied by  $(M^*)^{-1}$  and will be written as follows:

$$I \cdot \ddot{u} + (M^*)^{-1} \cdot C^* \cdot E \cdot \dot{u} + \Omega^2 \cdot u = (M^*)^{-1} \cdot E^T \cdot f \quad (6.21)$$

The equation above can be also written as:

$$\ddot{u}_i + \frac{c^*_{ii}}{m^*_{ii}} \cdot \dot{u}_i + \omega_i^2 \cdot u = \frac{F_i^*(t)}{m^*_{ii}} \quad (6.22)$$

where,

$$F_i^*(t) = \hat{x}_i^T \cdot f \quad (6.23)$$

The damping ratio is being calculated using the expression below:

$$\xi_i = \frac{c^*_{ii}}{c^{cr}_{ii}} = \frac{c^*_{ii}}{2 \cdot m^*_{ii} \cdot \omega_i} \quad (6.24)$$

Solving the expression above for the values of the modal damping matrix it yields:

$$c^*_{ii} = \xi_i \cdot 2 \cdot m^*_{ii} \cdot \omega_i \quad (6.25)$$

And given that the relation between the modal damping matrix and the real damping matrix is:

$$C^* = E^T \cdot C \cdot E$$

The real damping matrix is equal to:

$$C = (E^T)^{-1} \cdot C^* \cdot E^{-1} \quad (6.26)$$

Using the formula of  $\xi$ , the equation of motion above is then written as:

$$\ddot{u}_i + 2 \cdot \xi_i \cdot \omega_i \cdot \dot{u}_i + \omega_i^2 \cdot u = \frac{F_i^*(t)}{m^*_{ii}} \quad (6.27)$$

Assuming that a harmonic load is being applied at a specific node, the equation of motion can be written as:

$$\ddot{u}_i + 2 \cdot \xi_i \cdot \omega_i \cdot \dot{u}_i + \omega_i^2 \cdot u = \frac{\hat{x}_i^T \cdot f}{m^*_{ii}} \cdot \sin(\Omega \cdot t) \quad (6.28)$$

In the steady-state regime, the system will vibrate on the frequency of the external load but with a phase shift. The modal displacement is being given by the following equation.

$$u_i = \hat{u}_i \cdot \sin(\Omega \cdot t - \varphi_i) \quad (6.29)$$

And substituting the expression above in the equation of motion, the amplitude of the modal displacement for a system with damping is being given by:

$$\hat{u}_i = \frac{1}{\sqrt{\left(1 - \left(\frac{\Omega}{\omega_i}\right)^2\right)^2 + \left(2 \cdot \xi_i \cdot \frac{\Omega}{\omega_i}\right)^2}} \cdot \frac{1}{\omega_i^2} \cdot \frac{\hat{x}_i^T \cdot f}{m^*_{ii}} \quad (6.30)$$

And the phase shift is given by:

$$\tan(\varphi_i) = \frac{2 \cdot \xi_i \cdot \frac{\Omega}{\omega_i}}{1 - \left(\frac{\Omega}{\omega_i}\right)^2} \quad (6.31)$$

For a system without damping, the amplitude of the modal displacement for a system with damping is being given by:

$$\hat{u}_i = \frac{1}{\omega_i^2 - \Omega^2} \cdot \frac{\hat{x}_i^T \cdot f}{m^*_{ii}} \quad (6.32)$$

The modal amplitude frequency response function can be also evaluated by dividing the modal amplitude with the amplitude of the acting force. For a system with damping, it is equal to:

$$H_{u,Fp}^A(\Omega) = \frac{\hat{u}_i}{\hat{F}_p} \Rightarrow H_{u,Fp}^A(\Omega) = \frac{1}{\sqrt{\left(1 - \left(\frac{\Omega}{\omega_i}\right)^2\right)^2 + \left(2 \cdot \xi_i \cdot \frac{\Omega}{\omega_i}\right)^2}} \cdot \frac{1}{\omega_i^2} \cdot \frac{\hat{x}_{Pi}^T}{m^*_{ii}} \quad (6.33)$$

For a system without damping, it is equal to:

$$H_{u,Fp}^A(\Omega) = \frac{\hat{u}_i}{\hat{F}_p} \Rightarrow H_{u,Fp}^A(\Omega) = \frac{1}{\omega_i^2 - \Omega^2} \cdot \frac{\hat{x}_i^T}{m^*_{ii}} \quad (6.34)$$

The real frequency response function is equal to:

$$H_{x,Fp}^A(\Omega) = E \cdot H_{u,Fp}^A(\Omega) \quad (6.35)$$

And the real (structural) amplitude of the displacement is equal to:

$$\hat{x}(t) = E \cdot \hat{u}(t) = H_{x,Fp}^A(\Omega) \cdot f \quad (6.36)$$

## 6.8.2 Analysis

In order to perform the modal analysis of the structure, the natural frequencies ( $\omega_i$ ) and the corresponding Eigenmatrix (E) is being calculated using the undamped equation of motion of the structure. As shown in Table 2.10, the stiffness of the soil and the corresponding damping varies with the initial displacement applied on the top mass. In order to calculate the Mass and Stiffness matrices of the structure, the finite difference method code in Matlab was used. In the Matlab script, a constant stiffness for the soil springs is being assumed. For the undamped system, a harmonic load is assumed to act at the top node of the structure with a constant amplitude of 1000 KN and a varying frequency ( $\Omega$ ) between 0 – 40 rad/sec. For the damped system, realistic harmonic loads which correspond to the initial displacements applied on the Plaxis models, are being used. The range of the frequency of the external loading was chosen such as that it includes the first three natural frequencies of the structure which are:

Natural Frequencies (rad/sec)	
1st	1.743
2nd	11.582
3rd	31.417

Table 6.13: Natural Frequencies of the Structure (Hz)

### 6.8.2.1. System Without Damping

In the first part of the analysis, the structure is assumed to have zero damping, so its' equation of motion becomes:

$$M \cdot \ddot{x} + K \cdot x = f$$

The load is applied at the top of the structure, as shown in Figure 6.41.

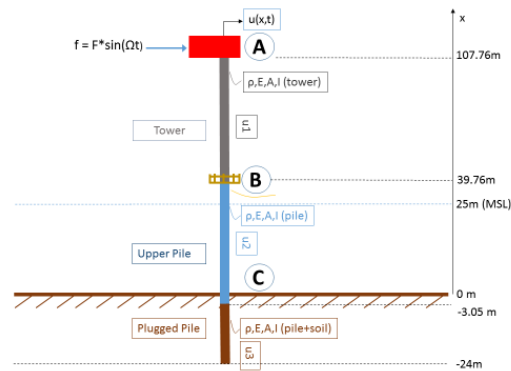


Figure 6.41: Point of Application of the Harmonic Load

The amplitude of the load,  $F = 1000 \text{ kN}$  and its' frequency varies between  $\Omega = 0 - 40 \text{ rad/sec}$ , in order to excite the first three natural frequencies of the structure. The Normal Modes have been calculated using both the formulas which correlate the amplitude of the structural displacement with the amplitude of the modal displacement and the Modal Frequency Response Function, respectively. For validation purposes of the Matlab script, the results of both the methods of calculation are being shown in Figure 6.42.

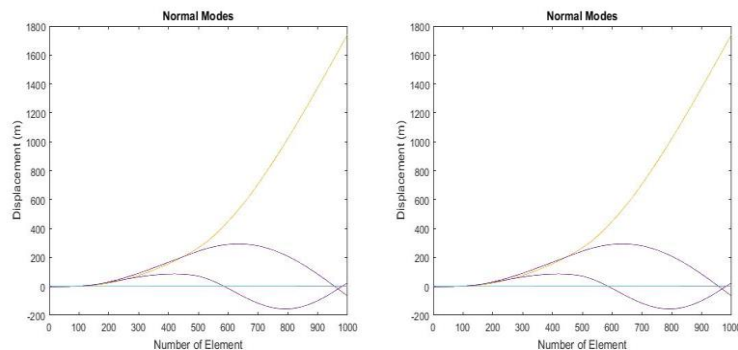


Figure 6.42: Normal Modes calculated using Modal Displacement (Left) and with Modal FRF (Right)

The FRF of the structure as a whole for a varying frequency of excitation is being shown in Figure 6.43.

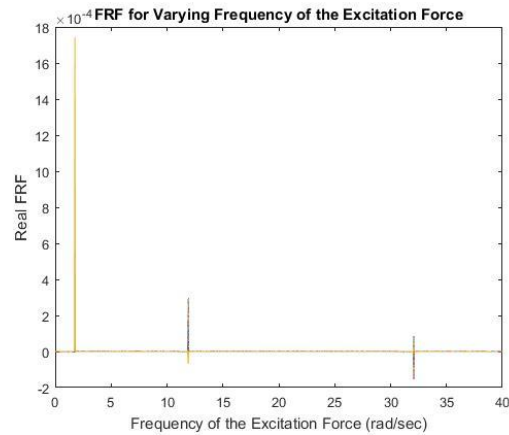


Figure 6.43: FRF for varying Frequency of Excitation

As shown in Figure 6.43, the FRF and, consequently, the displacement reached its maximum value when the frequency of the excitation force coincides with one of the natural frequencies of the structure. Due to the absence of any damping mechanism in the structure, the amplitude of the displacement at those frequencies practically tends to infinity.

#### 6.8.2.2 System with Damping

As shown in the previous paragraph imposing a bigger initial displacement (i.e. bigger load) applied at the top of the monopile led to a varying damping ratio of the structure (Table 6.12). As shown in Table 6.12, the percentage increase of the damping ratio due to the presence of sand-fill is bigger for larger initial displacements.

In order to calculate the Frequency Response Function (FRF) an equivalent harmonic load will be applied at the top mass of the monopile as modelled using the Finite Difference Method (FDM). The amplitude of the concentrated harmonic load which will cause the same initial displacement for each case shown in Table 6.12, is being presented in Table 6.14.

Case	Top Mass Displacement (m)	Equivalent Load on Top Mass (kN)
Case 1	0.05	95
Case 2	0.1	190
Case 3	0.2	355
Case 4	0.3	510
Case 5	0.4	640

Table 6.14: Equivalent Amplitude of the Harmonic Load

**Case 1**

The modal amplitude frequency response gives “the ratio of the displacement of mode a mode to that of the force applied to the degree of freedom at the top node” [4]. For the 1<sup>st</sup> Case under consideration, the FRF is shown in Figure 6.44.

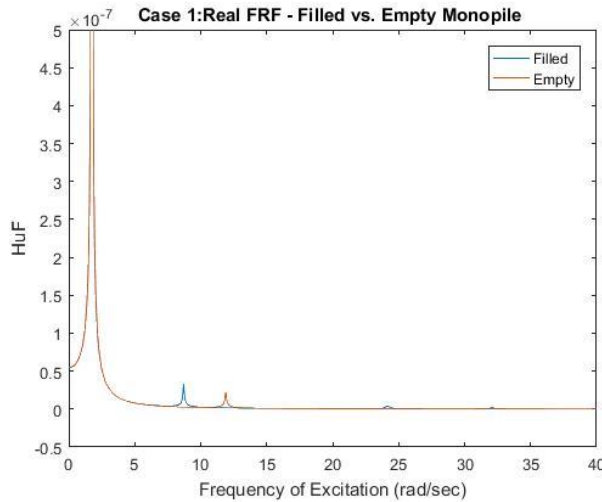


Figure 6.44: Real Frequency Response Function in Relation with the Frequency of the Excitation

As shown in Figure 6.44, the structural response maximizes at the points when the excitation force’s frequency coincides with one of the natural frequencies of the structure, due to resonance. The maximum displacement of the structure in relation with the frequency of the excitation force, for a force of 95 kN applied on the top of the structure, for the empty and the filled monopile, is being shown in Figure 6.45.

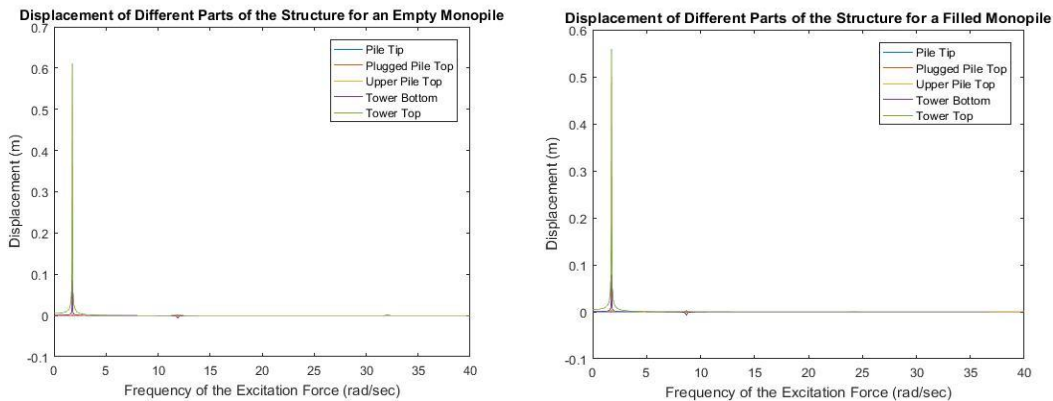


Figure 6.45: Displacement of each Part of the Structure for Varying Frequency of Excitation – (Left Empty – Right Filled)

More specifically, the effect of the corresponding damping ratios on the displacement of each node in the case of resonance at the fundamental frequency of the structure is shown in Figure 6.46.

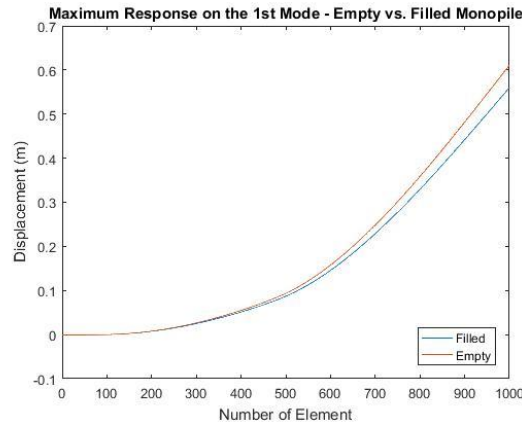


Figure 6.46: Maximum Displacement of each Element of the Structure –2<sup>nd</sup> Mode

As shown in Figure 6.46, the bigger damping due to the filling of the monopile leads to a decrease in the maximum displacement of the top node by approximately 8.4%. The detailed graphs obtained for the Cases 3 – 5 are shown in Appendix F. The collective results for Cases 1 – 5 are being presented in Table 6.15.

Case	Decrease on Top Mass' Displacement (%)
Case 1	8.4
Case 2	6.1
Case 3	9.5
Case 4	8.7
Case 5	12.2

Table 6.15: Percentage Decrease of Top Mass Displacement for varying Loading

## 6.9 Identification of Damping Coefficient Corresponding to the Sand-Fill (c)

In this paragraph, an estimation of the damping coefficient which corresponds to the presence of sand-fill is being presented. This coefficient is included in the Euler-Bernoulli beam for a system with damping, as shown below.

$$E \cdot I \frac{d^4 w}{dx^4} + c \frac{dw}{dt} + m \frac{d^2 w}{dt^2} = 0 \quad (6.37)$$

The script in Matlab which was created to calculate the natural frequency of the structure using normal modes, will be utilized to identify the corresponding damping coefficient for an increase of 0.04% on the total damping ratio of the structure.

### Procedure to Estimate “c”:

1. Assume that the damping ratio corresponding to the 1<sup>st</sup> mode of vibration of the empty monopile is caused mainly by the surrounding soil. Therefore, an initial damping ratio (i.e.  $\xi = 0.58\%$ , Table 2.8) is being used

2. Calculate the element of the modal damping matrix which corresponds to the 1<sup>st</sup> mode of the soil ( $c_{11}^*$ ), using the corresponding element of the modal mass matrix and the fundamental natural frequency of the structure
3. Calculate the approximate value of the damping coefficient, assuming constant damping ratio for the embedded part of the monopile, using the formula:

$$c_{mode\ 1,soil} = \frac{c_{mode\ 1,soil}^*}{\int_0^L \varphi_{mode\ 1}^2} \quad (6.38)$$

4. Add a damping coefficient on the element of the damping matrix corresponding to the filled part of the monopile. Find its' value as a percentage of the damping coefficient of the soil ( $c_{mode\ 1, soil}$ ).
5. Use trial-and-error method for the value of the constant damping assigned to the filled monopile, in order to achieve the measured damping ratio of the structure (i.e.  $\xi = 0.62\%$ ).

Performing the steps describes before, the damping coefficient for the embedded and the filled part of the monopile are:

$$c_{soil} = 5.6849 \cdot 10^9 \frac{N}{m \cdot sec} = 5.68 \frac{GN}{m \cdot sec}$$

$$c_{filled\ pile} = 4.2637 \cdot 10^3 \frac{N}{m \cdot sec} = 4.26 \frac{kN}{m \cdot sec}$$



## **7. Opportunity Window for the application of Sand-Fill Technology in the North Sea & Financial Analysis**

### **7.1 Introduction**

In this chapter, a financial analysis on the impact of the added sand on the total cost of the monopile is being presented. In the first paragraph, an overview of reports published by accredited organizations. These reports, record the current situation of offshore wind energy developments in Europe and also provide forecasts for the upcoming years. These forecasts are crucial in order to estimate the opportunity window of the application of the sand-filled monopiles in future developments. In this analysis, the main focus is given to the new developments by the year 2020. Since these forecasts are also based on the trendline of the offshore wind energy installations during the previous years, focusing at a year not so distant in the future, can be considered to increase the reliability of the forecasts. After presenting the forecasts, the potential of new developments in the North Sea is being estimated also by using an online platform which presents the current situation of the licensed fields in the North Sea. This estimation takes into consideration the under construction and the licensed fields in the North Sea, in combination with the forecasts presented. At the last part of this chapter, a financial analysis in order to estimate the impact of the added sand on the total cost of the monopile is being presented. The financial analysis focuses on the comparison of the costs (including material, the transportation and the installation costs) between a traditional (empty) monopile and a monopile filled with sand.

### **7.2 Opportunity Window for the Application of the “Sand-Fill” Technique on Monopiles**

In this chapter, the financial impact of the added sand to the total cost of the construction of a monopile in an offshore environment is being examined. Firstly, the opportunity window for this new technique needs to be estimated. To estimate the opportunity window, an estimation of the future offshore wind energy projects in the North Sea is needed. Various accredited organizations produce forecasts based on the current situation, the trend during the previous years and the estimated growth in the sector in the upcoming periods. These reports usually predict the future trends based on a low (pessimistic) scenario, a medium (neutral) scenario and a high (optimistic) scenario. Those forecasts, and depending on the organization, refer to a time span ranging from a few years up to decades in the future. Moreover, those reports refer to forecasts on the development of new offshore wind farms in various areas in the world.

Due to the variety of the reports which are produced at a global level, focus is only given to forecasts produced by well-known, accredited organizations. Organizations, such as, WindEurope [47,48], the European Wind Energy Association (EWEA) [49,50,51], the Global Wind Energy Council (GWEC) [52] and International Renewable Energy Agency (IRENA) [53,54,55] have been chosen to be used as reference in this report. The current status of the offshore/onshore wind installations and the estimated future development of offshore wind farms by each organization is being presented in the figures below:

### 7.2.1 WindEurope Report

The total installed power of offshore wind energy in Europe, as of 2016, is about 16%, as shown in Figure 7.1. The forecast for the installed power (onshore and offshore) for the years between 2017 – 2021 is being presented in Figure 7.2.

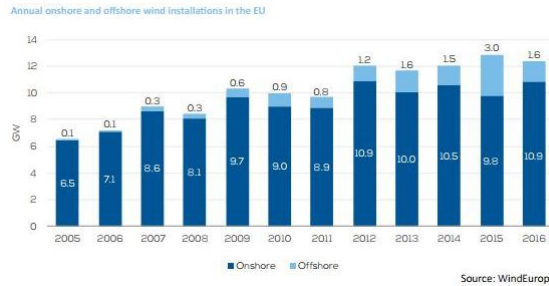


Figure 7.1: Current Situation of Offshore Installations in EU (2016) [48]

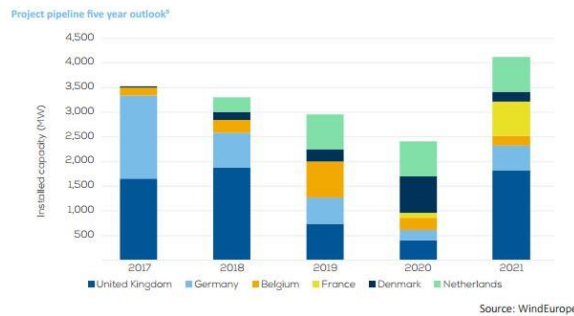


Figure 7.2: Forecast Offshore Wind Energy Developments each Year between 2017 - 2020 [47]

### 7.2.2 EWEA Report

EWEA’s and WindEurope’s reports present similar figures for the current situation in Europe. In EWEA’s report, the total recorded installed offshore wind capacity, as of 2015, is equal to 11.034 GW. The installed capacity per country is being installed in Figure 7.3.

Country	BE	DE	DK	ES	FI	IE	NL	NO	PT	SE	UK	Total
No. of farms	5	18	13	1	2	1	6	1	1	5	27	80
No. of turbines	182	792	513	1	9	7	184	1	1	86	1,454	3,230
Capacity installed (MW)	712	3,295	1,271	5	26	25	427	2	2	202	5,061	11,027

Figure 7.3: Current Situation per Country (2015) [50]

The expected installed offshore wind capacity in Europe, according to three distinctive forecast scenarios (low, central and high scenario) is equal to 20, 23 and 28 GW, respectively (Figure 7.4). In comparison with the WindEurope report, the EWEA report’s low scenario is higher. The offshore wind energy goal for each of the leading European countries in the offshore wind energy sector is being presented in Figure 7.5. If the total target for all the countries presented in Figure 7.5 is being met, the total installed capacity will be equal to approximately 31.5 GW. This goal can be considered to be highly optimistic, since it even exceeds EWEA’s high scenario.

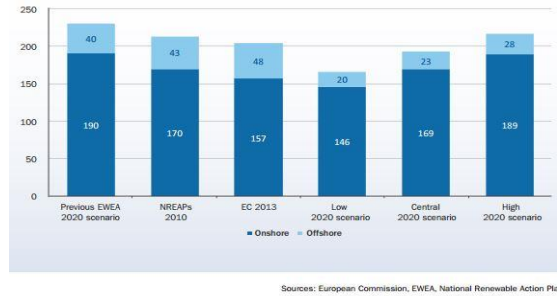


Figure 7.4: Forecast Offshore/Onshore Wind Energy Developments on 2020 [51]

	Spatial planning for offshore renewables	Installed offshore capacity (MW)	NREAP 2020 offshore renewables target (MW)	EEZ	Integrated MSP process
Belgium	Area composed of 7 concessions	195	2,000 <sup>99</sup> wind	Yes	Yes, gradual implementation
Denmark	Offshore renewables zoning <sup>98</sup>	386 (just for the North Sea)	1,335 <sup>84</sup> wind	Yes	No
Germany	MSP in EEZ (2009)	90 <sup>62</sup>	10,000 <sup>83</sup> wind	Yes	Yes, in EEZ
Netherlands	2 OWE area <sup>84</sup> and two search areas	228	5,178 wind	Yes	In the process of being implemented
UK	Criteria based MSP	1,341	12,990 wind 1,300 wave and tidal	Yes	A type of MSP in place

Source: Seenergy2020 project, Deliverable 2.3

Figure 7.5: Offshore Wind Energy Target per Country [51]

### 7.2.3 GWEC Report

GWEC’s report presents (Figure 7.6) that the total installed offshore wind capacity in Europe in the period 2008 – 2016 is approximately equal to 14 GW. This figure is slightly lower to the total capacity installed as is being recorded in the WindEurope report. GWEC’s report also presents a forecast for the cumulative wind energy capacity installed of 218.3 GW by 2020. This forecast (Figure 7.7) is in accordance with EWEA’s high scenario which predicts a cumulative wind energy capacity of 217 GW in Europe by 2020.

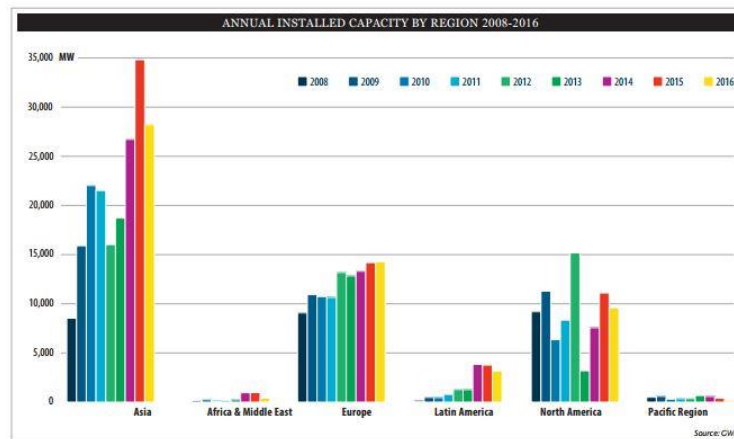


Figure 7.6: Current Situation Offshore Wind Developments (2016) [52]

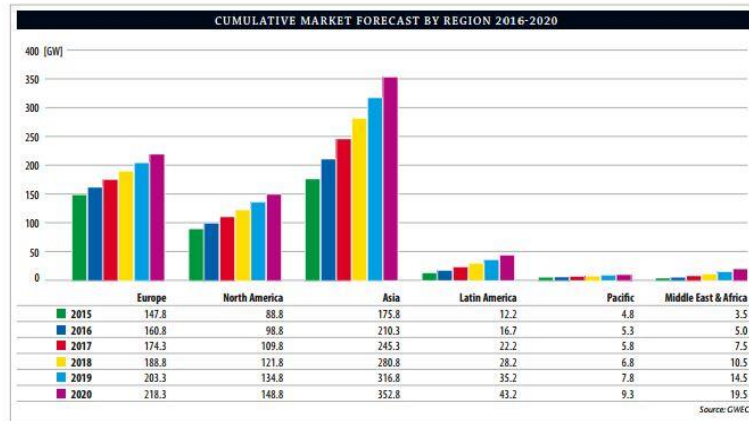


Figure 7.7: Forecasted Offshore/Onshore Wind Energy Developments on 2020 [52]

### 7.2.4 IRENA Report

IRENA’s report forecasts an average of about 2 GW/year new offshore wind energy developments per year (Figure 7.8), for the period between 2015 – 2020. After 2020, the forecast shows an increasing trend for the installed capacity per year. Given IRENA’s forecast, the total installed capacity for the period between 2015 – 2020 will be equal to approximately 16-17 GW. This forecast is similar to WindEurope’s forecast for the same time period ( $\approx 19$ -20 GW)

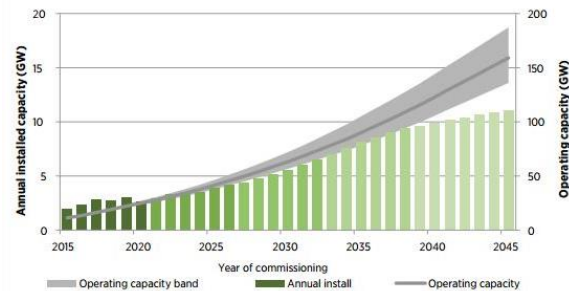


Figure 7.8: Forecast Offshore Wind Energy Developments on 2045 [53]

IRENA’s report also presents a forecast for the adjustments on various aspects of the offshore wind energy sector for the period between 2016 – 2045. As shown in Figure 7.9, the average wind farm size is expected to increase dramatically ( $\approx 12.7$  GW capacity per farm) and the Levelized Cost of Energy produced (LCOE) will be reduced to about 170 USD/MWh ( $\approx 145$  €/MWh).

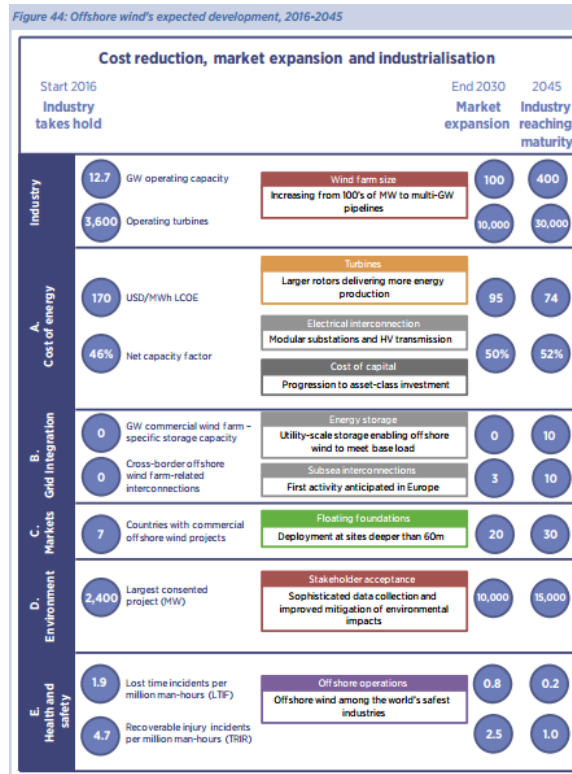


Figure 7.9: Forecasted Trend in the Offshore Wind Energy Market [53]

All the aforementioned forecasts, have been taken into consideration specific factors which are expected to have a crucial effect on the predicted growth of the sector in the future. Those factors can be split in factors will have an impact in the wind energy development at a global and at a European Region level (GWEC).

- a) At a Global Level the main factors to influence the growth are:
  - UN's agreement in Paris for 100% emissions-free power by 2050
  - Constant reduction in costs
  - US market stability
  
- b) At a European Level the main factors to influence the growth are:
  - The expected growth in Turkey's market
  - Southern European markets recover from financial crisis
  - 70 GW are expected to be added
  - The goal of 40 GW power from Offshore Wind Energy is assumed that it will be met

### 7.3 Exclusive Economic Zones

The opportunity window refers only to North Sea territory, which includes the Exclusive Economic Zones (EEZ) of the Netherlands, the UK, Norway, Denmark and Belgium. France's EEZ in the North Sea has been excluded due to the lack of sufficient data and projects already developed in the area. The EEZs for all the aforementioned countries are being shown in Figure 7.10.

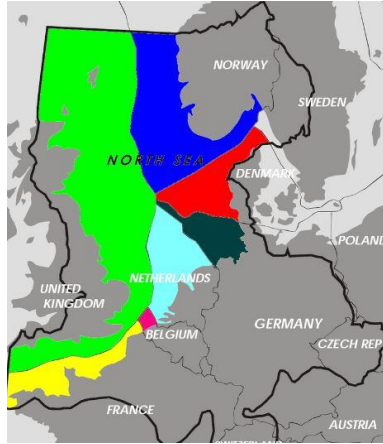


Figure 7.10: Borders of Area of Interest & EEZ (<https://upload.wikimedia.org>)

## 7.4 Data Collection & Methodology to Process the Data

In the previous paragraph, the current and forecasted installed capacity has been presented at a regional level (EU). Utilizing a specialized online platform ([www.4coffshore.com](http://www.4coffshore.com)) which keeps record of the licensed offshore fields and of the developed, planned and under construction projects, the current and planned projects per country have been estimated. To perform this analysis, all the licensed fields were recorded, along with their mean depth. This information was crucial, given the fact that the monopiles can be used as support structures for a depth up to approximately 35m. For every developed, planned or under construction project, the number of wind turbine generators along with their nominal power have been recorded as well. This information was important to estimate the mass of the rotor-nacelle assembly, which, in turn, affects the diameter of the monopile and the volume of the sand to be added. The results of the analysis described above are being presented in the following two paragraphs. Firstly, the current situation is being recorded and then the planned projects are being estimated. The current situation was recorded by using the data available online (Offshore Wind North Sea). These data are the most representative, since this platform is updated regularly. The data presented correspond on the data available on (Offshore Wind North Sea) on April 2016. For the estimation of the projects realized by the year 2020, the data available online have been cross analyzed with the forecasts, to provide a realistic estimation.

### 7.4.1 Current Situation North Sea

In order to create the figures presented in this paragraph, a file was created using Microsoft Excel, to record all the fields which belong in the EEZ of each country. The fields of each country have been separated in five categories:

1. Fully Commissioned
2. Under Construction
3. Licensed/Planned
4. Empty Fields
5. Fields Licensed but the Project got Cancelled

The analysis presented in the following paragraphs was limited to projects with maximum depths around 30 m. Projects realized at water depths higher than 35 m were excluded in this analysis, because the monopile concept is not usually applied on these depths. For water depths bigger than 35 m., the monopile cannot provide a feasible solution, and other foundation types are being used (i.e. jacket type, floating etc.)

In order to record the current situation realistically, only the fully commissioned fields are taken under consideration in this paragraph. In Figure 7.11, the total installed capacity per country is being presented. The biggest projects so far have been realized offshore UK, when Germany, Netherlands, Belgium and Denmark have demonstrated activity in the sector during the previous period.

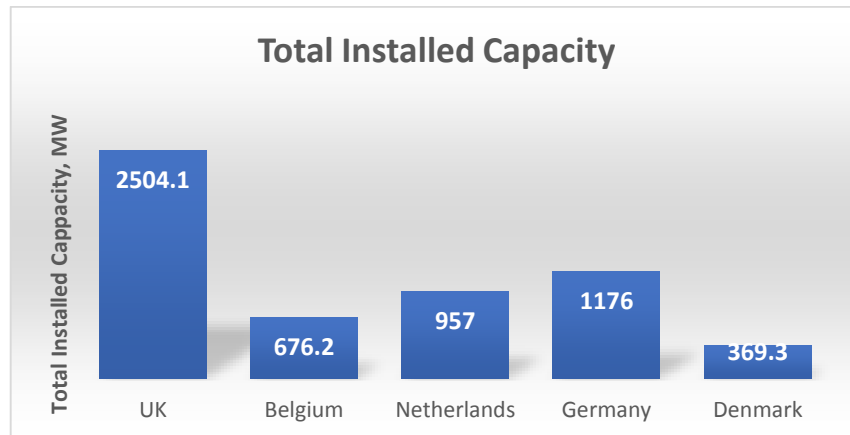


Figure 7.11: Current Installed Capacity (Offshore Wind) per Country

In Figure 7.12, the average installed capacity per wind generator per country has been estimated. A weighted average has been used, to correlate the capacity of the generator with its' rate of utilization in the offshore wind projects. The following formula was used for this calculation:

$$\text{Average Capacity (MW)} = \frac{\sum \text{Number of Turbines}_i \cdot \text{Turbine Capacity}_i}{\sum \text{Number of Turbines}_i} \quad (7.1)$$

where,  $i$  = Sequential Number of Project

This analysis has shown that all the aforementioned countries, except of Denmark, have shown preference to wind turbines with an average capacity between 3 – 4 MW/Generator. Denmark has utilized in its' OWFs relatively smaller turbines, with an average capacity about 2 – 2.5 MW. This might be due to the fact that Denmark has been a pioneer in offshore wind energy production and the projects have been realized much earlier. Therefore, using earlier technology led to an average of about 2-2.5 MW/turbine.

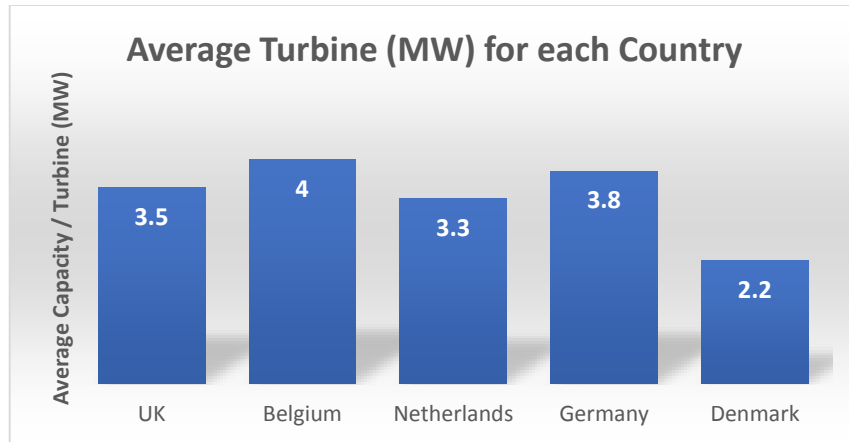


Figure 7.12: Average Turbine Capacity per Country

Also, the mean water depth for the projects at each country has been estimated. For the mean water depth, again a weighted average has been calculated, according to the formula below.

$$\text{Mean Water Depth (m)} = \frac{\sum \text{Total MW Installed}_i \cdot \text{Mean Water Depth}_i}{\sum \text{Total MW Installed}_i} \quad (7.2)$$

where, i = Sequential Number of Project

The mean water depth per country varies, depending naturally to the morphology of the seabed surrounding each country (Figure 7.13).

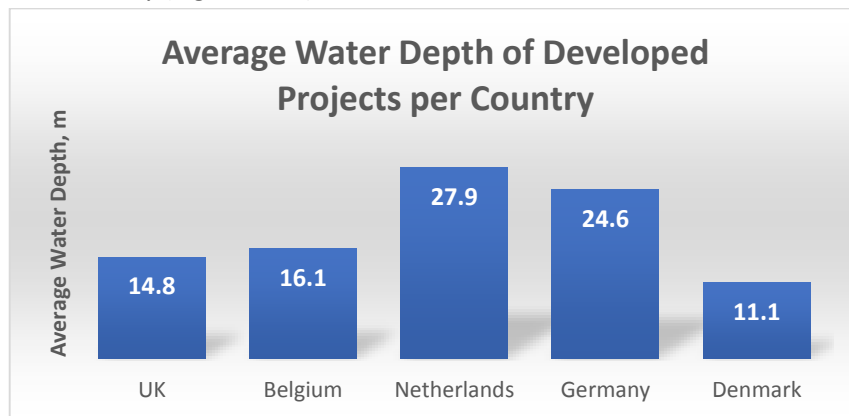


Figure 7.13: Mean Water Depth of Developed Fields per Country

Knowing the average capacity per generator per project, the total number of monopiles which have been installed already in each country was calculated, using the formula:

$$\text{Total Nr. of Installed Monopiles}_j = \frac{\sum \text{MW Installed}_i}{\sum \text{Average Turbine Capacity (MW)}_i} \quad (7.3)$$

where, i = Sequential Number of Project

J = Sequential Number of Country



For each wind generator located at a water depth smaller than 35m., one monopile structure is assumed to be placed as a support structure for the OWG.

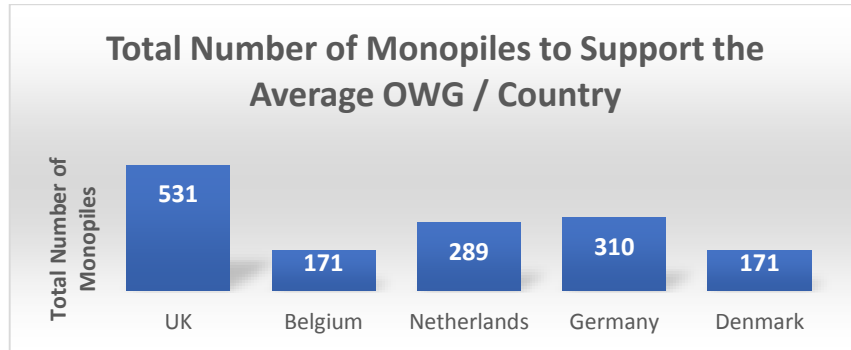


Figure 7.14: Number of Monopiles Installed per Country

To conclude, knowing the number of monopiles and the mean depth per country, an estimation has been done for the total length of the monopiles (above seabed level) installed per country. The formula applied is:

$$\begin{aligned} \text{Average Total Length of Installed Monopiles}_j(m) \\ = \text{Mean Water Depth}_{i,j} \cdot \text{Total Nr. of Monopiles}_{i,j} \quad (7.4) \end{aligned}$$

where, i = Sequential Number of Project

J = Sequential Number of Country

As it is shown in Figure 7.15, about 8 km “average total length” of monopiles have been installed in the UK, in the Netherlands and in Germany. Of course, the total length may be almost the same for the Netherlands, the UK and for Germany, but for each country the diameter of the equivalent monopile will vary, in a manner that the equivalent monopile should demonstrate adequate strength properties to withstand the weight of the average wind generator, which varies for each country.

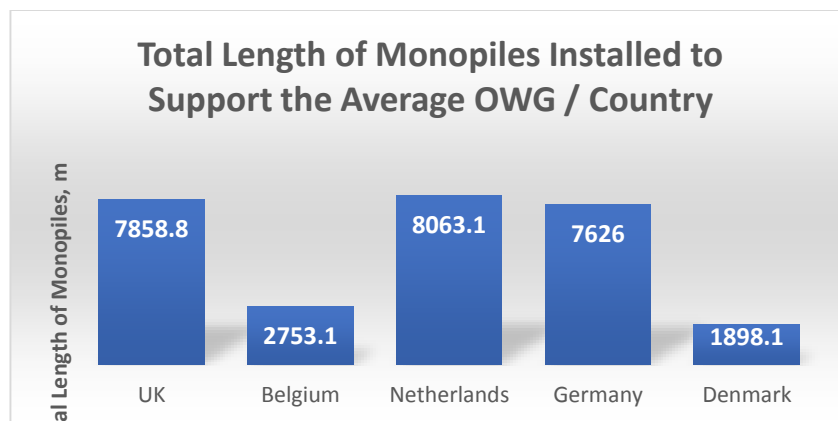


Figure 7.15: Average Total Length of Monopiles Installed in each Country

### 7.4.2 Variation of Parameters for the Planned Projects

After analyzing the current situation, a similar analysis has been performed for the planned projects. The projects which are planned for the future include every project which is under construction and every project which is licensed, so that its' construction will start in the upcoming years. The empty fields which have already allocated by the governments and are soon to be tendered are being included, as well. In the UK around 16 GW are expected to be built in the upcoming years, when in the Netherlands, in Germany and in Denmark, 8 GW, 7GW and 4 GW, respectively, are expected to be realized. The planned to be installed capacity is being shown in Figure 7.16.

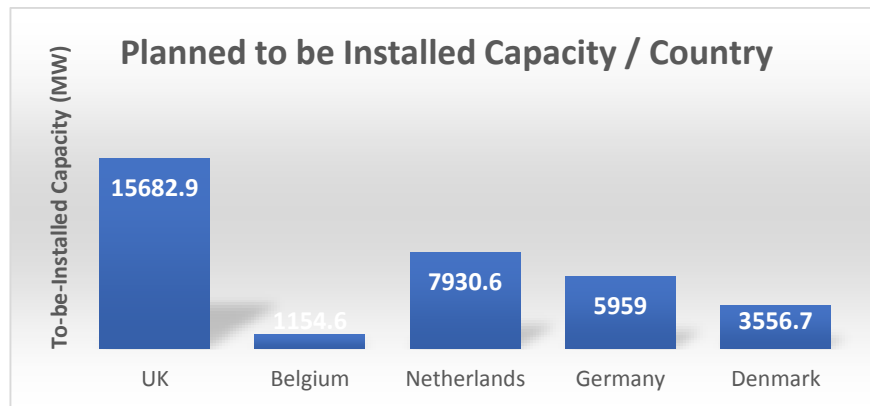


Figure 7.16: Planned to be in Installed Total Capacity per Country

At this point, it should be noted that those estimations are much higher than the forecasted installed capacity per country (Figure 7.2). This is normal, since this estimation is not restricted to the period between 2016 – 2021, but it refers on fields that are available to be developed at any point in the future. Also, in this paragraph, it is assumed that every licensed field will be developed. This assumption can be considered as highly optimistic and can only be used to provide an upper limit of the expected projects. Given the crucial divergence between the forecasts and the estimation done using the data on the licensed fields, in the final analysis, both results will be treated separately.

In order to restrict the analysis in the time period 2017 – 2020, the information obtained by 4C Offshore Ltd, has been analyzed in combination with the forecasts by various organizations. The forecasts presented in Figure 7.2, Figure 7.4 and Figure 7.8 for the developments by the year 2020, are being presented in Table 7.1.

Organization	Forecasted Installed Capacity (MW)
Wind EU	12250
EWEA	9000 (L)
	12000 (M)
	17000 (H)
IRENA	10000

Table 7.1: Forecasts for the Developed Offshore Wind Capacity in the North Sea (2020)

As shown in Table 7.1, the forecasts are estimating a developed capacity ranging between 9 – 17 GW. The extreme and the lowest values which are being presented only in the EWEA report are being excluded, and the expected value of the average scenario of the three reports will be used. Therefore, an average of about 11.40 GW is being used in as an upper limit for the developed capacity offshore by the year 2020. Therefore, in order to estimate the installed capacity by the year 2020 per country in the absence of more specific data the following method will be applied.

1. The potential of each country in future developments is estimated using the formula

$$\% \text{ Contribution}_i = \frac{\text{Planned Capacity}_i}{\text{Total Planned Capacity}} \quad (7.5)$$

where, i = Sequential Number of each Country

2. The total forecasted capacity is being separated in parts and assigned to each country, according to its percentage contribution on the total future projects.

The results of this analysis are being presented in Figure 7.17.

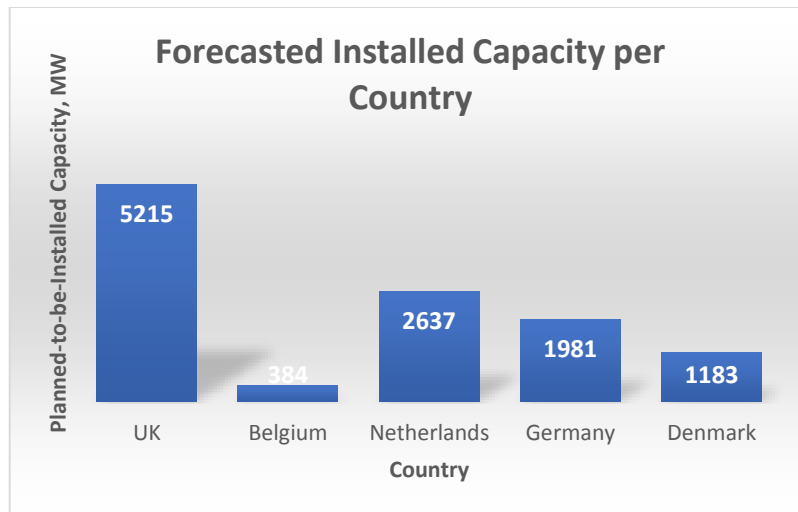


Figure 7.17: Forecasted Installed Capacity per Country

As shown in Figure 7.18, the trend is that in the upcoming years wind turbines of higher capacity (bigger than 6 MW/turbine) will be utilized in the new projects.

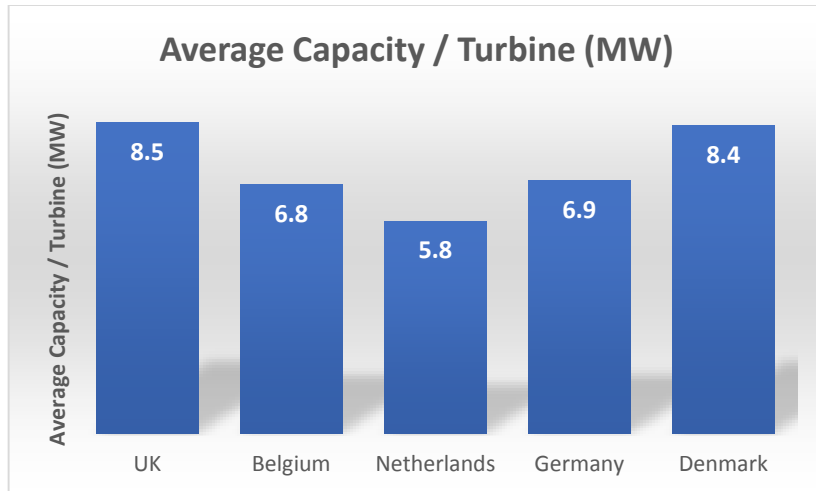


Figure 7.18: Future Trend for Average Capacity per Wind Generator (Offshore)

In Figure 7.19, the mean depth of the locations for the planned project is being presented.

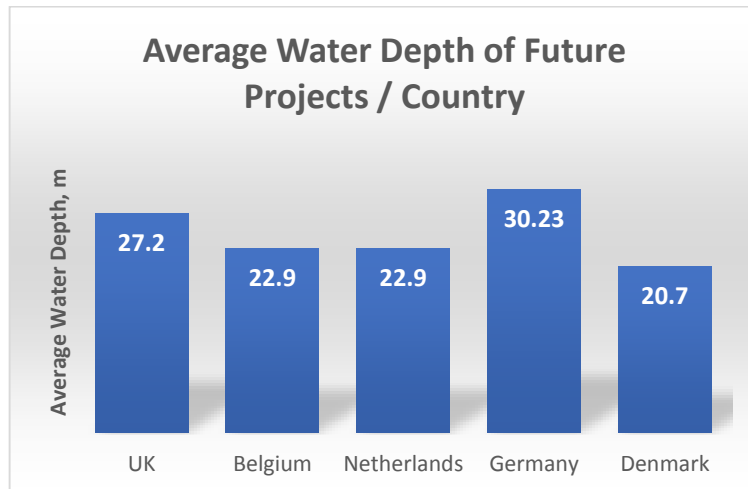


Figure 7.19: Average Water Depth for Projects to be Developed per Country

The number of the monopiles which are planned to be installed per country are being shown in Figure 7.20. About 600 monopiles are being forecasted to be installed in the UK, whereas, around 300 are being expected in Germany and about 450 are being expected in the Netherlands.

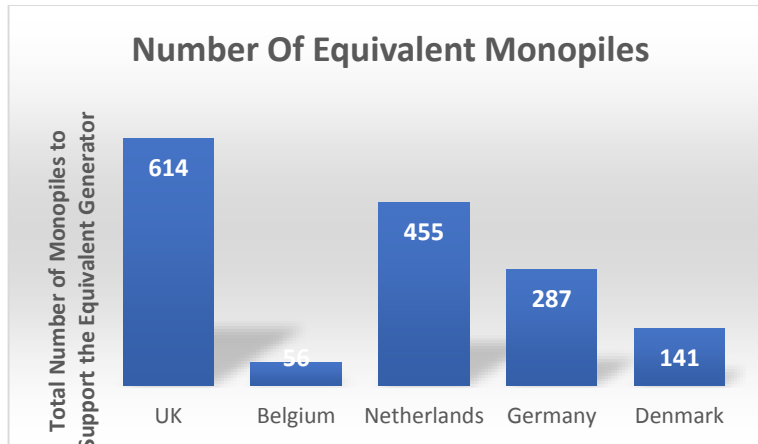


Figure 7.20: Total Number of Monopiles to be Installed per Country

The planned length of equivalent monopiles is more than 16 km for the UK and about 8.5 km and 10 km in Germany and in the Netherlands, respectively (Figure 7.21).

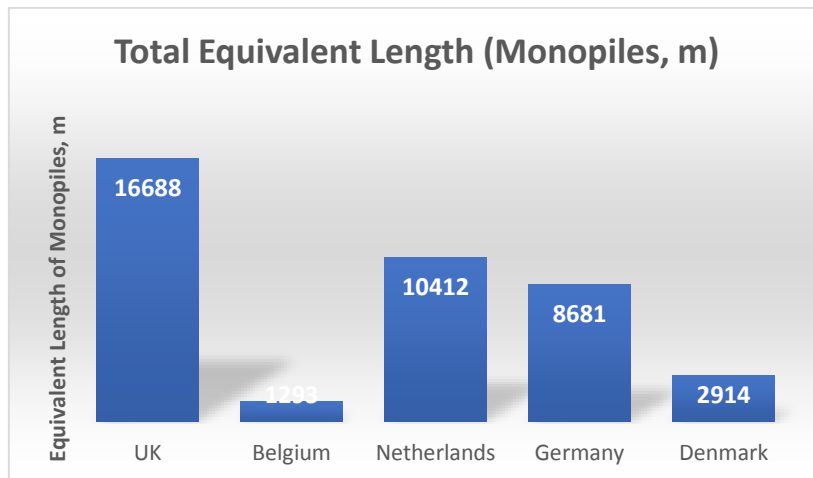


Figure 7.21: Total Length of Monopiles to be Installed per Country

### 7.4.3 Comparison between Constructed and Planned Projects

In this paragraph, a comparison between the current and planned situation is being presented. Denmark is expected to increase its' installed capacity by about 220% by 2020, whereas, the Netherlands has the potential to increase their installed capacity by 175%. The UK and Germany demonstrate increasing trends as well, with an expected increase of 108% and 68.5%, respectively. However, as the leader in the projects which are already connected to the grid, the UK is expected to install about 5.2 GW, which in absolute numbers, will be almost equal to the summation of the capacity which will be realized by all the other countries combined (Figure 7.22).

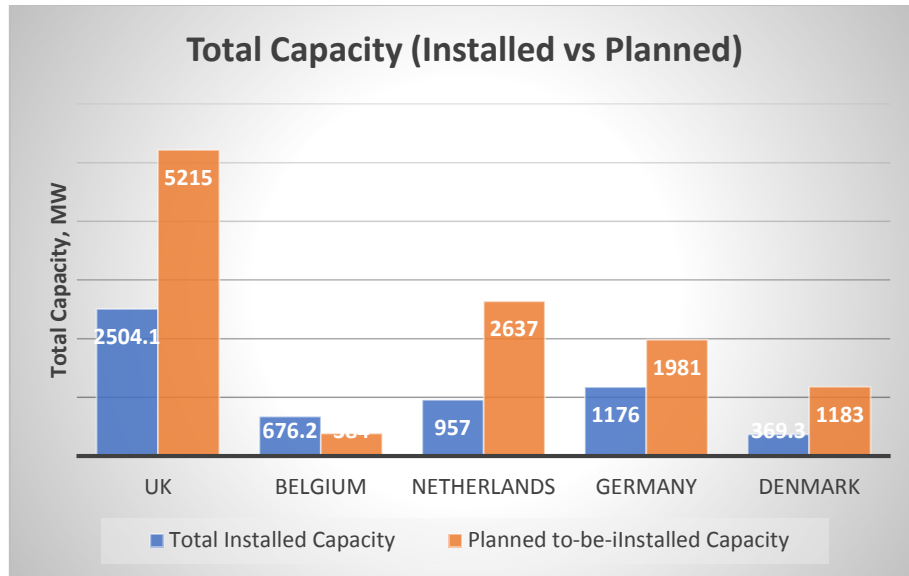


Figure 7.22: Current vs. Planned Capacity Installed

As shown in Figure 7.23, the trend for the upcoming projects is to install turbines of higher unit capacity. The increase in the capacity/turbine varies between 75% - 140%, for the various countries under consideration.

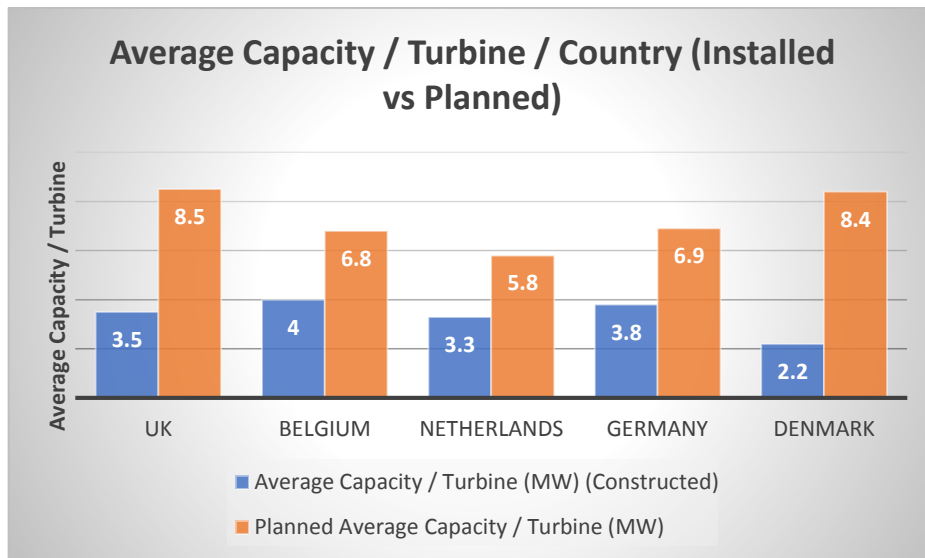


Figure 7.23: Average Capacity per Turbine per Country

Also, the trend is to realize projects in deeper water (Figure 7.24). Only for the Netherlands forecast of the future shows the development of projects in shallower waters. This forecast is mainly based on the fact that currently (April 2016), there are still many empty licensed fields in the EEZ of the country, located in low depths. However, this forecast should be further evaluated, since power production might be more beneficial further offshore, and new fields is possible to be licensed at any time in the near future.

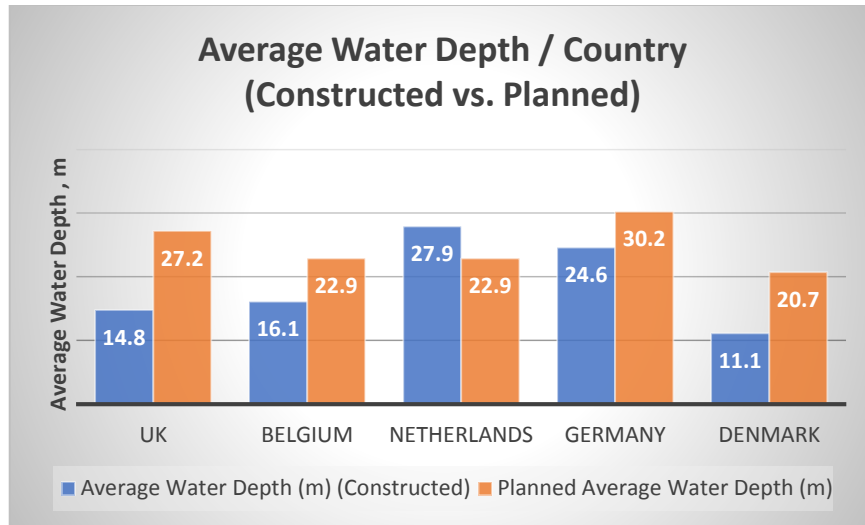


Figure 7.24: Average Water Depth of Current / Planned Projects per Country

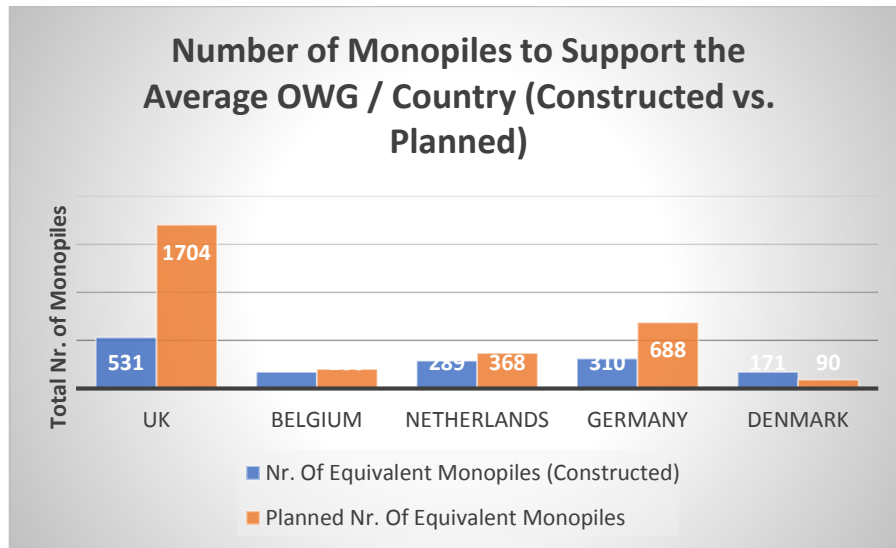


Figure 7.25: Total Number of Monopiles Constructed and Forecasted per Country

The “total length” of the monopiles which will be used to support the turbines of the new projects for the UK is about 16 km (Figure 7.26), showing an increase of about 112%. A significant increase is also estimated for Denmark, where the equivalent total length is expected to increase by 53.5%.

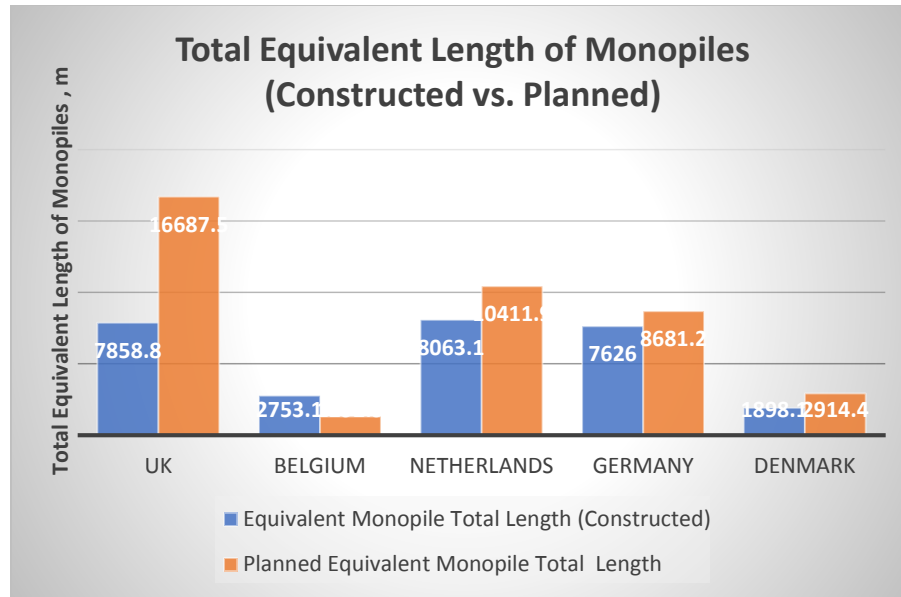


Figure 7.26: : Total Length of Monopiles to be Installed per Country

As mentioned before, the average offshore wind generator to be installed in the future varies for each country (Figure 7.22). This leads to a varying estimated Rotor-Nacelle Assembly (RNA) mass for each country. Setting the embedded length of the monopile, the soil properties, the diameter/thickness of the transition piece/tower and the thickness of the monopile as constants, a sensitivity analysis is being performed to identify the required monopile diameter to obtain the same natural frequency. The parameters which differentiate between the countries are the average water depth, due to the varying site locations, and the tower height, due to the different rotor dimensions for the various wind turbines. The natural frequency is set to be approximately 0.22 Hz, in order to exceed the upper limit of the 1P frequency of the rotor by at least 10%. The 1P frequency depends on the type of wind turbine. In the following analysis, the Siemens - SWT-6.0-154 turbine is chosen for the sites where the trend reveals that the average wind turbine generator capacity will be about 6 MW in the future. For the countries where the trend reveals the utilization of 8 MW turbines, the Vestas V164-8.0 MW turbine is being chosen, since is one of the few 8 MW turbines available currently in the market. The upper limit of the 1P frequency is set by the Vestas V164-8.0 MW turbine, which has the highest rotor speed (4.8 – 12.1 RPM) ([www.homepages.ucl.ac.uk](http://www.homepages.ucl.ac.uk)). Therefore, the target natural frequency in this analysis is about 0.2218 Hz. In the following tables (Table 7.2, Table 7.3), the required tower height and the resultant average diameter and thickness for each country is being presented.



Country	Nominal Power (MW)	Model	Top Mass (kg)	Typical Rotor Size (m)	Minimum Tower Length Required (m)
Netherlands	6	Siemens - SWT-6.0-154	360000	154	82
UK	8	MHI Vestas V164-8.0MW	495000	164	87
Belgium	6.5	Siemens - SWT-6.0-154	360000	154	82
Germany	6.5	Siemens - SWT-6.0-154	360000	154	82
Denmark	8	MHI Vestas V164-8.0MW	495000	164	87

Table 7.2: Wind Turbine and Minimum Tower Length Required

Country	Average Water Depth (m)	Monopile Length (above seabed) (m)	Diameter (m)	Thickness (m)	Natural Frequency (Hz)
Netherlands	23	28	6.1	0.08	0.2221
UK	27	32	6.5	0.1	0.2231
Belgium	23	28	6.1	0.08	0.2221
Germany	30	35	6.2	0.1	0.2224
Denmark	21	26	6.4	0.085	0.2239

Table 7.3: Minimum Monopile Length and its Required Minimum Dimensions

Taking into consideration the average water depth and the minimum diameter and thickness required, the inner area and volume of the average monopile per country is being presented in Table 7.4.

Country	Inner Area (m <sup>2</sup> )	Inner Volume (m <sup>3</sup> )
Netherlands	27.71	775.93
UK	31.17	997.52
Belgium	27.71	775.93
Germany	28.27	989.60
Denmark	30.48	792.57

Table 7.4: Area and Volume of the Upper Part of the Average Dimensions Monopile per Country

The values presented in Table 7.4 are essential in order to estimate the average cost of the sand which will be used as filling in the monopile, as well as, the costs related to the transportation and installation of sand, for each specific country.

## 7.5 Financial Analysis for the Sand-Filled Monopiles Technique – Case Study

The main goal of the financial analysis is to identify the effect of filling the monopile with sand, on the total cost for the foundation of an offshore wind turbine. As shown in Figure 7.27, the monopile's cost represents the 25% of the CAPEX of the investment for a project developed in the Netherlands (2014) [56]. In the US, the cost of the support structure is approximately 23% (Table 7.5), which is very similar to the cost of the support structure presented for the Netherlands. Therefore, it can be concluded that the support structure represents a significant percentage of the total cost and any reduction in its' total cost could be beneficial for the investment.

Table 3.1 Baseline parameters.

Type	Parameter	Units	4-A-14	4-D-14	8-A-14	8-D-14
CAPEX	Development	€/MW	101	108	90	95
	Turbine	€/MW	1,279	1,279	1,498	1,498
	Support structure	€/MW	677	861	689	722
	Array electrical	€/MW	98	99	89	91
	Construction	€/MW	543	645	320	496
OPEX	Operations and planned maintenance	€/MW/yr	31	37	23	28
	Unplanned service and other OPEX	€/MW/yr	65	78	48	57
AEP	Gross AEP	MWh/yr/MW	4,459	5,022	4,551	5,089
	Losses	%	18.6	17.3	17.6	16.2
	Net AEP	MWh/yr/MW	3,628	4,154	3,750	4,263
	Net capacity factor	%	41.4	47.4	42.8	48.7

Source: BVG Associates

Figure 7.27: Approximated Cost / MW for an Offshore Wind Turbine in the Netherlands (2014) [10]

Input category	Units	Tranche A	Tranche B	Tranche C
<b>CAPEX</b>				
Turbine	\$/kW	\$1,615	\$1,424	\$1,263
Support Structure	\$/kW	\$681	\$604	\$527
Installation (turbine and support structure)	\$/kW	\$369	\$349	\$324
Within Farm Array Cable	\$/kW	\$176	\$167	\$154
Development and permitting	\$/kW	\$191	\$171	\$144

Table 7.5: Cost / KW for the development of an offshore wind farm in the US [57]

Moreover, forecasts on the cost of the offshore wind turbines reveal the potential of 12% reduction of the total cost by 2020, and the potential for a 7% decrease on the cost related with the support structure (in comparison with cost values of 2011) [56].

### 7.5.1 Material Unit Costs related to the Support Structure (Monopile)

In order to perform the cost-benefit analysis, the costs related to the materials which will be used for the foundation of the monopile, along with the relevant transportation and installation costs need to be determined. The monopile is being constructed using steel (S355) welded plates. The price per tonne used in this analysis refer to an S355K2-G3 steel, which is suitable for design

of structures in marine environment. The mechanical properties of this type of steel are being shown in Table 7.6 ([www.tritonalloysinc.com](http://www.tritonalloysinc.com)).

MECHANICAL PROPERTIES OF GRADE S355 K2G3

Grade	Thickness(mm)	Min Yield (Mpa)	Tensile(MPa)	Elongation(%)	Min Impact Energy	
S355K2G3	8mm-100mm	315Mpa-355Mpa	450-630Mpa	18-20%	-20	40j
	101mm-200mm	285Mpa-295Mpa	450-600Mpa	18%	-20	33j
	201mm-400mm	275Mpa	450-600Mpa	17%	-20	33j

Table 7.6: Mechanical Properties of S355 K2G3 Steel for Offshore Applications

The cost per tonne for the aforementioned steel type, in form of a plate, ranges between 500 – 800 \$/tonne ([www.tritonalloysinc.com](http://www.tritonalloysinc.com)). The plates need to be welded and as ECN [58] suggests the expected final cost per tonne is about 2000 €/tonne. Therefore, the average value of the raw material is approximately 550 €/tonne (exchange rate August 2017) and the average value considered for the welded plates is approximately 2000 €/tonne, but in prices of 2002. The total plate cost/tonne shown in ECN’s report comprises of:

- a. The Price of Steel
- b. The Price for the Works on the Plates (welding, coating etc.)

A trendline for the price of hot rolled steel plates ([www.mesteel.com](http://www.mesteel.com)), has shown a variation in the price of steel plates 290 – 565\$/tonne (243 – 473€/tonne), for the time period between January 2003 – August 2017. Therefore, the cost for the works as of 2002 [58] is approximately 1710 €/tonne. Taking into consideration the average inflation rate between 2002 -2016 for the Netherlands ([www.inflation.eu](http://www.inflation.eu)) is approximately 1.58%. The equivalent present value for the works, assuming that the annual cumulative inflation is representative also for this type of manufacturing works, is being calculated by the following formula [59]:

$$Steel\ Value_{2016} = Steel\ Value_{2002} \cdot (1 + i)^N \quad (7.6)$$

Where the inputs of the formula are shown in Table 7.6.

Steel Value, 2002 (€)	Inflation Rate (%)	Years
1710	1.58	14

The total estimated cost per tonne for the steel is equal to (2016 prices):

$$1710 \cdot (1 + 0.0158)^{14} + 473 = 2129.7 + 473 = 2602.7 \text{ €/tonne}$$

An indicative cost per tonne for sand in Europe is approximately 15 €/tonne (UK prices, April 2017 ([www.orkagg.co.uk](http://www.orkagg.co.uk))). The required cost for steel per monopile (m3) for each is being shown in Figure 7.28.

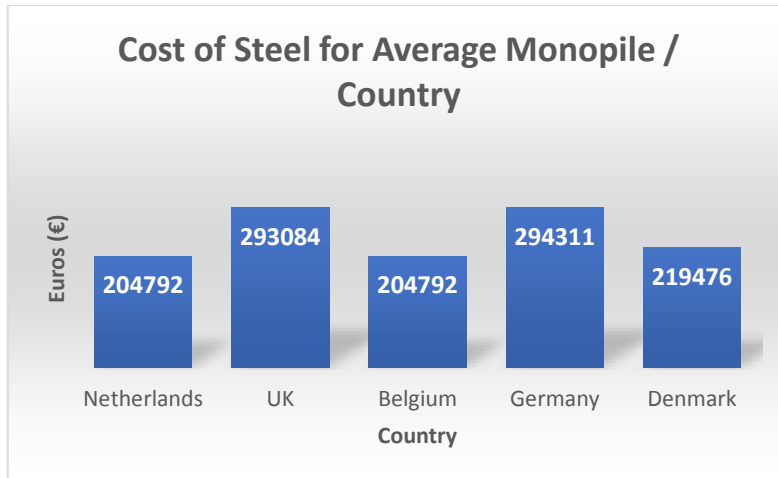


Figure 7.28: Cost of Steel / Monopile / Country

The required cost for the sand-fill (material only) for each country is being shown in Figure 7.29.

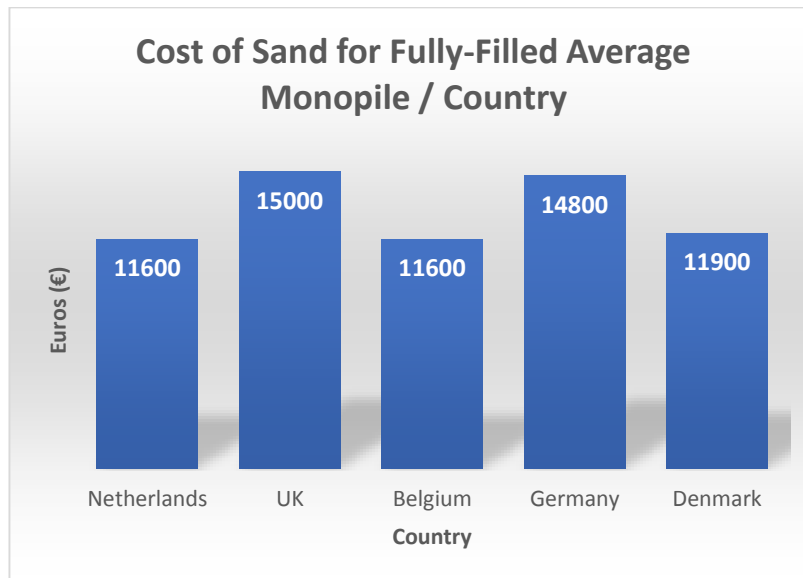


Figure 7.29: Cost of Sand / Fully Filled Monopile / Country

The percentage increase in the material costs between the empty and the sand-filled monopile can be calculated using the formula:

$$\frac{\text{Cost of Sand} - \text{Fill}}{\text{Cost of Steel}} \cdot 100 \quad (7.7)$$

The results are being shown in Figure 7.30.

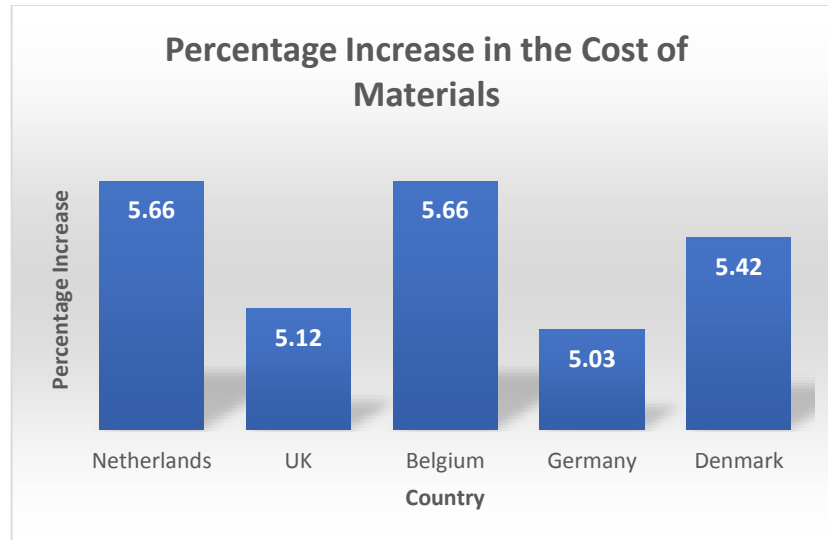


Figure 7.30: Percentage Increase in the Material Cost due to Sand-Fill / Country

## 7.5.2 Transportation and Installation Costs

Filling the monopile with sand, will also lead to an increase in the total transportation and installation costs of the foundations. A schematic representation of the transportation and installation process for an offshore wind turbine is being shown in Figure 7.31[60]. In this representation a jack-up (self-transport) structure is assumed to be used for both the transportation and the installation of the monopiles. The only variation between the process described in Figure 7.31 and the one followed in the current report, is the fact that the jack-up will only be used to install the monopiles. Barge vessels will be used to transport the monopiles from the port to the jack-up vessel, since the dayrate of these vessels are much lower. The latter is being presented in the following paragraphs. The two transportation strategies described above, are the only two available options for the transportation of offshore wind turbine [61].

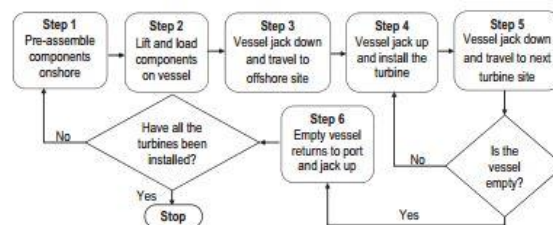


Figure 7.31: Flow Chart Describing the Transportation & Installation Process with a Jack-Up Vessel

The transportation time is totally dependent of the distance between the port and the installation area. Therefore, later in this chapter an area of the fictional wind farm in the Netherlands' EEZ is assumed. The installation time is dependent on the dimensions of the monopile to be driven in the ground (diameter and thickness). The expected time for the installation of a monopile, given the wind generator capacity, has been obtained by related publications [61]. Finally, indicative values for the day rates of the vessels which are required to

perform the transportation and installation have been obtained. Table 7.7 shows an approximate relation between the foundation installation time and the wind turbine capacity.

Foundation Installation Time	
Capacity (MW)	Expected Value (hrs)
2.5	40
3	54
3.6	60
4	84
5	96

Table 7.7: Expected Installation Time for Varying Wind Turbine Capacity [15]

Linear interpolation has been applied to estimate the average installation time for larger turbines (Figure 7.32).

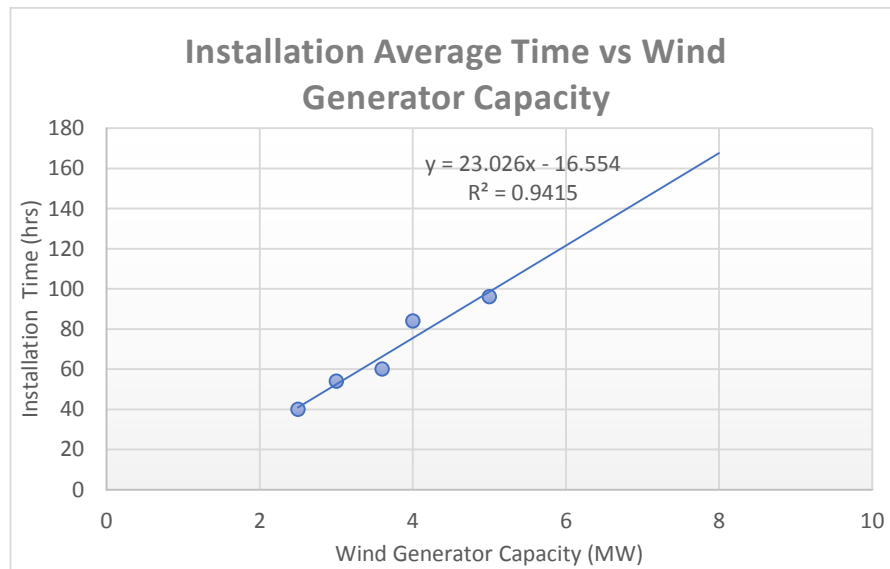


Figure 7.32: Expected installation time for wind generators of 2.5 – 8 MW

In order to fill the monopile with sand, a barge will be used to transport the sand and a specialized vessel will be used to transfer it to the installation (Jack-Up) vessel [61].

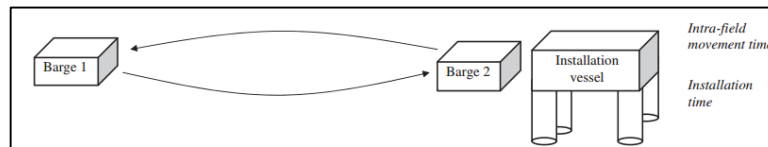


Figure 7.33: Transportation from the port to the jack-up structure procedure

The transfer of the sand from the installation vessel into the monopile, is assumed to be performed using a conveyor belt with an average unloading as estimated by Jones et al. [62]. A digital representation of a conveyor belt shown in Figure 7.34 (<https://i.ytimg.com>).

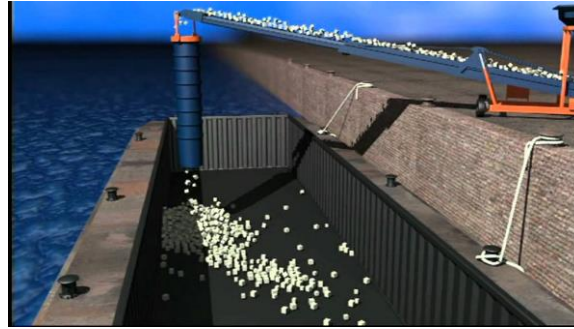


Figure 7.34: Conveyor Belt to Install Soil Offshore

Indicative day rates in the Netherlands for barges & jack up structures (for the monopile) and transportation & installation vessels (for the sand) are being shown in Figure 7.35 (2002 Prices) [58].

Parameter	Mobilisation costs	Day-rate	Significant wave height
2 tugs	36,000	20,000	1.5
1 cargo and 1 tug	38,000	35,000	1.5
Jack-up	200,000	75,000	2.0
Construction vessel	400,000	75,000	2.0
Sheer leg	150,000	75,000	1.5
Crane barge	200,000	100,000	2.0
Directional drill	not used	35,000	N.A.
Pontoon 80x25 + crane	not used	35,000	not used
Pontoon 60x20	not used	25,000	not used
2x trenching equipment	not used	10,000	N.A.
60 MT AHT	not used	15,000	not used
35 MT AHT	not used	10,000	not used
Tow tug	not used	10,000	not used
Divers	not used	10,000	N.A.
Cargo barge (large working area)	not used	35,000	not used
Cargo barge (normal working area)	not used	25,000	not used
Submarine cutting equipment	not used	25,000	N.A.

Figure 7. 35: Indicative Mobilization Costs and Day Rates (Netherlands, 2002)

Taking into consideration the inflation (Formula 7.6), the present value of the costs of the vessels under consideration in this report are being shown in Table 7.8.

#### Vessel Day Rates (Netherlands)

<b>Monopile Transport Vessel (Cargo Barge)</b>	31150	€/day
<b>Monopile Installation Vessel - including Installation Equipment (Jack-Up)</b>	343000	€/day
<b>Sand Transport Vessel (Cargo Barge)</b>	31150	€/day

Table 7.8: Present Value of the Cumulative Cost per Day for Transportation & Installation Vessels in the Netherlands

The values presented in Table 7.8 are estimations, but their accuracy is confirmed by an expert in the field. The expert in the field also provided an estimated cost for the more specialized vessel which will install the sand. The expected cost for it is about 75000 €/day.

### 7.5.3 Installation Time Estimation for a Single Monopile

For a single monopile, the average loading and movement time using a Jack-Up vessel is shown in Figure 7.36[61]. The average installation time per turbine capacity has been shown in Table 7.7.

Parameterization range for factors influencing foundation installation time.

Model	Load time, $L$ (h)	Installation time, $I$ (h)	Movement time, $M$ (h)	Weather uptime, $W$ (%)
Self-transport	2–4 (3)	36–96 (72)	4–8 (6)	75–95 (90)
Barge	NA	36–96 (72)	NA	75–95 (90)

Expected values are denoted in parentheses.

Figure 7.36: Average Load, Installation and Movement Time for Jack-Up Vessel

The total operational time for a Jack-Up, in order to install a monopile in each country is being shown in Table 7.9.

Country	Average Turbine Capacity (MW)	Indicative Model	Expected Installation Time (hrs)	Load + Installation + Movement Time (hrs)
Netherlands	6	Siemens - SWT-6.0-154	120	129
UK	8	MHI Vestas V164-8.0MW	170	179
Belgium	6.5	Siemens - SWT-6.0-154	135	144
Germany	6.5	Siemens - SWT-6.0-154	135	144
Denmark	8	MHI Vestas V164-8.0MW	170	179

Table 7.9: Total Operational Time for a Jack-Up to Install a Monopile for each Country

Assuming that the transportation vessel will travel once to a site with a distance to the port of 80 km and assuming a speed of 6 kn (11 km/hr) for the transport vessel, the operational time for the transport vessel is approximately 7.3 hrs ( $\approx 0.3$  days). The total transportation and installation costs for a single monopile is being shown in Table 7.10.



Country	Load + Installation + Movement Time (hrs)	Load + Installation + Movement Time (days)	Jack-Up Cost (M €)	Transp. Time (hrs)	Transp. Time (days)	Barge Cost (€)	Total Cost (M €)	Cost / MW (€)
Netherlands	129	5.4	1.85	7.3	0.3	9345	1.862	308700
UK	179	7.5	2.57	7.3	0.3	9345	2.582	321563
Belgium	144	6	2.06	7.3	0.3	9345	2.067	316615
Germany	144	6	2.06	7.3	0.3	9345	2.067	316615
Denmark	179	7.5	2.57	7.3	0.3	9345	2.582	321563

Table 7.10: Total Transportation and Installation Cost per Monopile for each Country

The estimation of the total cost is conservative, because the transportation barge was assumed to transfer only one monopile. However, and taking into consideration the fact that the transportation cost is less than 1% of the installation cost, this assumption cannot really affect the cost figures.

#### 7.5.4 Sand-Fill Transportation and Installation Cost Case Study - “Icarus” Offshore Wind Farm

The cost to transport and install the sand-fill at a site with a distance of 80 km from the port is shown in the table below. A specialized vessel to transport sand in the Netherlands has an average speed of 14.1km/h. Using a specialized vessel ([www.scheepvaartwest.be](http://www.scheepvaartwest.be)) for sand transportation and installation, with average tonnage of 12000 tonnes, the total cost of transportation and installation of sand per monopile for each country is being shown in Table 7.11.

Country	Inner Volume (m <sup>3</sup> )	Density Sand (kg/m <sup>3</sup> )	Weight of Sand (tn)	Vessel Capacity (tn)	Number of Turbines to be filled	Transp. Time (hrs)	Unloading Rate (tns/hr) [62]	Time to Fill Monopile (hrs)	Total Cost (€)
Netherlands	775.93	1900	1474.3	11500	7.8	5.7	1000	1.47	220000
UK	997.52	1900	1895.3	11500	6.1	5.7	1000	1.90	282500
Belgium	775.93	1900	1474.3	11500	7.8	5.7	1000	1.47	220000
Germany	989.60	1900	1880.2	11500	6.1	5.7	1000	1.88	281000
Denmark	792.57	1900	1505.9	11500	7.6	5.7	1000	1.51	225000

Table 7.11: Total Cost of Sand Filling / Monopile for each country

The percentage increase of the cost per monopile for each country, due to the added cost of the sand-fill, is shown in Table 7.12 and in Figure 7.37.

Country	Cost Of Steel (€)	Cost Of Sand (€)	Transportation & Installation Cost Steel (€)	Transportation & Installation Cost Sand (€)	Total Cost Empty Monopile (€)	Total Cost Filled Monopile (€)	Percentage Increase (%)
Netherlands	204800	11600	1861545	220000	2066345	2297945	11.2
UK	293100	15000	2581845	282500	2874945	3172445	10.3
Belgium	204800	11600	2067345	220000	2272145	2503745	10.2
Germany	294300	14800	2067345	281000	2361645	2657445	12.5
Denmark	219500	11900	2581845	225000	2801345	3038245	8.5

Table 7.12: Percentage Increase of the Cost / Monopile for each Country due to the Sand-Fill

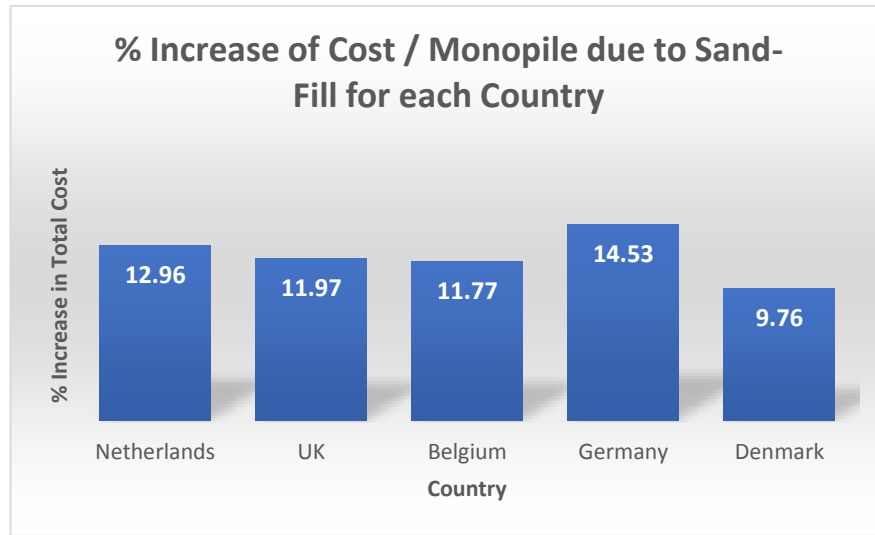


Figure 7.37: Percentage Increase of Cost / Monopile / Country due to Sand-Fill

Due to the varying dimensions of the “average forecasted diameter monopile” for each country, the cost of filling the monopile with sand varies. However, as shown in the previous chapters, in order to achieve the maximum effect on the increase of the damping ratio of the structure, the monopile should be totally filled. This is due to the fact, that placing more soil in the monopile, leads to a higher effect of the hysteretic damping values due to the shear deformations of the soil. However, this conclusion has been verified only for the Upwind report’s monopile, which has a diameter of 6.1 m and a thickness of 0.08 m. A suggested future research topic would be to verify this result for various dimensions of monopiles.

## 7.6 Conclusion

The increase on the total cost of the foundations, due to the added sand in the monopile (including material, transportation and installation costs), is significant, and is approximately 11% (Netherlands). This percentage corresponds to an approximate added value of about 231,500€. The analysis which was performed as the main objective of this report, revealed that the added stiffness to the structure is considerably lower than the added mass, so there is no possibility to increase the natural frequency of the structure by adding soil in the monopile. On the other hand,

the added sand has the ability to increase the damping of the system, with a consequent decrease of the amplitude of the stress cycles applied on the structure. The free vibration tests have shown an increase on the damping ratio of the structure by 0.04%, for a monopile embedded in sand. The increased damping ratio leads to a smaller maximum amplitude on the horizontal displacement of the structure. The increase of the damping of the structure is low, but still further research is suggested to examine the effect of the sand-fill on the amplitude of the stress cycles. Decrease in their amplitude could also decrease the fatigue damage on the structure. This could lead to lower maintenance costs and/or extension of the lifetime of the foundation. A future research could be focused in those aspects and then the evaluation of the financial loss or benefit of the added could be quantified.

*Page intentionally left blank*

## 8. Conclusions & Recommendations for Future Work

This research project focuses on the possible positive effect of added sand in monopiles. More specifically, it focuses on the effect of added sand on the structural and dynamic behavior of a monopile. The research objectives have been described in Paragraph 1.8. In the following paragraphs, a brief overview of the methods used to estimate the effect of sand-fill on each attribute of the structure is being presented. Also, the results obtained by the simulations are being presented and discussed.

### 8.1 Research Objective 1: Effect of Sand-Fill on the Local Buckling Resistance

The effect of sand-fill on the local buckling resistance is being examined using the relevant provisions of CUR211E [21] and in EN1993-4-3 [24]. Those design codes, suggest an indirect effect of the presence of sand-fill in the local buckling resistance of a pile. This positive effect is mainly due to the reduced ovalization of the monopile. The critical cross-section, which is prone to buckling, for an empty monopile has been identified [19] to be located at the area above the plugged part of the monopile. Then, an analysis has been performed in order to estimate the ovalization of an empty and a sand-filled tube. Ovalization occurs due to:

1. Initial out-of-roundness which is permitted in the production process of the pile
2. Ovalization due to direct and indirect soil pressure
3. Ovalization as a 2<sup>nd</sup> order effect due to bending

The difference between empty and sand-filled piles is that the latter are not expected to experience ovalization due to soil pressure (2), as the presence of soil in the pile is assumed to counteract the pressure outside of the monopile. This leads to significant decrease on the ovalization of the cross-section, and consequently, to an increase in the bending resistance of the monopile. The benefit of the added sand on the bending resistance of an empty pile was estimated to be approximately equal to 20%, for a loose sand used as sand-fill.

The positive effect of the sand-fill varies also with its' Young's Modulus. Using denser sand (i.e.  $E = 80 \text{ MPa}$ ), the increase on the bending resistance can be up to about 34%.

### 8.2 Research Objective 2: Effect of Sand-Fill on the Response of the Monopile to a Static Loading

In order to identify the effect of sand-fill on the displacement of the monopile, a model of the structure was created using Plaxis 3D. First, the lack of accuracy of the API p-y curves for large diameter monopiles was identified [14, 27]. Then, representative parameters to model a typical sand found in the North Sea were obtained by the literature [14]. Afterwards, a model presented in the literature was re-modeled in order to validate the accuracy of the model created in Plaxis 3D for this report. Having validated the model, a lateral load of a varying magnitude was applied to the top of an empty and a filled monopile. The displacements were measured at two different levels, namely, at the seabed level and at the top of the monopile. The effect of sand-fill on the reduction of the displacement at the seabed level is being presented in Figure 8.1.

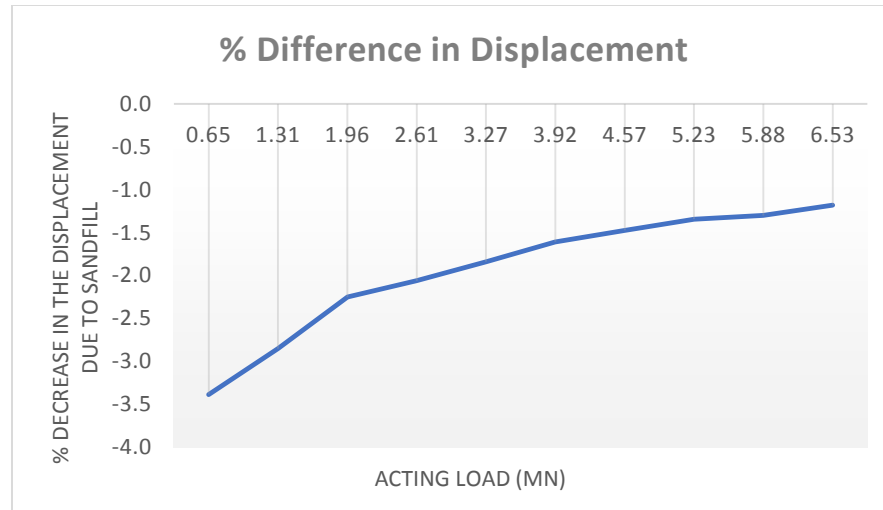


Figure 8.1: Percentage Decrease of Displacement due to Sand-Fill for varying Lateral Loading

As shown, as the magnitude of the acting load increases, the positive effect of the presence on sand-fill on the stiffness of the monopile decreases. This is reasonable, since the sand-filled was modelled in Plaxis using the Mohr-Coulomb material properties. Therefore, after some level of strains, the sand-fill is expected to reach its' plastic resistance. After reaching its' plastic resistance the sand-fill cannot contribute to the bending stiffness of the "composite" (steel and sand) section.

It was also noted, that the effect of the presence of sand-fill on the lateral displacement was more significant for the displacement at the seabed level, rather than for the displacement at the top of the monopile. This can be explained by the fact that at the seabed level the added sand can reduce the total displacement also due to its added mass on the structure. On the top of the monopile, only the additional bending stiffness further decreases the displacement, but the bending stiffness of the "sand column" in comparison with the bending stiffness of the monopile itself is very small.

### 8.3 Research Objective 3: Effect of Sand-Fill on the Natural Frequency of the Structure

The effect of sand-fill on the natural frequency of the structure was estimated by using two different models, namely, a model assuming a clamped connection for the monopile at a specific depth (fixity depth – Model A) and a model which included distributed soil springs with constant stiffness for the embedded part of the monopile (Model B). Two methods have been applied in order to perform the analysis, a numerical and an analytical one. In the numerical method, the Finite Difference Method was applied in Matlab, in order to discretize the structure and calculate the dynamic properties of an "N" degree of freedom system. In the analytical method, the actual equations of motion have been solved and the natural frequencies were determined graphically in Maple. Having estimated the natural frequencies, the coefficients which are required in the general solution of the equations of motion have been calculated, and the normal modes of a beam with constant stiffness and mass have been obtained (approximate modes). Utilizing the approximate modes as reference modes for the actual structure, the natural frequency of the structure is being calculated. Having established and validated the two alternative methods to

calculate the natural frequencies of the structure, a sensitivity analysis is being performed in order to identify the effect of:

- Monopile's Bending Stiffness
- Tower's Bending Stiffness
- Monopile's Mass
- Tower's Mass

on the 1<sup>st</sup> natural frequency of the structure. The results of the analysis have shown for all the models used in the analysis that:

- Increasing the bending stiffness of the monopile leads to a bigger increase in the natural frequency of the structure, in comparison with the case that the bending stiffness of the tower is increased
- Increasing the mass of the tower leads to a bigger decrease in the natural frequency of the structure, in comparison with the case that the mass of the monopile is increased

Then a sensitivity analysis was performed in order to identify the effect of filling the monopile with an "artificial material" of varying bending stiffness and density. This analysis was performed in order to identify the properties of the added material in order to increase the natural frequency of the monopile by 0.01 Hz, in comparison with the empty structure's natural frequency. The results for model A and B, for all the methods of analysis yielded that:

- Using the numerical solution for model A and B, for a material with average density of  $\rho = 2000 \text{ kg/m}^3$ , the required bending stiffness is equal to  $E = 9000 \text{ MPa}$
- Using the analytical solution for model A, for a material with average density of  $\rho = 2000 \text{ kg/m}^3$ , the required bending stiffness is equal to  $E = 6900 \text{ MPa}$
- Using the analytical solution for model B, for a material with average density of  $\rho = 2000 \text{ kg/m}^3$ , the required bending stiffness is equal to  $E = 4300 \text{ MPa}$

It can be concluded, that the analytical solutions which were obtained using the approximate modes of a beam with a constant dimensions and no top mass added on its' top yield somehow different results in comparison with the exact numerical solution which refers to the structure as described in Upwind report. Therefore, the approximate required characteristics of the artificial material are the following:

$$\rho = 2000 \frac{\text{kg}}{\text{m}^3}$$

$$E \cdot I = 9000 \text{ MN} \cdot \text{m}^2$$

It was also shown that assuming distributed soil springs instead of a fixity length, the added stiffness of the sand is located closer to the "connection" of the structure on the ground. This leads to an added stiffness and mass closer to the support, which enhances the positive effect of the filling on the structure's total stiffness. Therefore, a material with much lower bending stiffness is required in this case.

## 8.4 Research Objective 4: Effect of the Sand-fill on the Damping Ratio

In order to estimate the effect of the added sand on the damping ratio of the structure, a model was created in Plaxis. A free vibration analysis was performed and the logarithmic decrement method was applied in order to estimate the damping ratio of the structure. The logarithmic decrement method was applied on the normalized time history response, as the method suggests. In order to isolate the contribution of the sand-fill to the total damping of the structure, the only forms of damping included were the structural damping of steel and the damping due to the hysteretic behavior of the surrounding soil and the sand-fill. The Hardening Soil Small (HS Small) modeled offered in Plaxis 3D was used to model the soil. This type of soil is verified by other researchers that it can capture the damping ratio of the soil when the shear strains developed increase. An extensive literature review was performed in order to identify the main parameters which affect the shear stress/strain behavior of the soil. Then, experimental results which were considered as representative for the loading conditions on the sand-fill were found in the literature, in order to estimate the representative characteristics of the sand-fill and to model it in Plaxis 3D.

Moreover, a sensitivity analysis was performed in order to identify the effect of the mesh size and the measured number of cycles on the estimated damping ratio. After optimizing the number of cycles measures and the mesh size, the inputs needed to model a sand of loose, medium and high density were collected and used to model the surrounding soil and the sand-fill. Having identified all the inputs to model the sand in Plaxis, a sensitivity analysis was performed in order to identify the effect of a sand-fill of a varying density on a monopile embedded in a sand of a varying density. The results of this analysis have shown that the damping mechanism for an embedded monopile in loose sand leads significantly higher dissipation of energy, than for a monopile embedded in dense sand. Also the shear stresses on the sand-fill led to an added damping on the system, which was captured by Plaxis. A collective table (Table 8.1) which shows the results obtained by these simulations is shown below.

Type of Surrounding Soil	Type of Filling	Natural Frequency (rad/sec)	Damping Ratio (%)	Increase on Damping Ratio due to Sand Fill (%)
Loose	Empty	1.825	0.58	N/A
	Loose	1.810	0.62	6.9
	Dense	1.810	0.62	6.9
Medium	Empty	1.870	0.5	N/A
	Loose	1.860	0.54	8
Dense	Empty	1.915	0.38	N/A
	Loose	1.910	0.42	10.5
	Dense	1.910	0.42	10.5

Table 8.1: Variation of Damping Ratio with the Presence of Sand-fill and the Density of Soil



Then, the effect of filling partially the monopile with sand was tested. The analysis shown, that only by filling the monopile along its' height with sand can lead to the benefit obtained by its' presence on the damping ratio of the structure.

One more sensitivity analysis was performed, in order to identify the relation between the initial displacement imposed during the free vibration tests and the damping ratio of the structure. The analysis has shown an increase of the damping ratio as the imposed displacement increases. The results are shown in Table 8.2.

Initial Displacement (m)	FILLED		EMPTY	
	Natural Frequency (rad/sec)	Damping Ratio (%)	Natural Frequency (rad/sec)	Damping Ratio (%)
0.05	1.820	0.46	1.835	0.42
0.10	1.815	0.62	1.825	0.58
0.20	1.795	1.02	1.810	0.92
0.30	1.775	1.32	1.795	1.20
0.40	1.762	1.60	1.785	1.40

Table 8.2: Natural Frequency and Damping Ratio variation with Initial Displacement

Having identified the damping ratio variation due to the varying density of soil, the damping ratios of the structure as shown in Table 8.2, were used to identify the maximum displacement on each node and for each excitation frequency, taking into consideration the respective damping ratios obtained by Plaxis.

## 8.5 Financial Analysis of the “Sand-Filled Monopiles” Technique

In the last chapter of this report, a financial analysis was performed in order to estimate the added cost filling the monopiles offshore with sand. This estimation of this added cost is significant, because if the benefit of increasing the damping ratio of the structure is quantified using monetary values, then this added benefit should be compared with the added cost. Only by doing so, future investors can make an informed decision on how to proceed or not to the filling of monopiles offshore with sand.

Firstly, the opportunity window for the application of a new technology in the offshore wind turbine foundation in the future was estimated. The estimation of the future projects where a new technology could be applied, was performed using forecasts by accredited organizations, along with an online platform which presented the current situation of offshore wind farm developments in the North Sea. Having obtained the data of the online platform and taking into consideration the forecasts of the reports, the trends for the future for various characteristics of the wind farms were identified for each country which has an Exclusive Economic Zone in the North Sea. After processing the data statistically, parameters such as:

- Average Total Capacity / Country
- Average Capacity / Turbine
- Average Depth / Foundation

were estimated for the future projects at each country. This data was processed and an estimation of the total volume needed to be filled by sand / monopile / country was estimated.

Then, the unit costs for the materials included in this analysis were obtained, using current market values and the installation and transportation costs were obtained by the literature and had been confirmed through a conversation with an industry expert. After collecting all the cost related data, a fictional case study (“Icarus Offshore Wind Farm”) was analyzed in order to estimate the cost of applying the sand-filled technology on a future wind farm located at each country under consideration.

## 8.6 Recommendations for Future Research

- The calculation of the natural frequency of the structure for the analytical and the numerical models with the soil was performed assuming soil springs with constant stiffness along the embedded pile length. Modelling the stiffness of the soil varying with the depth, would lead to a more realistic representation of its’ stiffness, which might possibly affect the results related to the effect of the sand-fill on the fundamental natural frequency of the structure
- In the Free Vibration Analysis performed to calculate the damping ratio of the structure, only the damping due to the hysteretic behavior of the soil and the material damping of steel was included. This was done, because this research is focused on the comparison on the damping ratio of a structure with an empty and a sand-filled monopile. However, in order to measure a more realistic value for the total damping ratio of the structure, an additional damping of approximately 3% need to be added to the soil material as suggested by Brinkgreve et al [46]. This damping will be in the form of Rayleigh damping.
- In this research project, the additional cost for a sand-filled monopile was estimated during the financial analysis presented in Chapter 7. Having identified the positive effect of sand-fill on the damping ratio of the structure, further research should be focused to the effect of the reduced amplitude of the loading cycles and to the consequent possible decrease in the fatigue damage on the connections. Also, the possibility of the reduction on the maintenance related costs can be examined. Only after performing this analysis, the benefit of adding sand-fill in the monopile can be compared with the cost calculated in the financial analysis. This comparison will lead in the final verdict on whether the sand-fill technique is beneficial or not for the future investors, from a monetary point of view.
- During the analysis was shown that filling the monopile with a material with a Youngs Modulus of  $E = 6000 - 9000$  MPa (depending on the method of calculation) can have a beneficial effect on the stiffness of the structure. However, this Youngs modulus refers to composite materials which will increase the cost of the material and the installation costs. The technical feasibility of this solution along with a financial analysis is advised to be performed in order to examine its’ benefits.
- Concrete has a Youngs Modulus of  $E \approx 20000$  MPa, and there is also available underwater concrete, which in theory could be installed in the monopile. It is shown in this report, that filling the monopile with concrete would be highly beneficial for the structure’s stiffness. Again, a financial analysis should be performed in order to investigate the economic benefits of such a solution.

## References

1. Madabhushi G.S.P. and Haiderali A.E., "Evaluation of the p-y Method in the Design of Monopiles for Offshore Wind Turbines", Offshore Technology Conference, Houston, Texas, USA, May 2013
2. Byrne B. and Houlsby G., "Foundations for offshore wind turbines", Philosophical Transactions of the Royal Society A: Mathematical, Physical and Engineering Sciences, Vol. 361, Issue 1813, Pages 2909 – 2930, 2003
3. International Renewable Energy Agency, "Wind Power", Vol. 1, Issue 5, June 2012
4. Martinez-Chaluisant V., "Static and Dynamic Response of Monopiles for Offshore Wind Turbines", MSc Thesis, University of Wisconsin- Madison, 2011
5. Musial, W., Butterfield, S., & Ram, B., "Energy from Offshore Wind", Office of Energy Efficiency and Renewable Energy, U.S. Department of Energy. Golden: National Renewable Energy Laboratory, 2006
6. W. de Vries, "Integrated Wind Turbine Design", WP 4.2: Support Structure Concepts for Deep Water Sites, Deliverable D4.2.8: Offshore Foundations and Support Structures, Project Upwind, March 2011
7. Huang J.W., "Development of modified p-y curves for Winkler Analysis to characterize the lateral load behavior of a single pile embedded in improved soft clay", MSc Thesis, Iowa State University, USA, 2011
8. Tomlinson M.J., "Pile Design and Construction Practice", 4<sup>th</sup> Ed., E & FN Spon, London, UK, 2004
9. Poulos, H., "Behavior of Laterally Loaded Piles: I-Single Piles", Journal of the Soil Mechanics and Foundation Division, 97(SM5), 711-731, May 1971
10. Arany L., Bhattacharya S. et al., "Design of Monopiles for Offshore Wind Turbines in 10 Steps", Soil Dynamics and Earthquake Engineering 92 (2017): 126 – 152
11. Damgaard M., Andersen J., "Natural frequency and damping estimation of an offshore wind turbine structure", Proceedings of the Twenty-second (2012) International Offshore and Polar Engineering Conference, Vol. 4, Pages: 300 – 307, 2012
12. Lanzo G, D'Elia B, "Cyclic Properties of Toyoura Sand at Small to Medium Strains in Simple Shear Test"
13. Rosbjerg S. and Gravesen H., "OWA Offshore Wind Farm Foundations", UK Round 3, Design Basis, Version 1, Upwind Report, Grontmij Carl Bro, 2009
14. Rahman K., Achmus M., "Finite Element Modelling of Horizontally Loaded Monopile Foundations for Offshore Wind Energy Converters in Germany", Institute of Soil Mechanics, Foundation Engineering and Waterpower Engineering, University of Hannover, Germany, 2005
15. Fischer T., de Vries W., Schmidt B., "Upwind Design Basis - WP 4: Offshore Foundations and Support Structures", Project Upwind, October 2010
16. Jonkman J., Butterfield S., Musial W., Scott G., "Definition of a 5-MW Reference Wind Turbine for Offshore System Development", NREL/TP-500-38060, Colorado, USA, February 2009
17. Det Norske Veritas (DNV), "Design of Offshore Wind Turbine Structures", Offshore Standard: DNV-OS-101, DNV, May 2014

18. European Committee for Standardization (2003), "EN1993-1-1: Design of Steel Structures – Part 1.1: General Rules and Rules for Building", Brussels, European Committee for Standardization, 2003
19. Winkel J., "Large Diameter Dolphin Piles: The Effect of the Inner Soil on their Local Buckling Resistance", MSc Thesis, TUDelft & Royal Haskoning DHV, October 2016
20. European Committee for Standardization (2004), "EN1994-1-1: Design of Composite Steel and Concrete Structures – Part 1.1: General Rules and Rules for Building", Brussels, European Committee for Standardization
21. de Gijt J.G., Broeken M.L, "Quay Walls", 2<sup>nd</sup> Edition, SBRCURnet Publication 211E, CRC Press, 2014
22. European Committee for Standardization (2003), "EN1993-1-3: General Rules. Supplementary Rules for Cold-Formed Members and Sheeting", Brussels, European Committee for Standardization, March 2004
23. Abspoel R., "Steel Structures 3", TUDelft Course, TUDelft, Delft, the Netherlands, 2016
24. European Committee for Standardization (2007), "EN1993-4-3: Design of Steel Structures - Part 4-3: Pipelines", European Committee for Standardization, Brussels, 2007
25. Abdel-Rahman & Achmus, "Finite Element Modelling of Horizontally Loaded Monopiles for Offshore Wind Energy Converters in Germany", Institute of Soil Mechanics, Foundation Engineering and Waterpower Engineering, 2005, Hannover, Germany
26. Brinkgreve et al., "Validation of Empirical Formulas to Derive Model Parameters for Sands", 7<sup>th</sup> NUMGE Conference, 2010, Trondheim, Norway
27. Edgers L., "Finite Element Analysis of an Offshore Wind Turbine Monopile", GeoFlorida Conference, 2010, Florida, USA
28. Carswell J., Johansson J et al., "Foundation Damping and the Dynamics of Offshore Wind Turbine Monopiles", *Renewable Energy* 80 (2015), pp. 724 - 736
29. Chopra A.K., "Dynamics of Structures", Prentice Hall, USA, 1995
30. Metrikine A.V, "Dynamics, Slender Structures and an Introduction to Continuum Mechanics", CT4145 Lecture Notes, TUDelft, 2016
31. British Standards Institution (2005), BS EN1991-1-4, "Actions on Structures: General Actions - Wind Actions", London, BSI
32. Darendeli M.B., "Development of a New Family of Normalized Modulus Reduction and Material Damping Curves, PhD Thesis, University of Austin, Texas, USA, 2001
33. Oztoprak S., Bolton M.D., "Stiffness of Sands through a Laboratory Test Database", *Geotechnique* (2013), Vol. 1, pp. 54-70
34. Kokusho, T. (1980). "Cyclic Triaxial Test of Dynamic Soil Properties for Wide Strain Range," *Soils and Foundations*, Vol. 20, No. 2, pp. 45-60.
35. Vucetic, M. and Dobry, R. (1991). "Effect of Soil Plasticity on Cyclic Response," *ASCE, Journal of Geotechnical Engineering*, Vol. 117, No. 1, pp. 89-107.
36. Ishibashi, I. and Zhang, X. (1993). "Unified Dynamic Shear Moduli and Damping Ratios of Sand and Clay," *Soils and Foundations*, Vol. 33, No. 1, pp.182-191.
37. Feyissa A.G., "Shear Modulus and Damping Ratio of Soils Found in Adama", MSc Thesis, Adis Ababa Institute of Technology, November 2011
38. Lanzo G., D'Elia B., "Cyclic Properties of Toyoura Sand at Small to Medium Strains in Simple Shear Tests", *Rivista Italiana Di Geotecnica*, Italy, April 2003

39. Jafarzadeh F., Moridzadeh M., "Shear Modulus and Damping Ratio of Sands at Medium to Large Shear Strains with Cyclic Simple Shear Tests", 4<sup>th</sup> Geotechnical Conference of Earthquake Geotechnical Engineering, Paper No. 1732, June 2007, Thessaloniki, Greece
40. Stokoe K.H., Santamarina J.C. (2000), "Seismic-Wave-Based Testing in Geotechnical Engineering", International Conference on Geotechnical and Geological Engineering,, GeoEng 2000, Melbourne, Australia, 2000
41. Brinkgreve R.B.J., Kappert M.H., Bonnier P.G, "Behavior of Soils and Rocks", CIE4361 Lecture Notes, TUDelft
42. Giang P.H, van Impe P., van Impe W.F, Mnege P., Haegeman W., (2015), "Effects of Grain Size on the Initial Shear Modulus of Calcareous Sand", Proceedings of the XVI ECSMGE Geotechnical Engineering for Infrastructure and Development, ICE Publishing, 2015
43. Brinkgreve R.B.J, Engin E., Engin H.K., (2010) "Validation of Empirical Formulas to Derive Model Parameters for Sands", 7<sup>th</sup> NUMGE Conference, Trondheim, Norway, June 2010
44. Fonseca A.C.V, "Diameter Effects of Large Scale Monopiles: A Theoretical and Numerical Investigation of the Soil-Pile Interaction", MSc Thesis, University of Porto, Portugal, July 2015
45. van Es J., "Seismic Behaviour of a LNG Tank Foundation", MSc Thesis, TUDelft, the Netherlands, March 2014
46. Brinkgreve R.B.J., Kappert M.H., Bonnier P.G., (2007), "Hysteretic Dmping in a Small-Strain Stiffness Model", Numerical Models in Geomechanics, Taylor & Francis Group, London, UK
47. Wind Europe Business Intelligence, "The European Offshore Wind Industry: Key Trends and Statistics 2016", Wind Europe, Brussels, Belgium, January 2017
48. Wind Europe Business Intelligence, "Wind in Power: 2016 European Statistics", Wind Europe, Brussels, Belgium, February 2017
49. Moccia J., Arapogianni A., "Pure Power: Wind Energy Targets for 2020 and 2030", European Wind Energy Association, Brussels, Belgium, July 2011
50. Ho A., Mbistrova A., Corbetta G., "The European Offshore Wind Industry – Key Trends and Statistics 2015", European Wind Energy Association, Brussels, Belgium, February 2016
51. Moccia J., "Wind Energy Scenarios for 2020", European Wind Energy Association, Brussels, Belgium, July 2014
52. Global Wind Energy Council, "Global Wind Statistics 2016", Global Wind Energy Council, Brussels, Belgium, February 2017
53. International Renewable Energy Agency (IRENA), "Innovation Outlook: Offshore Wind", International Renewable Energy Agency, Abu Dhabi, UAE, 2016
54. International Renewable Energy Agency (IRENA), "Renewable Capacity Statistics 2017", International Renewable Energy Agency, Abu Dhabi, 2017
55. International Renewable Energy Agency (IRENA), "Renewable Energy Statistics 2016", International Renewable Energy Agency, Abu Dhabi, 2016
56. International Renewable Energy Agency (IRENA), "Renewable Energy technologies: Cost Analysis Series", Vol. 1, Issue 5/5, International Renewable Energy Agency, Abu Dhabi, June 2012
57. Kempton W., McClellan S., Ozkan D., "Massachusetts Offshore Wind Future Cost Study", Special Initiative of Offshore Wind, University of Delaware, March 2016

58. Herman S.A., Probabilistic Cost Model for Analysis of Offshore Wind Energy Costs and Potential, Energy Research Centre (ECN), Netherlands, May 2002
59. Brealey R.A., Myers S.C., Allen F., "Principles of Corporate Finance", 10<sup>th</sup> Edition, McGraw-Hill Irwin, New York, USA, 2011
60. Sarker B.R. ,Faiz T.I., "Minimizing Transportation and Installation Costs for Turbines in Offshore Wind Farms", Renewable Energy Journal, Vol. 101, Pg. 667 – 679, 2016
61. Kaiser M.J, Snyder B.F, "Modeling Offshore Wind Installation Costs on the U.S. Outer Continental Shelf", Renewable Energy Journal, Vol. 50, Pg. 676 – 691, February 2013
62. Jones R.M, Wright C.W., Smith C.S, "A Study of Large Self-Unloading Vessels", Society of Naval Architects and Marine Engineers (SNAME), Canada, 1972

## APPENDIX A: Vertical & Horizontal Effective Stresses of the Sand-Fill

Assuming the following characteristics for the saturated sand which surrounds monopile:

$$\gamma_{\text{sand},s} = 20 \text{ KN/m}^3$$

And taken into consideration the length of the pile (between seabed level and the soil plug) =  $0.5D = 3.05\text{m}$

And, using Rankine formulas the Passive and Active Earth Pressure Coefficients can be calculated as follows:

$$K_a = \frac{1 - \sin(\varphi)}{1 + \sin(\varphi)} \quad (\text{A.1})$$

And

$$K_p = \frac{1 + \sin(\varphi)}{1 - \sin(\varphi)} \quad (\text{A.2})$$

With dense sand friction angle:  $\varphi = 30-45^\circ$

Also,  $\gamma_{\text{water}} = 10 \text{ KN/m}^3$

The effective stress of the soil at a specific depth "d" is given by the formula:

$$\sigma_{zz} = \gamma_{\text{sand}} \cdot d - \gamma_{\text{water}} \cdot d \quad (\text{A.3})$$

And the Effective Active/Passive stresses are given by the formula:

$$\sigma_{xx} = K_a (\text{or } K_p) \cdot \sigma_{zz} \quad (\text{A.4})$$

Using the formulas above, the vertical effective stress on the soil for various depths of the monopile will be equal to:

$$\sigma_{zz} = 3.05 \cdot 20 = 61 \text{ kPa}$$

And,

$$\sigma_{zz,eff} = 61 - 3.05 \cdot 10 = 30.5 \text{ kPa}$$

The corresponding passive and active effective stresses are:

$$\sigma_{xx,eff,active} = 6.632 \text{ kPa}$$

$$\sigma_{xx,eff,passive} = 140.267 \text{ kPa}$$

## APPENDIX B: Natural Frequency Estimation (Analytical Solution)

In order to verify the accuracy of the Matlab script which was created to calculate the 1<sup>st</sup> natural frequency of the structure, the natural frequency was calculated also analytically. A representation of the equivalent system is shown in *Figure B.1*.

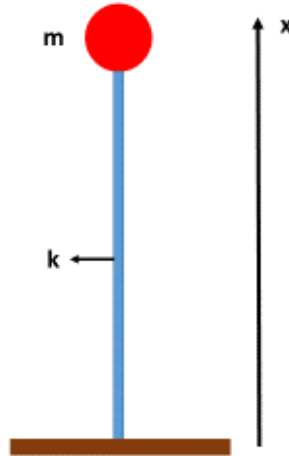


*Figure B.1: Graphic Representation Cantilever Beam with Concentrated Mass*

For a discrete system subject to free vibration, in which the beam is considered as massless with a concentrated mass at its free end, with no presence of damping, the equation of motion is:

$$m \cdot \ddot{x} + k \cdot x = 0 \quad (B.1)$$

Where,

$m$  = concentrated mass located at beam's tip

$k$  = stiffness of the beam

To perform the hand calculations, an equivalent model was created which represents the actual structure. In this model, the distributed self-weight of the pile was transformed to an equivalent mass acting at the top, together with the top mass. The way to create this equivalent model is being presented later in this paragraph.

Using the stiffness of materials deflection formula (Timoshenko and Young, 1961):

$$k = \frac{3 \cdot E \cdot I}{L^3} \quad (B.2)$$

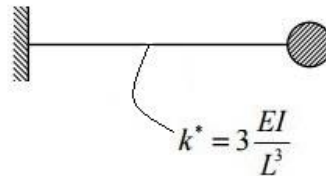


*Figure B.2: Bending Stiffness Fixed-Free Beam [30]*

Where,



$E = \text{Steel Young Modulus} = 2.1 \cdot 10^{11} \text{ N/m}^2$

$$I = \text{Circular Hollow Section 2nd Moment of Area} = \frac{\pi}{4} \cdot (r_{out}^4 - r_{in}^4) \quad (B.3)$$

$L = \text{Distance between Clamped Support and Free End}$

The un-damped circular natural frequency of the system can be calculated applying formula B.4:

$$\omega_n = \sqrt{\frac{k}{m}} = \sqrt{\frac{3 \cdot E \cdot I}{L^3 \cdot m_{tot}}} \quad (B.4)$$

where,

$$m_{tot} = m_{top} + m_{structure} \quad (B.5)$$

And the self-weight of the structure is:

$$m_{struct} = \rho \cdot A \cdot L \quad (B.6)$$

where,

$$A = \frac{\pi}{4} \cdot (D_{out}^2 - D_{in}^2) \quad (B.7)$$

$$\rho_{structure} = \rho_{steel} + \rho_{coating} = 8500 \frac{\text{kg}}{\text{m}^3} \quad (B.8)$$

The equivalent tip mass for the cantilever beam can be calculated as suggested by [**Σφάλμα! Το αρχείο προέλευσης της αναφοράς δεν βρέθηκε.**, **Σφάλμα! Το αρχείο προέλευσης της αναφοράς δεν βρέθηκε.**]. A small element of the beam at a distance “ $x$ ” from the free end is being considered, as shown in the figure below:

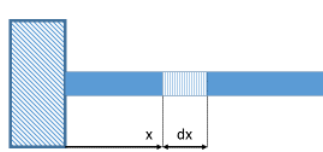


Figure 1. 8: Small Element on the Column

The moment at a point of a beam is related to the second derivative of the deflection with the following formula:

$$M = E \cdot I \cdot \frac{d^2y}{dx^2} \quad (B.9)$$

Where,  $\delta$  is the vertical deflection of the beam. So,

$$\frac{dy}{dx} = \int_{x=0}^x M(x) dx \quad (B.10)$$

But,

$$M(x) = -F \cdot L \cdot \left(1 - \frac{x}{L}\right) \quad (B.11)$$

So Eq. B.10 can be written as:

$$\frac{dy}{dx} = \int_{x=0}^x -F \cdot L \cdot \left(1 - \frac{x}{L}\right) dx = \frac{-F \cdot L}{E \cdot I} \cdot \left(x - \frac{x^2}{2 \cdot L}\right)$$

And,

$$y(x) = \int_{x=0}^x \frac{dy}{dx} dx = \frac{-F \cdot L}{E \cdot I} \cdot \left(\frac{x^2}{2} - \frac{x^3}{6 \cdot L}\right)$$

Which, for  $x=L$  it yields the a widely known expression for the tip displacement of a cantilever beam, loaded under a concentrated point load at its' tip. This expression is also shown in figure 1.4 [Σφάλμα! Το αρχείο προέλευσης της αναφοράς δεν βρέθηκε.], and is equal to:


$$y(x) = \delta = \frac{-F \cdot L^3}{3 \cdot E \cdot I}$$


Figure 1. 9: Deflection at the end of a cantilever beam

In the expression above, the minus sign means that the deflection occurs downwards. Knowing that this is the direction of deflection the minus sign can be eliminated in the expressions which will be presented later in this paragraph.

The displacement at any point along the beam's length is given by:

$$y(x) = \frac{1}{2 \cdot L^3} \cdot (3 \cdot L \cdot x^2 - x^3) \cdot \frac{F \cdot L^3}{3 \cdot E \cdot I} \quad (B.12)$$

If  $v$  is the transverse velocity at the free end of the beam, the velocity of the small element at a distance "x", will be equal to:

$$v(x) = \frac{dy}{dt} \quad (B.13)$$

And assuming that the max velocity is equal to  $v_{max}$  the velocity variation along the beam length will be equal to:

$$v(x) = \frac{3 \cdot L \cdot x^2 - x^3}{2 \cdot L^3} \cdot v_{max}$$

and the Kinetic Energy of the element is equal to:

$$dK = \frac{1}{2} \cdot \rho \cdot A \cdot dx \cdot \left(\frac{3 \cdot L \cdot x^2 - x^3}{2 \cdot L^3} \cdot v_{max}\right)^2 \quad (B.14)$$

The total Kinetic Energy of the beam is:

$$\begin{aligned}
 K &= \frac{1}{2} \cdot \int_0^L \rho \cdot A \cdot \left( \frac{3 \cdot L \cdot x^2 - x^3}{2 \cdot L^3} \cdot v_{max} \right)^2 dx = \frac{\rho \cdot A \cdot v_{max}^2}{8 \cdot L^6} \cdot \left[ \frac{9 \cdot L^2 \cdot x^5}{5} - \frac{6 \cdot L \cdot x^6}{6} - \frac{x^7}{7} \right]_0^L \\
 &= \frac{\rho \cdot A \cdot v_{max}^2}{8 \cdot L^6} \cdot \left( \frac{33 \cdot L^7}{35} \right) = \frac{1}{2} \cdot \left( \frac{33}{140} \cdot m_{struct} \right) \cdot v_{max}^2
 \end{aligned}$$

Therefore, if a mass with a magnitude of  $m_1^* = \frac{33}{140} \cdot m_{struct}$  is being placed at the free end of the cantilever beam, and, at the same time, the distributed mass of the column is being removed, the system created will be dynamically equivalent. Using this property, the equivalent tip mass which was needed in order to calculate the circular natural frequency of the system can be easily estimated. Having the total tip mass of the system, the first natural frequency is equal to:

$$f_1 = \frac{\omega_1}{2 \cdot \pi} \quad (B.15)$$

The same result could have been obtained, using the 1<sup>st</sup> normal mode coefficient ( $C_1$ ), for a cantilever beam. Using this procedure, the following formulas can be applied:

$$k^* = 3 \cdot \frac{E \cdot I}{L^3} \quad (B.16)$$

$$\omega_1^2 = C_1^2 \cdot \frac{E \cdot I}{\rho \cdot A \cdot L^4} \quad (B.17)$$

Where normal mode coefficients are as shown given in the figure below:

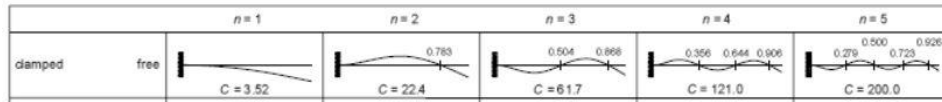


Figure 1.10 Normal Modes for Cantilever Beam

And,

$$m_2^* = \frac{3 \cdot \rho \cdot A \cdot L}{C_1^2} \approx 0.24 \cdot \rho \cdot A \cdot L \quad (B.18)$$

As it was shown, both the Kinetic Energy approach and the Normal Modes approach yield almost the same result:

$$m_1^* = \frac{33}{140} = 0.2357 \approx m_2^* = 0.24$$

## APPENDIX C: Finite Difference Method

### Equations of Motion & Boundary Conditions

#### Model A - Fixity Depth

In order to setup the model for the natural frequency analysis in MATLAB, the support structure was modelled using four different parts, each with its own displacement. Since the support structure was split in four parts, a total of four equations of motion had been implemented. The separation of the four parts is shown in the following figure.

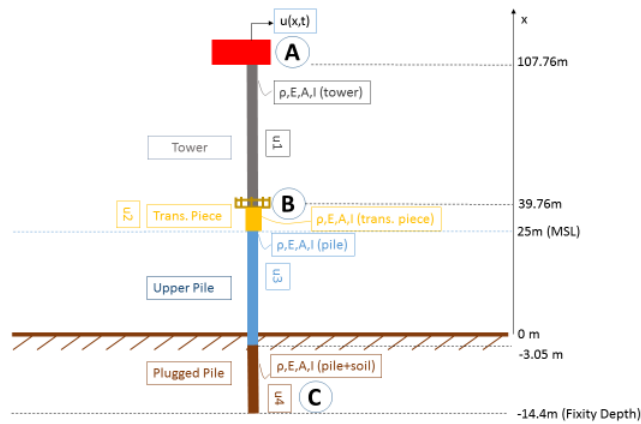


Figure C.1: Representation of Parts

$$\rho \cdot A \cdot \frac{d^2 u_i}{d_t^2} + E \cdot I \cdot \frac{d^4 u_i}{d_x^4} = 0 \quad (C.1)$$

$$i = 1, 2, 3, 4$$

#### Boundary Condition at point A

Point A is located at the top of the tower, where the Boundary Condition represents the balance between three forces, namely, the inertia force of the mass ( $M$ ), the wind Thrust Force ( $F_{thr}$ ) and the shear force of the beam. Also, the moments at the free end of the beam should be equal to zero.

$$-E \cdot I \cdot \frac{d^3 u_1(107.76)}{d_x^3} + M \cdot \frac{d^2 u_1(107.76)}{d_t^2} = 0 \quad (C.2)$$

$$E \cdot I \cdot \frac{d^2 u_1(107.76)}{d_x^2} = 0 \quad (C.3)$$

**Interface Condition at Transition Points between the Parts**

At the point of connection between two consecutive parts (i.e Point B), the relevant interface conditions have been taken into consideration. These interface conditions refer to the continuity of the structure, meaning, that at the specific point, the displacement, the rotation, the moment and the shear force will be exactly the same for both the equations of motion.

$$u_i(x, t) = u_{i+1}(x, t) \quad (C.4)$$

$$\frac{du_i(x, t)}{dx} = \frac{du_{i+1}(x, t)}{dx} \quad (C.5)$$

$$\frac{d^2u_i}{dx^2} = \frac{d^2u_{i+1}}{dx^2} \quad (C.6)$$

$$\frac{d^3u_i}{dx^3} = \frac{d^3u_{i+1}}{dx^3} \quad (C.7)$$

For  $i = 1, 2, 3$

**Boundary Condition at point C**

At point C, which is located at the seabed, a rigid connection has been assumed. This assumption, of course will lead, to a rough approximation of the natural frequency. However, at this point the purpose was to create a model just to perform a sensitivity analysis and define the effect of sand-fill on the natural frequency of the structure. Therefore, the focus was not on the exact value of the natural frequency, but on the incremental effect on it when filling the monopile with sand. The assumed rigid connection has restricted the movement and the rotation of the monopile at this specific point.

$$u_4(0, t) = 0 \quad (C.8)$$

$$u_4'(0, t) = 0 \quad (C.9)$$

**Model B – Soil Springs**

For the model with the soil springs, the Equations of Motion and the boundary conditions should correspond to the figure below.

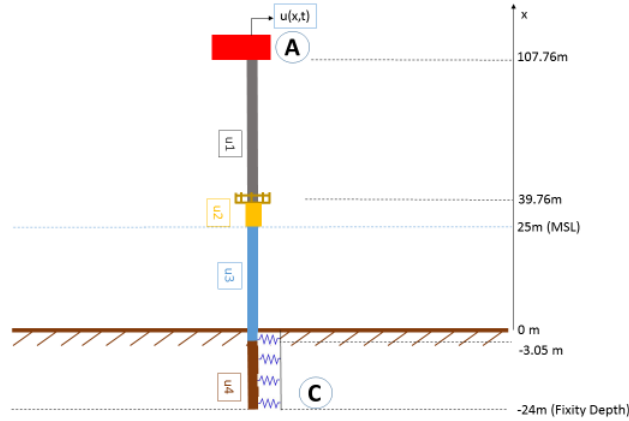


Figure C.2: Separation in Parts for EoM – Soil Spring

The equations of motion are:

$$\rho \cdot A \cdot \frac{d^2 u_i}{d t^2} + E \cdot I \cdot \frac{d^4 u_i}{d x^4} = 0 \quad (C.10)$$

For  $i = 1, 2, 3$

$$\rho \cdot A \cdot \frac{d^2 u_4}{d t^2} + E \cdot I \cdot \frac{d^4 u_4}{d x^4} + k_d \cdot u_4 = 0 \quad (C.11)$$

The interface conditions and the boundary condition at Point A, are identical with the ones presented for model A.

### Discretization using Finite Difference Method

For the discretization of the structure, the Finite Differences method, has been applied. To apply the finite difference method for a beam, the Taylor expansion around a point ( $x_n$ ) has been performed to calculate up to the fourth spatial derivative. This is due to the fact that the equations of motion of the beam include fourth order derivatives, as shown in the previous paragraph. The TSE will be performed for 5 points in total, 2 preceding and two succeeding the point under consideration, ( $x_n$ ).

The location and the IDs of these points are shown in the figure below:

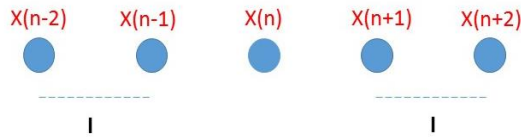


Figure C.3: Sequence of finite elements

Performing TSE for all the points shown in figure 2, around point  $x_n$  it yields:

$$w(x_{n-2}) = w(x_n) + (-2 \cdot l) \cdot w'(x_n) + \frac{(-2 \cdot l)^2}{2} \cdot w''(x_n) + \frac{(-2 \cdot l)^3}{6} \cdot w'''(x_n) + \frac{(-2 \cdot l)^4}{24} \cdot w''''(x_n) \quad (C.12)$$

$$w(x_{n-1}) = w(x_n) - l \cdot w'(x_n) + \frac{(l)^2}{2} \cdot w''(x_n) - \frac{(l)^3}{6} \cdot w'''(x_n) + \frac{(l)^4}{24} \cdot w''''(x_n) \quad (C.13)$$

$$w(x_n) = w(x_n) \quad (C.14)$$

$$w(x_{n+1}) = w(x_n) + l \cdot w'(x_n) + \frac{(l)^2}{2} \cdot w''(x_n) + \frac{(l)^3}{6} \cdot w'''(x_n) + \frac{(l)^4}{24} \cdot w''''(x_n) \quad (C.15)$$

$$w(x_{n+2}) = w(x_n) + (2 \cdot l) \cdot w'(x_n) + \frac{(2 \cdot l)^2}{2} \cdot w''(x_n) + \frac{(2 \cdot l)^3}{6} \cdot w'''(x_n) + \frac{(2 \cdot l)^4}{24} \cdot w''''(x_n) \quad (C.16)$$

It is:

$$w''''(x_n) + error = \alpha \cdot w(x_{n-2}) + \beta \cdot w(x_{n-1}) + \gamma \cdot w(x_n) + \delta \cdot w(x_{n+1}) + \varepsilon \cdot w(x_{n+2}) \quad (C.17)$$

$$\begin{aligned} &= (\alpha + \beta + \gamma + \delta + \varepsilon) \cdot w(x_n) + (-2 \cdot l \cdot \alpha - l \cdot \beta + l \cdot \delta + 2 \cdot l \cdot \varepsilon) \cdot w'(x_n) \\ &\quad + \left( 2 \cdot l^2 \cdot \alpha + \frac{l^2}{2} \cdot \beta + \frac{l^2}{2} \cdot \delta + 2 \cdot l^2 \cdot \varepsilon \right) \cdot w''(x_n) \\ &\quad + \left( -\frac{4}{3} \cdot l^3 \cdot \alpha - \frac{l^3}{6} \cdot \beta + \frac{l^3}{6} \cdot \delta + \frac{4}{3} \cdot l^3 \cdot \varepsilon \right) \cdot w'''(x_n) \\ &\quad + \left( \frac{2}{3} \cdot l^4 \cdot \alpha - \frac{l^4}{24} \cdot \beta + \frac{l^4}{24} \cdot \delta + \frac{2}{3} \cdot l^4 \cdot \varepsilon \right) \cdot w''''(x_n) \end{aligned}$$

In a matrix form it can be written as:

$$\begin{bmatrix} 1 & 1 & 1 & 1 & 1 \\ -2 \cdot l & -l & 0 & l & 2 \cdot l \\ 2 \cdot l^2 & \frac{l^2}{2} & 0 & \frac{l^2}{2} & 2 \cdot l^2 \\ -\frac{4 \cdot l^3}{3} & -\frac{l^3}{6} & 0 & \frac{l^3}{6} & \frac{4 \cdot l^3}{3} \\ \frac{2 \cdot l^4}{3} & \frac{l^4}{24} & 0 & \frac{l^4}{24} & \frac{2 \cdot l^4}{3} \end{bmatrix} \cdot \begin{bmatrix} \alpha \\ \beta \\ \gamma \\ \delta \\ \varepsilon \end{bmatrix} = \begin{bmatrix} 0 \\ 0 \\ 0 \\ 0 \\ 1 \end{bmatrix}$$

Solving the system of equations, it yields:

$$\alpha = \frac{1}{l^4}, \beta = \frac{-4}{l^4}, \gamma = \frac{6}{l^4}, \delta = \frac{-4}{l^4}, \varepsilon = \frac{1}{l^4}$$

So, the equation of motion (including the imaginary elements will be:

$$\ddot{w}(x_n) = \frac{-E \cdot I}{\rho \cdot A \cdot l^4} \cdot [1 \quad -4 \quad 6 \quad -4 \quad 1] \cdot \begin{bmatrix} w(x_{n-2}) \\ w(x_{n-1}) \\ w(x_n) \\ w(x_{n+1}) \\ w(x_{n+2}) \end{bmatrix} \quad (C.18)$$

For N=7:

$$\ddot{w}(x_n) = \frac{-E \cdot I}{\rho \cdot A \cdot l^4} \cdot \begin{bmatrix} 1 & -4 & 6 & 4 & 1 & 0 & 0 & 0 & 0 & 0 & 0 \\ 0 & 1 & -4 & 6 & -4 & 1 & 0 & 0 & 0 & 0 & 0 \\ 0 & 0 & 1 & -4 & 6 & -4 & 1 & 0 & 0 & 0 & 0 \\ 0 & 0 & 0 & 1 & -4 & 6 & -4 & 1 & 0 & 0 & 0 \\ 0 & 0 & 0 & 0 & 1 & -4 & 6 & -4 & 1 & 0 & 0 \\ 0 & 0 & 0 & 0 & 0 & 1 & -4 & 6 & -4 & 1 & 0 \\ 0 & 0 & 0 & 0 & 0 & 0 & 1 & -4 & 6 & -4 & 1 \end{bmatrix} \cdot \begin{bmatrix} w(-2) \\ w(-1) \\ w(1) \\ w(2) \\ w(3) \\ w(4) \\ w(5) \\ w(6) \\ w(7) \\ w(8) \\ w(9) \end{bmatrix}$$

Therefore, choosing for example 7 nodes per structural element,  $w(1)$  to  $w(7)$  represents the 7 finite elements which were used for the monopile (or tower) and  $w(-2)$ ,  $w(-1)$ ,  $w(8)$ ,  $w(9)$  are imaginary elements positioned after both ends of the column. These nodes are being introduced in order to provide the 5 nodes which are needed by the method to calculate the deflection on the first ( $w(1)$ ) and the last element ( $w(7)$ ).

After applying the fixed-free boundary conditions, the matrix above will be transformed with respect to the columns which refer to the last element and the element before it. This will happen by applying the finite difference method, which will provide a relationship between the real nodes and the imaginary ones. The imaginary ones should be eliminated from the matrix referring to the EoM, therefore a technique has been followed to express the displacements of the imaginary nodes in relation with the real ones. The boundary condition for the point A, ( $x=L$ ), states that the shear force and the moment should be equal to zero. This means that the following Equations C.2 and C.3 should be valid.

In a matrix form the EoM for a fixed- free beam in discretized form, including the boundary conditions will be:

$$\ddot{w}(x_n) = \frac{-E_i \cdot I_i}{\rho \cdot A_i \cdot l_i^4} \cdot \begin{bmatrix} 7 & -4 & 1 & 0 & 0 & 0 \\ -4 & 6 & -4 & 1 & 0 & 0 \\ 1 & -4 & 6 & -4 & 1 & 0 \\ 0 & 1 & -4 & 6 & -4 & 1 \\ 0 & 0 & 1 & -4 & 5 & -2 \\ 0 & 0 & 0 & 2 & -4 & 2 \end{bmatrix} \cdot \begin{bmatrix} w(2) \\ w(3) \\ w(4) \\ w(5) \\ w(6) \\ w(7) \end{bmatrix} + \begin{bmatrix} 0 \\ 0 \\ 0 \\ 0 \\ 0 \\ 0 \end{bmatrix} \quad (C.22)$$

Similarly, in a matrix form the EoM for a free - free beam (with soil springs) in discretized form, including the boundary conditions will be:

$$\ddot{w}(x_n) = \frac{-E_i \cdot I_i}{\rho \cdot A_i \cdot l_i^4} \cdot \begin{bmatrix} 2 & -4 & 2 & 0 & 0 & 0 \\ -2 & 5 & -4 & 1 & 0 & 0 \\ 1 & -4 & 6 + k_d^* & -4 & 1 & 0 \\ 0 & 1 & -4 & 6 + k_d^* & -4 & 1 \\ 0 & 0 & 1 & -4 & 5 & -2 \\ 0 & 0 & 0 & 2 & -4 & 2 \end{bmatrix} \cdot \begin{bmatrix} w(2) \\ w(3) \\ w(4) \\ w(5) \\ w(6) \\ w(7) \end{bmatrix} + \begin{bmatrix} 0 \\ 0 \\ 0 \\ 0 \\ 0 \\ 0 \end{bmatrix} \quad (C.22)$$



\*The above matrix is just a representation, meaning, the soil spring stiffness is being shown to be added on two random elements. The soil spring stiffness is added in reality to any element which is below the seabed.

### Modelling of the Interface Conditions Using FDM Example

The interface conditions are (Eq. C.4 – C.7):

$$\begin{aligned} w_p(x, t) &= w_t(x, t) \\ \frac{dw_p(x, t)}{dx} &= \frac{dw_t(x, t)}{dx} \\ \frac{d^2w_p}{dx^2} &= \frac{d^2w_t}{dx^2} \\ \frac{d^3w_p}{dx^3} &= \frac{d^3w_t}{dx^3} \end{aligned}$$

The second order approximation for the expressions above are the following:

$$\frac{dw}{dx}: D_1 - w_{n-1} = w_{n+1} - D_4 \quad (C.23)$$

$$\frac{d^2w}{dx^2}: E_p \cdot I_p \cdot (D_1 - 2 \cdot w_n + w_{n-1}) = (w_{n+1} - 2 \cdot w_n + D_4) \cdot E_t \cdot I_t \quad (C.24)$$

$$\begin{aligned} \frac{d^3w}{dx^3}: E_p \cdot I_p \cdot (D_2 - 2 \cdot D_1 + 2 \cdot w_{n-1} - w_{n-2}) \\ = (w_{n+2} - 2 \cdot w_{n+1} + 2 \cdot D_4 - D_3) \cdot E_t \cdot I_t \end{aligned} \quad (C.25)$$

And the 4<sup>th</sup> derivative, which appears in the equation of motion, can be written:

$$\begin{aligned} \frac{d^4w}{dx^4}: E_p \cdot I_p \cdot (D_2 - 4 \cdot D_1 + 6 \cdot w_n - 4 \cdot w_{n-1} + w_{n-2}) \\ = (w_{n+2} - 4 \cdot w_{n+1} + 6 \cdot w_n - 4 \cdot D_4 + D_3) \cdot E_t \cdot I_t \end{aligned} \quad (C.26)$$

The position of the fictional nodes, D1-4 is shown in the figure below:



Figure C.4: Graphic Representation of Nodes at Interface Point

Working on the above equations as you showed me on paper, I get the following results for the nodes D1-D4.

$$D_1 = w_{n-1} + w_{n+1} - D_4 \quad (C.27)$$

$$D_4 = \frac{(E_t \cdot I_t - E_p \cdot I_p) \cdot w_{n+1} - (E_t \cdot I_t - E_p \cdot I_p) \cdot 2 \cdot w_n - 2 \cdot E_p \cdot I_p \cdot w_{n-1}}{-(E_t \cdot I_t + E_p \cdot I_p)} = y \quad (C.28)$$

$$D_2 = \frac{(2 \cdot E_t \cdot I_t - 2 \cdot E_p \cdot I_p) \cdot y + E_t \cdot I_t \cdot w_{n+2} - (E_t \cdot I_t - E_p \cdot I_p) \cdot 2 \cdot w_{n+1} + E_p \cdot I_p \cdot w_{n-2} - E_p \cdot I_p \cdot D_3}{E_p \cdot I_p} \quad (C.29)$$

And,

$$D_3 = \frac{(6 \cdot E_t \cdot I_t - 6 \cdot E_p \cdot I_p) \cdot y + (2 \cdot E_t \cdot I_t + 6 \cdot E_p \cdot I_p) w_{n+1} + 2 \cdot E_p \cdot I_p \cdot w_{n-2} - (6 \cdot E_p \cdot I_p - 6 \cdot E_t \cdot I_t) \cdot 6 \cdot w_n - 8 \cdot E_p \cdot I_p \cdot w_{n-1}}{(E_t \cdot I_t + E_p \cdot I_p)} \quad (C.30)$$

Using the relationships above the fourth order derivative, which refers to the equation of motion for node 500 yields (node 500 belongs to the pile, when node 501 is located exactly at the interface between the pile and the tower):

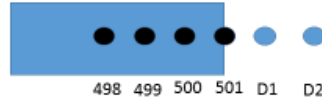


Figure C.5: Graphic Representation of Dummy Nodes at Interface Condition

$$\begin{aligned} & \rho \cdot A \cdot \frac{d^2 w_{500}}{dt^2} + \frac{E_p \cdot I_p}{l^4} (w_{498} - 4 \cdot w_{499} + 6 \cdot w_{500} - 4 \cdot w_{501} + D_1) \\ & \quad (D_1 \text{ was calculated before: } D_1 = w_{n-1} + w_{n+1} - D_4) \\ & = w_{498} - 4 \cdot w_{499} + 6 \cdot w_{500} - 4 \cdot w_{501} + w_{499} + w_{501} - D_4 \\ & = w_{498} - 3 \cdot w_{499} + 6 \cdot w_{500} - 3 \cdot w_{501} - D_4 \\ & = w_{498} - 3 \cdot w_{499} + 6 \cdot w_{500} - 3 \cdot w_{501} + \frac{(E_t \cdot I_t - E_p \cdot I_p)}{E_p \cdot I_p + E_t \cdot I_t} \cdot w_{501} - \frac{(E_t \cdot I_t - E_p \cdot I_p)}{E_p \cdot I_p + E_t \cdot I_t} \cdot 2 \cdot w_{500} \\ & \quad - \frac{2 \cdot E_p \cdot I_p}{E_p \cdot I_p + E_t \cdot I_t} \cdot w_{499} \\ & = w_{498} - \frac{3 \cdot (E_t \cdot I_t + E_p \cdot I_p) + 2 \cdot E_p \cdot I_p}{E_p \cdot I_p + E_t \cdot I_t} \cdot w_{499} + \frac{6 \cdot (E_t \cdot I_t + E_p \cdot I_p) - 2 \cdot (E_t \cdot I_t - E_p \cdot I_p)}{E_p \cdot I_p + E_t \cdot I_t} \\ & \quad \cdot w_{500} - \frac{3 \cdot (E_t \cdot I_t + E_p \cdot I_p) - (E_p \cdot I_p + E_t \cdot I_t)}{E_p \cdot I_p + E_t \cdot I_t} \cdot w_{499} \\ & = w_{498} - \frac{3 \cdot (E_t \cdot I_t + E_p \cdot I_p) + 2 \cdot E_p \cdot I_p}{E_p \cdot I_p + E_t \cdot I_t} \cdot w_{499} + \frac{6 \cdot (E_t \cdot I_t + E_p \cdot I_p) - 2 \cdot (E_t \cdot I_t - E_p \cdot I_p)}{E_p \cdot I_p + E_t \cdot I_t} \\ & \quad \cdot w_{500} - \frac{3 \cdot (E_t \cdot I_t + E_p \cdot I_p) - (E_p \cdot I_p + E_t \cdot I_t)}{E_p \cdot I_p + E_t \cdot I_t} \cdot w_{501} \end{aligned}$$

The expression above refers to the node before the last node of the pile (i.e. node 500).

Taking the equation of motion for the node 501 (last node of pile and first of the tower) the equation of motion can be written:

$$w_{499} - 4 \cdot w_{500} + 6 \cdot w_{501} - 4 \cdot D_1 + D_2$$

Using the known expression for D1

$$(D_1 \text{ was calculated before: } D_1 = w_{n-1} + w_{n+1} - D_4)$$

it yields:

$$w_{499} - 4 \cdot w_{500} + 6 \cdot w_{501} - 4 \cdot w_{500} - 4 \cdot w_{502} + 4 \cdot D_4 + D_2$$

## APPENDIX D: Approximate Modes – Sensitivity Analysis (Clamped-Free Beam)

### Approximate Modes Calculation

The three equations of motion are:

$$\rho \cdot A \cdot \ddot{u}_i + E \cdot I \cdot u_i'''' = 0 \quad (D.1)$$

For  $i = 1, 2, 3$

Where,

$\rho A$  = the mass per meter of the support structure

$EI$  = the bending stiffness per meter of the support structure

$u$  = the horizontal displacement

and,

$\ddot{u}$  = the horizontal acceleration ( $\frac{d^2u}{dt^2}$ ), as shown in the figure above

#### Boundary Conditions

$$u(0) = u'(0) = 0 \quad (D.2)$$

$$u''(122.16) = u'''(122.16) = 0 \quad (D.3)$$

#### Interface Conditions

$$u_1(14.4, t) = u_2(14.4, t) \quad (D.4)$$

$$\frac{du_1(14.4, t)}{dz} = \frac{du_2(14.4, t)}{dz} \quad (D.5)$$

$$\frac{d^2u_1(14.4, t)}{dz^2} = \frac{d^2u_2(14.4, t)}{dz^2} \quad (D.6)$$

$$\frac{d^3u_1(14.4, t)}{dz^3} = \frac{d^3u_2(14.4, t)}{dz^3} \quad (D.7)$$

And,

$$u_2(54.16, t) = u_3(54.16, t) \quad (D.8)$$

$$\frac{du_2(54.16, t)}{dz} = \frac{du_3(54.16, t)}{dz} \quad (D.9)$$

$$\frac{d^2u_2(54.16, t)}{dz^2} = \frac{d^2u_3(54.16, t)}{dz^2} \quad (D.10)$$

$$\frac{d^3u_2(54.16, t)}{dz^3} = \frac{d^3u_3(54.16, t)}{dz^3} \quad (D.11)$$

### General Solutions

$$u(x) = U(x) \cdot e^{i\omega t} \quad (D.12)$$

The space-related part of the equations of motion is:

$$U_{1,2,3}''''(x) - \left( \frac{\omega^2 \cdot \rho \cdot A}{E \cdot I} \right) \cdot U_{1,2,3}(x) = 0 \quad (D.13)$$

Setting,

$$\beta^4 = \left( \frac{\omega^2 \cdot \rho \cdot A}{E \cdot I} \right) \quad (D.14)$$

The space-related part for the EoMs which refer to the parts above the seabed level can be written as:

$$U_i''''(x) - \beta^4 \cdot U_i(x) = 0 \quad (D.15)$$

For  $i = 1, 2, 3$

The general solutions of the above equations are:

$$U_i(x) = A_i \cdot \cosh(\beta \cdot x) + B_i \cdot \sinh(\beta \cdot x) + C_i \cdot \cos(\beta \cdot x) + D_i \cdot \sin(\beta \cdot x) \quad (D.16)$$

Substituting the general solutions in the boundary conditions they yield:

$$U_1'(x) = A_1 \cdot \sinh(\beta \cdot x) + B_1 \cdot \cosh(\beta \cdot x) - C_1 \cdot \sin(\beta \cdot x) + D_1 \cdot \cos(\beta \cdot x)$$

So,

$$U_1(0) = 0 \Rightarrow A_1 = -C_1$$

$$U_1'(0) = 0 \Rightarrow B_1 = -D_1$$

and,

$$U_3''(x) = A_3 \cdot \cosh(\beta \cdot x) + B_3 \cdot \sinh(\beta \cdot x) - C_3 \cdot \cos(\beta \cdot x) - D_3 \cdot \sin(\beta \cdot x)$$

$$U_3'''(x) = A_3 \cdot \sinh(\beta \cdot x) + B_3 \cdot \cosh(\beta \cdot x) + C_3 \cdot \sin(\beta \cdot x) - D_3 \cdot \cos(\beta \cdot x)$$

So,

$$U_3''(122.16) = 0$$

$$\Rightarrow A_3 \cdot \cosh(\beta \cdot 122.16) + B_3 \cdot \sinh(\beta \cdot 122.16) - C_3 \cdot \cos(\beta \cdot 122.16) - D_3 \cdot \sin(\beta \cdot 122.16) = 0$$

$$U_3'''(122.16) = A_3 \cdot \sinh(\beta \cdot 122.16) + B_3 \cdot \cosh(\beta \cdot 122.16) + C_3 \cdot \sin(\beta \cdot 122.16) - D_3 \cdot \cos(\beta \cdot 122.16) = 0$$

Substituting the general solutions in the interface conditions they yield:

**At an elevation equal to 14.4m:**

$$U_1(14.4) = U_2(14.4)$$

$$\begin{aligned}
 U_1'(14.4) &= U_2'(14.4) \\
 &\Rightarrow A_1 \cdot \beta \cdot \sinh(\beta \cdot 14.4) + B_1 \cdot \beta \cdot \cosh(\beta \cdot 14.4) - C_1 \cdot \beta \cdot \sin(\beta \cdot 14.4) + D_1 \\
 &\quad \cdot \beta \cdot \cos(\beta \cdot 14.4) \\
 &= A_2 \cdot \beta \cdot \sinh(\gamma \cdot 14.4) + B_2 \cdot \beta \cdot \cosh(\gamma \cdot 14.4) - C_2 \cdot \beta \cdot \sin(\gamma \cdot 14.4) + D_2 \\
 &\quad \cdot \beta \cdot \cos(\gamma \cdot 14.4)
 \end{aligned}$$

$$\begin{aligned}
 U_1''(14.4) &= U_2''(14.4) \\
 &\Rightarrow \beta^2 \\
 &\quad \cdot [A_1 \cdot \cosh(\beta \cdot 14.4) + B_1 \cdot \sinh(\beta \cdot 14.4) - C_1 \cdot \cos(\beta \cdot 14.4) - D_1 \\
 &\quad \cdot \sin(\beta \cdot 14.4)] \\
 &= \beta^2 \\
 &\quad \cdot [A_2 \cdot \cosh(\beta \cdot 14.4) + B_2 \cdot \sinh(\beta \cdot 14.4) - C_2 \cdot \cos(\beta \cdot 14.4) - D_2 \\
 &\quad \cdot \sin(\beta \cdot 14.4)]
 \end{aligned}$$

$$\begin{aligned}
 U_1'''(14.4) &= U_2'''(14.4) \\
 &\Rightarrow \beta^3 \\
 &\quad \cdot [A_1 \cdot \sinh(\beta \cdot 14.4) + B_1 \cdot \cosh(\beta \cdot 14.4) + C_1 \cdot \sin(\beta \cdot 14.4) - D_1 \\
 &\quad \cdot \cos(\beta \cdot 14.4)] \\
 &= \beta^3 \\
 &\quad \cdot [A_1 \cdot \sinh(\beta \cdot 14.4) + B_1 \cdot \cosh(\beta \cdot 14.4) + C_1 \cdot \sin(\beta \cdot 14.4) - D_1 \\
 &\quad \cdot \cos(\beta \cdot 14.4)]
 \end{aligned}$$

**At an elevation equal to 44.4m:**

$$U_2(44.4) = U_3(44.4)$$

$$\begin{aligned}
 U_2'(44.4) &= U_3'(44.4) \\
 &\Rightarrow A_2 \cdot \sinh(\beta \cdot 44.4) + B_2 \cdot \cosh(\beta \cdot 44.4) - C_2 \cdot \sin(\beta \cdot 44.4) + D_2 \\
 &\quad \cdot \cos(\beta \cdot 44.4) \\
 &= A_3 \cdot \sinh(\beta \cdot 44.4) + B_3 \cdot \cosh(\beta \cdot 44.4) - C_3 \cdot \sin(\beta \cdot 44.4) + D_3 \\
 &\quad \cdot \cos(\beta \cdot 44.4)
 \end{aligned}$$

$$\begin{aligned}
 U_2''(44.4) &= U_2''(44.4) \\
 &\Rightarrow [A_2 \cdot \cosh(\beta \cdot 44.4) + B_2 \cdot \sinh(\beta \cdot 44.4) - C_2 \cdot \cos(\beta \cdot 44.4) - D_2 \\
 &\quad \cdot \sin(\beta \cdot 44.4)] \\
 &= [A_3 \cdot \cosh(\beta \cdot 44.4) + B_3 \cdot \sinh(\beta \cdot 44.4) - C_3 \cdot \cos(\beta \cdot 44.4) - D_3 \\
 &\quad \cdot \sin(\beta \cdot 44.4)]
 \end{aligned}$$

$$\begin{aligned}
 U_2'''(44.4) &= U_3'''(44.4) \\
 &\Rightarrow [A_2 \cdot \sinh(\beta \cdot 44.4) + B_2 \cdot \cosh(\beta \cdot 44.4) + C_2 \cdot \sin(\beta \cdot 44.4) - D_2 \\
 &\quad \cdot \cos(\beta \cdot 44.4)] \\
 &= [A_3 \cdot \sinh(\beta \cdot 44.4) + B_3 \cdot \cosh(\beta \cdot 44.4) + C_3 \cdot \sin(\beta \cdot 44.4) - D_3 \\
 &\quad \cdot \cos(\beta \cdot 44.4)]
 \end{aligned}$$

As in the analysis of the free-free beam, the approximated normal modes will be calculated for a structure with a constant cross-section along its length. Again a weighted average of the diameters and thicknesses of all the members is being taken.

$$D_{avg} = \frac{6.1 \cdot 54 + 5.65 \cdot 9.76 + 4.98 \cdot 68}{131.76} = 5.127 \text{ m} \quad (D.17)$$

And

$$t_{avg} = \frac{0.08 \cdot 54 + 0.06 \cdot 9.76 + 0.03 \cdot 68}{131.76} = 0.0527 \text{ m} \quad (D.18)$$

The dimensions above lead to the following values for the mass and stiffness related parameters:

Area (m <sup>2</sup> )	2 <sup>nd</sup> Moment of Area (m <sup>4</sup> )	Bending Stiffness (MNm <sup>2</sup> )	Density (kg/m <sup>3</sup> )	Mass per Meter (kg/m)
0.8401	2.7042	5.6789*105	8500	7140.85

Since,

$$\beta_i = \sqrt{\frac{\omega_i^2 \cdot \rho A}{EI}}$$

For  $i=1,2,3$ .

Substituting the expressions above in the frequency equation, the first three natural frequencies can be estimated graphically using a Maple script. The results for the first natural frequency are being shown in the figure below.

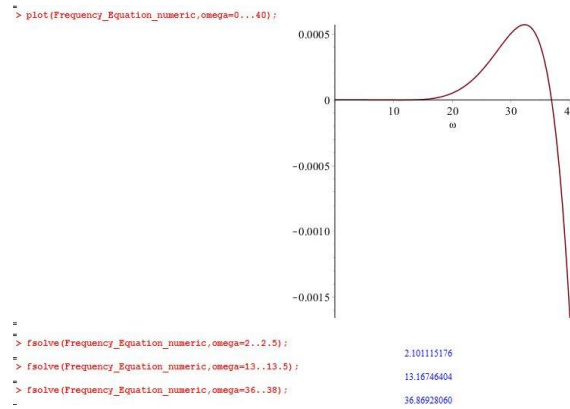


Figure 2. 6: 1<sup>st</sup>, 2<sup>nd</sup> and 3<sup>rd</sup> Natural Frequency (rad/sec)

Having calculated the first three natural frequencies, the values of “ $\beta_i$ ” for the first 3 normal modes ( $i=1,2,3$ ) are (Eq. D.14):

$$\omega_1 = 2.101115 = \beta_1^2 \cdot \sqrt{\frac{EI}{\rho A}} \Rightarrow \beta_1 = 0.01534957425$$

$$\omega_2 = 13.167464 = \beta_2^2 \cdot \sqrt{\frac{EI}{\rho A}} \Rightarrow \beta_2 = 0.03842576232$$

$$\omega_3 = 36.869280 = \beta_3^2 \cdot \sqrt{\frac{EI}{\rho A}} \Rightarrow \beta_3 = 0.0642989307$$

Since the 12 equations are linearly dependent, one random equation out of the twelve has to be removed. Since the new system of equations consists of 11 equations with 12 unknowns, one unknown should also be eliminated. This will happen by dividing all the coefficients by one coefficient (randomly chosen). In that way, the division of a coefficient with the coefficient itself, will lead to value equal to unity, thus eliminating one unknown of the system of equations. This procedure has been done in Maple for the first three natural frequencies. The equation which was eliminated was the interface condition which states that the shear force at the interface between the parts which are connected at an elevation of 14.4m and 54.4m will be equal for both parts. The coefficient which was eliminated was the "A1" coefficient.

Setting  $\frac{A_1}{A_1} = 1$ , the ratio of all the coefficients for each natural frequency have been calculated in three separate maple files (attached to this email). The first 3 normal modes for each part are:

$U_{i,j}$  where  $i =$  number referring to a part of the structure,  $j =$  mode nr.

### **First Part**

$$U_{11} = \cosh(\beta_1 \cdot x) - 1.0007839 \cdot \sinh(\beta_1 \cdot x) + \cos(0.3270857 \cdot x) - 1.0007839 \cdot \sin(\beta_1 \cdot x)$$

$$U_{12} = \cosh(\beta_2 \cdot x) - 1.0007766 \cdot \sinh(\beta_2 \cdot x) + \cos(\beta_2 \cdot x) - 1.0007766 \cdot \sin(\beta_2 \cdot x)$$

$$U_{13} = \cosh(\beta_3 \cdot x) - 1.0007779 \cdot \sinh(\beta_3 \cdot x) + \cos(\beta_3 \cdot x) - 1.0007779 \cdot \sin(\beta_3 \cdot x)$$

### **Second Part**

$$U_{21} = -1.33361 \cdot \cosh(\beta_1 \cdot x) - 41.0890653 \cdot \sinh(\beta_1 \cdot x) + 28.7598075 \cdot \cos(\beta_1 \cdot x) - 0.8054633 \cdot \sin(\beta_1 \cdot x)$$

$$U_{22} = 16.2553070 \cdot \cosh(\beta_2 \cdot x) - 16.1874621 \cdot \sinh(\beta_2 \cdot x) + 11.5317621 \cdot \cos(\beta_2 \cdot x) - 0.2722488 \cdot \sin(\beta_2 \cdot x)$$

$$U_{23} = 21.6323122 \cdot \cosh(\beta_3 \cdot x) - 21.6330615 \cdot \sinh(\beta_3 \cdot x) + 4.6411701 \cdot \cos(\beta_3 \cdot x) + 4.6260176 \cdot \sin(\beta_3 \cdot x)$$

### **Third Part**

$$U_{31} = 36.2035007 \cdot \cosh(\beta_1 \cdot x) - 41.0890653 \cdot \sinh(\beta_1 \cdot x) + 28.7598075 \cdot \cos(\beta_1 \cdot x) - 0.8054633 \cdot \sin(\beta_1 \cdot x)$$

$$U_{32} = 16.255307 \cdot \cosh(\beta_2 \cdot x) - 16.1874621 \cdot \sinh(\beta_2 \cdot x) + 11.5317621 \cdot \cos(\beta_2 \cdot x) - 0.2722488 \cdot \sin(\beta_2 \cdot x)$$

$$U_{33} = 21.6323122 \cdot \cosh(\beta_3 \cdot x) - 21.6330615 \cdot \sinh(\beta_3 \cdot x) + 4.6411701 \cdot \cos(\beta_3 \cdot x) + 4.6260176 \cdot \sin(\beta_3 \cdot x)$$

Where,

$$\beta_1 = 0.0153495$$

$$\beta_2 = 0.0384257$$

$$\beta_3 = 0.0642989$$



The first three normal modes have been calculated using the formulas above, and are being presented in the figures below.

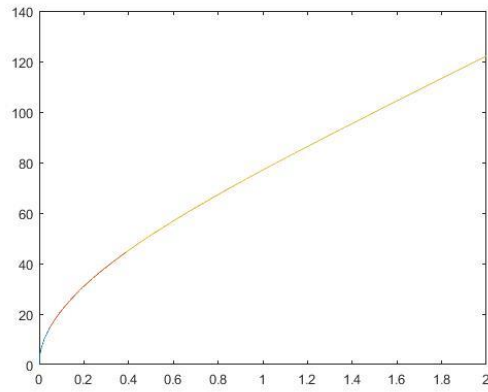


*Figure D.1: 1<sup>st</sup> Normal Mode*

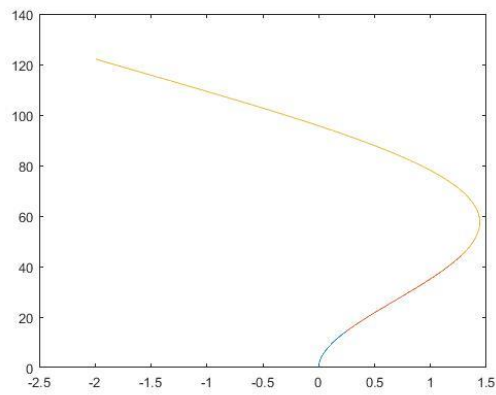


*Figure D.2: 2<sup>nd</sup> Normal Mode*

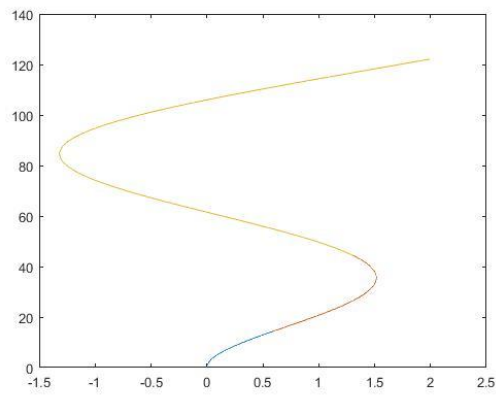


*Figure D.3: 3<sup>rd</sup> Normal Mode*

## Sensitivity Analysis

- In order to increase the 1<sup>st</sup> natural frequency by **1%**, the bending stiffness along with the maximum added mass is being presented in the figure below.

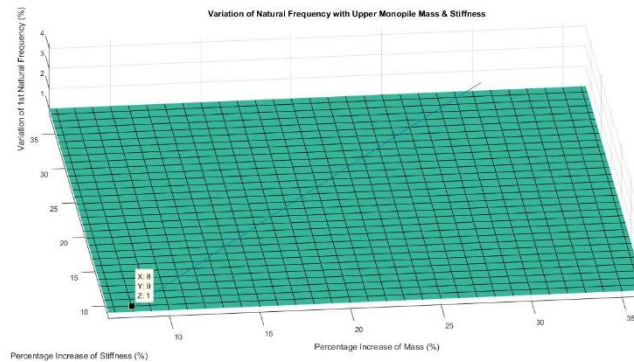


Figure D.4: Required minimum Added Stiffness and maximum Added Mass for 1% Increase

As shown in Figure D.4, the minimum required additional stiffness in order to achieve a 1% increase in the 1<sup>st</sup> natural frequency is about 8%, and it should be achieved with a maximum added mass of 8.08%.

- In order to increase the 1<sup>st</sup> natural frequency by **2%**, the bending stiffness along with the maximum added mass is being presented in the figure below.

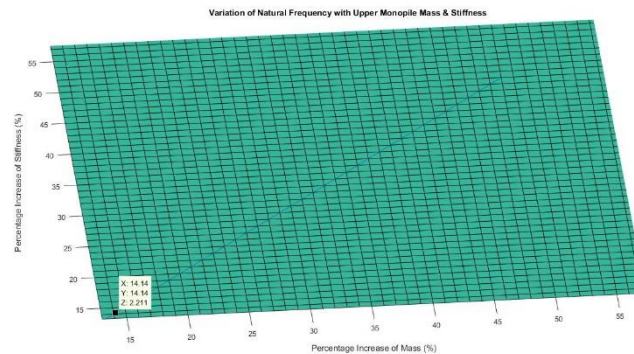


Figure D.5: Required minimum Added Stiffness and maximum Added Mass for 2% Increase

As shown in Figure D.5, the minimum required additional stiffness in order to achieve a 2% increase in the 1<sup>st</sup> natural frequency is about 13%, and it should be achieved with a maximum added mass of 13.13%.

- In order to increase the 1<sup>st</sup> natural frequency by **3%**, the bending stiffness along with the maximum added mass is being presented in the figure below.

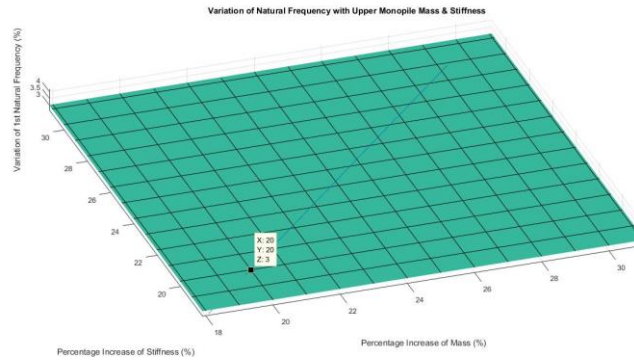


Figure D.6: Required minimum Added Stiffness and maximum Added Mass for 3% Increase

As shown in Figure D.6, the minimum required additional stiffness in order to achieve a 3% increase in the 1<sup>st</sup> natural frequency is about 20%, and it should be achieved with a maximum added mass of 20.4%.

- In order to increase the 1<sup>st</sup> natural frequency by **4%**, the bending stiffness along with the maximum added mass is being presented in the figure below.

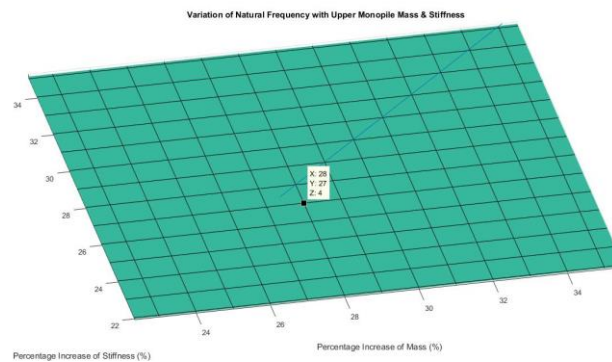


Figure D.7: Required minimum Added Stiffness and maximum Added Mass for 4% Increase

As shown in Figure D.7, the minimum required additional stiffness in order to achieve a 4% increase in the 1<sup>st</sup> natural frequency is about 27.5%, and it should be achieved with a maximum added mass of 27.8%.

The relation between the bending stiffness and the added mass is almost linear, so for an increase by 10% in the 1<sup>st</sup> natural frequency the added stiffness required will be equal to about 91% and will be achieved with an added mass of 91.9%, as shown in the figure below.

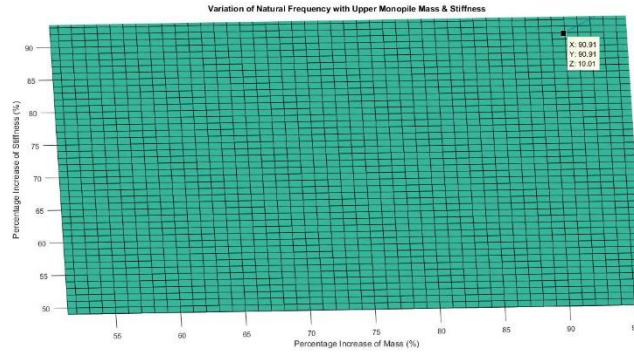


Figure D.8: Required minimum Added Stiffness and maximum Added Mass for 10% Increase

## APPENDIX E: Approximate Modes – Sensitivity Analysis (Free-Free Beam with Soil Springs)

### Approximate Modes Calculation

Therefore, 3 equations will be applied to determine the normal mode for each part. The three equations of motion are:

$$\rho \cdot A \cdot \ddot{u}_1 + E \cdot I \cdot u_1'''' + k_d \cdot u_1 = 0 \quad (E.1)$$

$$\rho \cdot A \cdot \ddot{u}_2 + E \cdot I \cdot u_2'''' = 0 \quad (E.2)$$

$$\rho \cdot A \cdot \ddot{u}_3 + E \cdot I \cdot u_3'''' = 0 \quad (E.3)$$

Where,

$\rho A$  = the mass per meter of the support structure

$EI$  = the bending stiffness per meter of the support structure

$u$  = the horizontal displacement

and,

$\ddot{u}$  = the horizontal acceleration ( $\frac{d^2u}{dt^2}$ ), as shown in the figure above

#### Boundary Conditions

$$u''(0) = u'''(0) = 0 \quad (E.4)$$

$$u''(131.76) = u'''(131.76) = 0 \quad (E.5)$$

#### Interface Conditions

$$u_1(24, t) = u_2(24, t) \quad (E.6)$$

$$\frac{du_1(24, t)}{dz} = \frac{du_2(24, t)}{dz} \quad (E.7)$$

$$\frac{d^2u_1(24, t)}{dz^2} = \frac{d^2u_2(24, t)}{dz^2} \quad (E.8)$$

$$\frac{d^3u_1(24, t)}{dz^3} = \frac{d^3u_2(24, t)}{dz^3} \quad (E.9)$$

And,

$$u_2(54, t) = u_3(54, t) \quad (E.10)$$

$$\frac{du_2(54, t)}{dz} = \frac{du_3(54, t)}{dz} \quad (E.11)$$

$$\frac{d^2u_2(54, t)}{dz^2} = \frac{d^2u_3(54, t)}{dz^2} \quad (E.12)$$

$$\frac{d^3u_2(54, t)}{dz^3} = \frac{d^3u_3(54, t)}{dz^3} \quad (E.13)$$

### General Solutions

$$u(x) = U(x) \cdot e^{i\omega t} \quad (E.14)$$

The space-related part of the equation of motion which refers to part 1 is:

$$U_1''''(x) - \left( \frac{\omega^2 \cdot \rho \cdot A - k_d}{E \cdot I} \right) \cdot U_1(x) = 0 \quad (E.15)$$

The space-related part of the equations of motion, which refers to parts 2,3 is:

$$U_{2,3}''''(x) - \left( \frac{\omega^2 \cdot \rho \cdot A}{E \cdot I} \right) \cdot U_{2,3}(x) = 0 \quad (E.16)$$

Setting,

$$\beta^4 = \left( \frac{\omega^2 \cdot \rho \cdot A - k_d}{E \cdot I} \right) < 0 \quad (E.17)$$

Due to the high magnitude of the soil subgrade modulus ( $k_d$ ), the value of expression of the numerator in the square root will be smaller than zero. This is valid for the first three (or six) natural frequencies which will be taken into consideration in this analysis. Therefore, the 4<sup>th</sup> order differential equation will have roots in the form of:

$$s_{1,2,3,4} = \frac{1}{\sqrt{2}} \cdot (\pm 1 \pm i) \cdot \beta_i \quad (E.18)$$

And a general solution in the form:

$$U_1(x) = e^{\beta \cdot x} \cdot (A_1 \cdot \cos(\beta \cdot x) + B_1 \cdot \sin(\beta \cdot x)) + e^{-\beta \cdot x} \cdot (C_1 \cdot \cos(\beta \cdot x) + D_1 \cdot \sin(\beta \cdot x))$$

The parameter “ $\gamma$ ”, is equal to:

$$\gamma^4 = \left( \frac{\omega^2 \cdot \rho \cdot A}{E \cdot I} \right) \quad (E.19)$$

The space-related part for the EoMs which refer to the parts above the seabed level can be written as:

$$U_2''''(x) - \gamma^4 \cdot U_2(x) = 0 \quad (E.20)$$

$$U_3''''(x) - \gamma^4 \cdot U_3(x) = 0$$

The general solutions of the above equations are:

$$U_1(x) = e^{\beta \cdot x} \cdot (A_1 \cdot \cos(\beta \cdot x) + B_1 \cdot \sin(\beta \cdot x)) + e^{-\beta \cdot x} \cdot (C_1 \cdot \cos(\beta \cdot x) + D_1 \cdot \sin(\beta \cdot x))$$

$$U_2(x) = A_2 \cdot \cosh(\gamma \cdot x) + B_2 \cdot \sinh(\gamma \cdot x) + C_2 \cdot \cos(\gamma \cdot x) + D_2 \cdot \sin(\gamma \cdot x)$$

$$U_3(x) = A_3 \cdot \cosh(\gamma \cdot x) + B_3 \cdot \sinh(\gamma \cdot x) + C_3 \cdot \cos(\gamma \cdot x) + D_3 \cdot \sin(\gamma \cdot x)$$

Substituting the general solutions in the boundary conditions they yield:

$$\begin{aligned} U_1'(x) = & A_1 \cdot (\beta \cdot e^{\beta \cdot x} \cdot \cos(\beta \cdot x) - \beta \cdot e^{\beta \cdot x} \cdot \sin(\beta \cdot x)) + B_1 \cdot (\beta \\ & \cdot e^{\beta \cdot x} \cdot \sin(\beta \cdot x) + \beta \\ & \cdot e^{\beta \cdot x} \cdot \cos(\beta \cdot x) + C_1 \cdot (-\beta \cdot e^{-\beta \cdot x} \cdot \cos(\beta \cdot x) - \beta \cdot e^{-\beta \cdot x} \cdot \sin(\beta \cdot x)) + D_1 \\ & \cdot (-\beta \cdot e^{-\beta \cdot x} \cdot \sin(\beta \cdot x) + \beta \cdot e^{-\beta \cdot x} \cdot \cos(\beta \cdot x)) \end{aligned}$$

$U_1''(x)$  and  $U_1'''(x)$  can be derived in a similar manner

So,

$$U_1''(0) = 0 \Rightarrow B_1 = D_1$$

$$U_1'''(0) = 0 \Rightarrow -2 \cdot A_1 + 2 \cdot B_1 + 2 \cdot C_1 + 2 \cdot D_1 = 0$$

and,

$$U_3''(x) = A_3 \cdot \cosh(\gamma \cdot x) + B_3 \cdot \sinh(\gamma \cdot x) - C_3 \cdot \cos(\gamma \cdot x) - D_3 \cdot \sin(\gamma \cdot x)$$

$$U_3'''(x) = A_3 \cdot \sinh(\gamma \cdot x) + B_3 \cdot \cosh(\gamma \cdot x) + C_3 \cdot \sin(\gamma \cdot x) - D_3 \cdot \cos(\gamma \cdot x)$$

So,

$$U_3''(131,76) = 0$$

$$\Rightarrow A_3 \cdot \cosh(\gamma \cdot 131,76) + B_3 \cdot \sinh(\gamma \cdot 131,76) - C_3 \cdot \cos(\gamma \cdot 131,76) - D_3 \cdot \sin(\gamma \cdot 131,76) = 0$$

$$U_3'''(131,76) = A_3 \cdot \sinh(\gamma \cdot 131,76) + B_3 \cdot \cosh(\gamma \cdot 131,76) + C_3 \cdot \sin(\gamma \cdot 131,76) - D_3 \cdot \cos(\gamma \cdot 131,76) = 0$$

Substituting the general solutions in the interface conditions they yield:

**At an elevation equal to 24m:**

$$U_1(24) = U_2(24)$$

$$U_1'(24) = U_2'(24) \Rightarrow$$

$$\begin{aligned} & AI e^{\beta x0} \cos(\beta x0) \beta - AI e^{\beta x0} \sin(\beta x0) \beta + BI e^{\beta x0} \cos(\beta x0) \beta + BI e^{\beta x0} \sin(\beta x0) \beta \\ & - CI \cos(\beta x0) e^{-\beta x0} \beta - CI \sin(\beta x0) e^{-\beta x0} \beta + DI \cos(\beta x0) e^{-\beta x0} \beta \\ & - DI \sin(\beta x0) e^{-\beta x0} \beta - A2 \gamma \sinh(\gamma x0) - B2 \gamma \cosh(\gamma x0) + C2 \gamma \sin(\gamma x0) \\ & - D2 \gamma \cos(\gamma x0) \end{aligned}$$

$$U_1''(24) = U_2''(24) \Rightarrow$$

$$\begin{aligned} & -2 AI e^{\beta x0} \sin(\beta x0) \beta^2 + 2 BI e^{\beta x0} \cos(\beta x0) \beta^2 + 2 CI \sin(\beta x0) e^{-\beta x0} \beta^2 \\ & - 2 DI \cos(\beta x0) e^{-\beta x0} \beta^2 - A2 \gamma^2 \cosh(\gamma x0) - B2 \gamma^2 \sinh(\gamma x0) + C2 \gamma^2 \cos(\gamma x0) \\ & + D2 \gamma^2 \sin(\gamma x0) \end{aligned}$$

$$U_1'''(24) = U_2'''(24) \Rightarrow$$

$$\begin{aligned} & -2 AI e^{\beta x0} \cos(\beta x0) \beta^3 - 2 AI e^{\beta x0} \sin(\beta x0) \beta^3 + 2 BI e^{\beta x0} \cos(\beta x0) \beta^3 \\ & - 2 BI e^{\beta x0} \sin(\beta x0) \beta^3 + 2 CI \cos(\beta x0) e^{-\beta x0} \beta^3 - 2 CI \sin(\beta x0) e^{-\beta x0} \beta^3 \\ & + 2 DI \cos(\beta x0) e^{-\beta x0} \beta^3 + 2 DI \sin(\beta x0) e^{-\beta x0} \beta^3 - A2 \gamma^3 \sinh(\gamma x0) \\ & - B2 \gamma^3 \cosh(\gamma x0) - C2 \gamma^3 \sin(\gamma x0) + D2 \gamma^3 \cos(\gamma x0) \end{aligned}$$

**At an elevation equal to 54m:**

$$U_2(54) = U_3(54)$$

$$\begin{aligned} U_2'(54) &= U_3'(54) \\ &\Rightarrow A_2 \cdot \sinh(\gamma \cdot 54) + B_2 \cdot \cosh(\gamma \cdot 54) - C_2 \cdot \sin(\gamma \cdot 54) + D_2 \cdot \cos(\gamma \cdot 54) \\ &= A_3 \cdot \sinh(\gamma \cdot 54) + B_3 \cdot \cosh(\gamma \cdot 54) - C_3 \cdot \sin(\gamma \cdot 54) + D_3 \cdot \cos(\gamma \cdot 54) \end{aligned}$$

$$\begin{aligned} U_2''(54) &= U_3''(54) \\ &\Rightarrow [A_2 \cdot \cosh(\gamma \cdot 54) + B_2 \cdot \sinh(\gamma \cdot 54) - C_2 \cdot \cos(\gamma \cdot 54) - D_2 \cdot \sin(\gamma \cdot 54)] \\ &= [A_3 \cdot \cosh(\gamma \cdot 54) + B_3 \cdot \sinh(\gamma \cdot 54) - C_3 \cdot \cos(\gamma \cdot 54) - D_3 \\ &\quad \cdot \sin(\gamma \cdot 54)] \end{aligned}$$

$$\begin{aligned} U_2'''(54) &= U_3'''(54) \\ &\Rightarrow [A_2 \cdot \sinh(\gamma \cdot 54) + B_2 \cdot \cosh(\gamma \cdot 54) + C_2 \cdot \sin(\gamma \cdot 54) - D_2 \cdot \cos(\gamma \cdot 54)] \\ &= [A_3 \cdot \sinh(\gamma \cdot 54) + B_3 \cdot \cosh(\gamma \cdot 54) + C_3 \cdot \sin(\gamma \cdot 54) - D_3 \cdot \cos(\gamma \cdot 54)] \end{aligned}$$

In order that the system of the above 12 equations with 12 unknowns does not have a trivial solution, the determinant of the co-efficients of  $A_1 \dots D_4$  must be equal to zero. This procedure gives the frequency equation.

In order to have a constant mass and stiffness along the total length of the structure, a weighted average of the diameters and thicknesses of all the members is being taken.

$$D_{avg} = \frac{6.1 \cdot 54 + 5.65 \cdot 9.76 + 4.98 \cdot 68}{131.76} = 5.127 \text{ m} \quad (E.21)$$

And

$$t_{avg} = \frac{0.08 \cdot 54 + 0.06 \cdot 9.76 + 0.03 \cdot 68}{131.76} = 0.0527 \text{ m} \quad (E.22)$$

The dimensions above lead to the following values for the mass and stiffness related parameters:

$$A = 0.8401 \text{ m}^2$$

$$I = 2.7042 \text{ m}^4$$

$$EI = 5.6789 \cdot 10^{11} \text{ N} \cdot \text{m}^2 \text{ per meter length}$$

$$\rho = 8500 \frac{\text{kg}}{\text{m}^3}$$

$$\rho A = 7140.85 \text{ kg per meter length}$$

Since,

$$\beta_i = \sqrt[4]{\frac{k_d - \omega_i^2 \cdot \rho \cdot A}{E \cdot I}}$$

And,

$$\gamma_i = \sqrt{\sqrt{\frac{\omega_i^2 \cdot \rho A}{EI}}}$$



For  $i= 1,2,3$ .

Substituting the expressions above in the frequency equation, the first three natural frequencies can be estimated graphically using a Maple script. The results for the first natural frequency are being shown in the figure below.

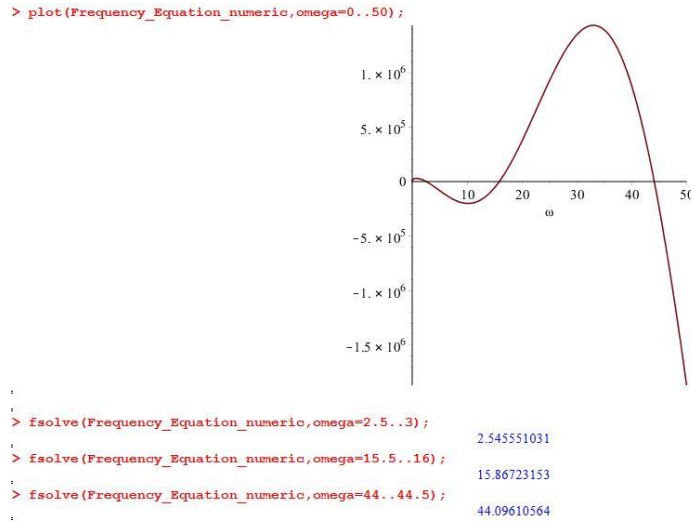


Figure E.1: 1<sup>st</sup>, 2<sup>nd</sup> and 3<sup>rd</sup> Natural Frequency (rad/sec)

Having calculated the first three natural frequencies, the values of “ $\beta_i$ ” and “ $\gamma_i$ ”s for the first 3 normal modes ( $i=1,2,3$ ) are:

$$\omega_1 = 2.54555 = \gamma_1^2 \cdot \sqrt{\frac{EI}{\rho A}} \Rightarrow \gamma_1 = 0.016895157$$

$$\omega_2 = 15.86723 = \gamma_2^2 \cdot \sqrt{\frac{EI}{\rho A}} \Rightarrow \gamma_2 = 0.042181498$$

$$\omega_3 = 44.09611 = \gamma_3^2 \cdot \sqrt{\frac{EI}{\rho A}} \Rightarrow \gamma_3 = 0.07031881523$$

And,

$$\Rightarrow \beta_1 = \sqrt[4]{\frac{k_d - \omega_1^2 \cdot \rho \cdot A}{E \cdot I}} = \sqrt[4]{\frac{6.5 \cdot 10^9 - 2.54555^2 \cdot 7140.85}{5.6789 \cdot 10^{11}}} = 0.32708567$$

$$\beta_2 = \text{abs}\left(\sqrt[4]{\frac{\omega_2^2 \cdot \rho \cdot A - k_d}{E \cdot I}}\right) \Rightarrow \beta_2 = \sqrt[4]{\frac{k_d - \omega_2^2 \cdot \rho \cdot A}{E \cdot I}} = 0.32706363$$

$$\beta_3 = \text{abs}\left(\sqrt[4]{\frac{\omega_3^2 \cdot \rho \cdot A - k_d}{E \cdot I}}\right) \Rightarrow \beta_3 = \sqrt[4]{\frac{k_d - \omega_3^2 \cdot \rho \cdot A}{E \cdot I}} = 0.32691142$$

The soil subgrade modulus  $k_d$ , is set equal to  $6.5 \cdot 10^9$  (N/m length) because this is the required value for the soil stiffness, in order that the monopile as described in the Upwind report will have the exact natural frequency, as presented in the report (0.277 Hz). In this approximation, the value of the soil subgrade modulus is considered to be constant and independent of the depth. Introducing this value for the soil stiffness in the Matlab script (considering both the ends of the structure as free as shown in Figure 2.1), the 1<sup>st</sup> natural frequency is being shown in the table below:

1595	15.4393
1596	14.1462
1597	10.1337
1598	4.9888
1599	1.8391
1600	0.2770

Figure E.2: Natural Frequencies – FD Model with Soil, for  $k_d = 6.5 \cdot 10^9$  N/m

Of course, the table above refers to the natural frequencies which have been calculated for the exact model of the monopile, as it has been analyzed using the FDM. In the modal analysis, the whole structure is considered to have constant dimensions along its length. Therefore, the natural frequency of this approximate structure will vary comparing to the natural frequency of the exact model.

Since the 12 equations are linearly dependent, one random equation out of the twelve has to be removed. Since the new system of equations consists of 11 equations with 12 unknowns, one unknown should also be eliminated. This will happen by dividing all the coefficients by one coefficient (randomly chosen). In that way, the division of a coefficient with the coefficient itself, will lead to value equal to unity, thus eliminating one unknown of the system of equations. This procedure has been done in Maple for the first three natural frequencies. The equation which was eliminated was the interface condition which states that the shear force at the interface between the parts which are connected at an elevation of 24m will be equal for both parts. The coefficient which was eliminated was the “A1” coefficient.

Setting  $\frac{A_1}{A_1} = 1$ , the ratio of all the coefficients for each natural frequency have been calculated in three separate maple files (attached to this email). The first 3 normal modes for each part are:

$$U_{i,j} \text{ where } i = \text{number referring to a part of the structure}, j = \text{mode nr.}$$

#### **First Part**

$$U_{11} = e^{\beta_1 \cdot x} \cdot (1 \cdot \cos(\beta_1 \cdot x) - 1.16226 \cdot \sin(\beta_1 \cdot x)) + e^{-\beta_1 \cdot x} \cdot (3.32452 \cdot \cos(\beta_1 \cdot x) - 1.16226 \cdot \sin(\beta_1 \cdot x))$$

$$U_{12} = e^{\beta_2 \cdot x} \cdot (1 \cdot \cos(\beta_2 \cdot x) - 1.52146 \cdot \sin(\beta_2 \cdot x)) + e^{-\beta_2 \cdot x} \cdot (4.04292 \cdot \cos(\beta_2 \cdot x) - 1.52146 \cdot \sin(\beta_2 \cdot x))$$

$$U_{13} = e^{\beta_3 \cdot x} \cdot (1 \cdot \cos(\beta_3 \cdot x) - 2.11726 \cdot \sin(\beta_3 \cdot x)) + e^{-\beta_3 \cdot x} \cdot (5.23451 \cdot \cos(\beta_3 \cdot x) - 2.11726 \cdot \sin(\beta_3 \cdot x))$$

Where,

$$\beta_1 = 0.3270857$$

$$\beta_2 = 0.3270636$$

$$\beta_3 = 0.3269114$$

### Second Part

$$U_{21} = -1.33361 \cdot \cosh(\gamma_1 \cdot x) - 41.0890653 \cdot \sinh(\gamma_1 \cdot x) + 28.7598075 \cdot \cos(\gamma_1 \cdot x) - 0.8054633 \cdot \sin(\gamma_1 \cdot x)$$

$$U_{22} = 16.2553070 \cdot \cosh(\gamma_2 \cdot x) - 16.1874621 \cdot \sinh(\gamma_2 \cdot x) + 11.5317621 \cdot \cos(\gamma_2 \cdot x) - 0.2722488 \cdot \sin(\gamma_2 \cdot x)$$

$$U_{23} = 21.6323122 \cdot \cosh(\gamma_3 \cdot x) - 21.6330615 \cdot \sinh(\gamma_3 \cdot x) + 4.6411701 \cdot \cos(\gamma_3 \cdot x) + 4.6260176 \cdot \sin(\gamma_3 \cdot x)$$

### Third Part

$$U_{31} = 36.2035007 \cdot \cosh(\gamma_1 \cdot x) - 41.0890653 \cdot \sinh(\gamma_1 \cdot x) + 28.7598075 \cdot \cos(\gamma_1 \cdot x) - 0.8054633 \cdot \sin(\gamma_1 \cdot x)$$

$$U_{32} = 16.255307 \cdot \cosh(\gamma_2 \cdot x) - 16.1874621 \cdot \sinh(\gamma_2 \cdot x) + 11.5317621 \cdot \cos(\gamma_2 \cdot x) - 0.2722488 \cdot \sin(\gamma_2 \cdot x)$$

$$U_{33} = 21.6323122 \cdot \cosh(0.071515 \cdot x) - 21.6330615 \cdot \sinh(0.071515 \cdot x) + 4.6411701 \cdot \cos(0.071515 \cdot x) + 4.6260176 \cdot \sin(0.071515 \cdot x)$$

$$\gamma_1 = 0.016895157$$

$$\gamma_2 = 0.042181498$$

$$\gamma_3 = 0.070318815$$

The first three normal modes have been calculated using the formulas above, and are being presented in the figures below.

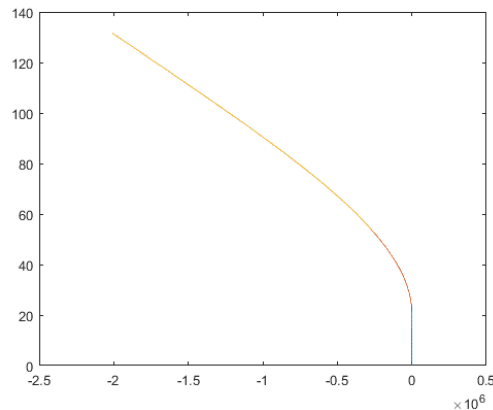


Figure E.3: 1<sup>st</sup> Normal Mode

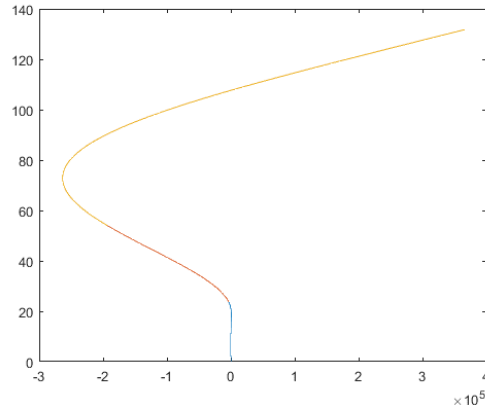


Figure E.4: 2<sup>nd</sup> Normal Mode

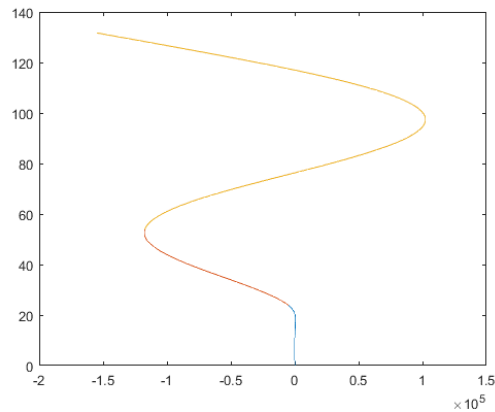


Figure E.5: 3<sup>rd</sup> Normal Mode

## Sensitivity Analysis

- In order to increase the 1<sup>st</sup> natural frequency by **1%**, the bending stiffness along with the maximum added mass is being presented in the figure below:

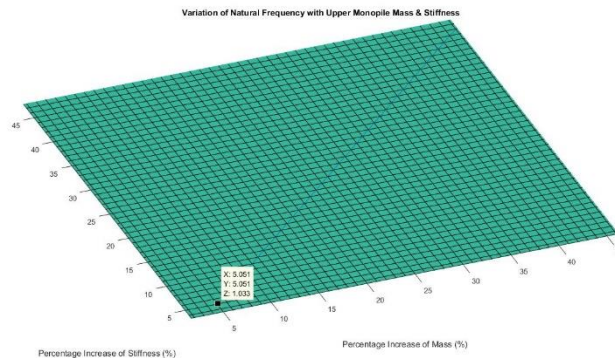


Figure E.6: Required minimum Added Stiffness and maximum Added Mass for 1% Increase

As shown in *Figure E.6*, the minimum required additional stiffness in order to achieve a 1% increase in the 1<sup>st</sup> natural frequency is about 5.05%, and it should be achieved with a maximum added mass of 5.10%.

- In order to increase the 1<sup>st</sup> natural frequency by **2%**, the bending stiffness along with the maximum added mass is being presented in the figure below:

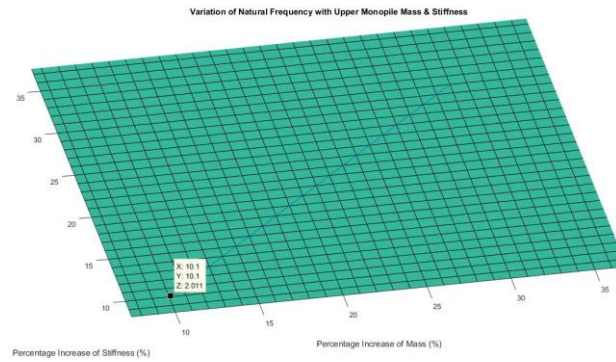


Figure E.7: Required minimum Added Stiffness and maximum Added Mass for 2% Increase

As shown in Figure E.7, the minimum required additional stiffness in order to achieve a 2% increase in the 1<sup>st</sup> natural frequency is about 10.5%, and it should be achieved with a maximum added mass of 10.61%.

- In order to increase the 1<sup>st</sup> natural frequency by **3%**, the bending stiffness along with the maximum added mass is being presented in the figure below:

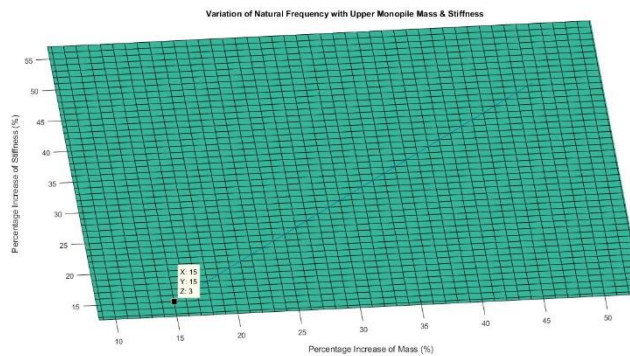


Figure E.8: Required minimum Added Stiffness and maximum Added Mass for 3% Increase

As shown in Figure E.8, the minimum required additional stiffness in order to achieve a 3% increase in the 1<sup>st</sup> natural frequency is about 15.5%, and it should be achieved with a maximum added mass of 15.66%.

- In order to increase the 1<sup>st</sup> natural frequency by **4%**, the bending stiffness along with the maximum added mass is being presented in the figure below:

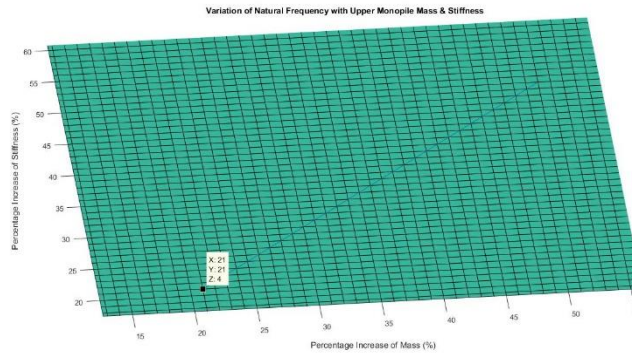


Figure E.9: Required minimum Added Stiffness and maximum Added Mass for 4% Increase

As shown in Figure E.9, the minimum required additional stiffness in order to achieve a 4% increase in the 1<sup>st</sup> natural frequency is about 21%, and it should be achieved with a maximum added mass of 21.21%.

The relation between the bending stiffness and the added mass is almost linear, so for an increase by 10% in the 1<sup>st</sup> natural frequency the added stiffness required will be equal to about 64.7% and will be achieved with an added mass of 65.36%, as shown in the figure below.

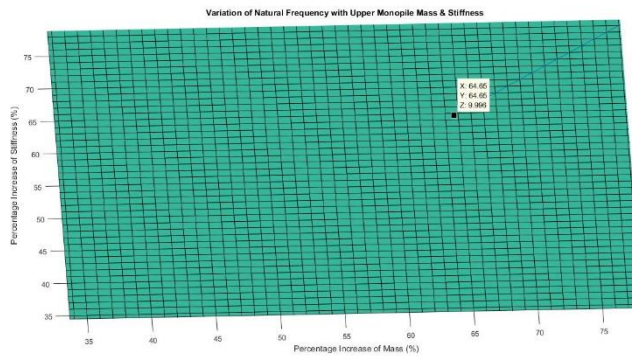


Figure E.10: Required minimum Added Stiffness and maximum Added Mass for 4% Increase

## APPENDIX F: Effect of the Density of the Surrounding Soil & the Sand-Fill

### ➤ Dense Surrounding Soil – Loose & Dense Sand-fill

The response time history, as obtained by Plaxis, for an empty and a fully filled monopile (dense sand) is being shown in Figure F.1.

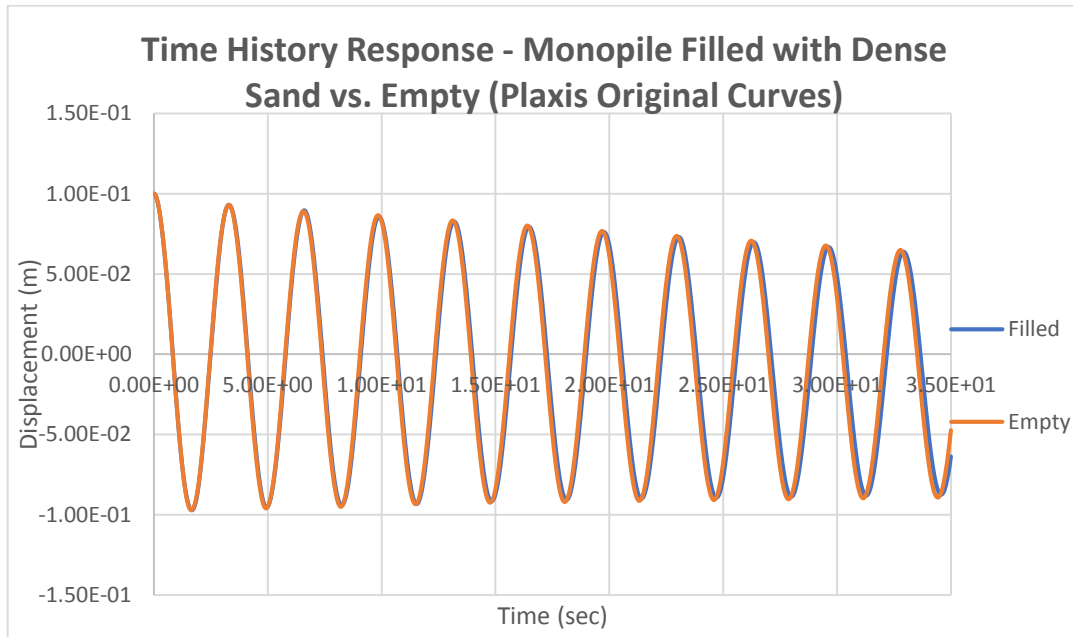


Figure F.1: Comparison of the Response of a Filled with an Empty Monopile Embedded in Dense Soil

The normalized time history response is shown in Figure F.2.

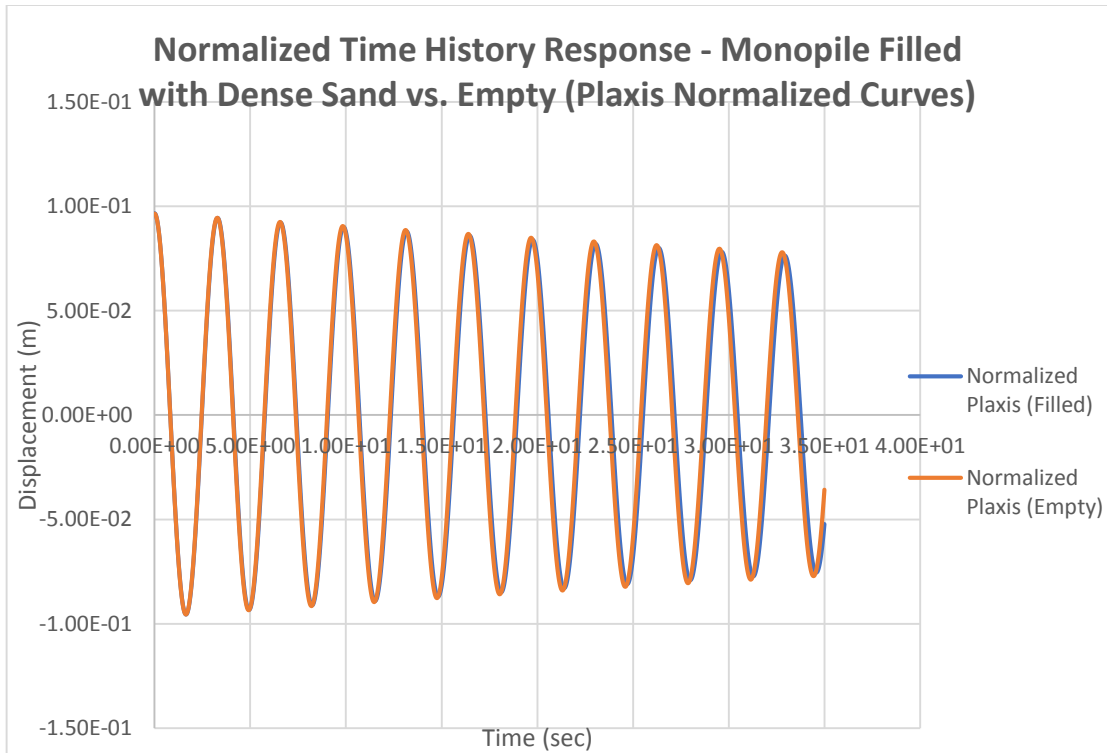


Figure F.2: Comparison of the Normalized Response of a Filled with an Empty Monopile Embedded in Dense Soil

As shown in Figure F.1 and Figure F.2 **Σφάλμα! Το αρχείο προέλευσης της αναφοράς δεν βρέθηκε.**, the effect of damping due to the sand-fill becomes visible after the 3<sup>rd</sup> cycle, and it increases towards the end of the simulation. However, the effect is not so significant.

The match of the normalized curves with the analytical solution for the empty and the filled monopile is being shown in Figure F.3 and Figure F.4.



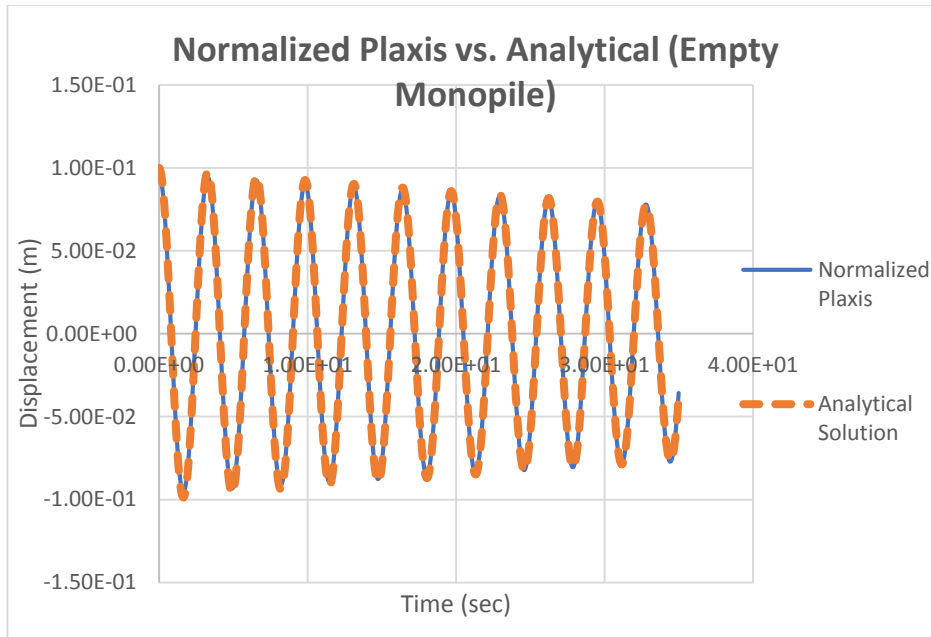


Figure F.3: Normalized Plaxis Response and Analytical Response for an Empty Monopile

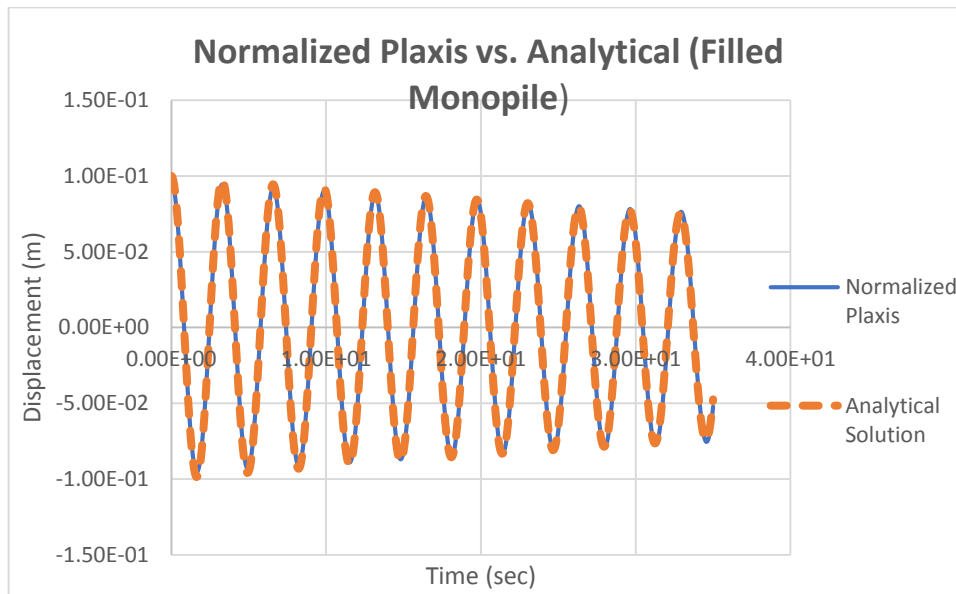


Figure F.4: Normalized Plaxis Response and Analytical Response for a Filled Monopile

The normalized curves coincide with the analytical solution, which was the goal of normalizing the curves obtained by Plaxis. By normalizing the Plaxis values, the damped/undamped natural frequencies and the damping ratio are known. The results for all the cases tested are being presented in a collective table at the end of this analysis. This comparison is being presented only for this case for brevity.

Using loose sand as filling has exactly the similar result (Figure F.5). For this reason, the effect of adding sand of medium density in the monopile is not examined.

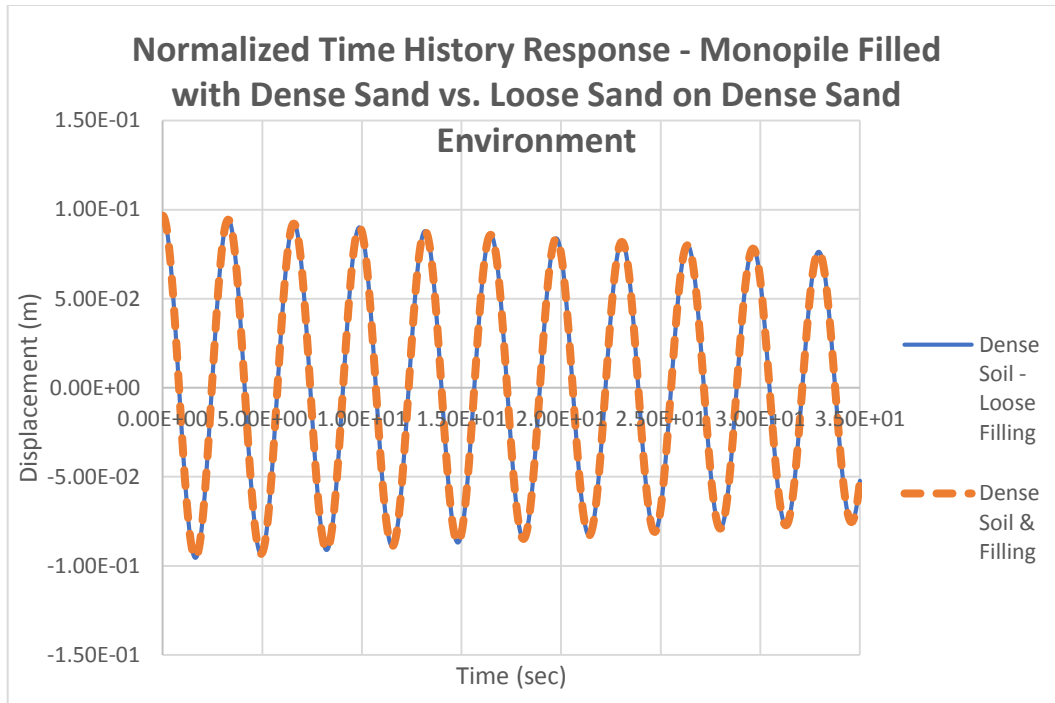


Figure F.5: Comparison of the Response of a Filled Monopile with Loose and Dense Sand

➤ Loose Surrounding Soil – Loose, Medium & Dense Sand-fill

The normalized time history response for an empty and a fully filled monopile (with loose sand) is being shown in Figure F.6.

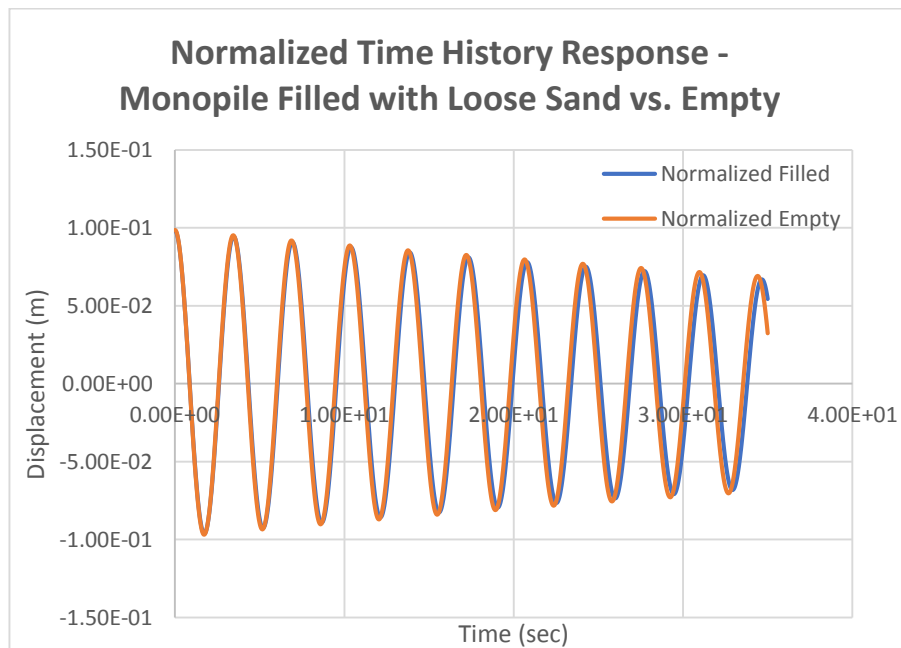


Figure F.6: Comparison of the Response of a Filled with an Empty Monopile Embedded in Loose Soil

As shown in Σφάλμα! Το αρχείο προέλευσης της αναφοράς δεν βρέθηκε., the effect of damping becomes visible already from the 2<sup>nd</sup> cycle. The magnitude of damping added in the

system is also higher, than in the case of adding sand-fill on a monopile embedded in dense sand (Figure F.1). The exact values and comparison are being presented at the table at the end of this paragraph.

➤ Medium Density Surrounding Soil – Loose, Medium & Dense Sand-fill

The response time history for an empty and a fully filled monopile (with medium dense sand) is being shown in Figure F.7. After recognizing that the density of the sand-fill does not affect the response, the analysis was performed for only one density for the sand fill (loose sand).

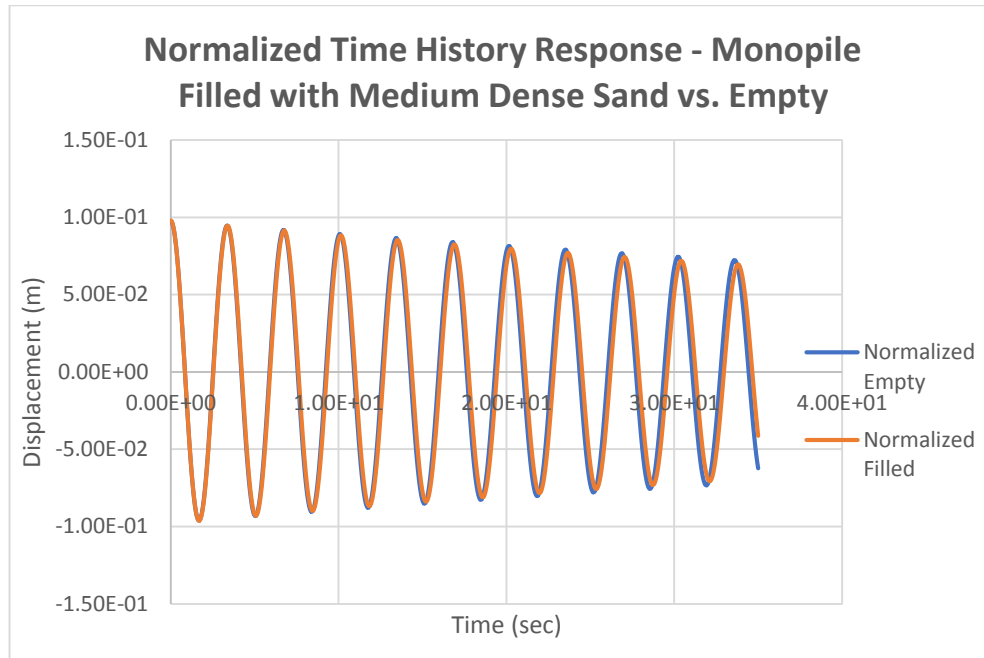
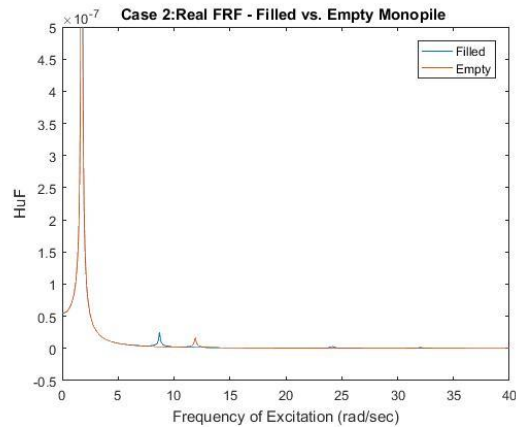


Figure F.7: Comparison of the Response of a Filled with an Empty Monopile Embedded in Medium Density Soil

## APPENDIX G: Modal Analysis – Frequency Response Functions

### Case 2

For the 2<sup>nd</sup> Case under consideration, the FRF is shown in *Figure 6.47*.



*Figure 6.47: Real Frequency Response Function in Relation with the Frequency of the Excitation*

The maximum displacement of the structure in relation with the frequency of the excitation force, for a force of 190 kN applied on the top of the structure, for the empty and the filled monopile, is being shown in *Figure 6.48*.

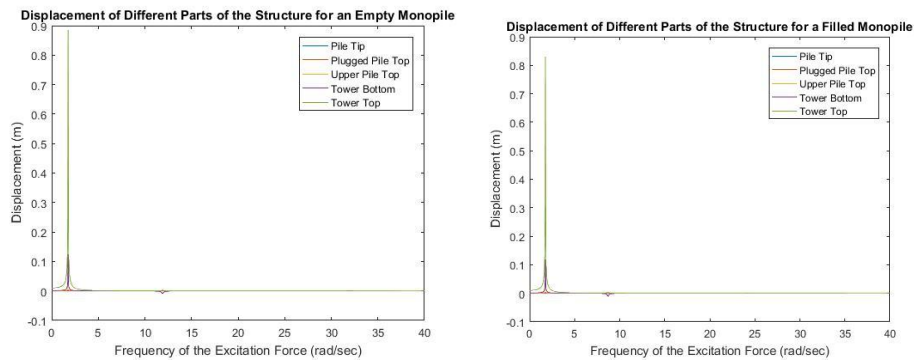


*Figure 6.48: Displacement of each Part of the Structure for Varying Frequency of Excitation – (Left Empty – Right Filled)*

More specifically, the effect of the corresponding damping ratios on the displacement of each node in the case of resonance at the fundamental frequency of the structure is shown in *Figure 6.49*.

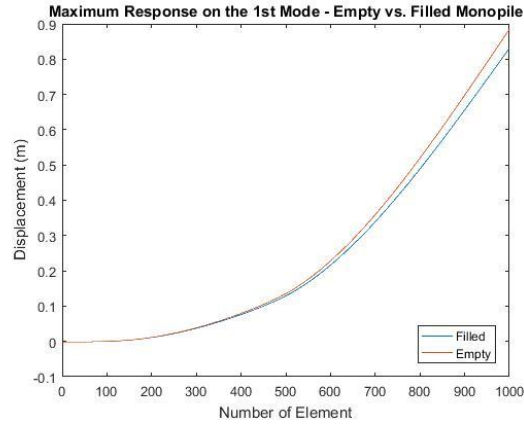


Figure 6.49: Maximum Displacement of each Node of the Structure

As shown in Figure 6.49, the bigger damping due to the filling of the monopile leads to a decrease in the maximum displacement of the top node by approximately 6.1%.

### Case 3

For the 3<sup>rd</sup> Case under consideration, the FRF is shown in Figure 6.50.

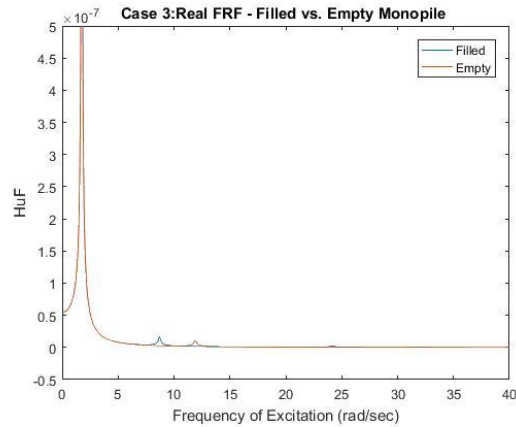


Figure 6.50: Real Frequency Response Function in Relation with the Frequency of the Excitation

The maximum displacement of the structure in relation with the frequency of the excitation force, for a force of 355 kN applied on the top of the structure, for the empty and the filled monopile, is being shown in Figure 6.51.

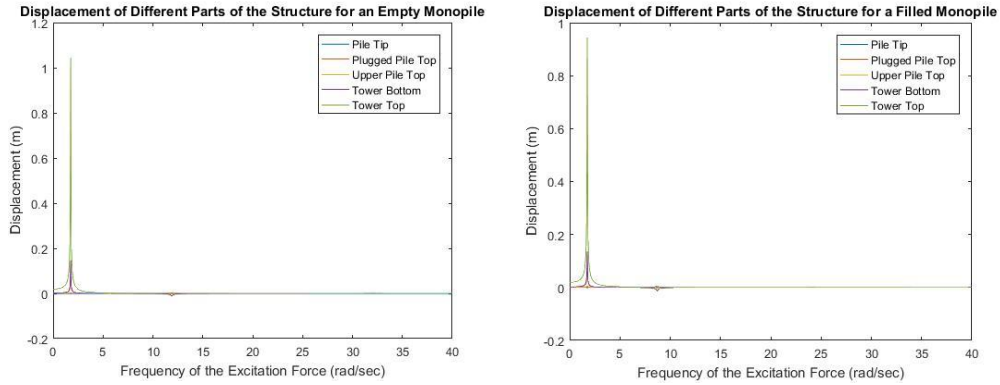


Figure 6.51: Displacement of each Part of the Structure for Varying Frequency of Excitation – (Left Empty – Right Filled)

More specifically, the effect of the corresponding damping ratios on the displacement of each node in the case of resonance at the fundamental frequency of the structure is shown in Figure 6.52.

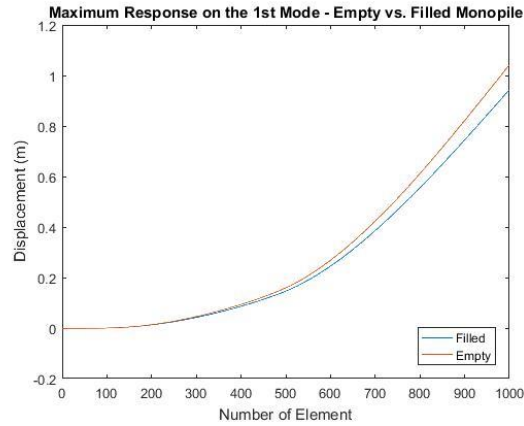


Figure 6.52: Maximum Displacement of each Node of the Structure

As shown in Figure 6.52, the bigger damping due to the filling of the monopile leads to a decrease in the maximum displacement of the top node by approximately 9.5%.

#### Case 4

For the 4<sup>th</sup> Case under consideration, the FRF is shown in Figure 6.53.

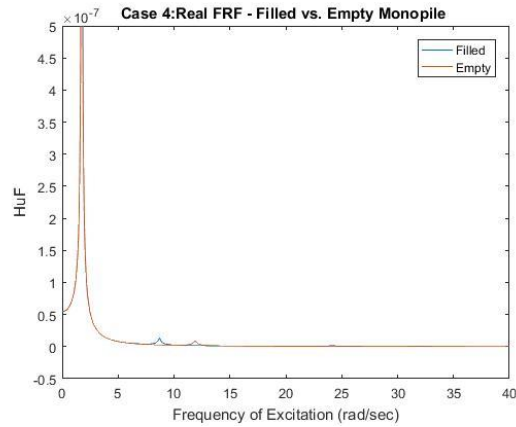


Figure 6.53: Real Frequency Response Function in Relation with the Frequency of the Excitation

The maximum displacement of the structure in relation with the frequency of the excitation force, for a force of 510 kN applied on the top of the structure, for the empty and the filled monopile, is being shown in Figures 2.8 and 2.9.

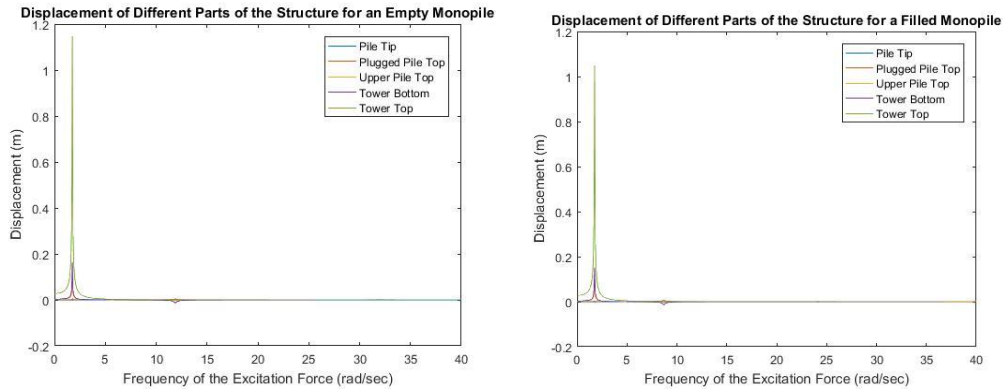


Figure 6.54: Displacement of each Part of the Structure for Varying Frequency of Excitation – (Left Empty – Right Filled)

More specifically, the effect of the corresponding damping ratios on the displacement of each node in the case of resonance at the fundamental frequency of the structure is shown in Figure 6.55.

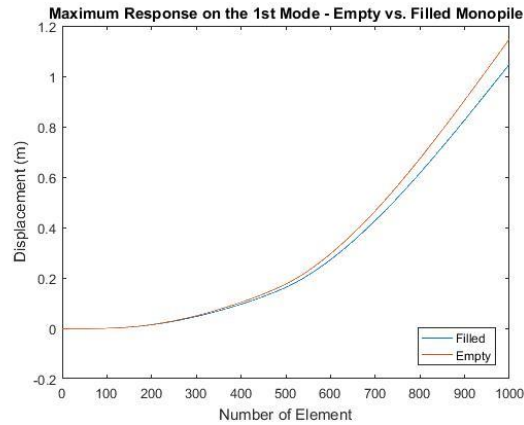


Figure 6.55: Maximum Displacement of each Node of the Structure

As shown in Figure 6.55, the bigger damping due to the filling of the monopile leads to a decrease in the maximum displacement of the top node by approximately 8.7%.

**Case 5**

For the 5<sup>th</sup> Case under consideration, the FRF is shown in Figure 6.56.

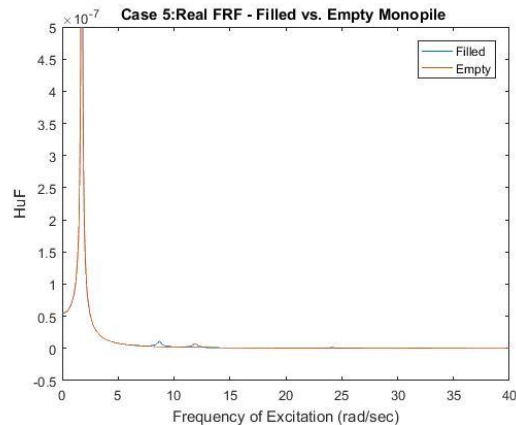


Figure 6.56: Real Frequency Response Function in Relation with the Frequency of the Excitation

As shown in Figure 6.56, the structural response maximizes at the points when the excitation force’s frequency coincides with one of the natural frequencies of the structure (resonance). The maximum displacement of the structure in relation with the frequency of the excitation force, for a force of 640 kN applied on the top of the structure, for the empty and the filled monopile, is being shown in Figures 2.8 and 2.9.



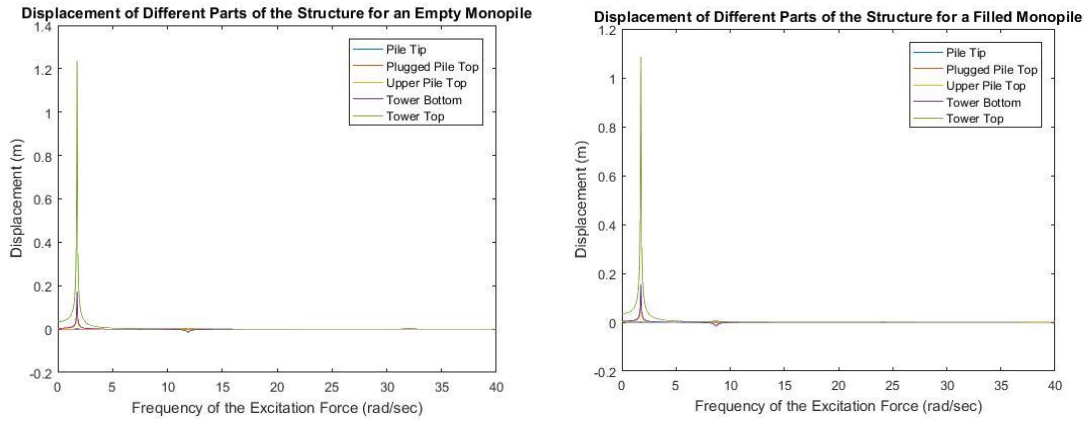


Figure 6.57: Displacement of each Part of the Structure for Varying Frequency of Excitation – (Left Empty – Right Filled)

More specifically, the effect of the corresponding damping ratios on the displacement of each node in the case of resonance at the fundamental frequency of the structure is shown in Figure 6.58.

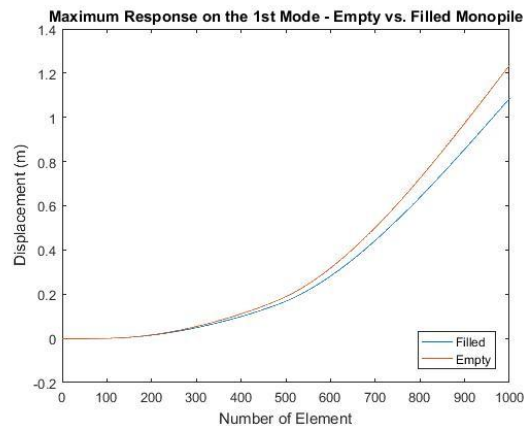


Figure 6.58: Maximum Displacement of each Node of the Structure

As shown in Figure 6.58, the bigger damping due to the filling of the monopile leads to a decrease in the maximum displacement of the top node by approximately 12.2%.